Spatio-Temporal Modelling of Fish Stocks: Deriving Spatially-Explicit MSY Reference Points Using a Metapopulation Model

by

Nicholas Gullage

A thesis submitted to the School of Graduate Studies
in partial fulfilment of the requirements for the degree of
Master of Science in Fisheries

Centre for Fisheries Ecosystems Research
Marine Institute, Memorial University of Newfoundland

May 2020

St. John's Newfoundland

Abstract

Many fisheries are successfully managed using reference points (RPs) based on the maximum sustainable yield (MSY), in particular f_{MSY}, the fishing mortality rate that achieves MSY. Typically, f_{MSY} is derived assuming fish are homogeneously distributed in space. However, fishing should be spatially allocated to optimize yields and reduce stock depletion, and f_{MSY} should be derived assuming fish are heterogeneously distributed. In this thesis, we apply a deterministic, age-structured model to derive spatially-explicit MSY RPs. We develop a metapopulation model with a source-sink, larval-advection dynamic to calculate f_{MSY} and other related RPs for a two-box model. We also derive MSY RPs for a three-box model for several unique connectivity patterns, and develop a framework to derive RPs for an n-box model. We conclude that spatially-explicit MSY RPs can be more sustainable than values derived through a one-box model RPs, but usually provide less yields.

Acknowledgements

I would like to thank my supervisor Dr. Noel Cadigan for his help through this thesis, and the Marine Institute for fostering a hospitable work environment.

I would also like to extend thanks to my cats Juno and Jupiter for copious amounts of stress relief when I needed it.

Contents

1 Introduction **1**

1.1 Fisheries Management and Management Reference Points . . . 1

1.2 Surplus Production Model 4

1.3 Practical Issues with Contemporary Models 6

1.4 Spatial Models 8

1.5 Source-Sink Metapopulations 11

1.6 Figures 15

2 MSY RPs for an Age-Structured Model **18**

2.1 Cohort Model 18

2.2 Parameter Choices 24

2.3 Forecast Projection 28

2.4 Per-Recruit Functions 29

2.5 Results 34

2.6 Discussion 38

2.7 Tables 42

2.8 Figures 44

3 The Two-Box Model **57**

3.1 Methods 57
3.2 Results 71
3.2.1 Verification of the Two-Box Forecast Projection Method 71
3.2.2 EQ System Equilibrium Results 71
3.2.3 Source and Sink Persistence 74
3.2.4 EQ MSY RP Results 77
3.2.5 EQ MSY RPs for Alternative Harvest Strategies 80
3.2.6 EQ MSY RPs for Alternative Parametrizations 82
3.2.7 MSY RPs for a HL System 83
3.2.8 MSY RPs for a DA System 84
3.2.9 MSY RPs for a HL & DA System 86
3.3 Discussion 87
3.4 Tables 94
3.5 Figures 98

4 The Three-Box Model 124
4.1 Methods 124
4.2 Results 131
4.2.1 Chain Pattern 132
4.2.2 Converging Pattern 133
4.2.3 Branching Pattern 135
4.2.4 Detouring Pattern 136
4.2.5 Cyclical Pattern 137
4.3 Discussion 138
4.4 Figures 141

5 Multiple dimensions and the n-Box Model **162**

5.1 Theory 162

5.2 Figures 169

6 Conclusion **170**

6.1 Future Research 170

6.2 Final Remarks 171

Appendix A **185**

Appendix B **188**

List of Tables

2.1 Values for stock characteristic used to estimate RPs. Weight are calculated as W_k, where $k = 0.1$, $k = 0.05$, and $k = 0.15$; selectivity are defined s_{a_r}, where $a_r = 6$ and $a_r = 8$; natural mortality rates are describe by $m_{constant} = 0.2$ and the Lorenzen natural mortality m_{lor}; and maturity ogives μ defined by $A_{50\%} = 8$ and $A_{95\%} = 10$, and $A_{50\%} = 10$ and $A_{95\%} = 12$. 42

2.2 Stock values calculated in the forecast projection and their respective equations. 43

2.3 RP estimates using the forecast projection method (FP) and through the per-recruit functions (PR), using the s_6, $\mu_{8,10}$, $W_{0.1}$, and $m_{constant}$ parametrizations (see Table 2.1 for parameter definitions). PR values were rounded to 3 significant figures to maintain the same precision as FP values. 43

3.1 MSY RP outputs for a two-box model using a forecast projection (FP) and the per-recruit functions (PR) under base conditions. Precision of PR outputs are rounded based on the precision FP outputs (3 significant figures). 94

3.2 Transfer proportions when $f_{MSY,1} = 0$ (p_{f0}) and $SSB_{eq,1} = 0$ (p_{ex}). Values for p_{f0} and p_{ex} are affected by changes in life history characteristics and SR models, and values for the equivalent (EQ), High-to-Low (HL), Downstream Advection (DA), and High-to-Low with Downstream Advection (HL & DA) will be different. 94

3.3 MSY RPs for various transfer proportions. The transfer proportion, p does not affect one-box model results. 95

3.4 MSY RPs under various two-box f harvest rules for an EQ system ($p = 0.2$), and a one-box f harvest rule. 96

3.5 MSY RPs from alternative parametrizations ($p = 0.2$). The first row displays RP values for the base assumptions (s_6, $W_{0.1}$, $m_{constant}$, and $\mu_{8,10}$). A Lorenzen mortality rate is applied to both the source and sink, simultaneously. All other parameters changes are applied to the source and sink independently, and are tabulated based on which sub-population is re-parametrized. Values for B_{MSY}, B_0, B_{MSY}/B_0 and MSY are the sum of source and sink values. 97

List of Figures

1.1 Precautionary approach as described by DFO (2006). Higher harvest rates are acceptable for healthy stocks. When stocks are healthy, harvest rates are set at a limit harvest reference point to optimize sustainable catches. As stock status deteriorates beyond an upper reference point due to overharvesting, harvest rates are reduced to allow the stock to recover. Reference points indicate when a stock's status transitions from the 'Healthy Zone' to the 'Caution Zone', and from the 'Caution Zone' to the 'Critical Zone', as well as the level of fishing permitted by a fishery given the stock's status. Management strategies aim to maximize harvests without exceeding predetermined reference points to avoid overexploitation and stock depletion. Recovering stocks (i.e. stocks in the Caution or Critical Zones) require reduced harvest rates to avoid further deterioration of the stock's health, whereas Healthy stocks can be harvested at the limit harvest reference point. 15

1.2 Equilibrium yield, Y_{eq}, for varying fishing mortality rates, Fs. Equilibrium yield is maximized (i.e. MSY) for $F = F_{MSY}$. No fishing ($F = 0$) or too much fishing ($F = F_{toogreat}$) will result in an equilibrium yield of zero. 16

1.3 Surplus production model equilibrium harvest ($Y_{eq} = B_{eq}H$) depends on the harvest rate, H, growth rate, r, and carrying capacity, K. Changes in r results in changes in both MSY and H_{MSY} (top left); changes in K only results in changes in MSY (top right). Over time biomass, B_t, approaches an equilibrium value when harvest rates are constant (bottom). Dashed lines indicate the respective B_{eq} for biomass projections under fixed harvest rates (solid), and the dashed grey line indicates B_{MSY}. 17

2.1 Cohort model with abundance denoted as $N_{year,age}$. Abundances are dependent on initial cohort abundance, i.e. recruitment, and abundance-at-age for the first year (green). Annual cohort abundances are projected forward following arrows, such that $N_{y+1,a+1} = N_{y,a}e^{-Z_{y,a}}$ for all y and a. Total mortality decreases abundance of each cohort by year, and recruitment increases annual abundance each year by adding a new cohort. 44

2.2 Bubble plot of abundances for a 500 year illustrative forecast projection ($f = 0.05$) using the BH_{100} SR model. (Top) Bubbles represent positive (blue) and negative (black) deviation of the standardized proportion abundance-at-age, $p_{y,a} = N_{y,a}/\Sigma_a N_{y,a}$, from the standardized mean proportion abundance-at-age, $\bar{p}_y = \Sigma_y p_{y,a}/500$, with standard deviation $\sigma_a = \sqrt{Var(p_{y,a}|a)}$. That is, $size = |\frac{p_{y,a}-\bar{p}_y}{\sigma_a}|$. Bubbles appear as solid lines in places where they are constant over time, i.e. line thickness is *size*, and colour is the sign of the deviation. Over time, all abundances-at-age and total abundances stabilize. (Bottom) Abundance of recruits (left) and total annual abundance (right) over time from forecast projection for five different initial abundances, N_{y_0,a_0}: 5 (solid), 15 (dashed), 25 (dotted), 35 (long-dash), and 45 (dot-dash). 45

2.3 Abundances for a 500 year forecast projection ($f = 0.05$) using the RK_{100} SR model. Additional details are provided in caption for Figure 2.2. 46

2.4 Cohort model where abundances are denoted $N_{year,age}$. Cohort abundances are typically projected forward from previous cohort abundance, $N_{y-1,a-1}$. However, per-recruit functions assume a stable state has been reached, such that $N_{y-1,a} = N_{y,a} = N_{y+1,a}$ for all years. The abundance at each age for a cohort is the same as the abundance at each age in a year (blue circle). 47

2.5 Replacement lines for various f's with respect to the BH_{100} SR curve. The replacement lines intersect the SR curve at $R = R_{eq}(f)$ and $S = SSB_{eq}(f)$, for some f. As f increases, the slope of the replacement line, $1/SPR(f)$, increases, and R_{eq} and SSB_{eq} strictly decrease for a BH SR model. When the slope of the replacement line is equal to the slope at the origin (i.e. at $SSB_{eq}(f) = 0$), the stock is unsustainable and collapses. Any greater f also results in stock collapse. 48

2.6 Maturity ogives and corresponding equilibrium yield and SSB curves. Maturities are defined by the $\mu_{8,10}$ (black) and $\mu_{10,12}$ distributions. Equilibrium yields and SSBs are calculated using per-recruit and the BH_{100} SR function. Dotted lines indicate f_{MSY} for the respective equilibrium curves. 49

2.7 Natural mortality rate distributions and corresponding equilibrium yield and SSB curves. Natural mortality rates are described by the constant $m = 0.2$ (black) and the Lorenzen natural mortality rate (blue). Equilibrium yields and SSBs are calculated using per-recruit and the BH_{100} SR function. Dotted lines indicate f_{MSY} for the respective equilibrium curves. 50

2.8 Selectivity curves and corresponding equilibrium yield and SSB curves. Selectivities are knife-edged, and fish are fully selected for ages $a \geq a_r$, where $a_r = 6$ (black) and $a_r = 8$ (blue). Equilibrium yields and SSBs are calculated using per-recruit and the BH_{100} SR function. Dotted lines indicate f_{MSY} for the respective equilibrium curves. 51

2.9 Weight-at-age distributions and corresponding equilibrium yield and SSB curves. Weights are modelled using a growth rate of $k = 0.1$ (black), $k = 0.05$ (blue), and $k = 0.15$ (red). Beginning-of-year weights (solid) use ages $a \in [5, 20]$, and mid-year weights (dashed) use ages $a \in [5, 20] + 0.5$. Equilibrium yields and SSBs are calculated using per-recruit and the BH_{100} SR function. Dotted lines indicate f_{MSY} for the respective equilibrium curves. 52

2.10 Stock-Recruitment using the BH (left) and RK (right) SR relationship, and corresponding equilibrium yield and SSB curves. Included are the BH_{100} and RK_{100} models (black), and the BH_{300} and RK_{300} models (blue). Equilibrium yields are calculated using per-recruit functions and equilibrium SSBs are calculated using the appropriate SR relationships. Dotted lines indicate f_{MSY} for the respective equilibrium curves. 53

2.11 Stock-Recruitment using the BH (left) and RK (right) steepness re-parametrizations, and their respective equilibrium yield and SSB curves. Stock-recruitment is modelled using a steepness of $h = 0.69$ (blue), $h = 0.78$ (red), and $h = 0.86$ (green). The BH_{100} and RK_{100} models (black) are also displayed for comparison. Equilibrium yields are calculated using per-recruit functions, and equilibrium SSBs are calculated using the appropriate SR relationships. Dotted lines indicate f_{MSY} for the respective equilibrium curves. Inset plots display the approximate linear relationship between f_{MSY} and steepness for both the BH and RK SR models ($f \in [0.2, 0.6]$, $h \in [0.6, 0.9]$). . . . 54

2.12 Percent deviation of RP outputs for alternative parametrizations with respect to outputs for base parametrizations. Row values are calculated using the following SR models: 1. BH_{100}, 2. BH_{300}, 3. RK_{100}, 4. RK_{300}, 5. BH_{low}, 6. BH_{med}, 7. BH_{up}, 8. RK_{low}, 9. RK_{med}, 10. RK_{up}. Base RP outputs (i.e. 0%) are indicated by dashed line. 55

2.13 A knife-edged (solid), sigmoid (dashed), and dome-shaped (dotted) selectivity curve, with their corresponding equilibrium yield curves. 56

3.1 Two-box models for (a) a source-sink system and (b) an MPA system. In (a) advection is a unidirectional flow between regions and in (b) advection is a result of spillover from MPAs into the fished region. 98

3.2 Abundances by age and year from a spatially-explicit forecast projection for $p = 0.2$, where $f_1 = f_2 = 0.05$. Over time, abundances for both the source and sink stabilize. Refer to the caption for Figure 2.2. 99

3.3 Equilibrium values for an EQ system using the BH_{50} SR model. Shown are the equilibrium yield (blue), SSB (red), and recruitment (green) for the source and sink, and the total of both. Equilibrium recruitment is measured as the pre-advection recruitment (i.e. $R_{eq,2} = R(SSB_{eq,2})$). The value of p varies by row. 100

3.4 Equilibrium values for an EQ system using the RK_{50} SR model. Shown are the equilibrium yield (blue), SSB (red), and recruitment (green) for the source and sink, and the total of both. Equilibrium recruitment is measured as the pre-advection recruitment (i.e. $R_{eq,2} = R(SSB_{eq,2})$) The value of p varies by row. 101

3.5 Equilibrium values for an EQ system using the BH_h SR model. Shown are the equilibrium yield (blue), SSB (red), and recruitment (green) for the source and sink, and the total of both. Equilibrium recruitment is measured as the pre-advection recruitment (i.e. $R_{eq,2} = R(SSB_{eq,2})$) The value of p varies by row. 102

3.6 Equilibrium values for an EQ system using the RK_h SR model. Shown are the equilibrium yield (blue), SSB (red), and recruitment (green) for the source and sink, and the total of both. Equilibrium recruitment is measured as the pre-advection recruitment (i.e. $R_{eq,2} = R(SSB_{eq,2})$) The value of p varies by row. 103

3.7 The pre-advection (left) and post-advection (right) equilibrium recruitment for the source and sink from $SSB_{eq} = B_{MSY}$, i.e. $R(B_{MSY})$. 104

3.8 Equilibrium curves for the source (a & d) and sink (b & e), and the total yield (c & f). Equilibrium yields were calculated using the BH_{50} SR model for select p values, with a constant f_2 with a varying f_1 (a, b, & c), and a constant f_1 with a varying f_2 (d, e, & f). The dots (a) indicate when $f_1 = f_{crash,1}(p)$ (i.e. $Y_{eq,1}(f_{crash,1}(p)) = 0$) for the respective yield curves. The vertical lines indicate $f_{MSY,1}$ (a) and $f_{MSY,2}$ (e) for the respect yields curves. 105

3.9 Equilibrium curves for the source (a & d) and sink (b & e), and the total yield (c & f). Yields are calculated for a constant $f_2 = 0.05$ (a, b, & c) and select f_1 values, and for a constant $f_1 = 0.05$ (d, e, & f) and select f_2 values. Equilibrium yields were calculated using the BH_{50} SR model. The dots (a & b) indicate the p for which $f_1 = f_{crash,1}(p)$ for the respective yield curves. Equilibrium yield in the source does not change with f_2 (d), and so all curves overlap. The value for $f_{crash,1}(p)$ do not change with f_2 and occurs at the p where $f_{crash}(p) = 0.03$ (a). 106

3.10 Contour plots of the source, sink, and total equilibrium yield (blue), SSB (red), and local recruitment (green) for $f = f_1 = f_2$. Yields were calculated using the BH_{50} for an EQ system. . 107

3.11 Equilibrium yield contours for the source sub-population. Equilibrium yields (blue) are non-zero for any f_1 and p where $f_1 < f_{crash,1}(p)$. Values for $f_{crash,1}(p)$ (purple) decrease as p increases, and the source is sustainable as long $f_1 < f_{crash,1}(p)$. Once $f_{crash,1}(p) = 0$ at $p = p_{ex}$, the source is extirpated. 108

3.12 The optimal f_{MSY}'s at different p's, for a EQ system using the BH_{50} (top-left), RK_{50} (top-right), BH_h (bottom-left), and RK_h (bottom-right) SR models. The vertical lines indicate p_{f0} (grey) and p_{ex} (black). 109

3.13 Total B_{MSY}, B_0, and biomass depletion at different p's, for a EQ system using the BH_{50} SR model. The vertical lines indicate p_{f0} (grey) and p_{ex} (black). 110

3.14 f_{MSY} at different p's for an EQ system using the BH_{50} (top-left), RK_{50} (top-right), BH_h (bottom-left), and RK_h (bottom-right) SR models. The optimal f's (brown) are displayed separately as f_1 (dashed) and f_2 (solid) (Refer to Figure 3.12). The vertical lines indicate p_{f0} (grey) and p_{ex} (black). Once $p = p_{f0}$, the f_{MPA} curve overlaps with the optimal $f_{MSY,2}$ curve because $f_{MSY,1} = 0$ and $f_{MSY,2} = f_{MPA}$. 111

3.15 Total B_{MSY}, B_0, and biomass depletion at different p's, for an EQ system using the BH_{50} (row 1), RK_{50} (row 2), BH_h (row 3), and RK_h (row 4) SR models. The vertical lines indicate p_{f0} (grey) and p_{ex} (black). Also see Figure 3.13. 112

3.16 Efficiency of sub-optimal harvest strategies at different p's for an EQ system, using the BH_{50} (top-left), RK_{50} (top-right), BH_h (bottom-left), and RK_h (bottom-right) SR models. The vertical lines indicate p_{f0} (grey) and p_{ex} (black). 113

3.17 f_{MSY} at different p's for a HL system using the BH_{50} (top-left), RK_{50} (top-right), BH_h (bottom-left), and RK_h (bottom-right) SR models. The vertical lines indicate p_{f0} (grey) and p_{ex} (black). 114

3.18 Total B_{MSY}, B_0, and biomass depletion at different ps, for a HL system using the BH_{50} (row 1), RK_{50} (row 2), BH_h (row 3), and RK_h (row 4) SR models. The vertical lines indicate p_{f0} (grey) and p_{ex} (black). 115

3.19 Total MSY from the optimal harvest strategy (i.e. $f_1 = f_{MSY,1}$ and $f_2 = f_{MSY,2}$) using the BH_{50} (top-left), RK_{50} (top-right), BH_h (bottom-left), and RK_h (bottom-right) SR models. . . . 116

3.20 Efficiency of sub-optimal harvest strategies at different ps for a HL system, using the BH_{50} (top-left), RK_{50} (top-right), BH_h (bottom-left), and RK_h (bottom-right) SR models. The vertical lines indicate p_{f0} (grey) and p_{ex} (black). 117

3.21 f_{MSY} at different p's, for a DA system using the BH_{50} (top-left), RK_{50} (top-right), BH_h (bottom-left), and RK_h (bottom-right) SR models. The vertical lines indicate p_{f0} (grey) and p_{ex} (black). 118

3.22 Total B_{MSY}, B_0, and biomass depletion at different p's, for a DA system using the BH_{50} (row 1), RK_{50} (row 2), BH_h (row 3), and RK_h (row 4) SR models. The vertical lines indicate p_{f0} (grey) and p_{ex} (black). 119

3.23 Efficiency of sub-optimal harvest strategies at different ps for a DA system, using the BH_{50} (top-left), RK_{50} (top-right), BH_h (bottom-left), and RK_h (bottom-right) SR models. The vertical lines indicate p_{f0} (grey) and p_{ex} (black). 120

3.24 f_{MSY} at different p's, for a HL & DA system using the BH_{50} (top-left), RK_{50} (top-right), BH_h (bottom-left), and RK_h (bottom-right) SR models. The vertical lines indicate p_{f0} (grey) and p_{ex} (black). 121

3.25 Total B_{MSY}, B_0, and biomass depletion at different ps, for a HL & NS system using the BH_{50} (row 1), RK_{50} (row 2), BH_h (row 3), and RK_h (row 4) SR models. The vertical lines indicate p_{f0} (grey) and p_{ex} (black). 122

3.26 Efficiency of sub-optimal harvest strategies at different p's for a HL and DA system, using the BH_{50} (top-left), RK_{50} (top-right), BH_h (bottom-left), and RK_h (bottom-right) SR models. The vertical lines indicate p_{f0} (grey) and p_{ex} (black). . . . 123

4.1 Three-box metapopulation structures with unidirectional transfer, where sub-populations P_1, P_2, and P_3 are connected through a (a) chain, (b) converging, (c) branching, (d) detouring, and (e) cyclical advection pattern. 141

4.2 Values for f_{MSY} for a three-box model with a chain advection connectivity pattern. Values are calculated for each sub-population according to Figure 4.1a. Changes in transfer proportions are mutually exclusive, where only one transfer proportion changes at a time (indicated by row). All non-changing transfer proportions a fixed at a constant $p = 0.1$. 142

4.3 Values for B_{MSY} for a three-box model with a chain advection connectivity pattern. Values are calculated for each sub-population according to Figure 4.1a. Total B_{MSY} is the sum of all B_{MSY} values for each sub-population. Changes in transfer proportions are mutually exclusive, where only one transfer proportion changes at a time (indicated by row). All non-changing transfer proportions a fixed at a constant $p = 0.1$. . . 143

4.4 Biomass depletion for a three-box model with a chain advection connectivity pattern. Values are calculated for each sub-population according to Figure 4.1a. Biomass depletion is the ratio of B_{MSY} to unfished biomass for each sub-population, and total biomass depletion is the ratio of the sum of all B_{MSY} values to the sum of all unfished biomasses. Changes in transfer proportions are mutually exclusive, where only one transfer proportion changes at a time (indicated by row). All non-changing transfer proportions a fixed at a constant $p = 0.1$. 144

4.5 MSY for a three-box model with a chain advection connectivity pattern. Values for MSY are calculated for each sub-population according to Figure 4.1a. Total MSY is the sum of optimized yields for all sub-populations. Changes in transfer proportions are mutually exclusive, where only one transfer proportion changes at a time (indicated by row). All non-changing transfer proportions a fixed at a constant $p = 0.1$. . . 145

4.6 Values for f_{MSY} for three-box model with a converging advection connectivity pattern. Values are calculated for each sub-population according to Figure 4.1b. Changes in transfer proportions are mutually exclusive, where only one transfer proportion changes at a time (indicated by row). All non-changing transfer proportions a fixed at a constant $p = 0.1$. . . 146

4.7 Values for B_{MSY} for three-box model with a converging advection connectivity pattern. Values are calculated for each sub-population according to Figure 4.1b. Total B_{MSY} is the sum of all B_{MSY} values for each sub-population. Changes in transfer proportions are mutually exclusive, where only one transfer proportion changes at a time (indicated by row). All non-changing transfer proportions a fixed at a constant $p = 0.1$. 147

4.8 Biomass depletion for a three-box model with a converging advection connectivity pattern. Values are calculated for each sub-population according to Figure 4.1b. Biomass depletion is the ratio of B_{MSY} to unfished biomass for each sub-population, and total biomass depletion is the ratio of the sum of all B_{MSY} values to the sum of all unfished biomasses. Changes in transfer proportions are mutually exclusive, where only one transfer proportion changes at a time (indicated by row). All non-changing transfer proportions a fixed at a constant $p = 0.1$. . . 148

4.9 MSY for a three-box model with a converging advection connectivity pattern. Values for MSY are calculated for each sub-population according to Figure 4.1b. Total MSY is the sum of optimized yields for all sub-populations. Changes in transfer proportions are mutually exclusive, where only one transfer proportion changes at a time (indicated by row). All non-changing transfer proportions a fixed at a constant $p = 0.1$. 149

4.10 Values for f_{MSY} for three-box model with a branching advection connectivity pattern. Values are calculated for each sub-population according to Figure 4.1c. Changes in transfer proportions are mutually exclusive, where only one transfer proportion changes at a time (indicated by row). All non-changing transfer proportions a fixed at a constant $p = 0.1$. . . . 150

4.11 Values for B_{MSY} for three-box model with a branching advection connectivity pattern. Values are calculated for each sub-population according to Figure 4.1c. Total B_{MSY} is the sum of all B_{MSY} values for each sub-population. Changes in transfer proportions are mutually exclusive, where only one transfer proportion changes at a time (indicated by row). All non-changing transfer proportions a fixed at a constant $p = 0.1$. 151

4.12 Biomass depletion for a three-box model with a branching advection connectivity pattern. Values are calculated for each sub-population according to Figure 4.1c. Biomass depletion is the ratio of B_{MSY} to unfished biomass for each sub-population, and total biomass depletion is the ratio of the sum of all B_{MSY} values to the sum of all unfished biomasses. Changes in transfer proportions are mutually exclusive, where only one transfer proportion changes at a time (indicated by row). All non-changing transfer proportions a fixed at a constant $p = 0.1$. . . 152

4.13 MSY for a three-box model with a branching advection connectivity pattern. Values for MSY are calculated for each sub-population according to Figure 4.1c. Total MSY is the sum of optimized yields for all sub-populations. Changes in transfer proportions are mutually exclusive, where only one transfer proportion changes at a time (indicated by row). All non-changing transfer proportions a fixed at a constant $p = 0.1$. 153

4.14 Values for f_{MSY} for a three-box model with a detouring advection connectivity pattern. Values are calculated for each sub-population according to Figure 4.1d. Changes in transfer proportions are mutually exclusive, where only one transfer proportion changes at a time (indicated by row). All non-changing transfer proportions a fixed at a constant $p = 0.1$. . . 154

4.15 Values for B_{MSY} for a three-box model with a detouring advection connectivity pattern. Values are calculated for each sub-population according to Figure 4.1d. Total B_{MSY} is the sum of all B_{MSY} values for each sub-population. Changes in transfer proportions are mutually exclusive, where only one transfer proportion changes at a time (indicated by row). All non-changing transfer proportions a fixed at a constant $p = 0.1$. 155

4.16 Biomass depletion for a three-box model with a detouring advection connectivity pattern. Values are calculated for each sub-population according to Figure 4.1d. Biomass depletion is the ratio of B_{MSY} to unfished biomass for each sub-population, and total biomass depletion is the ratio of the sum of all B_{MSY} values to the sum of all unfished biomasses. Changes in transfer proportions are mutually exclusive, where only one transfer proportion changes at a time (indicated by row). All non-changing transfer proportions a fixed at a constant $p = 0.1$. . . . 156

4.17 MSY for a three-box model with a detouring advection connectivity pattern. Values for MSY are calculated for each sub-population according to Figure 4.1d. Total MSY is the sum of optimized yields for all sub-populations. Changes in transfer proportions are mutually exclusive, where only one transfer proportion changes at a time (indicated by row). All non-changing transfer proportions a fixed at a constant $p = 0.1$. 157

4.18 Values for f_{MSY} for a three-box model with a cyclical advection connectivity pattern. Values are calculated for each sub-population according to Figure 4.1e. Changes in transfer proportions are mutually exclusive, where only one transfer proportion changes at a time (indicated by row). All non-changing transfer proportions a fixed at a constant $p = 0.1$. . . 158

4.19 Values for B_{MSY} for a three-box model with a cyclical advection connectivity pattern. Values are calculated for each sub-population according to Figure 4.1e. Total B_{MSY} is the sum of all B_{MSY} values for each sub-population. Changes in transfer proportions are mutually exclusive, where only one transfer proportion changes at a time (indicated by row). All non-changing transfer proportions a fixed at a constant $p = 0.1$. 159

4.20 Biomass depletion for a three-box model with a cyclical advection connectivity pattern. Values are calculated for each sub-population according to Figure 4.1e. Biomass depletion is the ratio of B_{MSY} to unfished biomass for each sub-population, and total biomass depletion is the ratio of the sum of all B_{MSY} values to the sum of all unfished biomasses. Changes in transfer proportions are mutually exclusive, where only one transfer proportion changes at a time (indicated by row). All non-changing transfer proportions a fixed at a constant $p = 0.1$. . . 160

4.21 MSY for a three-box model with a cyclical advection connectivity pattern. Values for MSY are calculated for each sub-population according to Figure 4.1e. Total MSY is the sum of optimized yields for all sub-populations. Changes in transfer proportions are mutually exclusive, where only one transfer proportion was change at a time (indicated by row). All non-changing transfer proportions a fixed at a constant $p = 0.1$. . . 161

5.1 A six-box metapopulation model with several advection connectivity patterns between sub-populations. 169

B.1 Contour plots of the source, sink, and total equilibrium yield (blue), SSB (red), and local recruitment (green) for $f = f_1 = f_2$. Yields were calculated using the RK_{50} under an EQ system. 189

B.2 Contour plots of the source, sink, and total equilibrium yield (blue), SSB (red), and local recruitment (green) for $f = f_1 = f_2$. Yields were calculated using the BH_h under an EQ system. 190

B.3 Contour plots of the source, sink, and total equilibrium yield (blue), SSB (red), and local recruitment (green) for $f = f_1 = f_2$. Yields were calculated using the RK_h under an EQ system. 191

B.4 Equilibrium values for a HL system using the BH_{50} SR model. Shown are the equilibrium yield (blue), SSB (red), and recruitment (green) for the source and sink, and the total of both. The value of p varies by row. 192

B.5 Equilibrium values for a HL system using the RK_{50} SR model. Shown are the equilibrium yield (blue), SSB (red), and recruitment (green) for the source and sink, and the total of both. The value of p varies by row. 193

B.6 Equilibrium values for a HL system using the BH_h SR model. Shown are the equilibrium yield (blue), SSB (red), and recruitment (green) for the source and sink, and the total of both. The value of p varies by row. 194

B.7 Equilibrium values for a HL system using the RK_h SR model. Shown are the equilibrium yield (blue), SSB (red), and recruitment (green) for the source and sink, and the total of both. The value of p varies by row. 195

B.8 Equilibrium values for a DA system using the BH_{50} SR model. Shown are the equilibrium yield (blue), SSB (red), and recruitment (green) for the source and sink, and the total of both. The value of p varies by row. 196

B.9 Equilibrium values for a DA system using the RK_{50} SR model. Shown are the equilibrium yield (blue), SSB (red), and recruitment (green) for the source and sink, and the total of both. The value of p varies by row. 197

B.10 Equilibrium values for a DA system using the BH_h SR model. Shown are the equilibrium yield (blue), SSB (red), and recruitment (green) for the source and sink, and the total of both. The value of p varies by row. 198

B.11 Equilibrium values for a DA system using the RK_h SR model. Shown are the equilibrium yield (blue), SSB (red), and recruitment (green) for the source and sink, and the total of both. The value of p varies by row. 199
B.12 Equilibrium values for a HL & DA system using the BH_{50} SR model. Shown are the equilibrium yield (blue), SSB (red), and recruitment (green) for the source and sink, and the total of both. The value of p varies by row. 200
B.13 Equilibrium values for a HL & DA system using the RK_{50} SR model. Shown are the equilibrium yield (blue), SSB (red), and recruitment (green) for the source and sink, and the total of both. The value of p varies by row. 201
B.14 Equilibrium values for a HL & DA system using the BH_h SR model. Shown are the equilibrium yield (blue), SSB (red), and recruitment (green) for the source and sink, and the total of both. The value of p varies by row. 202
B.15 Equilibrium values for a HL & DA system using the RK_h SR model. Shown are the equilibrium yield (blue), SSB (red), and recruitment (green) for the source and sink, and the total of both. The value of p varies by row. 203

List of Abbreviations

BH	Beverton-Holt
DA	Downstream Advection
DFO	Fisheries and Oceans Canada
EQ	Equivalent
HL	High-to-Low
MCDM	Multi-criteria Decision Making
MPA	Marine Protected Area
MSE	Management Strategy Evaluation
MSY	Maximum Sustainable Yield
PLD	Pelagic Larval Dispersal
RK	Ricker
RP	Reference Point
SaO	Slope at the Origin
SPM	Surplus Production Model

SPR	Spawner-per-Recruit
SR	Stock-Recruit
SSB	Spawning-Stock Biomass
YPR	Yield-per-Recruit

Chapter 1

Introduction

1.1 Fisheries Management and Management Reference Points

One of the critical concerns of fisheries scientists is the sustainability of commercial fisheries. Generally, this refers to the long-term maintenance of both the industry and the stock being fished, while optimizing returns in revenue or yields (i.e. annual catch biomass). To do this, the fisheries are regulated through management practices that promote sustainability. What is 'sustainable' is typically defined by management reference points (RPs), and a fundamental objective for fisheries scientists is to estimate these RPs, which are then used by managers to limit catches of commercial fisheries. As a result, RPs are widely considered an essential part of well-managed fisheries (Hilborn and Stokes, 2010; Hutchings and Rangeley, 2011).

A variety of RPs are available to fisheries managers to control harvesting,

and management strategies may use different RPs depending on the goals of the fishery. Fisheries and Oceans Canada (DFO), for example, use RPs based on a precautionary approach (DFO, 2006), which uses risk management protocols to maintain stock status at healthy levels (Figure 1.1). Other fisheries management organizations use similar precautionary approach frameworks with RPs for stock harvest (e.g., ICES, 2018; NAFO, 2004).

RPs are used to inform fisheries managers on how to adjust harvest rates to maintain a sustainable and healthy stock status. To define RPs, researchers rely on statistical, algorithmic population models, commonly referred to as stock assessment models, to quantify fish stocks (e.g., Beverton and Holt, 1957; Quinn and Deriso, 1999; Haddon, 2010).

Stock assessment models are typically used to gauge or assess the status of a fish stock, but they are also used to derive management RPs. To do this, these models require measures of fish abundance, as well as stock-specific traits like growth and maturation rates, which are often referred to as *life history characteristics*. It is vital to have accurate estimates of these life history characteristics to effectively manage a fish stock. These characteristics, however, can vary substantially over time and space, and management RPs may not be conducive to a sustainable fishery if life history characteristics, along with stock abundances, are not properly measured.

The most apt models for deriving management RPs are equilibrium models, which calculate stead-state yields for fixed harvest strategies, and are most commonly used to calculate the *Maximum Sustainable Yield* (MSY), which is considered an essential element of modern fisheries management (e.g., Worm et al., 2009; ICES, 2016; EC, 2010). In theory, MSY is the

maximum amount of stock that may be sustainably harvested annually, and indefinitely (see Beverton and Holt, 1957); that is, the maximum yield that is sustainable. Yield is the total catch biomass obtained from a predetermined level of fishing. This level of fishing, known as the *fishing mortality rate*, F, is related to the proportion of stock fished (see Chapter 2). Many management strategies are based on a long-term, average yield, referred to as equilibrium yield, Y_{eq}, that is obtained from fishing at a constant level, F, each year, i.e. $Y_{eq}(F)$. Annual yields may change between years from fluctuations in annual stock abundance, even under constant Fs, but average yields are expected to stabilize over long periods of time. Equilibrium yield $Y_{eq}(F)$ is a quasi-concave function (see Figure 1.2), meaning the function has a single maximum within a particular domain, $F \in [0, \infty)$, and at least one minimum at one of the endpoints (i.e. $Y_{eq} = 0$). Obviously, equilibrium yield where there is no fishing $Y_{eq}(0) = 0$. However, equilibrium yield where F is too great, $Y_{eq}(F_{toogreat}) = 0$, because the population is extirpated in the long-term. There is, therefore, some F, denoted F_{MSY}, that maximizes the equilibrium yield. The maximum potential yield that can be harvested without compromising the stock's status is defined as $MSY = Y_{eq}(F_{MSY})$ (e.g. Figure 1.2). Most management practices tend to focus on using RPs like F_{MSY} rather than MSY to define appropriate harvest levels, so we will focus primarily on determining MSY-based RPs like F_{MSY}.

A simple stock assessment model that may be used to derive MSY RPs is the Schaefer *surplus production model* (SPM; e.g., MacCall, 1990; Quinn and Deriso, 1999; Hilborn and Walters, 2013). SPMs are the simplest model used to derive MSY RPS. We present an SPM to introduce the general methods

used to derive these RPs, and discuss some issues with using these models to derive RPs.

1.2 Surplus Production Model

MSY is the maximum, average, long-term yield, and is a result of management strategies that set $F = F_{MSY}$. F_{MSY} is typically used in age-structured models, which we discuss in Chapter 2. Alternatively, it is common for equilibrium yields to be expressed in terms of the *harvest rate*, H. The harvest rate represents the proportion of stock biomass that is fished (i.e. harvested) annually. For example, a harvest rate of $H = 0.2$ indicates 20% of stock biomass is fished each year. A harvest rate of H_{MSY} is the proportion of stock biomass that can be fished annually, indefinitely, to maximize long-term yields. In some cases, MSY RPs can be calculated using H instead of F, for example in SPMs.

SPMs aggregate total stock abundance or biomass by year, and are often described by the time-discrete expression

$$B_{t+1} = B_t + rB_t\left(1 - \frac{B_t}{K}\right) - HB_t, \tag{1.1}$$

where B denotes the biomass, K is the carrying capacity, r is the growth rate, and t indicates the year.. From some initial biomass, subsequent biomasses are sequentially calculated.

SPMs are density dependent functions, meaning annual stock growth is affected by current stock biomass, and stock biomass has an *equilibrium*, B_{eq},

where total biomass will approach B_{eq} over time under constant harvest rates. When used for stock assessments, SPMs fit biomass data to estimate trends in biomass, but when deriving management RPs biomass values are projected forward until biomass reaches equilibrium. Equilibrium solutions to SPMs can be derived one of two ways: by forecasting biomass values forward in time using Equation 1.1 until values are stable, or deriving them through analytic equations. Forecasting biomass values requires initial values of biomass to begin the projection, and must be projected long enough for biomass to reach equilibrium. This forecast method is detailed more in Chapter 2

Deriving B_{eq} analytically is more efficient, and does not require starting values like the forecast method. Equilibrium biomass is defined as $B_{eq} = B_{t+1} = B_t$. In the absence of harvesting ($H = 0$), the equilibrium biomass is K. When the stock is harvested ($H > 0$), the equilibrium biomass depends on H (Figure 1.3). It can be shown that equilibrium biomass occurs when $r(1 - \frac{B_{eq}}{K}) - H = 0$, that is $B_{eq} = K(1 - \frac{H}{r})$ where $H \leq r$. It can also be shown that the optimal harvest rate (the harvest rate that achieves MSY) is $H_{MSY} = r/2$ and the optimal equilibrium biomass is $B_{MSY} = K/2$, where the optimal equilibrium yield is $MSY = B_{MSY}H_{MSY} = rK/4$.

SPMs are simple in structure and only rely on biomass data to estimate stock productivity parameters and calculate MSY RPs. However, SPMs may not provide reliable RPs for sustainable fisheries management. For example, Zhang (2013) calculated MSYs using an SPM and compared them to a "true" value for MSY (calculated using an age-structured model) and found that, in the presence of observation and process error, SPMs tended to overestimate MSY. Biased estimates for RPs may also be introduced by the error

associated with estimations of K and r.

Furthermore, SPMs conceal important information about the stock's age-structure. SPMs are a data-limited assessment method and they do not account for age-varying attributes such as maturation and growth rates, in such a way that stocks comprised primarily of older, slow-growing fish will have lower annual increases in biomass compared to stocks consisting of mostly younger fish. In spatially heterogeneous frameworks, it is common for different age-classes to occupy different habitats, for example juveniles and recruits may aggregate in nursery areas along coastlines (e.g., Walsh et al., 2004), or movement patterns may depend on age, as detailed in later this thesis. Age-aggregated SPMs cannot account for these age-segregated distributions, and in such cases age-structured models are ideal. We detail the methods for deriving MSY RPs using an age-structured model in Chapter 1.

1.3 Practical Issues with Contemporary Models

Recent studies indicate that global abundances of fish stocks are declining (Berkes et al., 2006; FAO, 2018; Worm et al., 2009). According to FAO (2018), 33.1% of fished stocks in 2015 were considered to be at a biologically unsustainable level; that is to say, they are 'overfished' (outside 'Healthy Zone'; see Figure 1.1). This is a 23.1% increase of overfished stocks since 1974. In Canada alone, 13.4% of stock are overfished, 11% of which have

management plans in place to help their recovery, yet only a small fraction of these plans have achieved their goals, and only 34% of fish Canadian fish stocks are known to be healthy (Oceana, 2018).

It is debated whether or not the prevalence of overfishing is attributed to the inability of contemporary management practices to produce sustainable outcomes as predicted by stock assessments (Larkin, 1977; Botsford et al., 1997; Hilborn and Ovando, 2014). For instance, Hilborn and Stokes (2010) propose that this prevalence may be a result of fisheries managers' definition of 'overfished', which sets biomass limits too high relative to true sustainable levels. The use of pre-determined harvest strategies based on reliable RPs is considered the best practice for recovering depleted and maintaining healthy stocks (Murawski, 2010), yet, this practice has had its share of failures. For example, since the adoption of MSY-based management procedures, North West Atlantic cod stocks have had little to no recovery in terms of biomass and provide consistently low landings (Shelton and Morgan, 2014). This may suggest that contemporary stock models are faulty and may provide unreliable indicators for sustainable fisheries management, for instance by not accounting for ecological process, as Shelton and Morgan (2014) point out.

To gain insight into the causes for declining fish stocks, fisheries scientists must consider alternative methods to model fish population dynamics. It is important to develop models which are cognizant of the stock's environment, unique species characteristics, and inter- and intra-specific interactions to understand how fish stocks vary through time and space, and how human intervention (e.g. fishing) may affect these changes. There is often trouble

deciding on an appropriate model structure, since both model under- and over-specification can lead to less accurate results (e.g., Goethel and Berger, 2017), and sensitivity analyses are sometimes recommended to decide the most appropriate formulation (Punt et al., 2015).

1.4 Spatial Models

Among other innovations, some research has adapted population dynamics models to include spatial variation in life history characteristics, as well as explicit spatial movement within or between populations. Models which incorporate these types of spatial structures are sometimes referred to as *spatially heterogeneous* models. Studies that have incorporated spatial heterogeneity into stock models have, for example, used telemetric tagging data to monitor individual fish movements over time (e.g., Goethel et al., 2014), or integrated oceanographic processes, like currents, that may effect fish distributions (e.g., Munroe et al., 2012; Pineda et al., 2007). These studies have provided vital information on species- and stock-specific dynamics, and Fogarty and Botsford (2007) gave an overview of recent developments in population connectivity models and spatial stock management. Cadrin and Secor (2009) conducted an extensive literature review on how spatial population structure has been accounted for in stock assessment and concluded, with some exceptions, that spatial aspects of demographic structure have been relatively ignored compared to other aspects like size, sex, maturity, etc. However, problems of exploiting sympatric populations, preventing local depletions, conserving essential fish habitats, and the designation of

marine-protected areas require the incorporation of spatial structure in stock assessments. Goethel et al. (2011) provided additional review of movement modelling in marine fish population dynamics.

Ignoring spatial structure or misdiagnosing appropriate connectivity dynamics in population models can provide inaccurate management goals which may lead to overharvesting. Goethel and Berger (2017) conducted a simulation for a metapopulation that considered different population connectivity structures, among other scenarios, to quantify the implications of structural misdiagnosis, and emphasized that population structure strongly influences outcomes and should be regularly integrated into population dynamics models when deriving management RPs.

Contemporary management practices involve determining F_{MSY} for a closed system. Population dynamics models typically assume that emigration and immigration between local populations are negligible, and only birth and death rates affect changes in local abundances (Gaines and Lafferty, 1995; Punt et al., 2015). In fact, the traditional concept of a fish 'stock' follows this definition (e.g., Quinn and Deriso, 1999). Stock models also typically assume that, within a population, fish are sympatric (i.e. randomly distributed in space) and have a panmictic nature (i.e. randomly mate). These assumptions, however, do not hold true most of the time. For example, fish may aggregate where food is abundant, and some species like Atlantic salmon are philopatric, meaning they return to their birth location to reproduce. In practice, it may be too simplistic to describe the complexities of stock dynamics under uniform conditions, and many studies suggests that models used to derive RPs should consider more realistic and accurate assumptions

about stock dynamics, either regarding ecological conditions, stock-specific characteristics, or both (Lipcius et al., 2008; Luzeńczyk, 2017). In this thesis, we consider how the inclusion of a spatial structure into stock models may affect management RPs, how spatially-varying life history characteristics may affect these RPs, and how these RP values differ from standard non-spatial model results.

Some studies have extended SPMs to include spatial heterogeneity and calculate spatial harvest goals, but there are issues in doing this, as well. Carruthers et al. (2011) ran simulations of a spatially explicit SPM for a variety of motile Atlantic species and concluded that these spatial models tend to provide precautionary management goals because they underestimate stock sizes and MSY. This can be beneficial for management strategies aimed at stock recovery, but spatially explicit SPMs can provide widely varying MSY estimates depending on the degree of mixing between local populations, the size and scale of the managed region, and the management regime used to determine MSY (Takashina and Mougi, 2015). In some cases, SPMs may be useful for precautionary approaches to fisheries management, but it is recommended (Zhang, 2013) that age-structured models be used when possible.

Additionally, Bosley et al. (2019) recently investigated optimal harvest rates (i.e. H_{MSY}) for homogeneous, heterogeneous and metapopulation stocks. They note that ignoring age-structure may not be appropriate for complex age-based movement patterns. Moreover, ignoring connectivity patterns could result in substantial overfishing and local population depletion, which could affect overall stock resiliency.

The integration of spatial heterogeneity into population dynamics models

has become more common in recent literature, but despite the increasing use of spatially structured models to describe population dynamics, little research has been published on providing spatial harvest advice and defining spatially-explicit RPs using an age-structured population model. Exceptions include Hintzen et al. (2015), who studied herring west of the British Isle, explicitly modelling mixing between local populations, and concluded that ignoring mixing effects can bias abundance estimates and provide inaccurate RPs. Ralston and O'Farrell (2008) investigated the effects various larval transport pathways had on spatially allocated harvests rates and MSY. They noted, among other things, that certain larval pathways allowed for higher total yields than that for a well-mixed population, provided F was large enough. Aside from the studies mentioned above, however, few others have considered management strategies that maximize spatially-allocated harvest, that is deriving MSY RPs, for an age-structured population.

Management RPs that take into account the movement of various age-groups are much more reliable indicators for sustainable harvests. Thus, it may be useful to develop a framework for a spatially explicit, age-based population that may be integrated into future stock assessment models to derive such RPs.

1.5 Source-Sink Metapopulations

Two commonly used spatial population dynamics models are the reaction-diffusion model and the metapopulation model (see Tyler and Rose, 1994). Reaction-diffusion models are useful for mapping continuous fish movements

and typically model random movements of individual fish. However, a weakness of reaction-diffusion models is that they are unable of addressing environmental heterogeneity in populations, i.e. diffusion coefficients are usually constant and spatially invariant.

Metapopulation models, on the other hand, are predicated on spatial aggregations of fish called 'sub-populations', which are typically grouped based on spatial boundaries or genetic structure. Metapopulation models are useful when assessing fish stocks of highly-motile species (e.g. Pacific tuna), for species that rely on the mobility of early-life stages for habitat selection (for example, when mature fish are sedentary), and where local hydrographic processes like currents and gyres influence fish distributions. More relevantly, metapopulation models are useful for assessing the distribution of resources, e.g. for exploitation by fisheries; further, metapopulations model long-term dynamics, upon which equilibrium yields are predicated. Therefore, in this thesis, we find it appropriate to develop a spatial equilibrium yield model using a metapopulation structure to derive area-specific MSY RPs.

Furthermore, we assume our metapopulation has a *source-sink* layout. It is well understood that a variety of species and fish stocks exhibit a source-sink dynamics structure (Kritzer and Sale, 2010). Source-sink populations are spatially segregated sub-populations which assume a highly productive source sub-population supplies the less productive sink sub-population with recruits to sustain the metapopulation. Models for such populations explicitly differentiate between source and sink fish, and often assume interconnectivity occurs via *larval advection*. Larval advection describes the movement of young fish (usually larvae, but we assume it refers to any fish pre-recruitment)

to more suitable locations for growth, like nurseries (Walsh et al., 2004).

Some literature relays the efficacy of using larval advection dynamics to model fish population connectivity. For example, Smedbol and Wroblewski (2002) analysed the spatial structure of the Northern Atlantic cod stocks using concepts of metapopulation theory, and proposed that using a spatially explicit metapopulation model with larval retention dynamics may aid in the recovery of those Northern cod stocks. Cowen and Sponaugle (2009) provided an overview of the ecological significance of larval advection for population persistence, and commented that population persistence, over long time scales, is fundamentally linked to rates of larval delivery and recruitment among populations. Larval advection is an essential mechanism for sustainability and population interconnectivity for many species, and should be frequently included in stock models that suggest any degree of stock mixing, especially at younger ages.

Often, larval advection is assumed to occur due to currents, since larvae are capable of adjusting their depth in the water column to take advantage of such waterways (e.g., Hart, 2003) to locate suitable habitats. Our model assumes fish are approximately sedentary over large scales, and therefore their only movement occurs at young ages via this larval advection process. Using this larval advection, metapopulation model, MSY RPs will be calculated to observe how different amounts of transferring larvae (henceforth pre-recruits) affect population sustainability and total fishery yields.

The objective of this thesis is to develop a heuristic age-structured model that can be used to calculate spatially-explicit MSY RPs for a metapopulation, and compare these values to spatially-implicit MSY RPs for a sym-

patric, panmictic population. In Chapter 2, we detail the established framework used to calculate RPs for a single, sympatric population through an age-structured model, and discuss how uncertainties can affect RP values. Although our models are deterministic, we discuss uncertainties to tie into the idea of structural uncertainties, and from it create motivation to develop new models to reduce potential errors in RP estimates. In Chapter 3, the one-box framework is modified to model two separate but connected populations of fish. Doing so allows fish to have varying characteristics depending on their resident location, and movement of fish between regions can be explicitly modelled. RPs are also calculated under various model parametrizations to demonstrate the robustness of these estimates. Finally, in chapter 4 we explicitly model three separate but connected populations to derive MSY RPs, and in chapter 5 we present a theoretical framework to calculate RPs for an n-dimensional metapopulation structure.

1.6 Figures

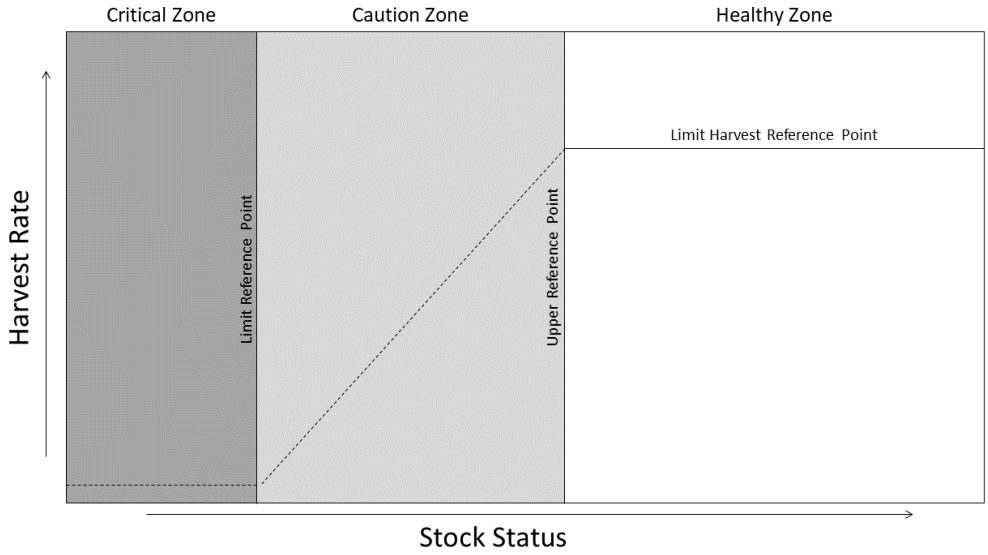

Figure 1.1: Precautionary approach as described by DFO (2006). Higher harvest rates are acceptable for healthy stocks. When stocks are healthy, harvest rates are set at a limit harvest reference point to optimize sustainable catches. As stock status deteriorates beyond an upper reference point due to overharvesting, harvest rates are reduced to allow the stock to recover. Reference points indicate when a stock's status transitions from the 'Healthy Zone' to the 'Caution Zone', and from the 'Caution Zone' to the 'Critical Zone', as well as the level of fishing permitted by a fishery given the stock's status. Management strategies aim to maximize harvests without exceeding predetermined reference points to avoid overexploitation and stock depletion. Recovering stocks (i.e. stocks in the Caution or Critical Zones) require reduced harvest rates to avoid further deterioration of the stock's health, whereas Healthy stocks can be harvested at the limit harvest reference point.

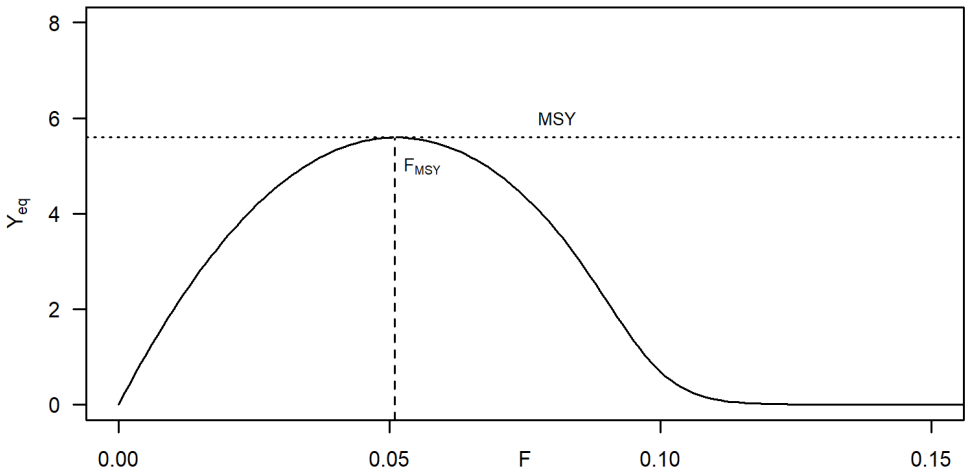

Figure 1.2: Equilibrium yield, Y_{eq}, for varying fishing mortality rates, Fs. Equilibrium yield is maximized (i.e. MSY) for $F = F_{MSY}$. No fishing ($F = 0$) or too much fishing ($F = F_{toogreat}$) will result in an equilibrium yield of zero.

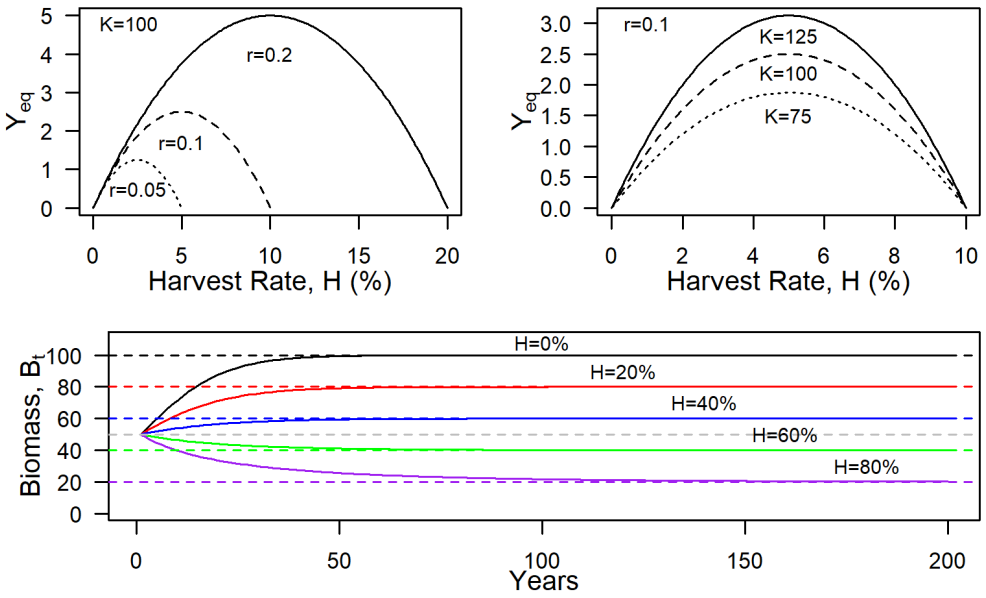

Figure 1.3: Surplus production model equilibrium harvest ($Y_{eq} = B_{eq}H$) depends on the harvest rate, H, growth rate, r, and carrying capacity, K. Changes in r results in changes in both MSY and H_{MSY} (top left); changes in K only results in changes in MSY (top right). Over time biomass, B_t, approaches an equilibrium value when harvest rates are constant (bottom). Dashed lines indicate the respective B_{eq} for biomass projections under fixed harvest rates (solid), and the dashed grey line indicates B_{MSY}.

Chapter 2

MSY RPs for an Age-Structured Model

2.1 Cohort Model

Age-structured models are commonly applied to describe the population dynamics of fish stocks that support important commercial fisheries. Age-structured models are responsive to changes in age-class composition of a population, and can account for age-dependent traits like maturation and growth rates. However, they require more data regarding the age distribution of the population. Rings on the fish ear-bones (i.e. otoliths), or scales, are used to measure age, which are then associated with fish size (i.e. length). These markers are time-consuming and difficult to measure, but when such age-length information is available, a more comprehensive understanding of a stock's age-composition is provided.

Age-structured models allow for the tracking of *cohorts*, that is, fish which

are born or recruited in the same year. Recruits are fish of the age at which they become liable to 'encounters' with the fishing or survey gears (Beverton and Holt, 1957); that is, fish at the youngest age caught by the gear. Each year, new recruits add to total stock abundance, and mortalities decrease total stock abundance. Mortalities consist of both fishing and natural deaths, and are often age- and year-dependent. Without an explicit age structure, net abundance (or biomass) increase would be condensed into a general growth rate term, e.g. r in Equation 1.1. Age-structured models expand the stock into individual age-class components, and separate cohorts can be modelled through an algorithmic cohort model. Age structured models allow for a decomposition of the growth rate term into reproduction and mortality. A cohort only declines in size due to mortality processes as time (i.e. age) increases.

Age-structured models are essentially constructed by a cohort model, which project forward abundances-at-age by year. The basic cohort model is motivated from the generic decay formula

$$\frac{dN(t)}{dt} = -Z \cdot N(t), \tag{2.1}$$

where $N(t)$ is cohort abundance at time t, and Z is the instantaneous total mortality rate. Solving this ordinary differential equation for *N(t)* gives

$$N(t) = N_0 e^{-Zt}, \tag{2.2}$$

where N_0 is some initial condition. The model assumes cohort abundance

decays in size over time, and Equation 2.1 assumes continuous time. However, it is common for total mortality to also vary in time (i.e. $Z \equiv Z(t)$), and this would make solutions to Equation 2.1 more complicated. In such cases, using a discrete time formulation of Equation 2.2 is more effective, which is expressed as

$$N_{y+1,a+1} = N_{y,a}e^{-Z_{y,a}}, \tag{2.3}$$

where time is reflected in years y, and a is age.

Total mortality rate, $Z_{y,a}$, is usually divided into two components: the loss of fish by natural causes (i.e. natural mortality), and the losses due to fishing (i.e. fishing mortality). It is common to assume the natural mortality rate, m, is known when deriving management RPs, and is usually constant over time for all ages. However, in later sections of this paper, natural mortality will be allowed to vary by age (see Section 2.2), therefore it will be denoted m_a. The fishing mortality rate, however, will generally vary between ages and years. Total mortality rate, Z, can be expressed as

$$Z_{y,a} = F_{y,a} + m_a. \tag{2.4}$$

When projecting abundances forward in time, F is assumed to be constant over time (i.e. $F_{y,a} \equiv F_a$), and is further separated into the *fully selected* fishing mortality rate, f, and fishing selectivity, s_a, such that $F_a = f \cdot s_a$, where $0 \leq f < \infty$, $0 \leq s_a \leq 1$, and $max_a s_a = 1$. Although the fishery selectivity is important in determining sustainable yields and RPs (e.g., Scott and Sampson, 2011), in this thesis, for simplicity, it is assumed that selectivity, s_a, is fixed and known for all ages. Selectivity is typically stratified by age or

length, where only fish above a certain age or length are caught. We assume selectivity is an age-based effect, and only fish above the age of recruitment, a_r, are caught. That is, selectivity for ages $a < a_r$ is zero.

MSY RPs are derived from long-term projections and the cohort model is used for the projections based on a values of f, s_a, and m_a. As Figure 2.1 illustrates, the initial abundance-at-age in the first year of the projection (i.e. $N_{1,a}, a = 1, ..., A$) and the abundances at the first age for all projection years (i.e. $N_{y,1}, y = 1, ...$) are required. The initial abundances ($N_{y,1}$) are derived using a stock-recruit model which is described below. Values for the initial abundance-at-age in the first year usually do not matter for long-term projections because equilibrium results will be independent of the starting value. We illustrate this feature later in this chapter. This is also true for the SPM, where equilibrium biomass as a function of H (i.e. $B_{eq}(H) = K(1 - H/r)$) is independent of B_0. Starting values for abundances for the cohort projection are set at arbitrary values, but abundances at the first age (i.e. youngest model age; usually called recruitment) play a direct role in determining MSY RPs.

In fisheries, it is common to assume initial cohort abundance, N_{y,a_0}, is related to parental spawning stock biomass (SSB) through functional relationships (Beverton and Holt, 1957) called stock-recruit (SR) relationships. Initial abundance is typically referred to as recruitment, R, where recruitment is modelled using a SR relationship as a function of SSB, and is typically expressed R(S), where $S \equiv SSB$. The recruitment for a year is dependent on the SSB the year a cohort was born, in this case a_0 years ago, and $N_{y,a_0} = R(S = SSB_{y-a_0})$. Recruitment is assumed to depend on parental

biomass (i.e. weight) rather than abundance (numbers) because total egg production is more related to total stock biomass than numbers. An SR relationship is essential for deriving MSY RPs because it provides information on stock reproduction rates, that is, how well the stock can maintain abundances through reproduction. The SR models used in this study are appropriate for an iteroparous species, meaning fish reproduce annually and contribute to the overall abundance increase so long as mature stock remains. The SR models are detailed in Section 2.2.

Modelling the relationship between parental stock size and reproduction and subsequent recruitmentof juveniles to a fishery is widely recognized as a fundamental component of sustainable fisheries management (Quinn and Deriso, 1999). SR functions are used to project stock size in response to proposed management actions, and to determine management RPs (e.g., Needle, 2001). Some RPs are derived directly from the SR relationship. An example of this is the spawning stock size corresponding to 50% of maximum recruitment which may be taken as a biomass limit (Myers et al., 1994). This RP is usually estimated using an SR model. Other RPs take into account other aspects of stock productivity, including MSY RPs like f_{MSY}. However, the SR model is still very important in determining MSY RPs. Reliable SR models are therefore important for successful fisheries management.

Stock biomass increases each year as fish grow in size (i.e. length) and weight increases. In age-based models, stock growth is calculated using stock abundances-at-age and their respective weights-at-age. It is assumed that most fishing occurs between spring and autumn, while spawning occurs at the beginning or end of each year. Therefore, stock biomass $B_{y,a}$ is measured at

the beginning of each year, and is calculated using beginning-of-year weights. This is different from catch biomass, $L_{y,a}$, referred to as *landings*, which use mid-year weights. Mid-year weights, W^m, are modelled using the same growth distribution as beginning-of-year weights ,W^b, but instead of using ages a_b, use ages $a_m = a_b + 0.5$ (i.e. half a year older; see Section 2.2).

Alongside f_{MSY}, B_{MSY} which is the equilibrium SSB from fishing at f_{MSY}, and biomass depletion which is the ratio of B_{MSY} to the unfished equilibrium SSB (i.e. B_{MSY}/B_0), are commonly used for fisheries management. This thesis will focus on deriving these three RPs.

Using an age-structured model, there are two methods through which these MSY RPs can be derived: a forecast projection, or *per-recruit* functions. The former method involves iterative calculations of quantities like yield over a long range of years through a numerical, algorithmic projection. The projection is re-initiated using different values for f's to determine which f (i.e. f_{MSY}) will provide the greatest equilibrium (i.e. long-term) yield (MSY). The method that uses per-recruit functions, on the other hand, uses explicit functions to directly solve for equilibrium solutions via a numerical optimization, assuming f does not vary over time. Furthermore, both the forecast and per-recruit methods require an SR model to calculate MSY RPs. There are benefits and drawbacks to using either method to estimate RPs: the projection method elucidates inter-annual changes in stock values, but can be time-consuming when projecting over a large number of years, whereas the method that uses per-recruit functions is preferred in situations which opt for brevity, but do not allow intermittent adjustments in life history traits.

Both a forecast projection (Section 2.3) and per-recruit functions (Section 2.4) are used to calculate f_{MSY}, B_{MSY}, and biomass depletion to demonstrate that both methods provide the same results. Of course, both methods should provide identical results if they are defined properly. The projection method is methodical, and its application in higher dimension is relatively simplistic and uninteresting. We primarily focus on the per-recruit method because our focus is to define closed-form functions for deriving MSY RPs for a spatially explicit population, and our use of the projection method will be purely demonstrative rather than heuristic.

2.2 Parameter Choices

In this thesis, MSY RPs are calculated under fixed biological and fishing effects, that is, we assume the age-distributions of various stock and fisheries characteristic are consistent over time. These characteristics include the selectivity (s), the natural mortality rate (m), the maturity-at-age (μ), and the weight-at-age (W). To understand the impact each of these characteristics have on RP estimates, a variety of different parametrizations and age-distributions were considered. An SR relationship is also required to estimate MSY RPs, and several are considered. The age-distributions of these characteristics range from starting age $a_0 = 5$ to the max age of $A = 20$. For each unique pair of characteristics and SR models, f_{MSY}, B_{MSY}, and biomass depletion are calculated. Changes for parameters were mutually exclusive, meaning they were changed independently, to emphasize the effect each characteristic has on RP results. The age-distributions of each charac-

teristic (Table 2.1) were calculated as follows:

- **Selectivity, *s*.** Selectivity is flat (constant) for ages $a \geq a_r$, where fish of ages $a \geq a_r$ are considered *fully selected* (s=1), and fish below this age are not selected (s=0). This is referred to as *knife-edged* selectivity. Two selectivity curves were used: (1) s_6, such that $a_r = 6$; (2) s_8 such that $a_r = 8$.

- **Maturity, $\boldsymbol{\mu}$.** Maturities are described by an age-dependent model,

$$\mu(a) = \frac{e^{\theta_0 + \theta_1 a}}{1 + e^{\theta_0 + \theta_1 a}}, \tag{2.5}$$

  where θ_0 and θ_1 are derived from fixing age-at-percent-maturities. Two maturity distributions (i.e. *maturity ogives*) were used: (1) $\mu_{8,10}$, where the age at 50% maturity (that is, the age for which 50% of fish are mature) $A_{50\%} = 8$, such that $\mu(8) = 0.5$, and the age at 95% maturity $A_{95\%} = 10$, such that $\mu(10) = 0.95$ ($\theta_0 \approx -11.78$, $\theta_1 \approx 1.472$); (2) $\mu_{10,12}$, where $A_{50\%} = 10$, and $A_{95\%} = 12$, ($\theta_0 \approx -14.72$, $\theta_1 \approx 1.472$).

- **Weight, *W*.** Weights are described by a Von Bertalanffy age-dependent equation (Haddon, 2010),

$$W(a) = W_\infty (1 - e^{-k \cdot (a - a')})^3, \tag{2.6}$$

  where k is the growth rate, the asymptotic weight (i.e. $\lim_{a \to \infty} W(a)$) $W_\infty = 2$, and a' is defined by $W(0) = 0.001 W_\infty$ ($a' \approx -1.054$). Three weight distributions were used: (1) $W_{0.1}$, such that $k = 0.1$; (2) $W_{0.05}$, such that $k = 0.05$; (3) $W_{0.15}$, such that $k = 0.15$.

- **Natural Mortality Rate, *m*.** Two distributions for the natural mortality rate were used: (1) $m_{constant}$, where $m_a = 0.2$ for all ages and years; (2) m_{lorenz}, where the natural mortality rate is described by an age-based distribution known as a *Lorenzen mortality* rate, expressed as a function of weight-at-age,

$$m(a) = m_\infty \left(\frac{W(a)}{W_\infty} \right)^c, \tag{2.7}$$

where m_∞ is the asymptotic natural mortality rate, W_∞ is the asymptotic weight (see Equation 2.6), $W(a)$ is the weight-at-age, and $c = -0.305$ (see Powers, 2014), where m_∞ is defined by $m(a)|_{W(a)=0.5W_\infty} = 0.2$ ($m_\infty \approx 0.162$).

- **Stock-Recruitment.** Two SR relationships are considered, as well as alternative parametrizations for both models: (1) The most commonly used SR relationship, the Beverton-Holt (BH) model (Beverton and Holt, 1957), is

$$R(S) = \frac{\alpha S}{\beta + S}, \tag{2.8}$$

where α and β are parameters and $S \equiv SSB$. For this model, $\lim_{S\to\infty} R(S) = \alpha$, and the stock size that provides half the max recruitment $S_{50\%} = \beta$, where $R(S_{50}) = 0.5R_{max}$. The slope at the origin (SaO) is $\frac{dR}{dS}|_{S=0} = \frac{\alpha}{\beta}$. We assume a constant $SaO = 1$, for simplicity, so $\alpha = \beta$. Two parametrizations were considered: (i) $\alpha = \beta = 100$; (ii) $\alpha = \beta = 300$. (2) The second most commonly used SR relationship is the Ricker (RK) model (Ricker, 1958),

$$R(S) = \alpha S e^{-\beta S}, \tag{2.9}$$

where α and β are parameters and $S \equiv SSB$. For this model, it can be shown that $\lim_{S\to\infty} R(S) = 0$, and $R_{max} = \alpha/(e \cdot \beta)$ when $S = 1/\beta$, and $SaO = \frac{dR}{dS}|_{S=0} = \alpha$. We assume a constant $SaO = 1$, and β is defined based on R_{max}; since we fix $\alpha = 1$, $\beta = 1/(e \cdot R_{max})$. Two parametrizations were considered: (i) $\beta = 0.00368$ for $R_{max} = 100$; (ii) $\beta = 0.00123$ for $R_{max} = 300$.

Both SR relationships were also re-parametrized in terms of the steepness parameter, h (see Francis, 1992; Punt and Cope, 2017). Steepness is a measure of stock productivity, and represents the ratio of unfished recruitment, R_0, to 20% unfished SSB, S_0. (1) The steepness version of the BH SR relationship is

$$R_h(S) = \frac{R_0}{S_0} \frac{4hS}{(1 - h + (5h - 1)S/S_0)}. \tag{2.10}$$

(2) The steepness version of the RK SR relationship is

$$R_h(S) = \frac{R_0}{S_0} S \cdot e^{\ln(5h)(1-S/S_0)/0.8}. \tag{2.11}$$

For both Equations 2.10 and 2.11, $R_0 = 100$ and $S_0 = R_0 \cdot SPR(0)$. SPR is a function that provides the ratio of SSB to recruitment with respect to f, and is defined in Section 2.4. Three steepness values are used to model the SR relationship. These values were taken from Shertzer and Conn (2012), who performed a meta-analysis of steepness for 94 stocks and calculated a median (inter-quartile range) of 0.78 (0.69-0.86). Similar results for steepness were found for pleuronectiformes by Myers et al. (1999) and

various species by Hilborn (2010). SR relationships were modelled using (i) the median value (*med*, $h = 0.78$), (ii) the lower quartile value (*low*, $h = 0.69$), and (iii) the upper quartile value (*up*, $h = 0.86$).

Initially, parameters are set as: s_6, $\mu_{8,10}$, $W_{0.1}$, and $m_{constant}$; these are considered the base conditions. When parameters were changed to calculate RPs for alternative life history characteristics, all parameters, other than that which is specified to change, followed these configurations.

2.3 Forecast Projection

The forecast requires initial conditions to calculate subsequent values. We assume the initial abundance for any year y, $N_{y,a}$, depends on SSB for the year they were born through an SR relationship. Our initial age $a_0 = 5$, and therefore, the relationship between spawning stock and recruitment entails a 5-year lag, where $N_{y,a_0} = R(SSB_{y-5})$. Due to this five-year lag, initial abundances must be set for the first *five* years to calculate subsequent abundances.

Forecast projections are structured similar to SPMs, where stock values are calculated iteratively, and over time abundances will eventually reach a stable state (Figures 2.2 and 2.3). To initialize the forecast projection, abundances-at-age for the first five years were all set at $N_{y,a} = 20$. It can be shown that equilibrium solutions for forecast projections are independent of initial abundances for the BH (Figure 2.2) and RK (Figure 2.3) SR models. Biomass, SSB, catch, and landings were calculated from abundances-at-age for each year (see Table 2.2 for equations) for ages 5 to 20 ($a \in [5, 20]$), over

500 years ($y \in [6, 500]$; values for the first five years are not forecasted because abundances were fixed). The forecast projections are reiterated for $f \in [0, 0.5]$ in increments of 0.001. The f that maximizes total annual landings (yield) is denoted f_{MSY}, the yield for the final year from fishing at f_{MSY} is MSY (i.e. $Y_{f_i=f_{MSY},y=500} = MSY$), and the SSB for the final year from fishing at f_{MSY} is B_{MSY} (i.e. $SSB_{f_i=f_{MSY},y=500}$).

2.4 Per-Recruit Functions

Equilibrium biomass and yield for an SPM can be found by simply finding the solution B_{eq} to Equation 1.1 when $B_{t+1} = B_t = B_{eq}$. This equilibrium biomass is a function of H (also r and K); that is, $B_{eq}(H) = K(1 - H/r)$. The same procedure can be used for age-structured models. At equilibrium the stock abundances-at-age do not change from year to year. In particular, the SSB is the same each year, and is also the same as the SSB produced by a cohort over its lifespan (see Figure 2.4). The basic quantities involved to derive equilibrium results for a cohort model are the fishery yield-per-recruit (YPR), the spawner-biomass-per-recruit (SPR), and the SR function. The per-recruit quantities are functions of f and give the total SSB per unit of recruitment produced by a cohort over its lifespan, or the total yield produced per unit of recruitment. Equations for SPR(f) and YPR(f) are developed below.

Equilibrium yield can be calculated using these per-recruit functions. To elaborate, let $R_{eq}(f)$ and $SSB_{eq}(f)$ denote the equilibrium values of recruitment and SSB, respectively, that we project at some specific f. At equilib-

rium, the sum of the mature biomass for all ages each year (i.e. SSB) is the same as the sum of mature biomass produced by a cohort over its lifespan. That is, $SSB_{eq}(f) = SPR(f)R_{eq}(f)$. Using the SR function and the fact that $SSB_{eq}(f)$ is the same each year, $SSB_{eq}(f) = SPR(f) \cdot R(SSB_{eq}(f))$. Since SPR(f) is a fixed value for a given *f*, $SSB_{eq}(f)$ may be obtained as the x solution to $x = SPR(f)R(x)$. Also, $R_{eq}(f) = R(SSB_{eq}(f))$ and equilibrium yield is $Y_{eq}(f) = YPR(f)R_{eq}(f)$.

Values for SSB_{eq} are also sometimes conceptualized as the intersect of the SR curve and a *replacement line*. The replacement line indicates the capacity for a stock to replace, and therefore sustain, itself through reproduction. The replacement is defined as $R = S/SPR(f)$ where the slope of the replacement line $1/SPR(f)$ depends on f (Figure 2.5). The values for $SSB_{eq}(f)$ and $R_{eq}(f)$ are the x and y values of the point of intersection, respectively.

Solutions for SSB_{eq} are simple to derive for the standard, spatially homogeneous BH and RK SR functions. Derivations become more complicated, however, when spatial dimensions are considered (see Chapter 3).

YPR is the ratio of landings with respect to abundance of recruits as a function of *f*. A discrete formulation for YPR is provided by Haddon (2010),

$$YPR(f) = W^m_{a_r} P_{a_r}(f) + \sum_{i=a_r+1}^{A} W^m_i P_i(f) e^{-\left(\sum_{j=a_r}^{i-1} f s_j + m_j\right)}, \tag{2.12}$$

and

$$P_a(f) = (1 - e^{-Z_{y,a}}) \frac{F_{y,a}}{Z_{y,a}}, \tag{2.13}$$

is the proportion of stock fished. The term $(1 - e^{-Z_{y,a}})$ in Equation 2.13 is the amount of fish lost through total mortality, and it is assumed $F_{y,a}/Z_{y,a}$ is

the proportion of those losses that are a result of fishing (see Baranov, 1918). SPR is calculated as

$$SPR(f) = W^b_{a_r}\mu_{a_r} + \sum_{i=a_r+1}^{A} W^b_i \mu_i e^{-\left(\sum_{j=a_r}^{i-1} fs_j + m_j\right)}. \tag{2.14}$$

The SSB_{eq} needed to calculate equilibrium yield will depend on the SR model used. For the BH model, for example, SSB_{eq} is defined as

$$SSB_{eq}(f) = SPR(f) \cdot \frac{\alpha SSB_{eq}(f)}{\beta + SSB_{eq}(f)}. \tag{2.15}$$

Solving Equation 2.15 for SSB_{eq} provides the following,

$$SSB_{eq}(f) = \alpha SPR(f) - \beta. \tag{2.16}$$

Doing the same for the RK model, where

$$SSB_{eq}(f) = SPR(f) \cdot \alpha SSB_{eq}(f) e^{-\beta SSB_{eq}(f)}, \tag{2.17}$$

SSB_{eq} can be expressed as

$$SSB_{eq}(f) = ln(\alpha SPR(f))/\beta. \tag{2.18}$$

Solving for SSB_{eq} for the steepness formulation of the BH model in the same way provides

$$SSB_{eq}(f) = \frac{S_0}{5h-1}\left(\frac{4hR_0 SPR(f)}{S_0} + h - 1\right), \tag{2.19}$$

and for the steepness RK model provides

$$SSB_{eq}(f) = S_0 \left(1 - 0.8\frac{ln(S_0/(R_0 SPR(f)))}{ln(5h)}\right). \tag{2.20}$$

Equilibrium yield, for some f is defined as

$$Y_{eq}(f) = \frac{YPR(f)}{SPR(f)} SSB_{eq}(f). \tag{2.21}$$

Equilibrium yield using the BH SR model is then

$$Y_{eq}(f) = \frac{YPR(f)}{SPR(f)}(\alpha SPR(f) - \beta), \tag{2.22}$$

and for the RK SR model is

$$Y_{eq}(f) = \frac{YPR(f)}{SPR(f)} \frac{log(\alpha SPR(f))}{\beta}. \tag{2.23}$$

Optimizing equilibrium yield with respect to f will provide f_{MSY}, such that $Y_{eq}(f_{MSY}) = MSY$. To elaborate, f_{MSY} is the f that maximizes Y_{eq}, such that $\frac{d}{df} Y_{eq}(f)|_{f=f_{MSY}} = 0$. For the BH,

$$\frac{d}{df} Y_{eq}(f) = \frac{d}{df}\left[\frac{YPR(f)}{SPR(f)}(\alpha SPR(f) - \beta)\right]. \tag{2.24}$$

The root (i.e. f_{MSY}) for Equation 2.24 is dependent on both α and β. However, because we assume $\alpha = \beta$, f_{MSY} is independent of α and β, since

it is a scalar term for the equilibrium yield. For the RK,

$$\frac{d}{df}Y_{eq}(f) = \frac{d}{df}\left[\frac{YPR(f)}{SPR(f)}\frac{log(\alpha SPR(f))}{\beta}\right]. \tag{2.25}$$

Here, β is a scalar and does not affect the value of f that maximizes Equation 2.25, so f_{MSY} is independent of β, but is dependent on α.

It is important to note that the YPR function itself is responsible for the quasi-concavity of the equilibrium yield curve mentioned previously. When there is no fishing ($f = 0$) the yield is zero, and when fishing is at too large a value, reproduction is insufficient to sustain the population where any further fishing would also provide zero yield. It is generally understood that YPR, as well as equilibrium yield, are dome-shaped and concave down, where yield increases with f until some point, then decreases until yield is zero. This is primarily a result of the Baranov catch proportion (i.e. Equation 2.13). Both SSB_{eq} and SPR functions are monotonically decreasing function with respect to f and effectively scale the optimal f and Y_{eq} values. Therefore, it is simple to conclude equilibrium yield is maximized for some value of *f*.

Values for f_{MSY} are found by using *nlminb* in ***R*** to optimize the equilibrium yield equations, and the optimized yield $MSY = Y_{eq}(f = f_{MSY})$ is recorded. Values for B_{MSY} are also calculated by using the equilibrium SSB equations, where $B_{MSY} = SSB_{eq}(f = f_{MSY})$, and biomass depletion (i.e. B_{MSY}/B_0) is derived using B_{MSY} and $B_0 = SSB_{eq}(f = 0)$.

2.5 Results

The long-range forecast and the per-recruit/SR methods provide relatively equal outputs, and the discrepancy between the forecast and per-recruit results are due to the limited precision in f for the forecast projection (0.001). The results derived through the per-recruit method are assumed to be the correct RP values. For all further calculations, the per-recruit functions were used for higher precision and quicker calculations.

Equilibrium yield and SSB were also calculated for different maturity ogives (Figure 2.6), natural mortality rate distributions (Figure 2.7), selectivity curves (Figure 2.8), and weight-at-age distributions (Figure 2.9). Equilibrium yield and SSB were also calculated for different SR relationships (Figures 2.10 and 2.11). Values for f_{MSY}, B_{MSY}, B_{MSY}/B_0, and MSY were calculated for each alternative parametrization and compared to the RP outputs under the base parametrizations (Figure 2.12). Percent changes in RP values were calculated as

$$\%\Delta x = \left(\frac{x - x_0}{x_0}\right) \cdot 100\%, \tag{2.26}$$

where x_0 are RP values under the base conditions, and x are RP values from alternative parametrizations.

Values for f_{MSY}, MSY, and B_{MSY} were larger for the steepness SR models than the standard SR models, and values for the RK models (standard and steepness) were always larger than their BH counterparts (Table 2.3). Biomass depletion from f_{MSY} had larger values (i.e. less biomass was depleted) for the standard BH and RK models, and using the steepness SR

models resulted in more depleted biomass compared to the standard SR models. In general, for f_{MSY} and MSY, values ordered (smallest-largest): standard BH, standard RK, steepness BH, and steepness Ricker. For B_{MSY} and biomass depletion, this order was reversed. It is clear that stock productivity (e.g. h) has a relationship with MSY RP values; increasing reproduction rates allows larger fs and total yields, but results in lower SSB_{eq}. Estimates of f_{MSY} are known to have an approximately linear relationship with steepness (see Punt and Cope, 2017), and our results for both the BH and RK models show a similar trend (see Figure 2.11).

As f_{MSY} and MSY increase, B_{MSY} and B_{MSY}/B_0 usually decrease, although there are exceptions to this as a result of our choices for α and β. For the standard BH SR relationship, changes in α and β did not affect f_{MSY} or biomass depletion (see Table 2.3). For a BH SR relationship, changes in α and β each may have separate effects on f_{MSY} (see Zheng et al., 2019, Appendix 7.2), but because $\alpha = \beta$, changes only affect the scale of SSB_{eq} and B_{MSY} without affecting f_{MSY} of biomass depletion. For the standard RK SR relationship, changes in β did not affect f_{MSY} or biomass depletion, similar to the BH model (Table 2.3). When using the RK SR model, changes in either α or β can affect B_{MSY}, and changes in α can affect f_{MSY}. However, α is constant for our calculations, resulting in a stable f_{MSY} between RK models. Biomass depletion for both the standard SR models did not change from increases in α and β (BH) or increases in β (RK), because these SR parameters only scale the SSB_{eq} (see Section 2.4) and the unfished equilibrium biomass, $SSB_{eq}(f = 0)$, scales equivalently with B_{MSY}.

Overall, MSY RPs were most sensitive to factors that affected biomass

increase, like the steepness h (see Table 2.3), and the growth rate, k (Figure 2.12). Values for all MSY RPs were zero for the standard BH and RK SR models when $k = 0.05$, implying fish did not grow quickly enough to allow sustainable harvesting. Meanwhile, f_{MSY} was largest for each SR model when $k = 0.15$, likely because faster fish growth can compensate for larger harvest rates, but this growth rate provided the lowest (non-zero) values for biomass depletion (see Figure 2.12). Harvest RPs rely on accurate estimations of growth rates, and small estimation errors in k can be fatal for a fish stock by promoting unsustainable harvest rates.

Changes in the maturation rate decreased all MSY RP estimates except for values for biomass depletion under the standard BH and RK SR models (Figure 2.12), and these deviations were unsubstantial ($\%\Delta x \leq 5\%$; e.g. Equation 2.26). This suggest that the presence of less mature fish results in a decrease in total harvest and lower harvest rates, which leaves higher levels of SSB as a result of decreased fishing.

Typically, increases in f_{MSY} result in decreases in B_{MSY} (and increased biomass depletion) because more of the spawning stock is fished, and this is reflected in all parameter changes, except for the age of recruitment (i.e. selectivity). When age of recruitment was increased for a knife-edged fishing selectivity, f_{MSY} *and* B_{MSY} increase, likely because only selecting older fish leaves younger fish with more time to mature (higher SSB) and more time to increase in size (higher biomass). Increasing the age of recruitment also increased MSY and reduced biomass depletion (i.e B_{MSY}/B_0 increased). Changing the age of selectivity provided only positive results in terms of MSY RPs, but changes in the selectivity curve can have unpredictable effects

on harvest rates. Moreover, knife-edged selectivity curves are not realistic. Fishing selectivity is usually described by a sigmoid curve, where selectivity increases with age, or a dome-shaped curve, where selectivity increases with age but decreases at the oldest ages (see Figure 2.13). For example, a dome-shaped selectivity can be seen in gill-nets which may allow younger, smaller fish to pass through, while older fish are too large to be captured, and so mostly middle-aged fish are captured. Selectivity can be difficult (i.e. expensive) to estimate since it is usually a component of the total fishing mortality rate, F, in stock assessment models, and is often estimated outside the assessment models. Further, fishing selectivity is related to the type of fishing gear used (e.g. mesh size) or the haul time for the gear (e.g. for purse seines), and several such factors may simultaneously affect the selectivity age-distribution. However, when possible, fishing selectivity can be used to directly constrain fishing rates, and is often considered an effective means of harvest control (e.g., Kanik et al., 2015).

Using a Lorenzen natural mortality rate almost always reduced MSY RP estimates. Biomass was less depleted when using the standard BH and RK model, and MSY was slightly greater when using the steepness SR models, likely due to relative stock productivity. Otherwise, using a Lorenzen natural mortality rate provided lower RPs compared to a constant m_a. However, changes in the Lorenzen natural mortality rate parameters, primarily the asymptotic mortality m_∞, can produce varying responses in RP outputs. For example, the Lorenzen natural mortality rate we used ($m_\infty \approx 0.161$) produces lower f_{MSY} values compared to estimates that use a constant natural mortality rate of $m_a = 0.2$. Some choices in of m_∞, however, will produce

an f_{MSY} greater than that for the constant $m = 0.2$. Therefore, for some value of m_∞, model outputs from both natural mortality rate distributions are equal. Using a Lorenzen natural mortality rate when $m_\infty \approx 0.154$ and $k = 0.1$—since the Lorenzen natural mortality rate depends on weight—MSY RP results are about equal to those calculated using the natural mortality rate $m_a = 0.2$. It is important to be aware of the adverse effects a Lorenzen natural mortality rate can have on RP outputs, and to note that RPs can be much more sensitive to age-based natural mortality rates compared to constant ones.

2.6 Discussion

As we have demonstrated, changes in parameters used to describe stock characteristics can have significant impacts on MSY RPs. Deviations in outputs are relevant when considering associated uncertainties in parameters, which makes it difficult to accurately define management RPs. It is standard for stock models to incorporate some form of uncertainty, for example in productivity parameters, and several studies have explored the impact stochasticity may have on RP estimates. Okamura et al. (2014) calculated MSY for BC lingcod using both a stochastic and deterministic delay-difference model. MSY results showed large variances, with 90% confidence intervals in most cases ranging from $\sim$ 50% of the estimated median MSY (5th percentile) to $\sim$ 200% of the median MSY (95th percentile). Horbowy and Luzeńczyk (2012) derived F_{MSY} and various alternative RPs through per-recruit functions using stochastic simulations. They showed that relative error in RP val-

ues can increase as process error increases in SR relationships, up to $\sim 50\%$ for the RK model and $\sim 30\%$ for the BH. Cadigan (2013) also examined the error in F_{MSY} and B_{MSY} estimates through simulations using per-recruit functions and several SR models, and showed that RP confidence intervals could be large when using the BH and RK SR models.

Estimates of f_{MSY} and B_{MSY} can be highly sensitive to changes in parameters which may be associated with uncertainty in one or more life history characteristics, as well as SR parameter estimates, since recruitment can be difficult to accurately estimate, assuming a relationship exists at all. Horbowy and Luzeńczyk (2012) performed stochastic simulations to derive f RPs using per-recruit functions, and noted that when the SR relationship is unknown, RPs which rely on stock recruitment had large associated error ($\sim 70\% - 130\%$ of estimates).

Due to the inevitability of errors in model outputs, some management plans utilize RP 'estimators' in lieu of direct estimates to approximate RPs, but these estimators can result in an even greater deviance from the true value compared to RPs that are calculated directly (Haltuch et al., 2008). Alternatives to using fixed RPs are also considered in some fisheries. Assessing and configuring management strategies according to previously employed management tactics and recent trends in fish stocks (i.e. *grandfathering*) is one (Geromont et al., 1999). Some stocks are reasonably well-managed without the use of population models, provided policy makers and fisheries scientist reach a consensus on appropriate parameters regarding total allowable catches (TACs; often a landings limit per fisherman or percentage of total MSY). Management goals and procedures that result from stock mod-

els may perform poorly due to biases in estimations. Simple decision-based rules are sometimes sufficient for setting harvest goals and protocol (Parma, 2002). Conversely, Goethel and Berger (2017) recommend using operating models for deterministic RP calculations, because they can test several RP-based harvest strategies at a time and allow managers to choose the strategy that is most effective. Sethi (2010) outlines a number of operating models used specifically for risk appraisal for fisheries management procedures, like mulitcriteria decision making (MCDM) and management strategy evaluations (MSEs), which may be applied to standard stock models to narrow down the most appropriate management options.

A variety of methods, like those mentioned above, have been developed to circumvent or mitigate the prevalent effect uncertainties have on estimates of harvest objectives. Nevertheless, if stock assessments are frequent and management procedures are responsive to changes in recent stock trends, i.e. a precautionary approach, RP-based management strategies can be highly effective (Nowlis and Bollermann, 2002). Although life history characteristics can have substantial associated errors, stock models may still provide inaccurate results even when these errors are small. In such cases, the model itself may be flawed by providing unreliable outputs. Thus, for our purposes, forgoing a stochastic model for a simpler, deterministic model is sufficient to present the methods for deriving MSY RPs and, in the upcoming chapters, to develop a framework for deriving area-specific MSY RPs.

For fisheries scientists, one of the main objectives is to construct and apply population dynamics models to quantify fish stocks and derive management RPs. Before developing novel frameworks and applying them to

fish stocks, it is important for stock assessors to understand and implement existing models for RP derivations. As shown in this chapter, the methods for calculating MSY RPs using an age-structured model for a spatially homogeneous stock are well-defined, yet within this framework, defining reliable management RPs can be difficult due to parameter uncertainties. However, structural misdiagnosis of a population dynamics can also reduce the accuracy of RP estimates substantially (Bosley et al., 2019; Goethel and Berger, 2017). Therefore, constructing more appropriate models to describe fish population dynamics, in particular adding spatial components to stock structures, may improve the reliability of RP estimates.

In the next chapter, the per-recruit and equilibrium SSB functions are adjusted to consider a spatial structure and used to derive area-specific RPs for a two-area system. More specifically, a theoretical and deterministic spatial population dynamics model will be constructed, taking into account a movement pattern known as *larval advection*, and MSY RPs will be derived for two distinct regions in space. Movement patterns like larval advection are common for many fish, even those that are approximately sedentary as adults, and these movement patterns should be accounted for in stock assessment models. Developing such a model may encourage the use of spatially explicit RPs for future management practices.

2.7 Tables

Table 2.1: Values for stock characteristic used to estimate RPs. Weight are calculated as W_k, where $k = 0.1$, $k = 0.05$, and $k = 0.15$; selectivity are defined s_{a_r}, where $a_r = 6$ and $a_r = 8$; natural mortality rates are describe by $m_{constant} = 0.2$ and the Lorenzen natural mortality m_{lor}; and maturity ogives μ defined by $A_{50\%} = 8$ and $A_{95\%} = 10$, and $A_{50\%} = 10$ and $A_{95\%} = 12$.

Age	$W_{0.1}$	$W_{0.05}$	$W_{0.15}$	s_6	s_8	$m_{constant}$	m_{lor}	$\mu_{8,10}$	$\mu_{10,12}$
5	0.187	0.054	0.380	0.000	0.000	0.200	0.333	0.012	0.001
6	0.259	0.074	0.510	1.000	0.000	0.200	0.302	0.050	0.003
7	0.338	0.098	0.643	1.000	0.000	0.200	0.278	0.187	0.012
8	0.423	0.125	0.775	1.000	1.000	0.200	0.260	0.500	0.050
9	0.510	0.155	0.901	1.000	1.000	0.200	0.246	0.813	0.187
10	0.599	0.187	1.021	1.000	1.000	0.200	0.234	0.950	0.500
11	0.687	0.222	1.132	1.000	1.000	0.200	0.224	0.988	0.813
12	0.775	0.259	1.234	1.000	1.000	0.200	0.216	0.997	0.950
13	0.860	0.298	1.326	1.000	1.000	0.200	0.209	0.999	0.988
14	0.942	0.338	1.409	1.000	1.000	0.200	0.204	1.000	0.997
15	1.021	0.380	1.483	1.000	1.000	0.200	0.199	1.000	0.999
16	1.096	0.423	1.549	1.000	1.000	0.200	0.194	1.000	1.000
17	1.167	0.466	1.607	1.000	1.000	0.200	0.191	1.000	1.000
18	1.234	0.510	1.659	1.000	1.000	0.200	0.188	1.000	1.000
19	1.296	0.554	1.704	1.000	1.000	0.200	0.185	1.000	1.000
20	1.355	0.599	1.743	1.000	1.000	0.200	0.182	1.000	1.000

Table 2.2: Stock values calculated in the forecast projection and their respective equations.

Value	Equation
Abundance, $N_{y,a}$	$N_{y-1,a-1}e^{-Z_{y-1,a-1}}$
Biomass, $B_{y,a}$	$N_{y,a}W_a^b$
Spawning Biomass, $SB_{y,a}$	$B_{y,a}\mu_a$
Total Annual Abundance, N_y	$\sum_a N_{y,a}$
Total Annual Biomass, B_y	$\sum_a B_{y,a}$
Spawning-Stock Biomass, SSB_y	$\sum_a SB_{y,a}$
Catch, $C_{y,a}$	$N_{y,a}(1-e^{-Z_{y,a}})\frac{F_{y,a}}{Z_{y,a}}$
Total Annual Catch, C_y	$\sum_a C_{y,a}$
Landings, $L_{y,a}$	$C_{y,a}W_a^m$
Total Annual Landings (Yield), Y_y	$\sum_a L_{y,a}$

Table 2.3: RP estimates using the forecast projection method (FP) and through the per-recruit functions (PR), using the s_6, $\mu_{8,10}$, $W_{0.1}$, and $m_{constant}$ parametrizations (see Table 2.1 for parameter definitions). PR values were rounded to 3 significant figures to maintain the same precision as FP values.

	f_{MSY}		MSY		B_{MSY}		B_{MSY}/B_0	
	FP	PR	FP	PR	FP	PR	FP	PR
BH_{100}	0.047	0.047	2.42	2.42	39.0	39.1	0.437	0.438
BH_{300}	0.047	0.047	7.26	7.26	117	117	0.437	0.438
RK_{100}	0.051	0.051	5.60	5.60	82.8	82.4	0.477	0.475
RK_{100}	0.051	0.051	16.8	16.8	248	247	0.477	0.475
BH_{low}	0.167	0.167	14.1	14.1	55.3	55.3	0.292	0.292
BH_{med}	0.206	0.206	15.9	15.9	48.1	48.0	0.254	0.254
BH_{up}	0.255	0.255	17.7	17.7	40.3	40.3	0.213	0.213
RK_{low}	0.148	0.148	17.7	17.7	80.3	80.1	0.424	0.423
RK_{med}	0.169	0.169	20.2	20.2	78.0	78.1	0.412	0.412
RK_{up}	0.186	0.186	22.3	22.3	76.7	76.5	0.405	0.404

2.8 Figures

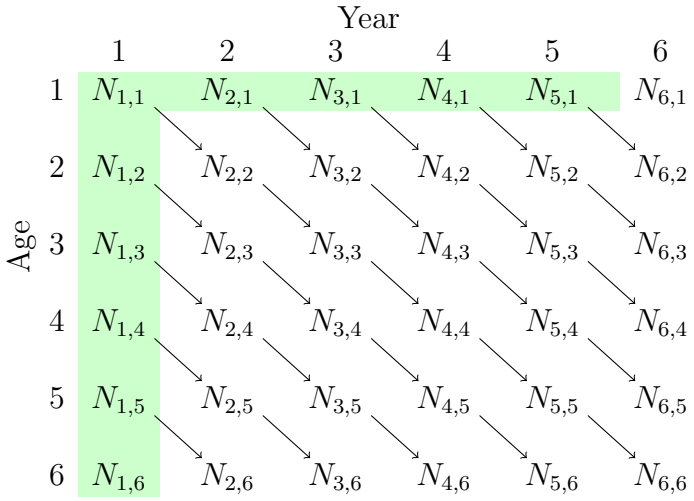

Figure 2.1: Cohort model with abundance denoted as $N_{year,age}$. Abundances are dependent on initial cohort abundance, i.e. recruitment, and abundance-at-age for the first year (green). Annual cohort abundances are projected forward following arrows, such that $N_{y+1,a+1} = N_{y,a}e^{-Z_{y,a}}$ for all y and a. Total mortality decreases abundance of each cohort by year, and recruitment increases annual abundance each year by adding a new cohort.

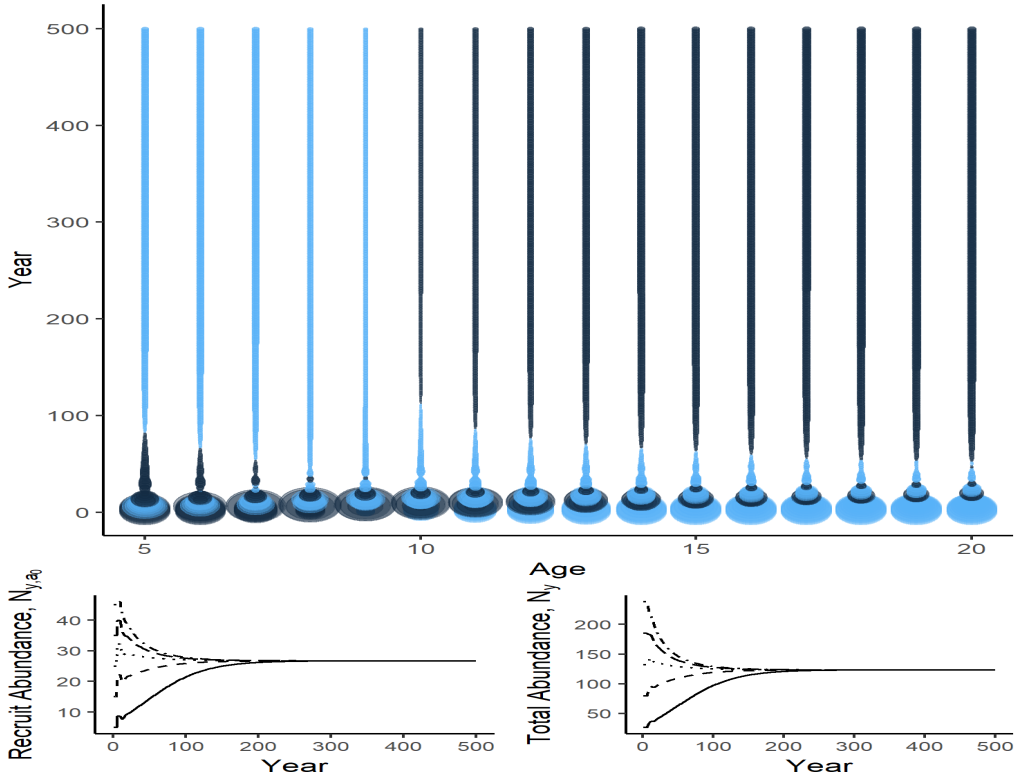

Figure 2.2: Bubble plot of abundances for a 500 year illustrative forecast projection ($f = 0.05$) using the BH_{100} SR model. (Top) Bubbles represent positive (blue) and negative (black) deviation of the standardized proportion abundance-at-age, $p_{y,a} = N_{y,a}/\Sigma_a N_{y,a}$, from the standardized mean proportion abundance-at-age, $\bar{p}_y = \Sigma_y p_{y,a}/500$, with standard deviation $\sigma_a = \sqrt{Var(p_{y,a}|a)}$. That is, $size = |\frac{p_{y,a}-\bar{p}_y}{\sigma_a}|$. Bubbles appear as solid lines in places where they are constant over time, i.e. line thickness is *size*, and colour is the sign of the deviation. Over time, all abundances-at-age and total abundances stabilize. (Bottom) Abundance of recruits (left) and total annual abundance (right) over time from forecast projection for five different initial abundances, N_{y_0,a_0}: 5 (solid), 15 (dashed), 25 (dotted), 35 (long-dash), and 45 (dot-dash).

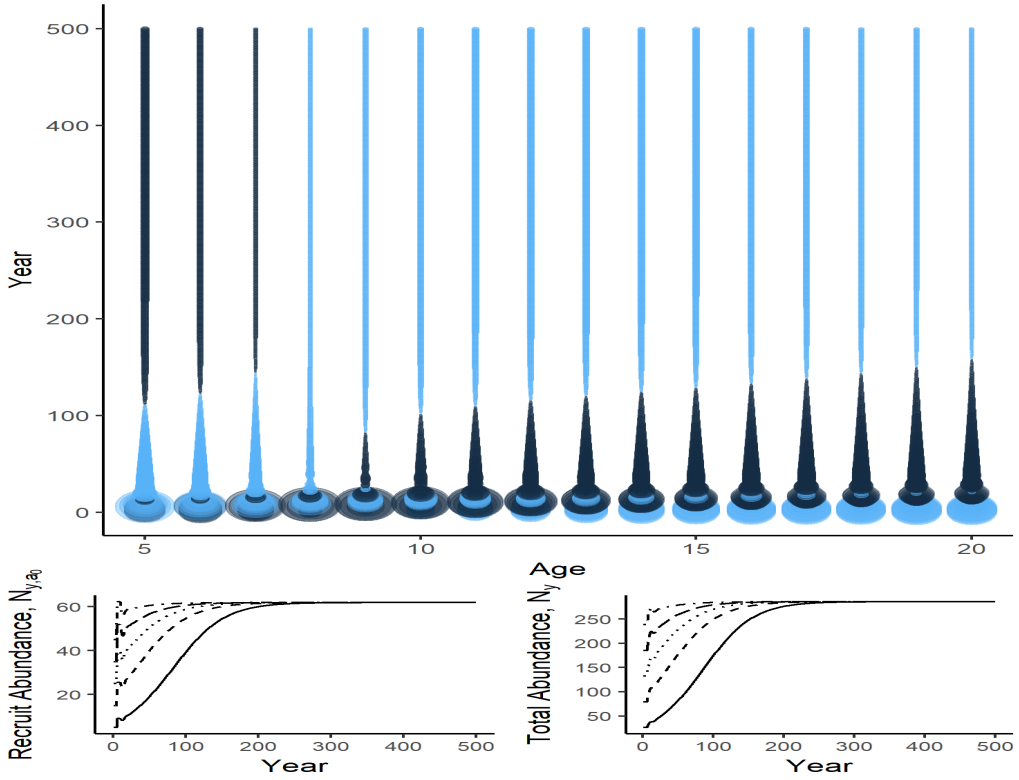

Figure 2.3: Abundances for a 500 year forecast projection ($f = 0.05$) using the RK_{100} SR model. Additional details are provided in caption for Figure 2.2.

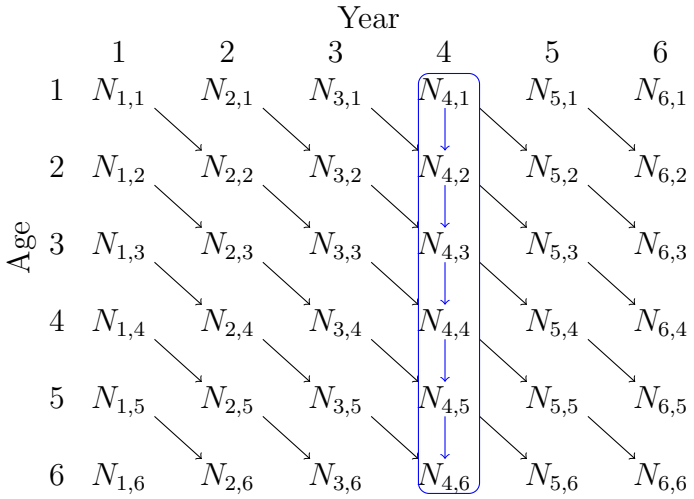

Figure 2.4: Cohort model where abundances are denoted $N_{year,age}$. Cohort abundances are typically projected forward from previous cohort abundance, $N_{y-1,a-1}$. However, per-recruit functions assume a stable state has been reached, such that $N_{y-1,a} = N_{y,a} = N_{y+1,a}$ for all years. The abundance at each age for a cohort is the same as the abundance at each age in a year (blue circle).

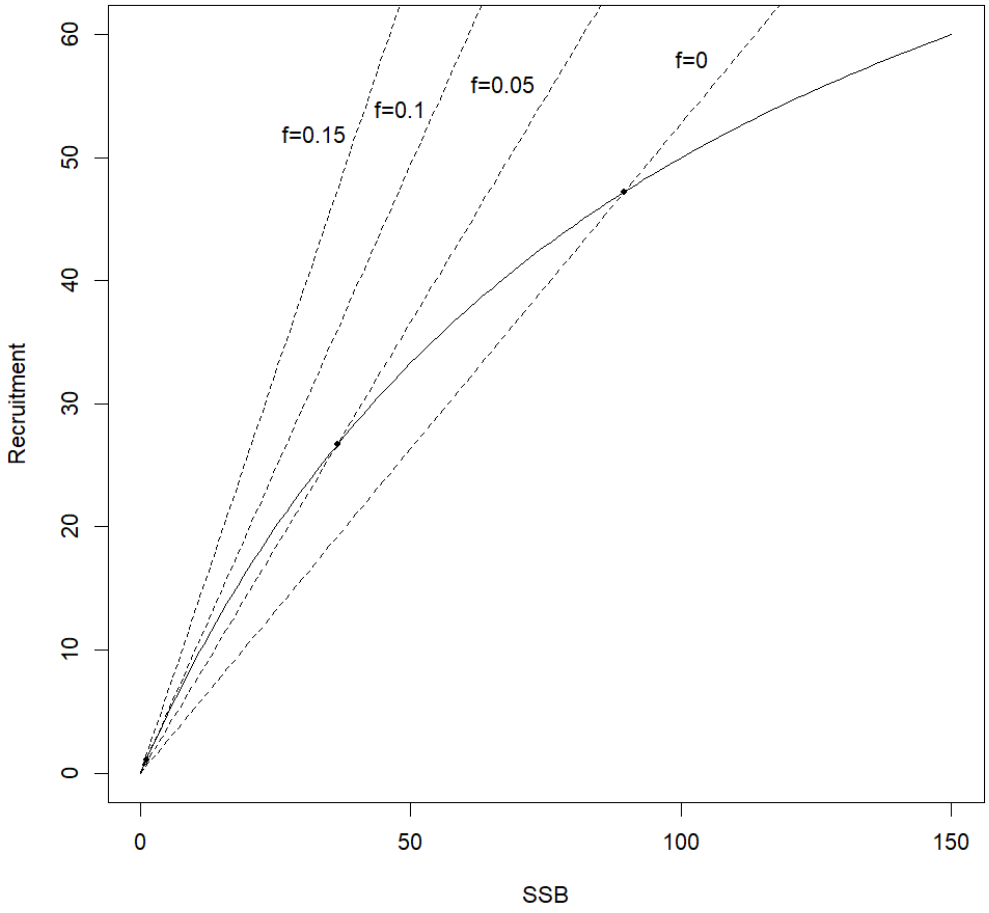

Figure 2.5: Replacement lines for various f's with respect to the BH_{100} SR curve. The replacement lines intersect the SR curve at $R = R_{eq}(f)$ and $S = SSB_{eq}(f)$, for some f. As f increases, the slope of the replacement line, $1/SPR(f)$, increases, and R_{eq} and SSB_{eq} strictly decrease for a BH SR model. When the slope of the replacement line is equal to the slope at the origin (i.e. at $SSB_{eq}(f) = 0$), the stock is unsustainable and collapses. Any greater f also results in stock collapse.

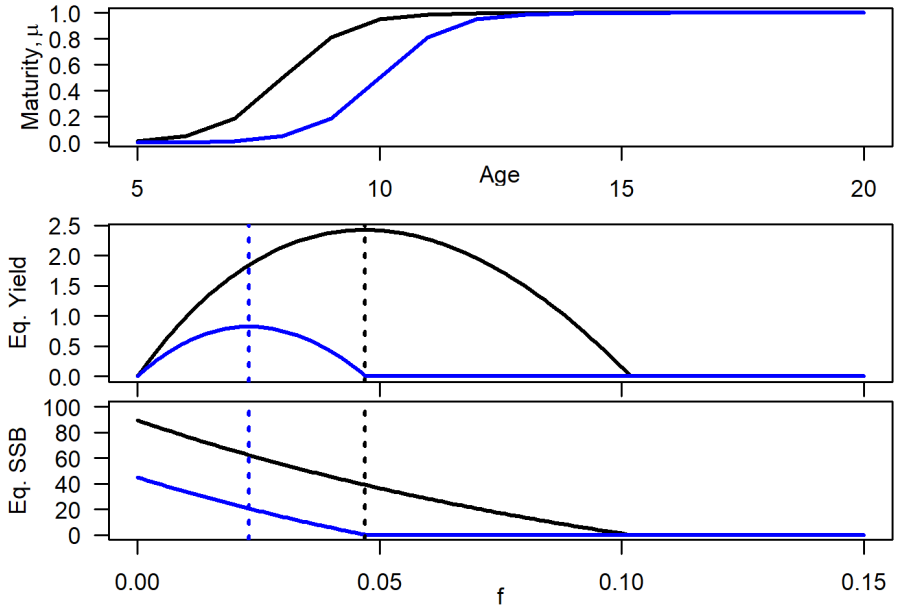

Figure 2.6: Maturity ogives and corresponding equilibrium yield and SSB curves. Maturities are defined by the $\mu_{8,10}$ (black) and $\mu_{10,12}$ distributions. Equilibrium yields and SSBs are calculated using per-recruit and the BH_{100} SR function. Dotted lines indicate f_{MSY} for the respective equilibrium curves.

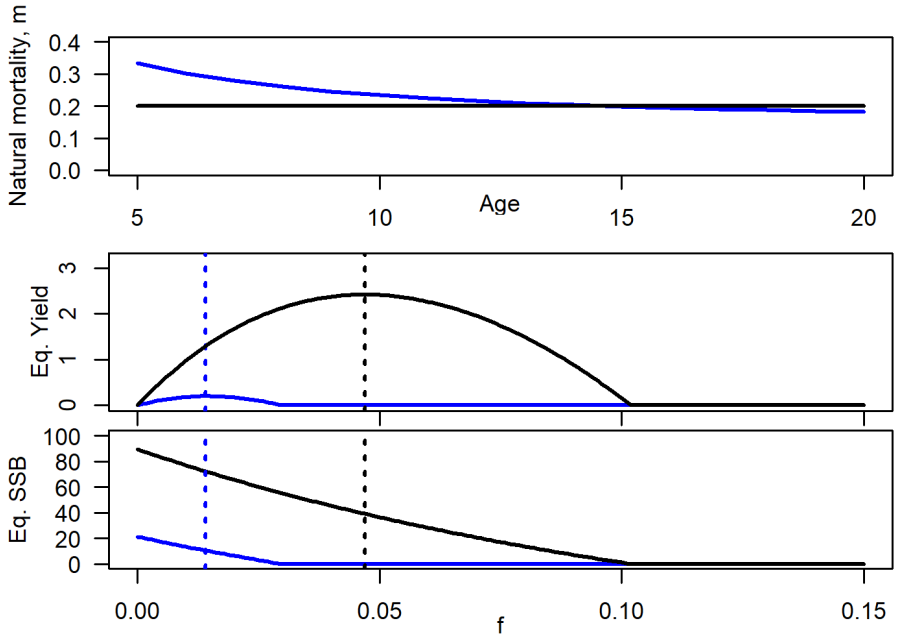

Figure 2.7: Natural mortality rate distributions and corresponding equilibrium yield and SSB curves. Natural mortality rates are described by the constant $m = 0.2$ (black) and the Lorenzen natural mortality rate (blue). Equilibrium yields and SSBs are calculated using per-recruit and the BH_{100} SR function. Dotted lines indicate f_{MSY} for the respective equilibrium curves.

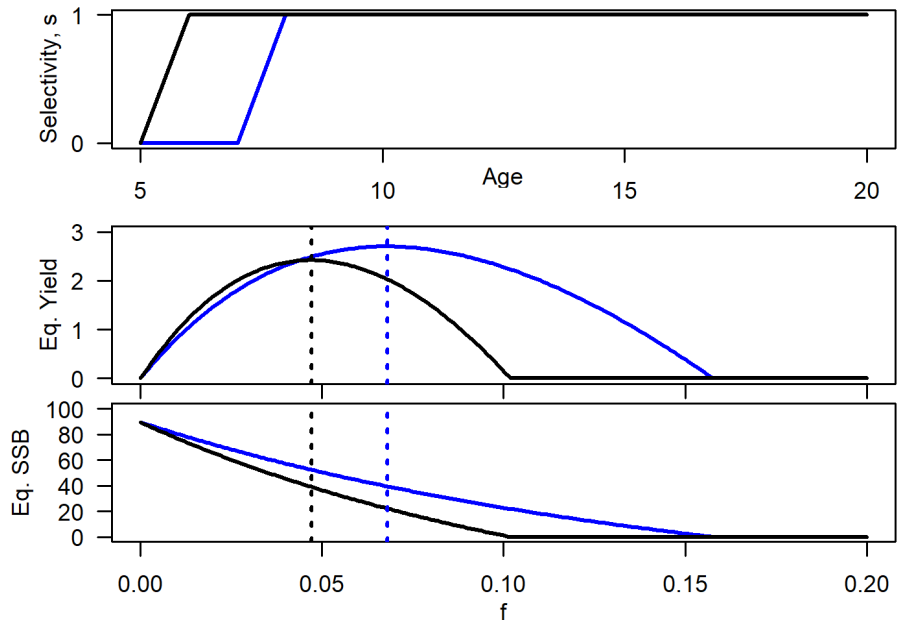

Figure 2.8: Selectivity curves and corresponding equilibrium yield and SSB curves. Selectivities are knife-edged, and fish are fully selected for ages $a \geq a_r$, where $a_r = 6$ (black) and $a_r = 8$ (blue). Equilibrium yields and SSBs are calculated using per-recruit and the BH_{100} SR function. Dotted lines indicate f_{MSY} for the respective equilibrium curves.

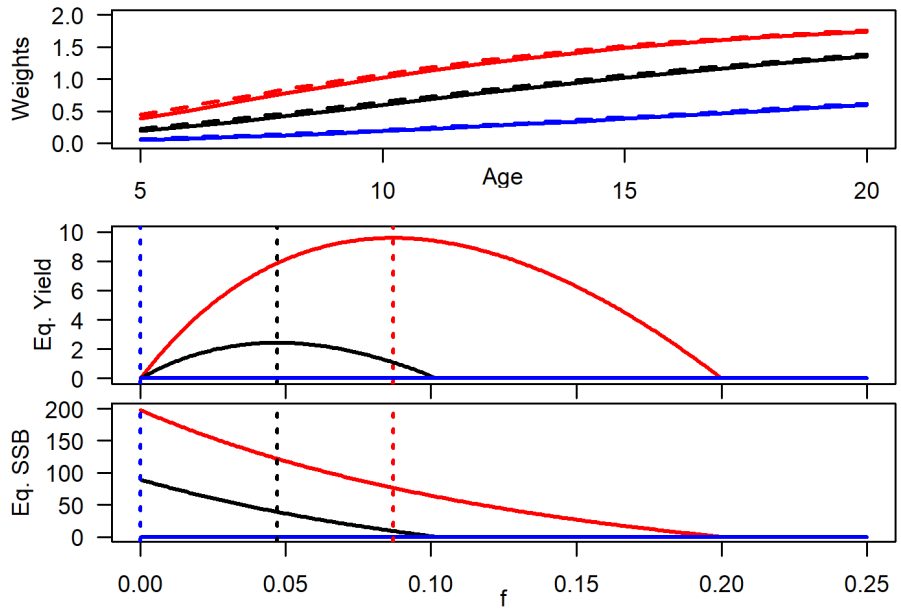

Figure 2.9: Weight-at-age distributions and corresponding equilibrium yield and SSB curves. Weights are modelled using a growth rate of $k = 0.1$ (black), $k = 0.05$ (blue), and $k = 0.15$ (red). Beginning-of-year weights (solid) use ages $a \in [5, 20]$, and mid-year weights (dashed) use ages $a \in [5, 20] + 0.5$. Equilibrium yields and SSBs are calculated using per-recruit and the BH_{100} SR function. Dotted lines indicate f_{MSY} for the respective equilibrium curves.

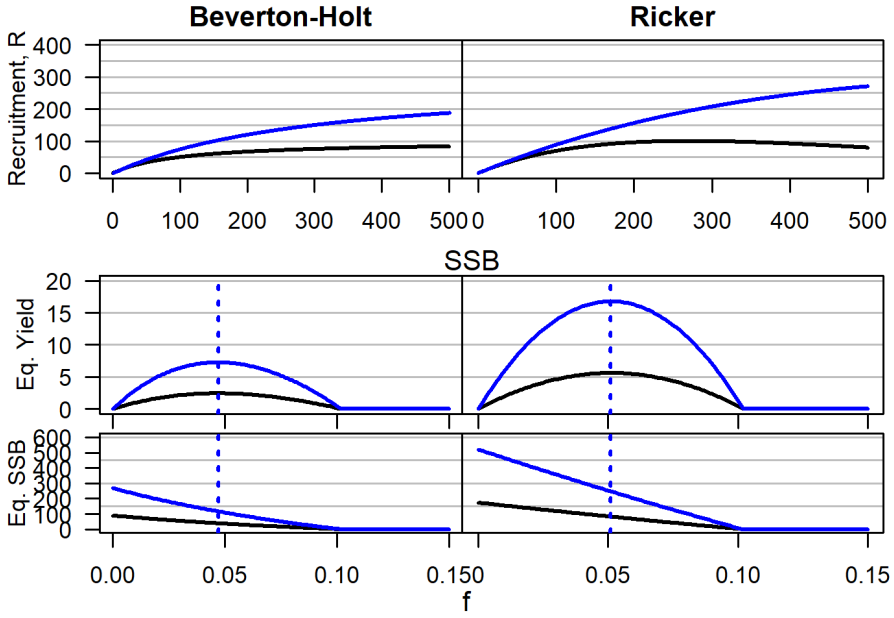

Figure 2.10: Stock-Recruitment using the BH (left) and RK (right) SR relationship, and corresponding equilibrium yield and SSB curves. Included are the BH_{100} and RK_{100} models (black), and the BH_{300} and RK_{300} models (blue). Equilibrium yields are calculated using per-recruit functions and equilibrium SSBs are calculated using the appropriate SR relationships. Dotted lines indicate f_{MSY} for the respective equilibrium curves.

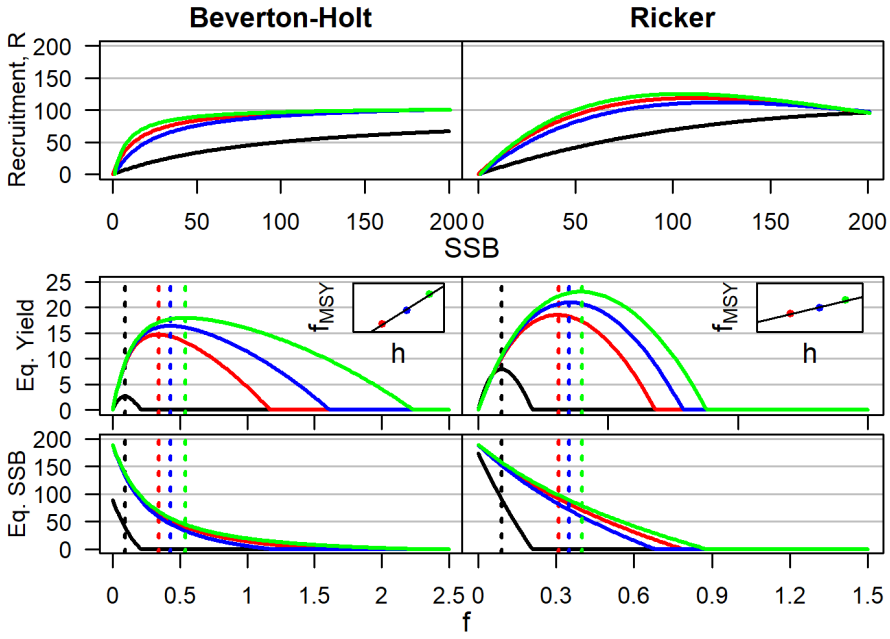

Figure 2.11: Stock-Recruitment using the BH (left) and RK (right) steepness re-parametrizations, and their respective equilibrium yield and SSB curves. Stock-recruitment is modelled using a steepness of $h = 0.69$ (blue), $h = 0.78$ (red), and $h = 0.86$ (green). The BH_{100} and RK_{100} models (black) are also displayed for comparison. Equilibrium yields are calculated using per-recruit functions, and equilibrium SSBs are calculated using the appropriate SR relationships. Dotted lines indicate f_{MSY} for the respective equilibrium curves. Inset plots display the approximate linear relationship between f_{MSY} and steepness for both the BH and RK SR models ($f \in [0.2, 0.6]$, $h \in [0.6, 0.9]$).

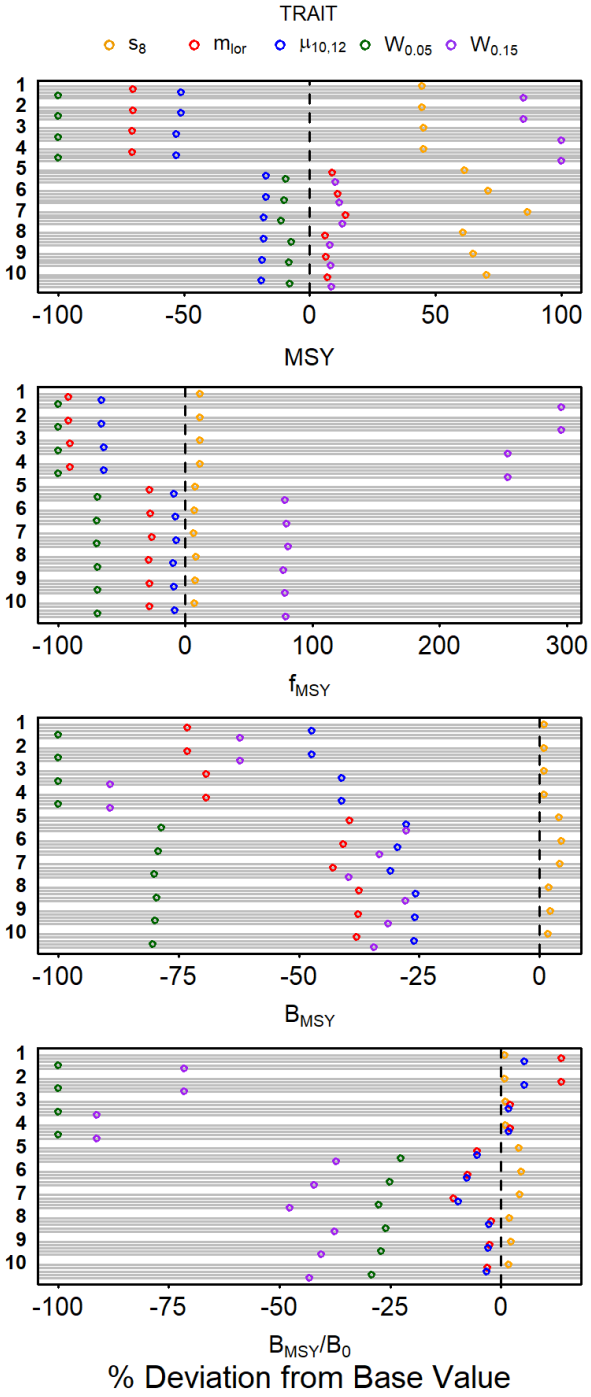

Figure 2.12: Percent deviation of RP outputs for alternative parametrizations with respect to outputs for base parametrizations. Row values are calculated using the following SR models: 1. BH_{100}, 2. BH_{300}, 3. RK_{100}, 4. RK_{300}, 5. BH_{low}, 6. BH_{med}, 7. BH_{up}, 8. RK_{low}, 9. RK_{med}, 10. RK_{up}. Base RP outputs (i.e. 0%) are indicated by dashed line.

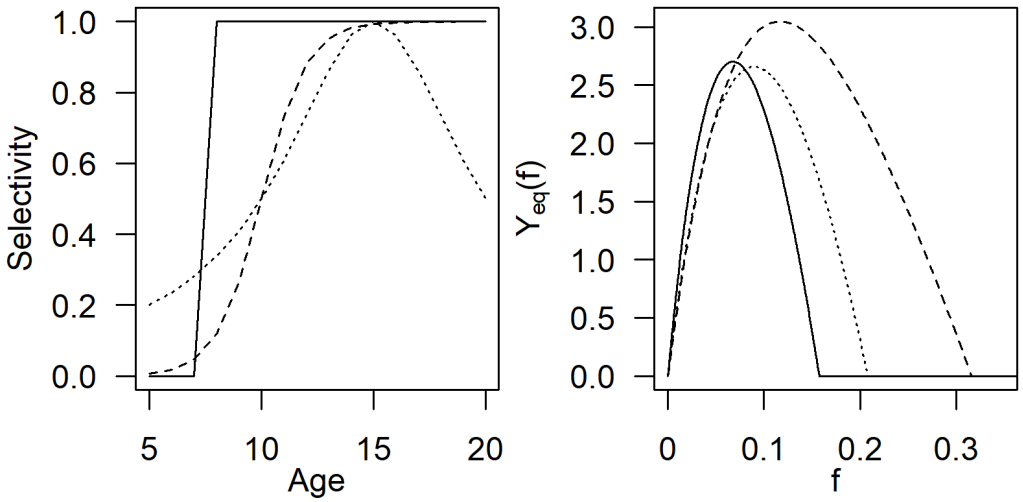

Figure 2.13: A knife-edged (solid), sigmoid (dashed), and dome-shaped (dotted) selectivity curve, with their corresponding equilibrium yield curves.

Chapter 3

The Two-Box Model

3.1 Methods

Transforming models from a spatially homogeneous to a spatially heterogeneous framework can be complicated because it requires *a priori* assumptions about the population structure and the connectivity and movement patterns of the stock. Further, spatial data is often limited and the application of spatial models is rare as a result. Although most stocks exhibit clear spatially-varying behaviour and characteristics, obtaining the required data and developing the appropriate models to fit the data has hitherto been undermined; this is no different for management RP calculations. Nevertheless, it is important to develop and a framework within which to incorporate such spatial data for when it is available. Understanding the base mechanisms of heterogeneous populations from spatial models beforehand may help with future implementations of these models.

In this chapter, we extend upon the one-box model framework for deriv-

ing MSY RPs to account for possible spatial variation in recruitment and life history characteristics, among other things, and investigate its impact on sustainability and yields. We do this assuming the stock has a *true* metapopulation structure with a source-sink dynamic, where the source and sink are distinct sub-populations within the stock, and fish transfer from source to sink via a larval advection process. Alongside the optimal two-box RPs, we also investigate the affects of alternative harvest strategies and compare them to the affects of one-box RPs when the stock is misdiagnosed as a single sympatric, panmictic population.

For our metapopulation model, we assume that fish move between at least two areas, and any movement of fish between areas is instantaneous (similar to the total mortality rate each year). We will start with a *two-box* model where fish transfer between two sub-populations. We consider a source-sink model, which is a commonly used two-box model (Lindegren et al., 2014; Wilberg et al., 2008) where fish flow unidirectionally from one region to the other (Figure 3.1a). That is, fish are only allowed to move from the source (typically higher reproduction rates and unfished) to the sink (typically lower reproduction rates and fished). We allow both sub-populations to be fished, and we initially assume both areas have equivalent reproduction rates, although later we allow for spatially-varying reproduction rates between the source and sink.

We use the transfer proportion, p, to denote the percentage of recruits that are advected annually, and we assume this percentage remains stable over time. For example, $p = 0.2$ means that 20% of recruits move from source to sink each year. We also assume that the SR relationships are

known, where transfer proportion, p, does not affect the SR relationships and only affects the SSB_{eq} and R_{eq} for each sub-population. To clarify, SR parameters are often estimated using abundance of recruits and total SSB, and transferring recruits would therefore affect how these parameters are estimated. However, equilibrium equations provide long-term solutions based on initial SR equations. We assume p is accounted for in SR parameter estimates and the initial SR relationships use the *true* parameters.

For a two-box model stock-recruitment is defined separately for each region. The SR relationships for each area are modelled via a density-dependent recruitment function, where the local recruitment is determined by the area occupied by the sub-population. Assume density dependence occurs via fish density in the stock area and only indirectly in terms of the total biomass of parents. Let ρ_R denote the density of recruits (i.e. number of recruits per unit area) and let ρ_S denote the density of adult biomass. The SR model is

$$\rho_R(\rho_S) = f(\rho_S; \alpha, \beta).$$

For example, the simple spatial BH model is

$$\rho_R(\rho_S) = \frac{\alpha\rho_S}{\beta + \rho_S}.$$

The total number of recruits in an area of size A is $R = \rho_R A$ and the total biomass of parents is $S = \rho_S A$. The relationship between R and S is

$$R(S; A, \alpha, \beta) = Af(\mu_S = S/A; \alpha, \beta).$$

For the BH model,

$$R(S; A, \alpha, \beta) = \frac{\alpha \rho_S A}{\beta + S/A} = \frac{A\alpha S}{A\beta + S}.$$

Consider a two-box model in which the density-dependent recruitment parameters are the same in each box. If the total area of the two boxes is A then the total BH model can be written

$$R(S; A, \alpha, \beta) = \frac{\alpha_o S}{\beta_o + S},\ \alpha_o = \alpha A \, and \, \beta_o = \beta A.$$

If the area of the first box is qA and the area of the second box is $(1-q)A$ then the BH model for box 1 has parameters $\alpha_1 = q\alpha_o$ and $\beta_1 = q\beta_o$ and the model for box 2 has parameters $\alpha_2 = (1-q)\alpha_o$ and $\beta_2 = (1-q)\beta_o$. For example, if the area of both boxes is half the total area then the BH parameters for each box are half of the parameters for both boxes. For a RK SR model, the density-dependent recruitment can be written

$$R(S; \alpha, \beta) = \alpha \rho_S A e^{-\beta S/A} = \alpha S e^{(-\beta_o)S}, \beta_o = \beta/A.$$

We assume areas $A_1 = A_2$, where $q = 1 - q = 0.5$, and the density of SSB, ρ_S, for the source and sink are equal to the SSB density for the one-box model. This is done to formulate a two-box SR model that has a total SSB and total recruitment equivalent to that of the one-box model, where is $S_1 = S_2 = S$ and $R_1(S_1) = R_2(S_2) = R(S)$ for some S. Note, the sum of recruitment $R(S_1) + R(S_2)$ is typically not the same as $R(S_1 + S_2)$ because recruitment is non-linear, but for our model $R(S_1) + R(S_2) = R(S_1 + S_2)$ if

$S_1 = S_2$.

If the SR parameters for each sub-population are defined based on the total area of the box (e.g. $\alpha_1 = \alpha_o A_1$ and $\alpha_2 = \alpha_o A_2$) where $A_1 = A_2$, it can be shown that the BH SR parameters α and β for the two-box model will be half that for the one-box model, and the RK SR parameter α will be the same as that for the one-box model while β will be twice that for the one-box model. For example, the one-box SR model BH_{100} where $\alpha = \beta = 100$ is equivalent to the two-box BH_{50} model where $\alpha = \beta = 50$, and the RK model RK_{100} where $\alpha = 1$ and $\beta = 1/(e \cdot 100)$ is equivalent to the two-box RK_{50} model where $\alpha = 1$ and $\beta = 1/(e \cdot 50)$. For the steepness models, unfished recruitment and SSB for the two-box model will be half that for the one-box model ($R_0 = 50$, $S_0 = 50 \cdot SPR(0)$).

Recall the per-recruit functions, like SPR, depend on the life history characteristics of a population. For a two-box model, we assume the life history characteristics, and therefore per-recruit functions, vary spatially. We assume the SPR functions are defined based on the region the recruits reside and grow in. That is, we assume the source and sink have distinct life history characteristics, and once recruits advect from the source they adapt the life history characteristics of the sink. We denote the per-recruits functions for the source as SPR_1 and YPR_1, and SPR_2 and YPR_2 for the sink. However, we initially assume life history characteristics in the source and sink are equal, and $SPR_1 = SPR_2$ and $YPR_1 = YPR_2$.

Equilibrium SSB for a one-box model may be derived as

$$SSB_{eq} = SPR(f)R_{eq}(f),$$

where equilibrium recruitment $R_{eq} = R(SSB_{eq})$. For a two-box model, the source and sink have different equilibrium recruitment functions, and the equilibrium SSB for each sub-population depends on the transfer proportion, p. For the source, a proportion p of the recruits are advected out of the area each year, and equilibrium recruitment, $R_{eq,1}$, is defined as $R_{eq,1}(f_1) = (1-p)R_1(SSB_{eq,1}(f_1))$, where $(1-p)$ recruits are left in the source after advection and f_1 is the fishing mortality rate in the source. That is, $R_1(SSB_{eq,1}(f_1))$ is the *pre-advection* (i.e. local) equilibrium recruitment, and $(1-p)R_1(SSB_{eq,1}(f_1))$ is the *post-advection* (i.e. residual) equilibrium recruitment for the source. Similar to the one-box model, equilibrium SSB in the source using the BH model is

$$SSB_{eq,1}(f_1) = (1-p)\alpha_1 SPR_1(f_1) - \beta_1, \tag{3.1}$$

where α_1 and β_1 are the SR parameters for the source, and $SPR_1(f_1)$ is the SPR function for the source.

Equilibrium recruitment in the sink component, $R_{eq,2}$, depends on both local recruitment, R_2, and recruitment in the source, R_1, since some proportion of recruits from the source immigrate into the sink annually. For example, if $R_1 = R_2 = 100$ and $p = 0.1$, then the post-advection recruitment in the source is 10% less than what was locally produced, i.e. $R_1 = 90$, and recruitment in the sink increases by the the amount, i.e. $R_2 = 110$. The definition for equilibrium recruitment generally assumes $R_{eq} = R(SSB_{eq})$, but for the sink this definition is incomplete because the sink may rely on the source for recruits. Equilibrium recruitment in the sink is the sum of local

recruitment, $R_2(SSB_{eq,2})$, and a proportion p of equilibrium recruitment in the source, $pR_1(SSB_{eq,1})$. Using a BH SR model, $SSB_{eq,2}$ is

$$SSB_{eq,2} = \frac{\alpha_2 SSB_{eq,2}}{\beta_2 + SSB_{eq,2}} SPR_2(f_2) + p\frac{\alpha_1 SSB_{eq,1}}{\beta_1 + SSB_{eq,1}} SPR_2(f_2), \tag{3.2}$$

where $SSB_{eq,1} = SSB_{eq,1}(f_1)$ and $SSB_{eq,2} = SSB_{eq,2}(f_1, f_2)$, and α_2 and β_2 are the sink SR parameters. Recall, initially $SPR_1(f) = SPR_2(f)$. In Appendix A we show that the solution to Equation 3.2 is

$$SSB_{eq,2}(f_1, f_2) = \frac{-B(f_1, f_2) \pm \sqrt{B(f_1, f_2)^2 + 4\beta_2 \cdot p \cdot R(SSB_{eq,1}(f_1))SPR_2(f_2)}}{2}, \tag{3.3}$$

where

$$B(f_1, f_2) = \beta_2 - \alpha_2 SPR_2(f_2) + p \cdot R_1(SSB_{eq,1}(f_1))SPR_2(f_2). \tag{3.4}$$

This is different than the one-box result because the sink population is affected by recruitment and consequently fishing in the sink and source regions. For the BH model, $SSB_{eq,2}$ relies on the quadratic formula, meaning there are two solutions. However, it can be shown that the negative-root solution always returns a negative SSB_{eq}, and the only plausible solution is the positive-root (see Appendix A).

Equilibrium SSB for the RK model is

$$SSB_{eq,1}(f_1) = \frac{ln((1-p)\alpha_1 SPR_1(f_1))}{\beta_1}, \tag{3.5}$$

for the source, which is similar to equilibrium SSB for the one-box model.

Equilibrium SSB for the sink has no analytic solution when using the RK SR model. We derive the values for $SSB_{eq,2}$ numerically, which is detailed below.

For the steepness version of the BH model,

$$SSB_{eq,1}(f_1) = \frac{S_0}{5h_1 - 1}\left(\frac{(1-p)\cdot 4h_1 R_0 SPR_1(f_1)}{S_0} + h_1 - 1\right), \tag{3.6}$$

for the source, where h_1 is the steepness for the source,

$$SSB_{eq,2}(f_1, f_2) = \frac{-B(f_1, f_2) + \sqrt{B(f_1, f_2)^2 + 4C(f_1, f_2)(5h_2 - 1)/S_0}}{2(5h_2 - 1)/S_0}, \tag{3.7}$$

for the sink, where h_2 is the steepness for the sink,

$$B(f_1, f_2) = (1-h_2) - \frac{4h_2 R_0}{S_0} SPR_2(f_2) - p\cdot\frac{5h_2 - 1}{S_0} R_{eq,1}(SSB_{eq,1}(f_1)) SPR_2(f_2), \tag{3.8}$$

and

$$C(f_1, f_2) = p \cdot SPR_2(f_2)(1 - h_2) R_{eq,1}(SSB_{eq,1}(f_1)). \tag{3.9}$$

For the steepness version of the RK SR model,

$$SSB_{eq,1}(f_1) = S_0\left(1 + 0.8\frac{ln((1-p)\cdot R_0 SPR_1(f_1)/S_0)}{ln(5h)}\right), \tag{3.10}$$

for the source. No analytic equation can be derived for equilibrium SSB for the sink using either the conventional or steepness versions of the RK SR model. Instead, numerical solutions are calculated from the definition of

equilibrium SSB. For the standard RK model, equilibrium SSB is defined as

$$S_2 = \alpha_2 S_2 e^{-\beta_2 S_2} SPR_2(f_2) + p \cdot \alpha_1 S_1 e^{-\beta_1 S_1} SPR_2(f_2), \tag{3.11}$$

where $S_2 \equiv SSB_{eq,2}(f_1, f_2)$ and $S_1 \equiv SSB_{eq,1}(f_1)$. Numerical solutions for equilibrium SSB in the sink for any f_1 and f_2 can be found by solving for the roots of Equation 3.11. For some values of f_1 and f_2, two *Real* roots exists, one of which is zero, and in such cases the non-zero root is used. A similar numerical solution is found for $SSB_{eq,2}$ for the steepness RK model, where equilibrium SSB for the sink is defined as

$$S_2 = \frac{R_0}{S_0} S_2 e^{ln(5h_2)(1-S_2/S_0)/0.8} SPR_2(f_2) + p\frac{R_0}{S_0} S_1 e^{ln(5h_1)(1-S_1/S_0)/0.8} SPR_2(f_2). \tag{3.12}$$

As described above, we illustrate our two-box equilibrium results using the BH_{50} and RK_{50} SR models. When using the steepness formulations BH_h and RK_h, we assume a constant steepness of $h_1 = h_2 = h = 0.78$. Furthermore, we assume a a set of base conditions for life history characteristics for both boxes, where the selectivity curve is defined by s_6, the natural mortality rate $m_{constant} = 0.2$, the maturity ogive $\mu_{8,10}$, and the growth rate $k = 0.1$ (see Table 2.1 for values). We assume these life history characteristics, along with the SR relationships, are consistent between both regions unless specified otherwise.

In Chapter 2, we calculated equilibrium yields using both a forecast projection and per-recruit functions, and derived MSY RPs to confirm both methods produce the same values. We perform the same comparison for

two-box model RPs. The forecast model is modified to calculate values for each sub-population separately, and recruitment advection is explicitly modelled. The two-box forecast model includes a tertiary *region* component, r, e.g. $N_{y,a,r}$, where $r = 1$ indicates values for the source and $r = 2$ indicates values for the sink. For the one-box model, we defined abundance at the first age, $N_{y,a_0} = R(SSB_{y-5})$. For the two-box model, we have two arrays of abundances, calculated as $N_{y,a_0,1} = (1-p)R_1(SSB_{y-5,r=1})$ and $N_{y,a_0,2} = R_2(SSB_{y-5,r=2}) + pR(SSB_{y-5,r=1})$. All other stock values for each sub-population are calculated according to Table 2.2. Optimal MSY RPs are based on the sum of yields from both sub-populations, i.e. $Y_{y=500,r=1} + Y_{y=500,r=2}$. We use the forecast projection method to verify MSY RP outputs are equal to those derived through the per-recruit function approach.

Equilibrium yield is calculated for each region. When using the per-recruit and SR function method, equilibrium yield for the source is

$$Y_{eq,1}(f_1) = \frac{YPR(f_1)}{SPR_1(f_1)} SSB_{eq,1}, \tag{3.13}$$

equilibrium yield for the sink is

$$Y_{eq,2}(f_1, f_2) = \frac{YPR(f_2)}{SPR_2(f_2)} SSB_{eq,2}(f_1, f_2), \tag{3.14}$$

and the total equilibrium yield is

$$Y_{eq,tot}(f_1, f_2) = Y_{eq,1}(f_1) + Y_{eq,2}(f_1, f_2). \tag{3.15}$$

Equilibrium yields, as well as SSB and recruitment, are calculated for a range of f_1 and f_2 to demonstrate the effects spatially-varying f's have on total yield. Moreover, we use the equilibrium yield functions to derive MSY RPs. Our interest is to maximize total yield with respect to both f_1 and f_2, simultaneously, and observe how these f's change as the transfer proportion, p, changes. The f's that optimize total yield will be denoted $f_{MSY,1}$ and $f_{MSY,2}$ for the source and sink, respectively. MSY, total B_{MSY}, and total biomass depletion will also be calculated for the two-box model using the appropriate SSB_{eq} equations. Total $B_{MSY} = B_{MSY,1} + B_{MSY,2}$ and total biomass depletion is $B_{MSY}/B_0 = (B_{MSY,1} + B_{MSY,2})/(B_{0,1} + B_{0,2})$, where $B_{0,r}$ is the unfished equilibrium SSB for the source (r=1) and sink (r=2). We also calculated these RPs for alternate parametrizations of life history characteristics, similar to in Chapter 2. In this case, MSY RPs are calculated from independent changes in source and sink parameters, to see how these changes can affect estimates for both areas. Similar to in Chapter 1, we optimize $Y_{eq,tot}$ and derive f_{MSY} using the *nlminb* function in **R**.

Many fisheries are restricted by the presence of Marine Protected Areas (MPAs). MPAs are regions in which fishing is either limited or prohibited to protect marine habitats or vulnerable fish species. However, on the boundaries of these areas where spillover occurs, fish are transferred into fished waters, creating a dynamic similar to the source-sink system discussed above (Figure 3.1b). Source-sink dynamics are often discussed alongside MPA and marine reserve implementation (e.g., Neubert, 2003; Crowder et al., 2000). Understanding the effects of spillover from MPAs is important to account for when defining spatial management RPs. If the metapopulation model above

assumes fishing does not occur in the source (i.e. $f_1 = 0$), an MPA-like system is replicated. Of course, we assume that only recruits spillover to the fished area, and the spillover is unidirectional. We define f_{MPA} as the f_2 that maximizes $Y_{eq,tot}$ when no fishing occurs in the MPA. RPs for an MPA-like system are compared to the optimal RPs for the two-box model to investigate how MPAs affect MSY RPs. In our simple setting an MPA-like harvest strategy has to be sub-optimal compared to fishing with optimal f's in both regions, and we investigate the loss of fishery efficiency caused by the MPA (i.e. compared $Y_{eq,tot}(f_1 = 0, f_2 = f_{MPA})/Y_{eq,tot}(f_1 = f_{MSY,1}, f_2 = f_{MSY,2})$).

We also investigate the optimal f assuming the fishing mortality rates in both sub-populations are *uniform*, i.e. $f_1 = f_2 = f_U$. This harvest strategy is investigated to examine the consequences of a spatially balanced harvest strategy, which is consistent with advice sometimes given in stock assessments that catches should not be concentrated in ways that result in high exploitation rates on any stock components (e.g., DFO, 2014). Even without setting separate f RPs for each region, incorporating a spatial structure into stock models can affect RP values. If the objective of a fishery is to sustain a fish stock and avoid sub-population extirpation, then f_U may be valuable. Similar to above, this harvest strategy is sub-optimal, and we investigate the loss of fishery efficiency (i.e. the ration of $Y_{eq,tot}(f_1 = f_U, f_2 = f_U)/Y_{eq,tot}(f1 = f_{MSY,1}, f_2 = f_{MSY,2})$).

So far we have assumed that both sub-populations have equal reproduction rates. We will refer to this as an *Equivalent* (EQ) system. However, it is common for source-sink systems, and also typical when designating MPAs, for the source (or MPA) to have higher reproduction rates than the sink. We

emulate a similar *High-to-Low* (HL) system, where recruitment is relatively greater in the source, by giving the source and sink different SR relationships:

1. For a BH SR model, the density-independent parameter (i.e. α) typically does not vary spatially (White, 2010), and we only vary β between the source and sink. For the BH_{50} model, we maintain $\alpha = \beta = 50$ in the sink, but let $\alpha = 50$ and $\beta = 40$ in the source, since a lower density-dependent term will increase recruitment. Changing β in a BH model does not affect the asymptotic (as $S \to \infty$) max recruitment. Since $SaO = \alpha/\beta$ for a BH model with the above SR parameters, $SaO = 1.25$ for the source and $SaO = 1$ for the sink, while $R_{max} = \alpha = 50$ is constant for both.

2. Extending this rationale to the RK SR model, we assign the source the same SaO and R_{max} for the RK_{50} as the BH_{50} model, where $SaO = \alpha$ and $R_{max} = \alpha/(e \cdot \beta)$. Therefore, we let $\alpha = 1.25$ and $\beta = 1.25/(e \cdot 50)$, since we define β as $\beta = \alpha/(e \cdot R_{max})$. Scaling β equally with α will force R_{max} to remain constant, while changing the SaO.

We also apply similar changes to the BH_h and RK_h models.

3. Steepness is directly related to the SaO, where $SaO = 4h/(1-h)$ for the BH (see White, 2010) and $SaO = \alpha = e^{ln(5h)/0.8}$ for the RK (derived from the recruitment function; see Punt and Cope, 2017). Proxy values of steepness can be calculated for the BH_{50} and RK_{50} SR models as $h = SaO/(4 + SaO)$ and $h = e^{0.8ln(SaO))}/5$ for the BH and RK, respectively. For the BH, $h_{source} = 0.24$ and $h_{sink} = 0.2$, where h_{source} is 1.2 times greater than h_{sink}. If we increase the SaO in the

source for the steepness models by the same amount as the standard models (that is, by 1.2), and $h_{sink} = 0.78$, then $h_{source} = 1.2h_{sink} = 0.93$.

4. For the RK, $h_{source} = 0.24$ and $h_{sink} = 0.2$, as well, and the source steepness is 1.2 times greater than the sink, so $h_{sink} = 0.78$, then $h_{source} = 1.2h_{sink} = 0.93$, identical to the BH. We calculate the same RPs as above (e.g. $f_{MSY,1}$ & $f_{MSY,2}$, f_{MPA}, and f_U) using these spatially varying reproduction rates, and compare values to those for the EQ system.

A *Downstream Advection* (DA) is also common in source-sink systems, where recruits transfer from a colder, northern area into warmer waters in the south. It is well known that colder temperatures promote slower growth rates, and similarly warmer waters promote faster growth rates. Assuming that the reproduction rates in the source and sink are equal, we calculate MSY RPs with a spatially varying growth rates, where $k_{source} = 0.075$ and $k_{sink} = 0.1$. Model outputs are compared to values for the two-box EQ and HL systems..

Lastly, we calculate the same MSY RPs assuming a high-to-low reproduction system with a downstream advection (HL & DA). MSY RP outputs from this model will be compared to the previous three (i.e EQ, HL, and DA).

3.2 Results

3.2.1 Verification of the Two-Box Forecast Projection Method

A forecast projection (2000 years) was iterated for a range of f_1 and f_2 values, where $f_1, f_2 \in [0, 0.5]$ and $p = 0.2$. Stock values, e.g. abundances, for both sub-populations approach an equilibrium over time, similar to a one-box forecast projection (Figure 3.2), and the sum of source and sink abundances (and all other values) also stabilize. We calculated MSY RPs for the two-box model using the forecast projection and compared them to results using the per-recruit functions (Table 3.1). Results from both methods provide approximately equal outputs. The discrepancies between values are due to the precision of f in the forecast projection (0.005), and values derived through the per-recruit functions are assumed to be the exact values. For all further RP estimations, we exclusively use the per-recruit functions.

3.2.2 EQ System Equilibrium Results

Equilibrium yield, SSB, and recruitment for the source and sink were calculated under an EQ system for a range of f_1 and f_2 values, and for several values of p, using the BH_{50} (Figure 3.3), RK_{50} (Figure 3.4), BH_h (Figure 3.5), and RK_h (Figure 3.6) SR models. Total equilibrium values were also calculated as the sum of equilibrium values for the source and sink. Note, equilibrium recruitment was calculated as $R_{eq,1} = R_1(SSB_{eq,1})$

for the source and $R_{eq,2} = R_2(SSB_{eq,2})$ for the sink. This is the pre-advection (i.e. local) recruitment, as opposed to the post-advection recruitment, which would be calculated as $R_{eq,1} = (1-p)R_1(SSB_{eq,1})$ for the source and $R_{eq,2} = R_2(SSB_{eq,2}) + pR_1(SSB_{eq,1})$ for the sink (see Figure 3.7). However, the total equilibrium recruitment remains constant before and after advection.

Generally, equilibrium values had a larger scale when using the steepness SR relationships compared to the conventional SR models. That is, both the source and sink could provide larger yields, and could provide non-zero yields for a larger range of f_1 and f_2 values. This is because the steepness models had higher reproduction rates and could sustain higher harvest rates.

When $p = 0$, equilibrium values in the source for any $f_1 = f$ were the same for equilibrium values for the same $f_2 = f$ in the sink. For example, using the BH_{50} SR model, $Y_{eq,1}(f_1 = 0.05) = Y_{eq,2}(f_2 = 0.05) = 1.21$, when $p = 0$. Also when $p = 0$, equilibrium SSB and recruitment were greatest when $f_1 = f_2 = 0$, while equilibrium yield was greatest (i.e. maximized) for some non-zero $f_1 = f_{MSY,1}$ and $f_2 = f_{MSY,2}$, where $f_{MSY,1} = f_{MSY,2}$ (see section 3.2.4). Equilibrium values in the source were independent of f_2 for all p. When $p = 0$, equilibrium values for the sink were independent of f_1. This is to be expected, since the source and sink are unconnected when $p = 0$. For any $p > 0$, equilibrium values in the sink were dependent on f_1 and f_2. Furthermore, equilibrium values in the source generally decreased and values in the sink generally increased for larger p's, although this depends on the value of p and the sustainability of the source (see section 3.2.3).

It is difficult to discern changes in equilibrium values from changes in

f_1, f_2, and p in Figures 3.3 to 3.6. To further elucidate these changes, we calculated the equilibrium yields for fixed p's for a range of f_1's and f_2's (Figure 3.8), as well as for fixed f_1's and f_2's for a range of p's (Figure 3.9). Equilibrium yields for these figures were calculated using the BH_{50} SR model for illustration purposes, since all other SR models produce similar trends in equilibrium results. We also calculated equilibrium yields, SSB, and recruitment over a range of p's for $f_1 = f_2$ for the BH_{50} model (Figure 3.10). The corresponding equilibrium results for the RK_{50}, BH_h, and RK_h SR models are also provided (Figures B.1 to B.3; Appendix B).

For a fixed value of f_2, equilibrium yields in the source decreased as p increased, and the equilibrium yield for some f, $Y_{eq,1}(f_1 = f)$ when $p = 0$ was greater than the yield for the same f for any $p > 0$ (Figure 3.8a). For certain f's, equilibrium yield in the source was zero because the source did not persist. Equilibrium yields in the sink typically increased as p increased (Figure 3.8b), but if the source did not persist, equilibrium yields in the sink were constant because f_2 was constant. For a fixed value of f_1, equilibrium yields in the source did not change with f_2 because the source was independent from the sink. However, equilibrium yields still decreased as p increased (Figure 3.8d) when f_1 was constant.

Equilibrium yields in the sink may increase or decrease with increases in p (e.g. Figures 3.8b & 3.8e) depending on the value of p. Furthermore, equilibrium yield in the sink for large f_2's was zero when $p = 0$, but if $p > 0$ (and the source persists) equilibrium yield in the sink was never be zero (Figure 3.8e). This is because the source provides a constant supply of recruits to the sink, and even if fishing temporarily depletes the sink, the

sink sub-population will be restored by the advecting recruits. Depending on p, the equilibrium yield in the sink from large f's may be insubstantial, but they cannot be zero, i.e. $\lim_{f_2 \to \infty} Y_{eq,2}(f_1, f_2) > 0$.

3.2.3 Source and Sink Persistence

Increases in p decreased R_{eq} and subsequently SSB_{eq} and Y_{eq} in the source, but increased R_{eq}, SSB_{eq} and Y_{eq} in the sink (e.g. Figure 3.10) for low p's. As p increased, more recruits were advected out of the source each year. This advection can be thought of as an increase in local recruitment in the sink and a decrease in local recruitment in the source, where the source has a lower reproduction rate than the sink. Indeed, the BH SSB_{eq} for the source has a negative linear relationship with p (see Equations 3.1 and 3.6), and the RK SSB_{eq} for the source has a negative logarithmic relationship with p (see Equations 3.5 and 3.10). As a result, p directly affected the sustainability of the source. As p increased, equilibrium recruitment and SSB in the source strictly decreased.

If p was large enough, the source could not be sustainably fished, where even a low fishing rates could deplete the source (e.g. Figure 3.8a). For certain values of p, the source became depleted even with no fishing. The conditions of source depletion are detailed below. Meanwhile, the sink could still allow fishing as p increased, despite the source being unfishable (e.g. Figures 3.8b). When p was low, the sustainability of the sink (i.e. $SSB_{eq,2}$) increased with p (e.g. Figure 3.10), and increasing p allowed greater sustainable harvest rates (e.g. Figures 3.8b & 3.8e). However, there are exceptions

to this–where increasing p does not necessarily increase harvest rates–which are also discussed below.

For any p where the source sub-population persisted, there was some f that would lead to extirpation (see Figure 3.8a). That is, there is some f where the equilibrium SSB in the source goes to zero. The f for which $SSB_{eq} = 0$ is the upper limit for sustainable fishing, and fishing rates beyond this threshold are unsustainable (i.e. overfishing). This value is sometimes denoted f_{crash} in fisheries science (see Cook, 1998). We denote this as $f_{crash,1}(p)$, since its value depends on p. Values for $f_{crash,1}(p)$ can be derived numerically, where

$$SSB_{eq,1}(f_{crash,1}(p)) = 0, \tag{3.16}$$

for any p. This may also be derived as $SaO = 1/((1-p)SPR_1(f_{crash,1}))$, where the slope of the replacement line cannot exceed slope of the SR curve at the origin (refer to Figure 2.5). The value for $f_{crash,1}(p)$ decreases as p increases, where the upper limit of fishing in the source decreases when more fish transfer out each year, and $f_{crash,1}(p)$ is greatest when $p = 0$ such that $f_{crash,1}(p > 0) < f_{crash,1}(p = 0)$. Sustainable yields can be obtained from the source as long as $f_1 < f_{crash,1}(p)$ for any p (see Figure 3.11). That is, the source can sustain more fishing when no recruits transfer to the sink (Figure 3.8a).

As p increased, equilibrium SSB_{eq} in the source decreased, and $f_{crash,1}(p)$ decreased with it since less fishing was required to deplete the source population. When $f_{crash,1}(p) = 0$, the source is extirpated regardless of fishing because too many recruits transfer from the source to allow the population

to persist. The p value for which $f_{crash,1}(p) = 0$ is denoted p_{ex}, where the sub-population in the source is effectively extirpated when $p = p_{ex}$. Also, $f_{crash,1}(p) = 0$ for any $p \geq p_{ex}$. Values for p_{ex} can be derived analytically from the SSB_{eq} equation for the source. The value for p_{ex} is defined as the p for which $SSB_{eq,1}(f_1 = 0) = 0$. For example, consider the BH model, where equilibrium SSB is expressed by Equation 3.1. The value for p_{ex} is defined as

$$(1 - p_{ex})\alpha_1 SPR_1(0) - \beta_1 = 0 \tag{3.17}$$

Solving Equation 3.17 for p_{ex} gives $p_{ex} = 1 - \beta_1/(\alpha_1 SPR_1(0))$.

Using the RK model where SSB_{eq} is expressed by Equation 3.5, it can be shown that $p_{ex} = 1 - 1/(\alpha_1 SPR_1(0))$. Values for p_{ex} were derived for each SR model (Table 3.2). For our choices of α_1 and β_1, p_{ex} will be the same for the BH_{50} and RK_{50} SR models, because $\beta_1/\alpha_1 = 100/100$ for the BH model and $1/\alpha_1 = 1/1$ for the RK model (and $SPR_1(0)$ is constant).

Equilibrium values in the sink depended on f_1 when $p > 0$ provided $f_1 < f_{crash,1}(p)$ and $p < p_{ex}$. If $f_1 \geq f_{crash,1}(p)$ or $p \geq p_{ex}$, equilibrium values in the sink were independent of f_1, since the source sub-population was extirpated. There were no values of p that resulted in sink extirpation the same way that $p \geq p_{ex}$ lead to extirpation in the source (see Figures 3.9b and 3.9e). As long as the source persisted and the sub-populations were connected, there were no values of p for which the sink sub-population was depleted, regardless of f. If the source did not persist, however, the sink was effectively a one-box system which could be depleted. In fact, the equilibrium SSB for the sink when the source is extirpated, that is when $R_{eq,1} = 0$ (i.e.

when $p = 0$, $p \geq p_{ex}$, or $f_1 \geq f_{crash,1}(p)$), is the same as the equilibrium SSB for the one-box model. The value of f that depletes the sink when no recruits advected from the source is denoted $f_{crash,2}$, and can be derived from $SSB_{eq,2}$ where $SSB_{eq,2}(f_1, f_{crash,2}) = 0$, and f_1 is irrelevant since the source is depleted. For, example, for the BH SR model, $f_{crash,2}$ can be derived as

$$SSB_{eq,2}(f_{crash,2}) = \alpha_2 SPR_2(f_{crash,2}) - \beta_2 = 0. \tag{3.18}$$

Note, $f_{crash,2}$ does not depend on p since the sink can only crash if there are no transferring recruits.

3.2.4 EQ MSY RP Results

MSY RPs were calculated for various p's for each SR model, and RPs were tabulated for select values of p (Table 3.3). Recall that MSY RPs are calculated by optimizing the total equilibrium yield, rather than the equilibrium yield of each sub-population, independently. When $p \geq p_{ex}$, all MSY RPs in the source are zero, since the source is extirpated. In this case, because of our choices for SR parameters, and because recruitment in the source and sink were equal, MSY and B_{MSY} for the sink were half the values for MSY and B_{MSY} when $p = 0$, while $f_{MSY,2}$ and biomass depletion when $p \geq p_{ex}$ were the same as the values when $p = 0$ (see Table 3.3). For example, for the BH_{50} SR model, $p_{ex} = 0.48$ (Table 3.2), so for a value of $p = 0.6 > p_{ex}$, $MSY = 1.211$ which is half $MSY = 2.421$ when $p = 0$; also $B_{MSY}/B0 = 0.438$ when $p = 0$ and when $p = 0.6$, and $f_{MSY,2} = 0.047$ when $p = 0$ and when $p = 0.6$ (Table 3.3).

When $p = 0$, f_{MSY}, B_{MSY}, and biomass depletion were the same for both regions (Table 3.3); MSY was also the same for both regions. This was also the case for equilibrium values (e.g. Figure 3.3). When populations were unconnected, they behaved as isolated, independent populations. Moreover, when $p = 0$, the total MSY, B_{MSY}, and biomass depletion from both sub-populations were equal to that of the one-box model, assuming life history characteristics and SR relationships were the same for both regions (see Table 3.3). That is to say, MSY, B_{MSY}, and biomass depletion for each area can be derived from one-box model results if the populations are unconnected.

For some p values, obtaining the optimal sustainable yield involves fishing in the source, that is $f_{MSY,1} \neq 0$. This is typical for moderate to low p's but for high p's, the source cannot be fished for yields to be optimized. At some p, and for all larger p values, $f_{MSY,1} = 0$; this p value is denoted p_{f0}. Our MSY RPs are derived by maximizing the total equilibrium yield with respect to f_1 and f_2. When $f_{MSY,1} = 0$ the optimal sustainable yield is obtained by exclusively fishing in the sink. The source may still persist when $p \geq p_{f0}$ as long as $p < p_{ex}$, and the source may still be fished so long as it persists, but fishing in the source when $p \geq p_{f0}$ provides sub-optimal yields. In other words, the upper limit of fishing $f_{crash,1}(p = p_{f0}) > 0$ and fishing in the source is possible, but not recommended. Values for p_{f0} were calculated for each SR relationship (Table 3.2), alongside values for p_{ex}. Generally, p_{f0} and p_{ex} increase concomitantly with productivity, and both values were larger when using the steepness SR models compared to the values for the standard SR models. This is because the steepness models had greater reproduction rates, and greater reproduction rates can accommodate larger harvest rates

as well as reduce the risk of extirpation.

When $p = 0$, $f_{MSY,1} = f_{MSY,2}$ (see Table 3.3). As p increased, $f_{MSY,1}$ decreased and $f_{MSY,2}$ increased until $p = p_{f0}$ (Figure 3.12), where $f_{MSY,1} = 0$. For values of p where $p \geq p_{f0}$, $f_{MSY,2}$ decreased, and the total yield was only dependent on f_2 because the source was not fished. As p increased further (to p_{ex}), the source sub-population became extirpated. Once the source was extirpated, increases in p no longer affected $f_{MSY,2}$, and $f_{MSY,2}$ remained at a constant value, which was the same value for $f_{MSY,2}$ when $p = 0$. For all values of p, $f_{MSY,2}$ was greater than or equal to f_{MSY} for the one-box model, and $f_{MSY,1}$ was always equal to it or less (see Table 3.3).

Total B_{MSY} strictly decreased as p increased until it reached half of the B_{MSY} when $p = 0$ (Figure 3.13); B_0 also decreased to half the B_0 when $p = 0$. MSY decreased as p increased, and was largest when $p = 0$ (see Table 3.3). Biomass depletion changed very little as p increased (Figure 3.13). This is because B_{MSY} and B_0 changed approximately the same with p, where SSB_{eq} scaled with p. Values for biomass depletion peaked (i.e. biomass was least depleted) when $p = p_{f0}$ for each SR model, otherwise it remained at or close to the biomass depletion for the one-box model.

When $p \geq p_{ex}$ and the source sub-population is effectively extirpated, the sink sub-population behaves as a spatially homogeneous population, i.e. a single population stock. Therefore, we must assume $p < p_{ex}$ when using a spatially explicit model to derive MSY RPs. That is to say, there would not be two populations if $p \geq p_{ex}$. For some RP calculations, we considered a constant, moderate transfer proportion of $p = 0.2$ (see Table 3.4). At this p, the source was still fishable (i.e. $p < p_{f0}$) for all SR models (see Table 3.2).

3.2.5 EQ MSY RPs for Alternative Harvest Strategies

Values for $f_{MSY,1}$ and $f_{MSY,2}$ are the optimal values for f, and total B_{MSY} and biomass depletion for these f's were also derived. MSY RPs were derived under MPA-like conditions, i.e. $f_1 = 0$, where $f_2 = f_{MPA}$ is the f that optimizes equilibrium yield when the source is not fished. MSY RPs were also calculated assuming fishing effort was uniform for both regions, i.e. $f_1 = f_2 = f_U$. Values for these sub-optimal f's were calculated for a range of p's and were compared to the optimal f's and $f_{MSY,1box}$ (Figure 3.14). Values for B_{MSY} and biomass depletion for the sub-optimal harvest strategies were were also compared to the optimal results (Figure 3.15); B_0 (i.e. $SSB_{eq}(f = 0)$) for the two-box model was calculated as well for completeness. MSYs were calculated for each harvest strategy for comparison (Table 3.4).

The unfished SSB and B_0, for the two-box model was always less than unfished SSB for the one-box model, except when $p = 0$ at which point they were equal. This is because the SR relationships are density-dependent, and overall productivity decreases as the density of SSB in each area decreases. The optimal, MPA-like, and uniform harvest strategies used the same unfished SSB since they are all two-box harvest strategies.

When p was low, f_{MPA} (Figure 3.14) and the total B_{MSY} from f_{MPA} (Figure 3.15) were larger compared to the optimal harvest strategy. This is because the source would retain more SSB and provide more recruits to the sink, but fishing in the sink would have to increase to compensate for the loss of yields in the source. Biomass was less depleted from fishing at f_{MPA} than the optimal harvest strategy when p was low. MSY from f_{MPA},

$Y_{eq,tot}(f_1 = 0, f_2 = f_{MPA})$, was less than MSY from the optimal harvest strategy (Table 3.4). We calculated the efficiency of yields as the ratio of MSY from alternative harvest strategies to the optimal MSY (Figure 3.16). When p was large enough (i.e. $p \geq p_{f0}$), the efficiency was 100% and both the optimal and MPA harvest strategies produced equal yields, since $f_{MSY,1} = 0$ for the optimal strategy when $p \geq p_{f0}$. Otherwise, yields were lost and were reduced by up to 50% percent (when $p = 0$).

Values for f_U were always less than f_{MSY} for the one-box model, except when the source was extirpated or unconnected to the sink (Figure 3.14). Furthermore, source extirpation occurred at a $p < p_{ex}$ for the f_U harvest strategy. Recall that $f_{crash,1}(p)$ depends on p (see Figure 3.11), where $f_{crash,1}(p)$ decreases as p increases. Since $f_1 = f_U > 0$ for any p, $f_1 = f_{crash}(p)$ when $f_{crash,1}(p) > 0$ for some $p < p_{ex}$. At the p that the source is extirpated, the yields in the source are zero even though $f_1 = f_U \neq 0$, and any amount of fishing in the source will provide zero catch. Once the source is extirpated, f_1 is irrelevant and the sink is fished as an independent population. When the source persisted, B_{MSY} from fishing at f_U was always lower than the optimal B_{MSY} for the standard SR models, but higher for the steepness models (Figure 3.15). Furthermore, fishing at f_U resulted in greater biomass depletion than the optimal harvest strategy for the standard SR models, but the steepness models resulted in less depleted biomass than the optimal strategy (Figure 3.15). Also, $f_U \geq f_{MSY,1}$ and $f_U \leq f_{MSY,2}$ for all p. Using a uniform harvest strategy usually resulted in underfishing in the sink and overfishing in the source. As a result, the f_U harvest strategy was sub-optimal (Figure 3.16). Fishing at f_U reduced total yields by more than 50% for some

p's, and yields were only 100% efficient when the source was extirpated or unconnected.

3.2.6 EQ MSY RPs for Alternative Parametrizations

MSY RPs were calculated under alternative parametrizations of life history characteristic distributions, and therefore using different SPR and YPR function for the source and sink. The alternative parameters include the selectivity, s_8, weights-at-age $W_{0.05}$ and $W_{0.15}$, the natural mortality rate m_{lor}, and the maturity ogive $\mu_{10,12}$ (see Table 3.5). Most notably, the source was unfishable when its growth rate was $k_{source} = 0.05$ and when its maturation rate was described by the $\mu_{10,12}$ ogive, as well as when using the Lorenzen natural mortality rate (Table 3.5). Interestingly, biomass was less depleted when using the Lorenzen natural mortality rate or $\mu_{10,12}$ ogive in the sink compared to the base conditions, while MSY for these alternative parametrizations was significantly lower compared to the base conditions. Most parameter changes in the sink resulted in larger results for MSY RPs, with the major exceptions being B_{MSY} and biomass depletion for $k_{sink} = 0.05$ and B_{MSY} using the $\mu_{10,12}$ ogive. The largest increase in MSY from the base conditions was from an increase in the growth rate for either sub-population, while the largest decrease was from using the Lorenzen mortality which made both populations nearly unfishable. In general, MSY RPs were most sensitive to growth rates and natural mortality rates.

The affects these parameter changes had on MSY RPs were made ambiguous by the division of the stock into segregated sub-populations, and

more importantly their connection through larval advection. For example, although harvesting in the sink did not directly affect harvesting in the source, changing source parameters affected how RPs were calculated to optimize MSY. Changing one parameter in the sink, like $k_{sink} = 0.05$ may increase $f_{MSY,1}$ yet reduce total MSY (Table 3.5). It is difficult to fully understand how parameter perturbations affect two-box model RPs, since RPs for each area are dependent on one another. A detailed analyses of these perturbation effects in spatial models may be left to future research.

3.2.7 MSY RPs for a HL System

Equilibrium yields, SSB and recruitment were calculated under a HL system, where the reproduction rate in the source was higher than that in the sink. Results were very similar to the EQ system, with the main difference being the increase in yield, SSB, and recruitment in the source. Equilibrium results for the HL system can be found in Appendix B (see Figures B.4 to B.7).

Values for p_{f0} and p_{ex} were derived using each SR models (Table 3.2). Increasing source recruitment increased p_{f0} and p_{ex} for all SR models.

MSY RPs were calculated for various p values. Values for $f_{MSY,1}$ were significantly affected by the increase in reproduction rate, where $f_{MSY,1} > f_{MSY,2}$ for very low values of p (Figure 3.17). Furthermore, the scales of the f's increased, for example $f_{MSY,2}$ at $p = p_{f0}$ ($f_{MSY,2} \approx 0.10$) was greater then the $f_{MSY,2}$ at $p = p_{f0}$ for the EQ system ($f_{MSY,2} \approx 0.08$). Values for f_U changed significantly under this system, where harvest rates in the source could allow more fishing in both regions for low p values, similar to $f_{MSY,1}$

for to the optimal harvest strategy (Figure 3.17).

Total B_{MSY} increased with the increased recruitment in the source, and B_0 increased for the standard SR models at low p (Figure 3.18). However, B_{MSY} and B_0 for the BH_h SR model were lower than that for the EQ system when p was low. Biomass estimates changed very little for the RK_h SR model.

Total MSY was calculated for the HL system and compared to total MSY for the EQ system (Figure 3.19). Relative to the EQ system, the increased recruitment in the HL system provided substantially greater yields. Both the MPA and uniform harvest strategies still provided sub-optimal harvests, or equal harvests at best (Figure 3.20).

3.2.8 MSY RPs for a DA System

Equilibrium yields, SSB and recruitment were calculated under a DA system, where the growth rate in the sink is higher than that in the source. Results are provided in Appendix B. The main difference in equilibrium values was the decrease in the scale for the BH_{50} and RK_{50} SR model (Figures B.8 and B.9), while having little difference for the steepness models (Figures B.10 and B.11). This is likely due to the higher recruitment rates from the steepness models which can compensate for the reduced growth with high recruitment.

Values for p_{f0} and p_{ex} were derived using each SR models (Table 3.2). For the DA system, p_{f0} and p_{ex} decreased for the BH_{50} and RK_{50} SR models, but did not change for the BH_h and RK_h models.

MSY RPs were calculated for various p values. Both $f_{MSY,1}$ and $f_{MSY,2}$ were greatly reduced for all p (Figure 3.21), although $f_{MSY,2}$ was still always greater than $f_{MSY,1box}$. Values for f_{MPA} were also greatly reduced for the standard SR models compared to the EQ system, while $f_U = 0$ regardless of p.

For the standard SR models, total B_{MSY} and B_0 decreased dramatically until $p = p_{ex}$, since values for p_{ex} were small. Values for B_{MSY} and B_0 were much lower than that for EQ system, and biomass was more depleted, as well (Figure 3.22). For the standard SR models, biomass was significantly more depleted under the uniform harvest strategy compared to the EQ system when p was small. B_{MSY} was constant for changes in p because f_U was constant. For the steepness SR models, B_{MSY} and B_0 decreased slightly compared the EQ system results, and changes in biomass depletion compared to EQ results were negligible, likely due to high reproduction rates compensating for the reduction of growth in the source.

MSYs were substantially lower for the DA system compared to the EQ and HL systems, but MSY increased as p increased for low p's (Figure 3.19) because as recruits advected into the sink, they obtained higher growth rates which resulted in a larger total biomass . Furthermore, changes in p resulted in minimal changes in f_{MPA} and f_U, and therefore provide minimal reductions in yield efficiency (Figure 3.23). That is, aside from at very low p's, all harvest strategies provided approximately equal yields.

3.2.9 MSY RPs for a HL & DA System

Finally, for the HL & DA system, equilibrium yields, SSB, and recruitment were calculated where the source had higher reproduction rates but slower growth rates than the sink. Results are provided in Appendix B (Figures B.12 to B.15). Values for p_{f0} and p_{ex} were also calculated (Table 3.2).

MSY RPs for various p values were calculated. Since this system is a combination of both the HL and DA systems, its RP results resemble results from both. Values for $f_{MSY,1}$ and $f_{MSY,2}$ decreased from the reduction in growth rate, but increased from the increase in reproduction rate (Figure 3.24), although the negative effects from the reduced growth rate was more prominent than from the increase in source reproduction rate.

For the standard SR models, B_{MSY} and B_0 from the conventional SR models decreased rapidly similar to the the DA system; biomass depletion showed similar trends (Figure 3.25). B_{MSY}, B_0, and biomass depletion from the steepness SR models, however, did not change much compared to that for the DA system.

The alternative harvest strategies always provided sub-optimal harvests to the optimal harvest strategy (Figure 3.26), but provided greater yields than the DA system alone, although not as great as the EQ or HL systems (Figure 3.19). Moreover, MSY increased with p similar to the DA system because recruits from the source grew quicker once advected into the sink, and the increase in MSY was greater than that for the DA system because higher reproduction rates in the source provide more recruits to the sink to grow.

It should be noted that, for all systems (i.e. EQ, HL, DA, and HL & DA), once $p \geq p_{ex}$, MSY, B_{MSY}, and B_0 for all SR models and all harvest rules were half their value for the one-box model. Changes in the system structure, e.g. to have higher reproduction rates in the source, only affected the source. Once the source was extirpated, these changes did not manifest in the sink MSY RP values because the sink behaved as a one-box system.

3.3 Discussion

A two-box population, particularly a source-sink system can result in substantially more complex dynamics than a standard one-box system. With the added spatial dimension, the degrees of freedom increase and allow for more variation within a stock in the form of spatially-varying life history characteristics, the transfer proportion, and local recruitment. Variation may also be allowed for in the applied harvest strategy, but to optimize yields and maintain a sustainable harvest, implementing a spatially-explicit harvest strategy with area-specific RPs is necessary. Moreover, the transfer proportion directly impacts the fishability and sustainability of the source sub-population, and remaining aware of metapopulation interconnectivity is imperative for effective fisheries management.

For a source-sink system with a larval advection process, the sink sub-population can accommodate a greater f than the source due to the constant supply of recruits transferring from the source. However, this heavily depends on the reproductive rates of each sub-population. If reproduction in the source is high and net flux of fish out of the source is low, the source may

accommodate higher harvest rates (see Lundberg and Jonzén, 1999). The optimal harvest rates and optimal sustainable harvest heavily depend on the SR relationship and sub-population life history characteristics (e.g. Figure 3.19).

Source extirpation occurred at much lower p's for the conventional BH or RK SR model than when using the steepness models, for all systems (Table 3.2), and MSY and B_{MSY} for the steepness models were far greater than the values for the conventional SR models for most p's (see Table 3.3). This is because the steepness versions of our the SR relationships had higher reproduction rates compared to the conventional SR relationships.

Moreover, when reproduction rates in the source were greater than the sink (e.g. HL system), MSY and B_{MSY} for low p's were larger than values for the EQ system (e.g. Figures 3.15, 3.18 and 3.19). When growth rates in the source were lower than that in the sink (DA), MSY and B_{MSY} were much lower than estimates for the EQ system (e.g. Figures 3.16 and 3.22). Higher source reproduction rates were unable to compensate for slow fish growth rates for our choices of k_{source} and SR parameters (HL & DA system), and the MSY is always lower than EQ estimates (Figure 3.19), while B_{MSY} was almost always lower than EQ estimates (see Figures 3.15 and 3.26). Choices of local reproduction and growth rates can have drastic effects on RP values, and perturbations of source parameters can have significant impacts on results for sink RPs (also see Table 3.5).

Optimal harvest rates are sensitive to the transfer proportion, and usually to differ substantially from one-box model values. If a stock consists of two connected sub-populations, contemporary harvest strategies which base

harvest rates on a one-box model may promote over-harvesting in the source and under-harvesting in the sink. Furthermore, fisheries may continue to fish at levels indicated by a one-box model, even if one-box model RPs are not sustainable harvest objectives, because results for MSY are usually greater for a one-box model. Unless fishing concentrates in areas where abundances are higher, i.e. the sink, overexploitation and even extirpation is possible using one-box model RPs.

To maximize overall catch, fishing effort tends to increase in areas with relatively higher local abundances (Branch et al., 2006). Ying et al. (2011), who simulated three mixing sub-populations to derive management RPs, concluded that fishing in these high-abundance areas can cause over-exploitation, and concentrating fishing in places where abundances were highest could lead to local depletion. To reduce the chances of overexploiting a sub-population, sub-optimal harvest rates can be implemented, e.g. f_{MPA}. However these options can further reduce yields (see Figure 3.16). The priority of fishery should be to sustain populations, and although focusing fishing where abundances are largest will produce the greatest yields, they may not be sustainable if mixing between sub-populations is not properly accounted for in RP derivations. Using spatial RPs like the two-box model MSY RPs will ensure fishing is properly spatially allocated and will reduce the chances of overexploitation.

MPAs can be used as an effective way to conserve populations, but they tend to decrease total yields (e.g. Figure 3.16). When spillover is minimal (i.e, $p < p_{f0}$), MPAs are an effective means of sustaining stock levels where biomass is far less depleted compared to the optimal harvest strategy (see

Figure 3.15). However, when spillover is high, their efficacy diminishes, although Takashina and Mougi (2014) argue they can also be effective for stock recovery if spillover is sufficiently large. Notwithstanding, our results show that if the advection of recruits between regions (i.e. p) is low, MPAs provide a considerable sustainable harvest, albeit sub-optimal. An MPA-like harvest rule can provide more risk-averse management RPs, but allowing an optimized harvest in both sub-populations can provide a greater total harvest (see Figure 3.16).

A uniform harvest strategy (i.e. f_U), designed to maintain a constant fishing mortality rate in both regions, has no benefit over the other harvest strategies. A uniform harvest rule always provides lower yields and f RPs than the optimal harvest rule, and almost always a lower yield and f RPs than the MPA-like harvest rule (see Figure 3.16). Employing a uniform harvest rate has very few benefits over spatially-allocated harvest rates. Although a uniform fishing mortality rate can be used as a measure for preventing overfishing in some cases, it is sub-optimal to the other tested harvest strategy.

Measurements of life history characteristics directly affect RP values, as we've noted in Chapter 2. Spatially-explicit RPs are no exception (Table 3.5), and reliably estimating stock parameters, like growth and maturation rates, for both sub-populations is critical. Life history characteristics tend to vary spatially, and may differ due to local temperatures (e.g. a DA system), for example. Accounting for these distinctions in life history characteristics is important to derive reliable MSY RPs, and parameter estimates can affect RP values in both the source and sink if population are connected.

To derive spatially-explicit RPs and properly allocate fishing to different areas, measurements of p are required. Not only does p affect RP values but also affects SR parameter estimation. Hintzen et al. (2015) performed a simulation and MSE on mixing populations of British herring, and concluded that without knowledge of the proportion of mixing, spatial RPs would result in overexploitation due to biased estimates of productivity. Having accurate information on pre-recruit movement may not only reduce the chances of overexploitation, but may also improve a fishery's yields. Botsford et al. (2009) found that modelling explicit larval advection provides yields higher than that from conventional (one-box) models when the connectivity patterns are known, even with the presence of MPAs. Spatial harvesting can provide higher MSYs in some cases, but requires knowledge of the connectivity of the populations.

There is difficulty in accurately estimating stock-recruitment for larval advection spatial models due to the lack of data for juvenile and larval movement. Spatial variation in productivity and movement of spawners may be entangled with movement of pre-recruits, which complicates the task of measuring local recruitment (Thorson et al., 2015). The transfer proportion, p, relies on the dispersal distance of larvae or the larval phase duration (pelagic larval duration, PLD; see Cowen and Sponaugle, 2009), and may also require information on ocean current pathways and current speeds, along with water depth (Cowen et al., 2006; Werner et al., 2007) because larvae take advantage of local waterways by repositioning themselves within water columns. Without data on the movement of pre-recruits like larvae, values for p cannot be estimated, and it is not possible to effectively apply this two-box model,

since RP results tend to depend on p. There has been some recent development of technologies designed to measure larval transportation processes, for example by monitoring waterway trajectories (see Gawarkiewicz et al., 2007). However, there are still many gaps in knowledge of pre-recruit dispersion processes, and accurately defining the transfer proportions is a necessary prerequisite for deriving spatially-explicit harvest RPs.

We assume pre-recruits move unidirectionally and consider a metapopulation to model explicit larval advection. Future studies could permit broader assumptions about overall stock dynamics by allowing more (or all) age-classes to move between sub-populations, allowing bidirectional (or philopatric) movements, and even modelling dispersal dynamics to further develop an understanding of how spatial dynamics of fish stocks influence management RPs for source-sink systems. These alternative conditions, alongside potential spatial variability life history characteristics and recruitment, may produce more reliable and possibly different conclusions about source-sink persistence and sustainable harvests.

It is also worth mentioning the effect uncertainties in parameter estimates may have on RP results, for example SR parameters, since the methods described herein rely heavily on productivity and pre-recruit movement. We noted in Chapter 1 that small deviations in parameters used to describe life history characteristics and SR relationships can have substantial effects on RP model outputs. This is no different for spatial models, and we performed a similar analysis on parameters for the two-box model. However, augmenting this model to allow errors in parameter estimates, or performing a stochastic simulation, may provide a more detailed understanding of source-sink harvest

RPs. Nonetheless, developing a simple, deterministic model provides a solid basis from which to extend the framework used to derive spatially explicit management RPs, and builds an understanding of how spatial variability and movement may affect these values.

The mobility of a species determines the significance of the indirect effects of fishing (Jonzén et al., 2001), and most MSY RPs are significantly affected by the amount of recruits that advect from source to sink. Although a two-box model may provide unreliable outputs if the transfer proportion is unknown or uncertain, a one-box model is insufficient to estimate MSY RPs for fisheries management, especially when the primary objective of the fishery is sustainability. One-box model values of $f_{MSY,1box}$ usually promoted overfishing in the source (i.e. $f_{MSY,1box} > f_{MSY,1}$), and employing a one-box model harvest rate could extirpate the source and reduce overall long-term yields. When deriving management RPs, it is critical that stock models are structured to account for spatial variability and population connectivity to optimize yields and avoid unnecessary stock depletion .

3.4 Tables

Table 3.1: MSY RP outputs for a two-box model using a forecast projection (FP) and the per-recruit functions (PR) under base conditions. Precision of PR outputs are rounded based on the precision FP outputs (3 significant figures).

SR model	$f_{MSY,1}$		$f_{MSY,2}$		MSY		B_{MSY}		B_{MSY}/B_0	
	FP	PR	FP	PR	FP	PR	FP	PR	FP	PR
BH_{50}	0.015	0.016	0.070	0.072	2.365	2.367	39.680	38.561	0.480	0.467
RK_{50}	0.020	0.020	0.075	0.077	5.476	5.478	82.196	81.447	0.505	0.501
BH_h	0.170	0.169	0.240	0.238	15.904	15.905	47.367	47.809	0.251	0.253
RK_h	0.130	0.130	0.200	0.202	20.119	20.121	78.463	77.865	0.415	0.412

Table 3.2: Transfer proportions when $f_{MSY,1} = 0$ (p_{f0}) and $SSB_{eq,1} = 0$ (p_{ex}). Values for p_{f0} and p_{ex} are affected by changes in life history characteristics and SR models, and values for the equivalent (EQ), High-to-Low (HL), Downstream Advection (DA), and High-to-Low with Downstream Advection (HL & DA) will be different.

		BH_{50}	RK_{50}	BH_h	RK_h
EQ	p_{f0}	0.30	0.31	0.77	0.68
	p_{ex}	0.48	0.48	0.93	0.82
HL	p_{f0}	0.38	0.41	0.89	0.73
	p_{ex}	0.58	0.58	0.99	0.86
DA	p_{f0}	0.12	0.13	0.77	0.68
	p_{ex}	0.22	0.22	0.93	0.82
HL & DA	p_{f0}	0.22	0.23	0.89	0.73
	p_{ex}	0.37	0.37	0.99	0.86

Table 3.3: MSY RPs for various transfer proportions. The transfer proportion, p does not affect one-box model results.

		BH_{50}	RK_{50}	BH_h	RK_h
One-box	f_{MSY}	0.047	0.051	0.206	0.169
	B_{MSY}	39.1	82.4	48.0	78.1
	B_0	89	174	189	189
	B_{MSY}/B_0	0.438	0.475	0.254	0.412
	MSY	2.42	5.60	15.9	20.2
$p = 0$	$f_{MSY,1}$	0.047	0.051	0.206	0.169
	$f_{MSY,2}$	0.047	0.051	0.206	0.169
	B_{MSY}	39.1	82.4	48.0	78.1
	B_0	89.4	174	189	189
	B_{MSY}/B_0	0.438	0.475	0.254	0.412
	MSY	2.42	5.60	15.9	20.2
$p = 0.2$	$f_{MSY,1}$	0.016	0.020	0.169	0.130
	$f_{MSY,2}$	0.072	0.077	0.238	0.202
	B_{MSY}	38.6	81.4	47.8	77.9
	B_0	82.6	163	189	189
	B_{MSY}/B_0	0.467	0.501	0.253	0.412
	MSY	2.37	5.48	15.9	20.1
$p = 0.3$	$f_{MSY,1}$	0.000	0.002	0.148	0.108
	$f_{MSY,2}$	0.080	0.087	0.251	0.217
	B_{MSY}	37.2	80.2	47.5	77.5
	B_0	74.0	147	188	188
	B_{MSY}/B_0	0.502	0.544	0.253	0.412
	MSY	2.30	5.33	15.8	20.0
$p = 0.6$	$f_{MSY,1}$	0.000	0.000	0.069	0.026
	$f_{MSY,2}$	0.047	0.051	0.286	0.255
	B_{MSY}	19.6	41.2	45.7	75.2
	B_0	44.7	86.8	181	176
	B_{MSY}/B_0	0.438	0.475	0.252	0.426
	MSY	1.21	2.80	15.5	19.2
$p = 1$	$f_{MSY,1}$	0.000	0.000	0.000	0.000
	$f_{MSY,2}$	0.047	0.051	0.206	0.169
	B_{MSY}	19.6	41.2	24.0	39.1
	B_0	44.7	86.8	94.7	94.7
	B_{MSY}/B_0	0.438	0.475	0.254	0.412
	MSY	1.21	2.80	7.97	10.1

Table 3.4: MSY RPs under various two-box f harvest rules for an EQ system ($p = 0.2$), and a one-box f harvest rule.

MSY RP	BH_{50}	RK_{50}	BH_h	RK_h
One-box				
f_{MSY}	0.047	0.051	0.206	0.169
B_{MSY}	39.1	82.4	48.0	78.1
B_{MSY}/B_0	0.438	0.475	0.254	0.412
MSY	2.42	5.60	15.9	20.2
Two-box				
$f_{MSY,1}$	0.016	0.020	0.169	0.130
$f_{MSY,2}$	0.072	0.077	0.238	0.202
B_{MSY}	38.6	81.4	47.8	77.9
B_{MSY}/B_0	0.467	0.501	0.253	0.412
MSY	2.37	5.48	15.9	20.1
MPA				
f_{MSY}	0.078	0.084	0.243	0.201
B_{MSY}	46.5	99.8	99.6	122
B_{MSY}/B_0	0.586	0.637	0.532	0.646
MSY	2.22	4.98	10.4	12.9
Uniform				
f_{MSY}	0.039	0.041	0.201	0.159
B_{MSY}	37.8	80.3	48.8	80.0
B_{MSY}/B_0	0.458	0.494	0.258	0.424
MSY	1.91	4.35	15.7	19.3

Table 3.5: MSY RPs from alternative parametrizations ($p = 0.2$). The first row displays RP values for the base assumptions (s_6, $W_{0.1}$, $m_{constant}$, and $\mu_{8,10}$). A Lorenzen mortality rate is applied to both the source and sink, simultaneously. All other parameters changes are applied to the source and sink independently, and are tabulated based on which sub-population is re-parametrized. Values for B_{MSY}, B_0, B_{MSY}/B_0 and MSY are the sum of source and sink values.

		$f_{MSY,1}$	$f_{MSY,2}$	B_{MSY}	B_0	B_{MSY}/B_0	MSY
	—	0.016	0.072	38.6	82.6	0.467	2.37
	m_{lorenz}	0.000	0.014	5.09	10.6	0.482	0.098
Source	s_8	0.021	0.081	37.9	82.6	0.459	2.54
	$W_{0.15}$	0.053	0.105	57.3	143	0.402	5.79
	$W_{0.05}$	0.000	0.047	19.6	44.7	0.438	1.21
	$\mu_{10,12}$	0.000	0.056	28.0	56.6	0.495	1.51
Sink	s_8	0.018	0.093	39.1	82.6	0.474	2.44
	$W_{0.15}$	0.015	0.099	57.4	134	0.429	5.98
	$W_{0.05}$	0.019	0.341	17.7	39.2	0.453	0.980
	$\mu_{10,12}$	0.011	0.077	30.1	63.2	0.476	1.81

3.5 Figures

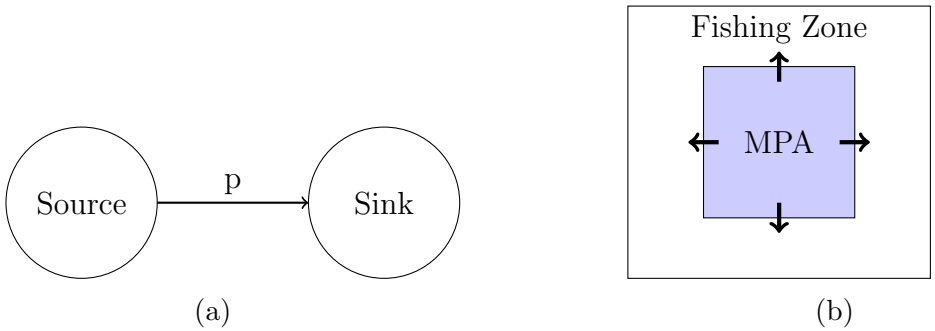

Figure 3.1: Two-box models for (a) a source-sink system and (b) an MPA system. In (a) advection is a unidirectional flow between regions and in (b) advection is a result of spillover from MPAs into the fished region.

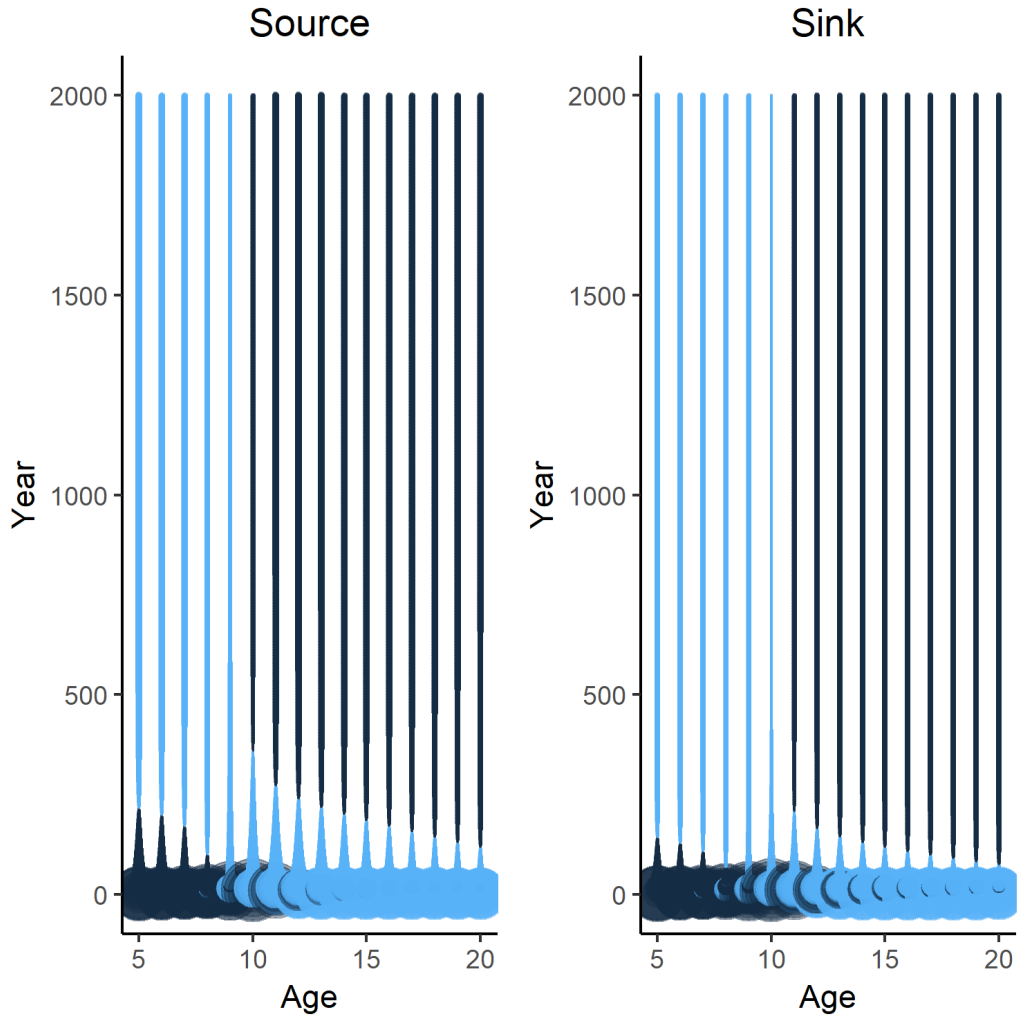

Figure 3.2: Abundances by age and year from a spatially-explicit forecast projection for $p = 0.2$, where $f_1 = f_2 = 0.05$. Over time, abundances for both the source and sink stabilize. Refer to the caption for Figure 2.2.

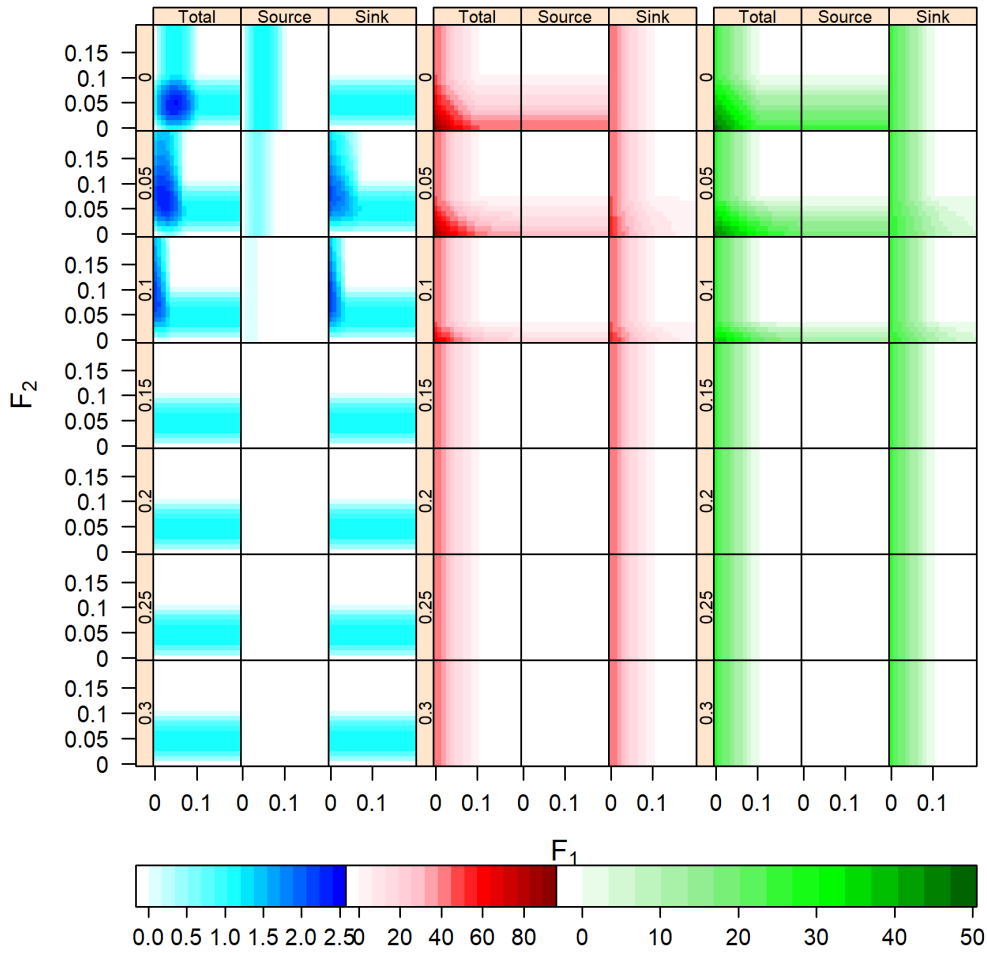

Figure 3.3: Equilibrium values for an EQ system using the BH_{50} SR model. Shown are the equilibrium yield (blue), SSB (red), and recruitment (green) for the source and sink, and the total of both. Equilibrium recruitment is measured as the pre-advection recruitment (i.e. $R_{eq,2} = R(SSB_{eq,2})$). The value of p varies by row.

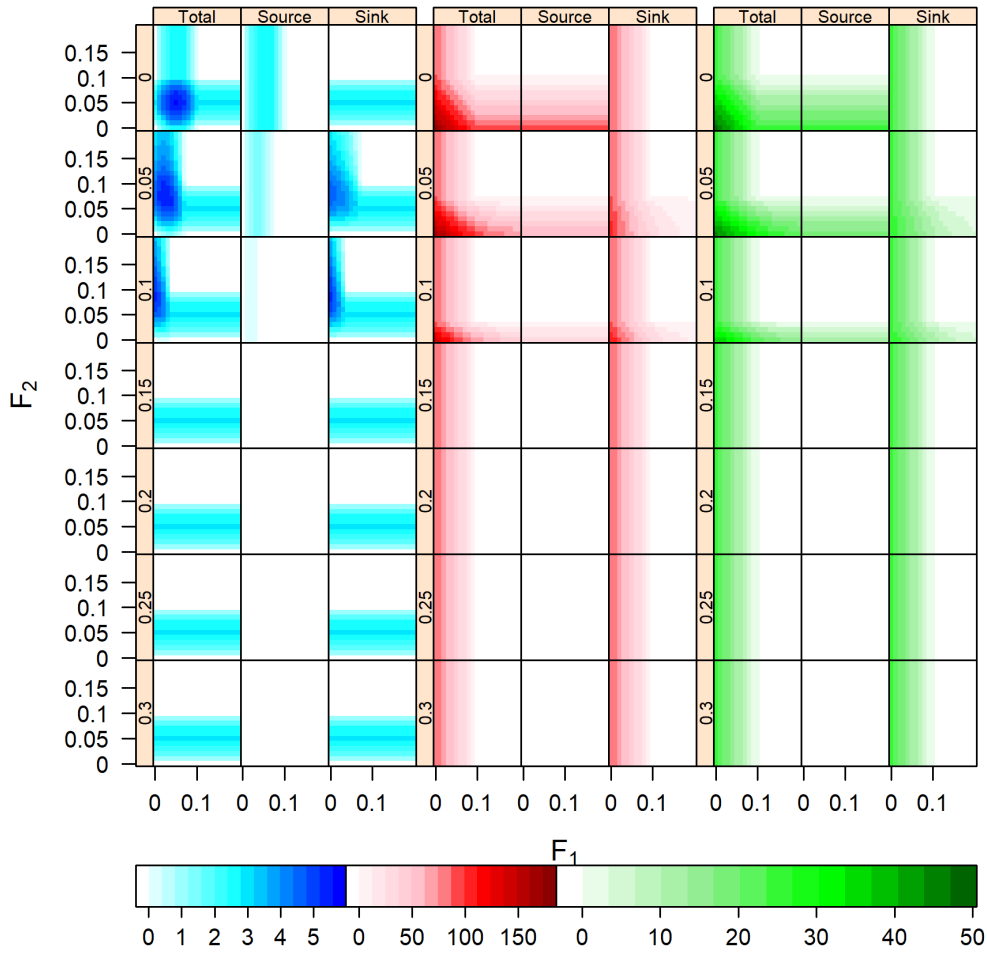

Figure 3.4: Equilibrium values for an EQ system using the RK_{50} SR model. Shown are the equilibrium yield (blue), SSB (red), and recruitment (green) for the source and sink, and the total of both. Equilibrium recruitment is measured as the pre-advection recruitment (i.e. $R_{eq,2} = R(SSB_{eq,2})$) The value of p varies by row.

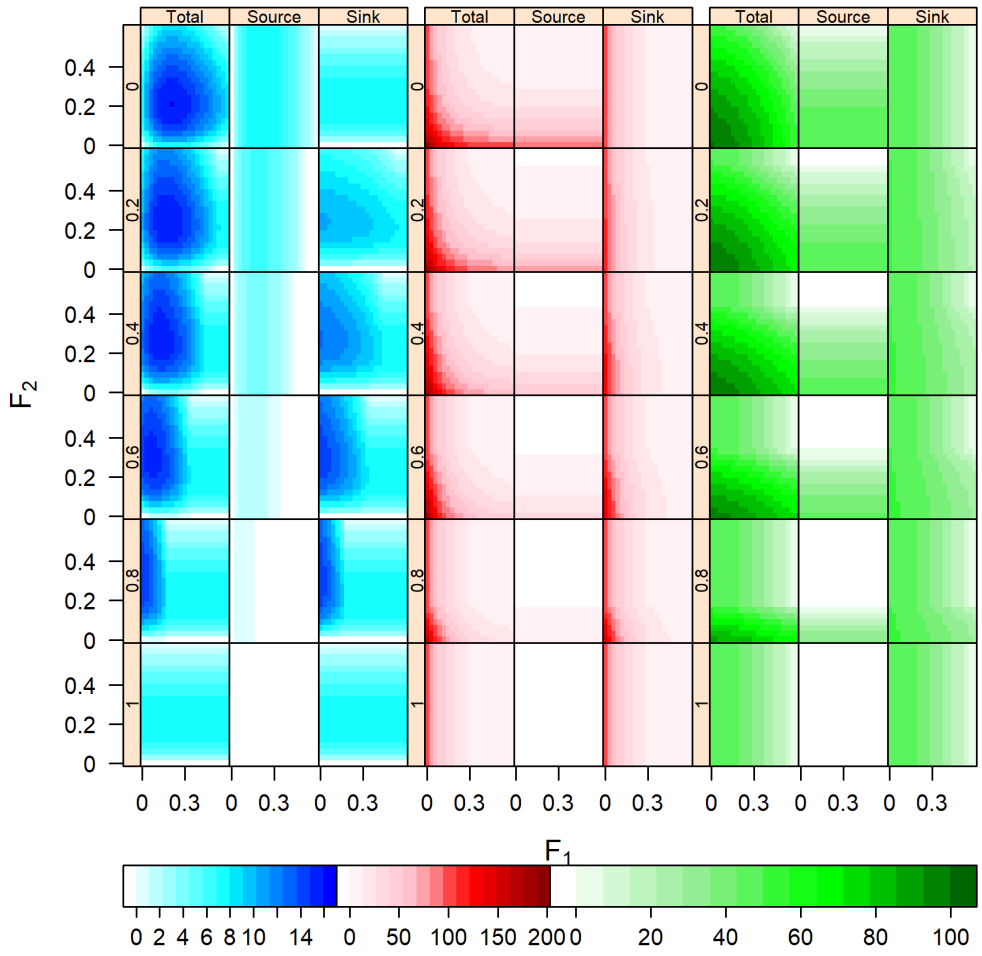

Figure 3.5: Equilibrium values for an EQ system using the BH_h SR model. Shown are the equilibrium yield (blue), SSB (red), and recruitment (green) for the source and sink, and the total of both. Equilibrium recruitment is measured as the pre-advection recruitment (i.e. $R_{eq,2} = R(SSB_{eq,2})$) The value of p varies by row.

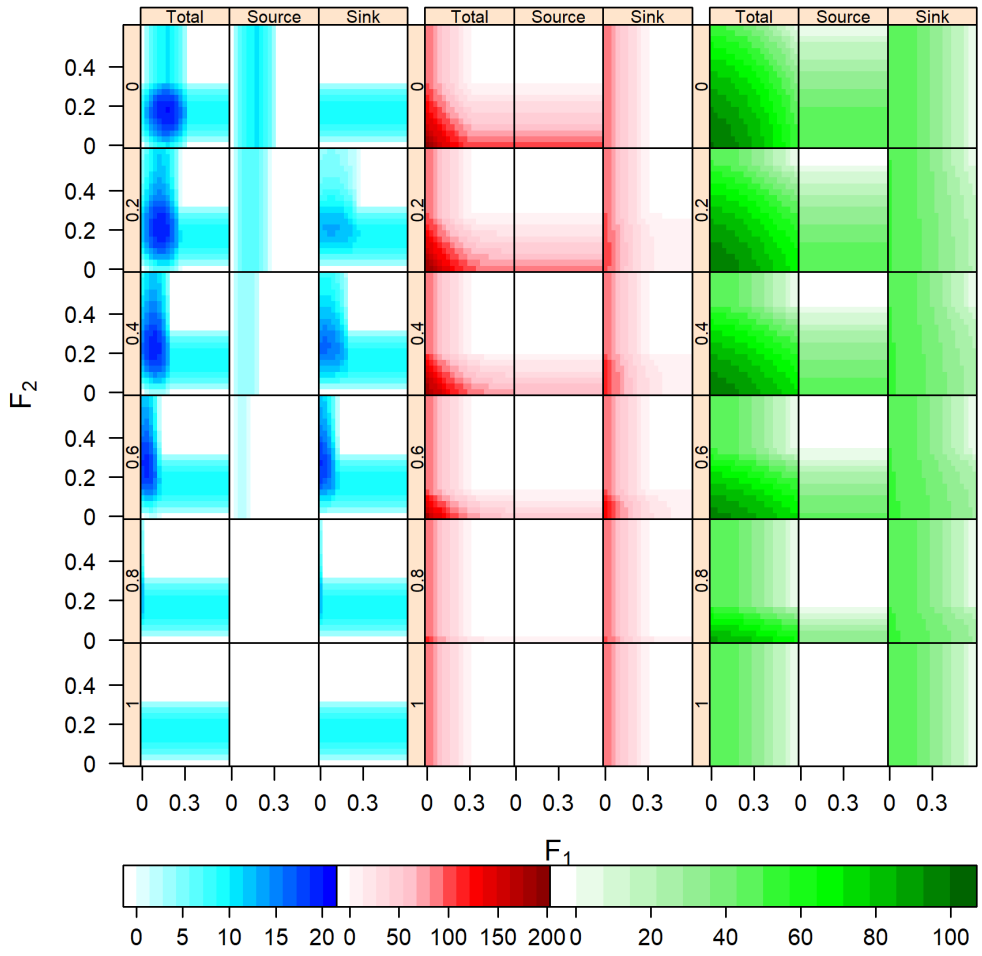

Figure 3.6: Equilibrium values for an EQ system using the RK_h SR model. Shown are the equilibrium yield (blue), SSB (red), and recruitment (green) for the source and sink, and the total of both. Equilibrium recruitment is measured as the pre-advection recruitment (i.e. $R_{eq,2} = R(SSB_{eq,2})$) The value of p varies by row.

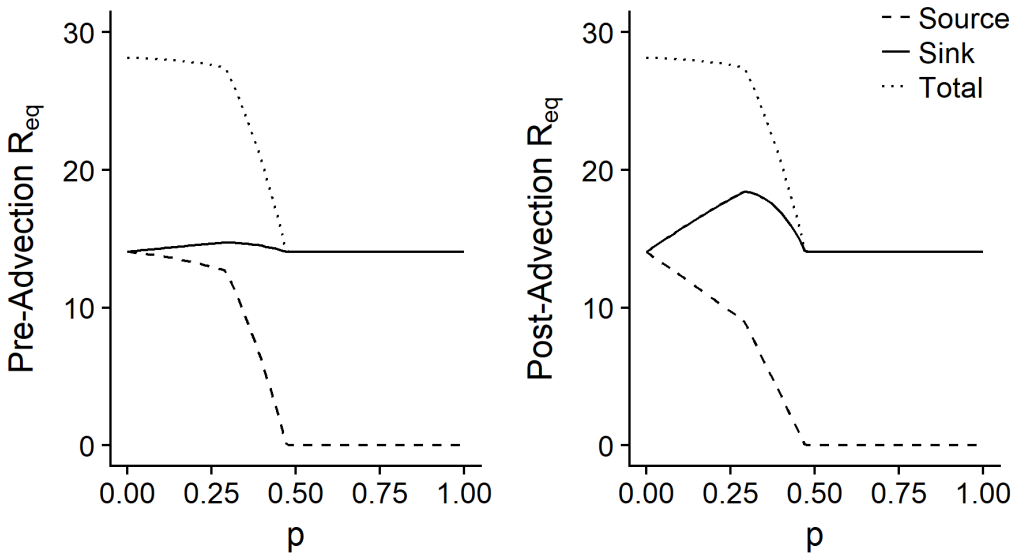

Figure 3.7: The pre-advection (left) and post-advection (right) equilibrium recruitment for the source and sink from $SSB_{eq} = B_{MSY}$, i.e. $R(B_{MSY})$.

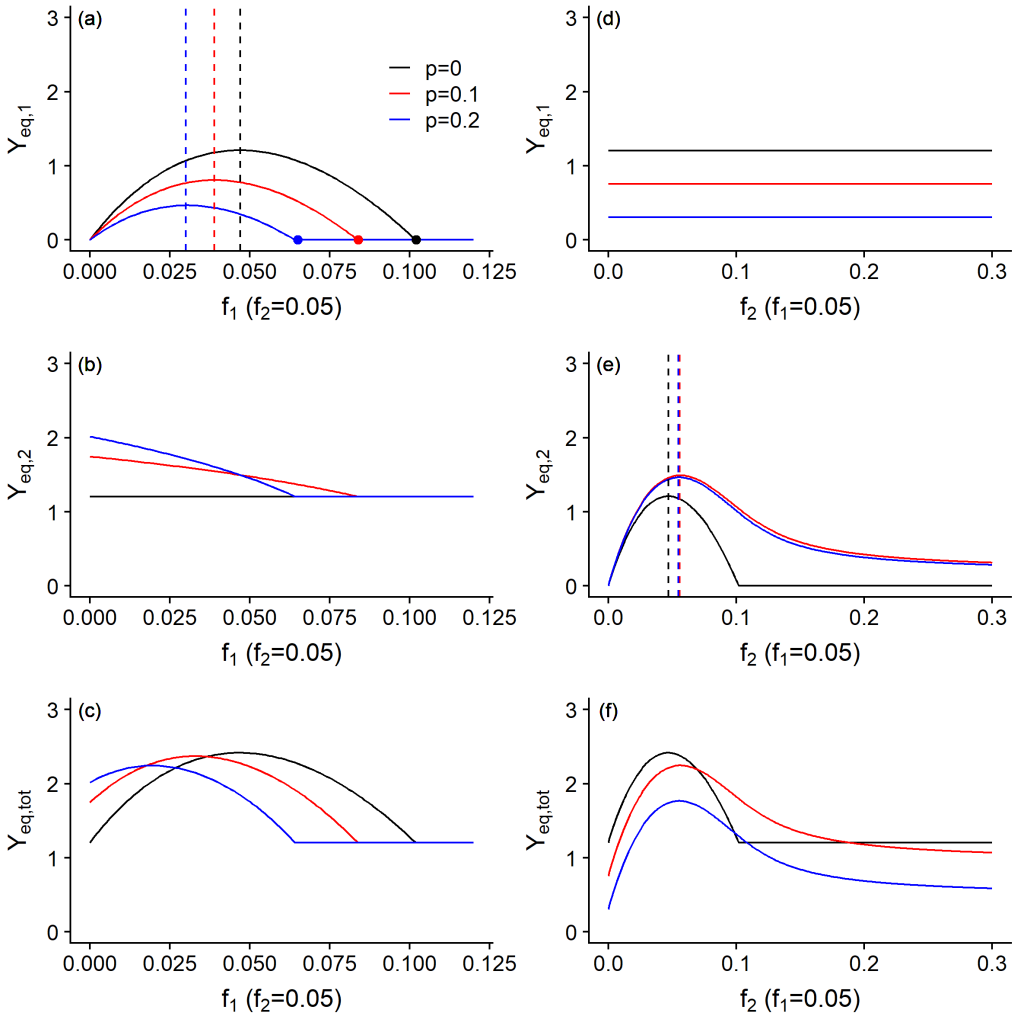

Figure 3.8: Equilibrium curves for the source (a & d) and sink (b & e), and the total yield (c & f). Equilibrium yields were calculated using the BH_{50} SR model for select p values, with a constant f_2 with a varying f_1 (a, b, & c), and a constant f_1 with a varying f_2 (d, e, & f). The dots (a) indicate when $f_1 = f_{crash,1}(p)$ (i.e. $Y_{eq,1}(f_{crash,1}(p)) = 0$) for the respective yield curves. The vertical lines indicate $f_{MSY,1}$ (a) and $f_{MSY,2}$ (e) for the respect yields curves.

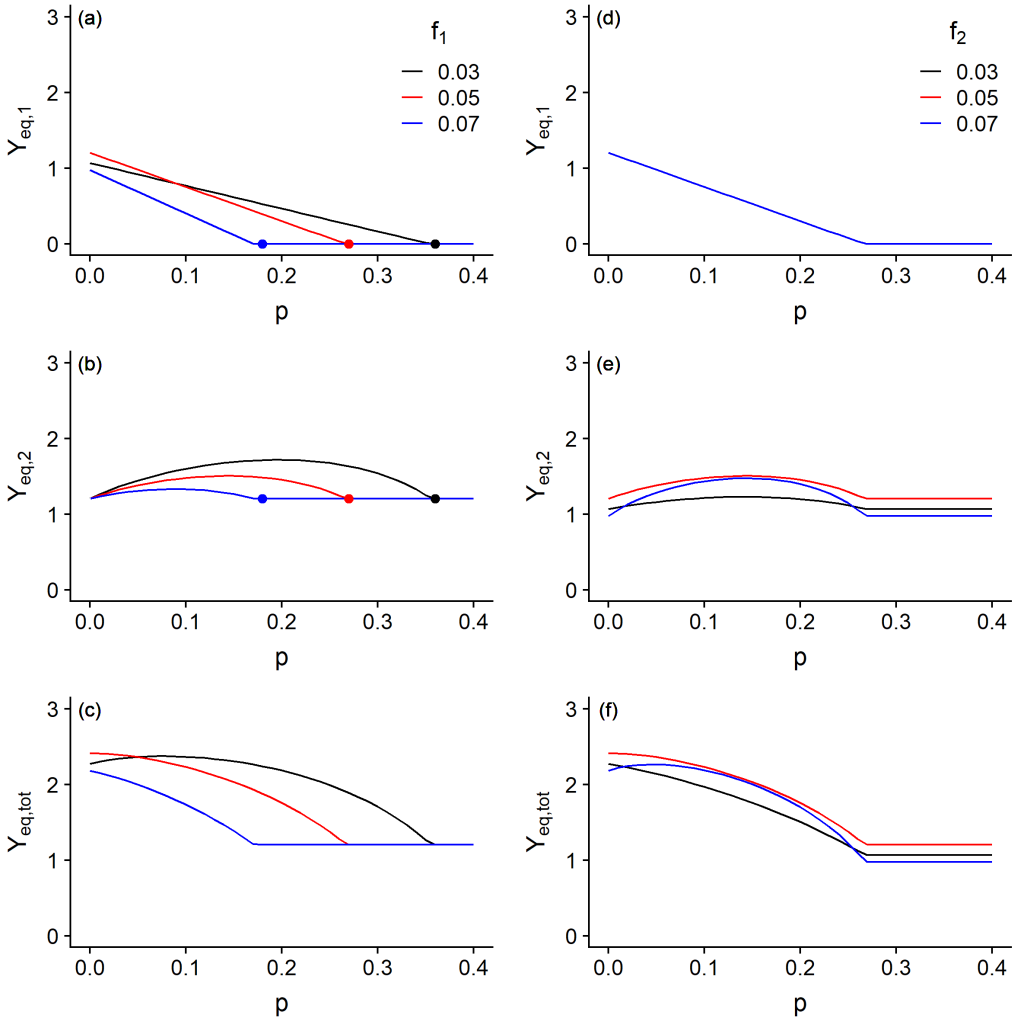

Figure 3.9: Equilibrium curves for the source (a & d) and sink (b & e), and the total yield (c & f). Yields are calculated for a constant $f_2 = 0.05$ (a, b, & c) and select f_1 values, and for a constant $f_1 = 0.05$ (d, e, & f) and select f_2 values. Equilibrium yields were calculated using the BH_{50} SR model. The dots (a & b) indicate the p for which $f_1 = f_{crash,1}(p)$ for the respective yield curves. Equilibrium yield in the source does not change with f_2 (d), and so all curves overlap. The value for $f_{crash,1}(p)$ do not change with f_2 and occurs at the p where $f_{crash}(p) = 0.03$ (a).

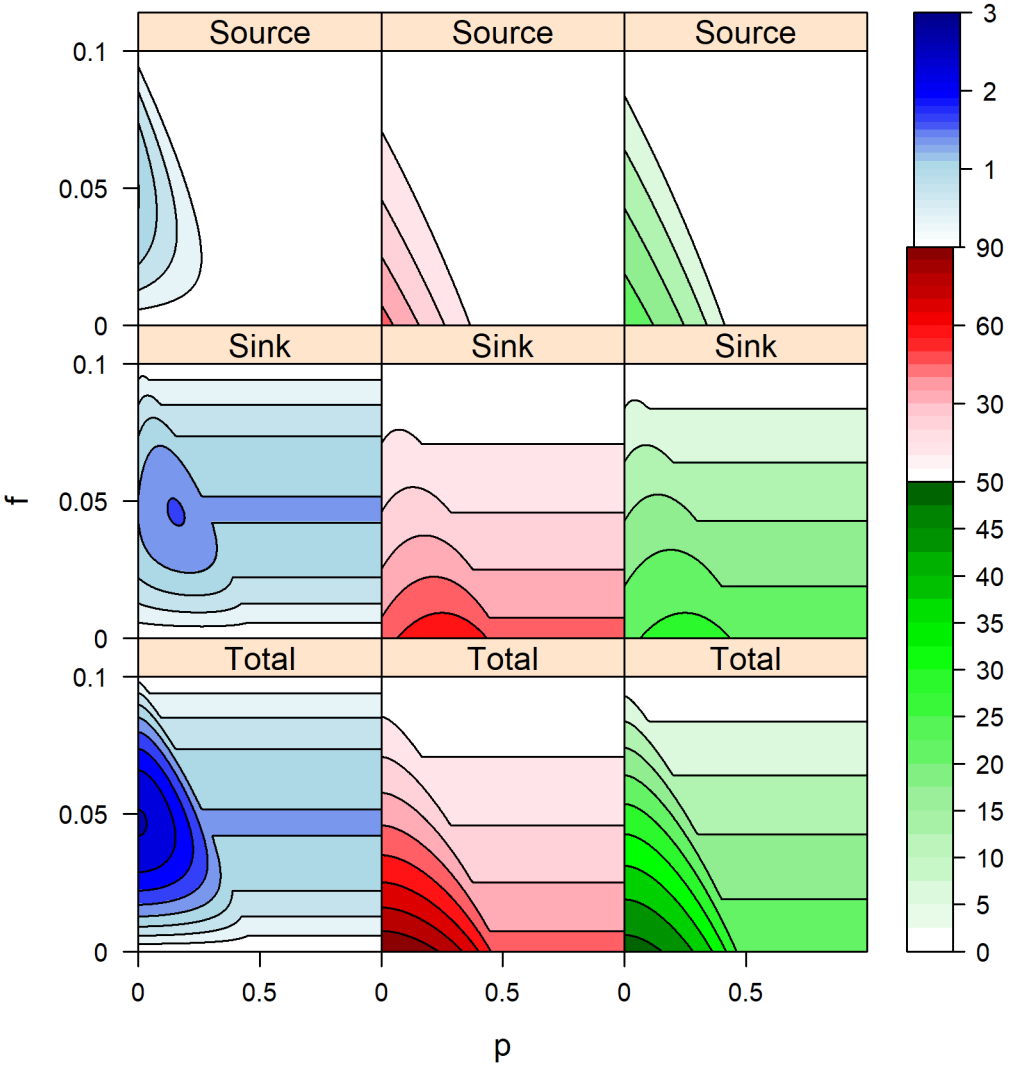

Figure 3.10: Contour plots of the source, sink, and total equilibrium yield (blue), SSB (red), and local recruitment (green) for $f = f_1 = f_2$. Yields were calculated using the BH_{50} for an EQ system.

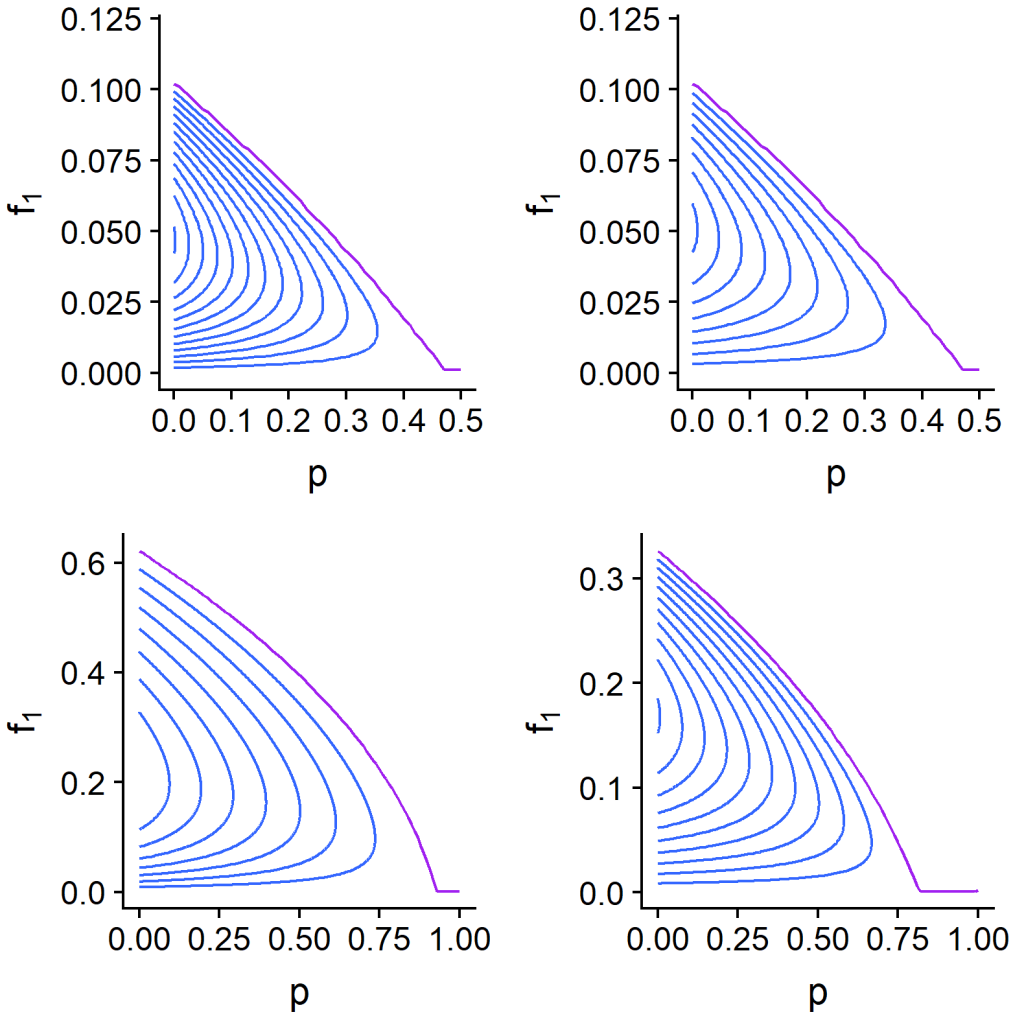

Figure 3.11: Equilibrium yield contours for the source sub-population. Equilibrium yields (blue) are non-zero for any f_1 and p where $f_1 < f_{crash,1}(p)$. Values for $f_{crash,1}(p)$ (purple) decrease as p increases, and the source is sustainable as long $f_1 < f_{crash,1}(p)$. Once $f_{crash,1}(p) = 0$ at $p = p_{ex}$, the source is extirpated.

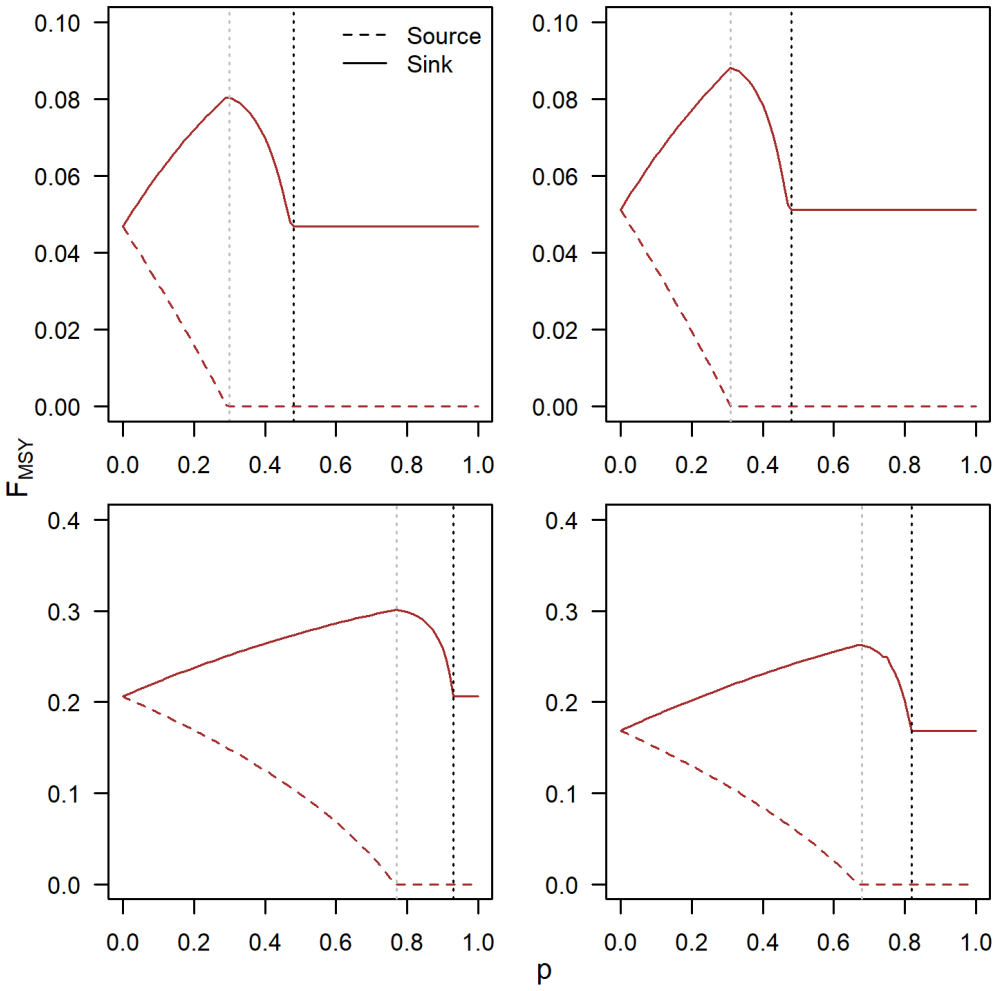

Figure 3.12: The optimal f_{MSY}'s at different p's, for a EQ system using the BH_{50} (top-left), RK_{50} (top-right), BH_h (bottom-left), and RK_h (bottom-right) SR models. The vertical lines indicate p_{f0} (grey) and p_{ex} (black).

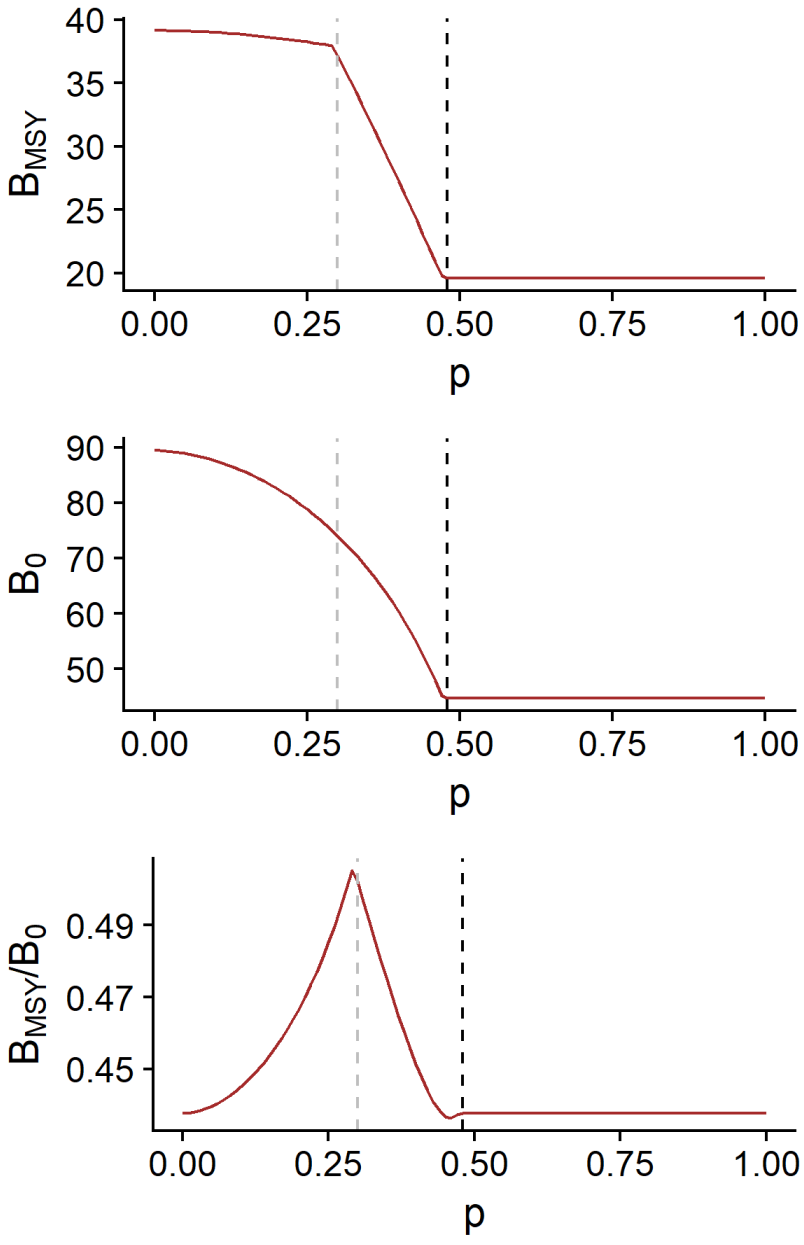

Figure 3.13: Total B_{MSY}, B_0, and biomass depletion at different p's, for a EQ system using the BH_{50} SR model. The vertical lines indicate p_{f0} (grey) and p_{ex} (black).

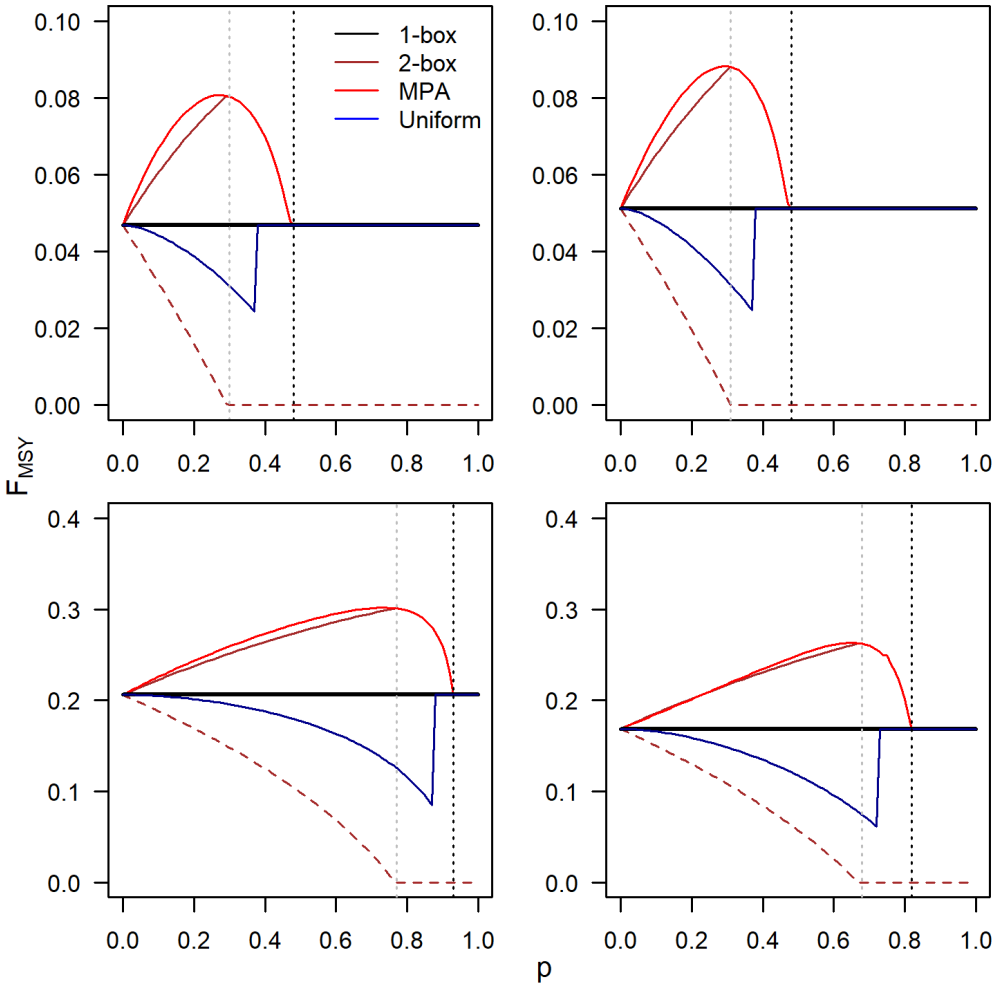

Figure 3.14: f_{MSY} at different p's for an EQ system using the BH_{50} (top-left), RK_{50} (top-right), BH_h (bottom-left), and RK_h (bottom-right) SR models. The optimal f's (brown) are displayed separately as f_1 (dashed) and f_2 (solid) (Refer to Figure 3.12). The vertical lines indicate p_{f0} (grey) and p_{ex} (black). Once $p = p_{f0}$, the f_{MPA} curve overlaps with the optimal $f_{MSY,2}$ curve because $f_{MSY,1} = 0$ and $f_{MSY,2} = f_{MPA}$.

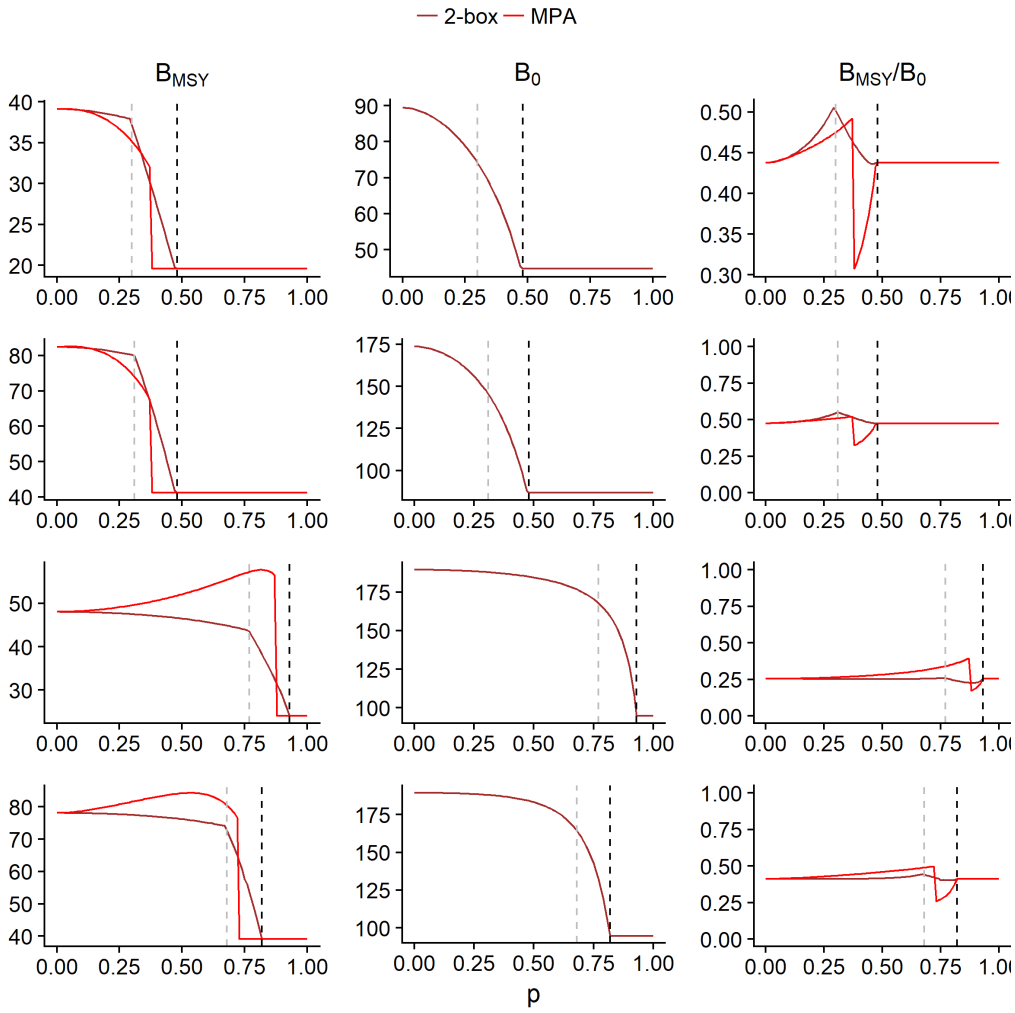

Figure 3.15: Total B_{MSY}, B_0, and biomass depletion at different p's, for an EQ system using the BH_{50} (row 1), RK_{50} (row 2), BH_h (row 3), and RK_h (row 4) SR models. The vertical lines indicate p_{f0} (grey) and p_{ex} (black). Also see Figure 3.13.

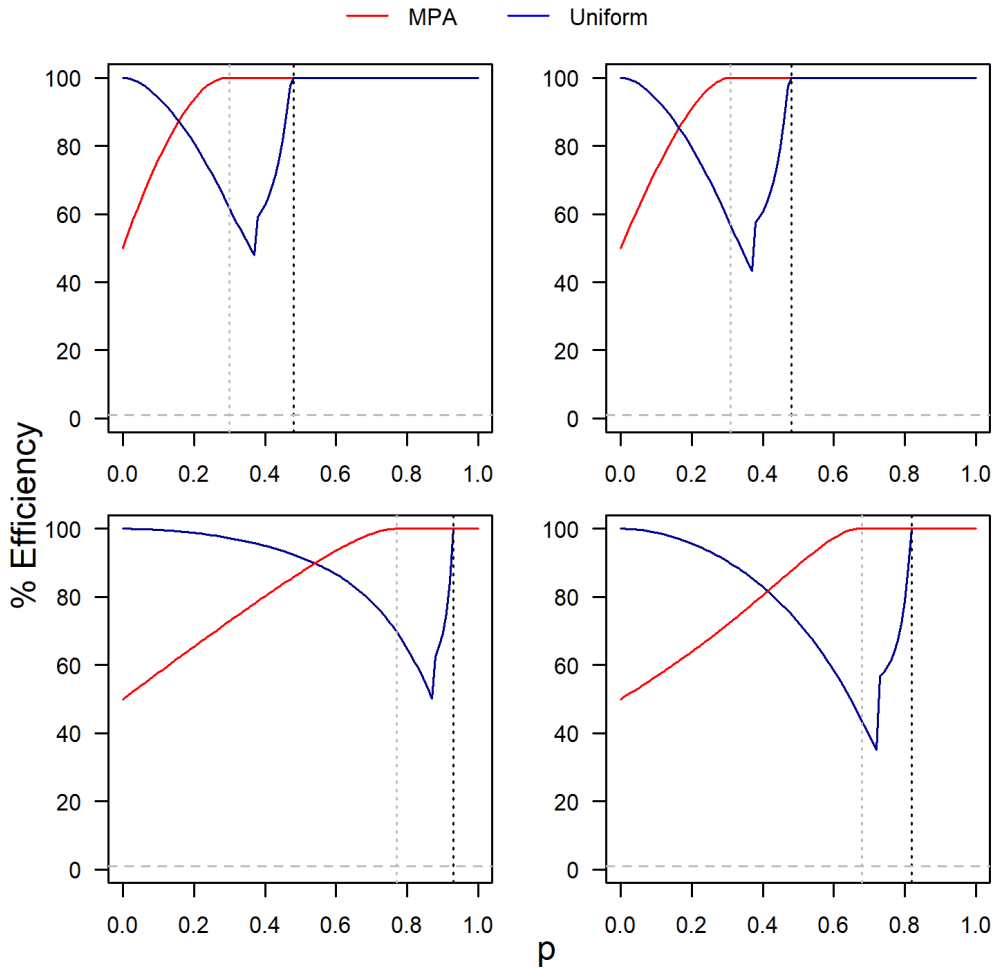

Figure 3.16: Efficiency of sub-optimal harvest strategies at different p's for an EQ system, using the BH_{50} (top-left), RK_{50} (top-right), BH_h (bottom-left), and RK_h (bottom-right) SR models. The vertical lines indicate p_{f0} (grey) and p_{ex} (black).

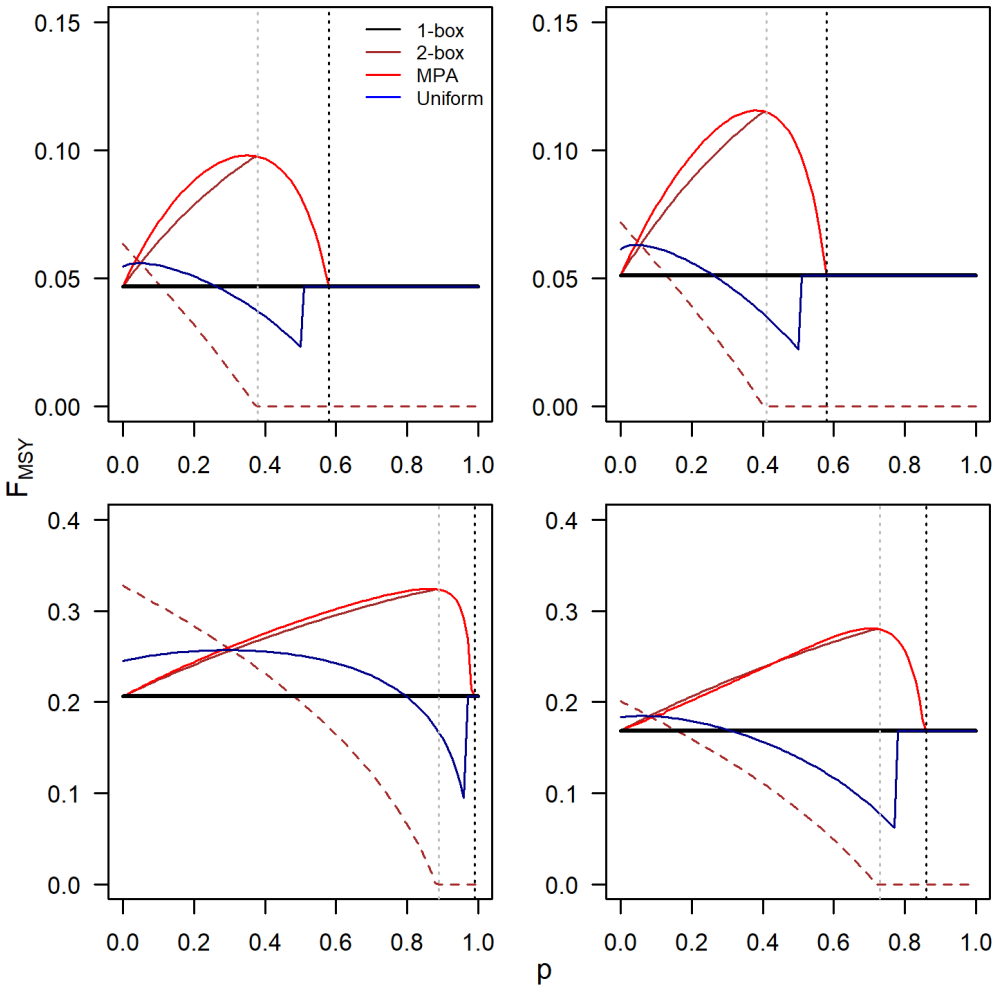

Figure 3.17: f_{MSY} at different p's for a HL system using the BH_{50} (top-left), RK_{50} (top-right), BH_h (bottom-left), and RK_h (bottom-right) SR models. The vertical lines indicate p_{f0} (grey) and p_{ex} (black).

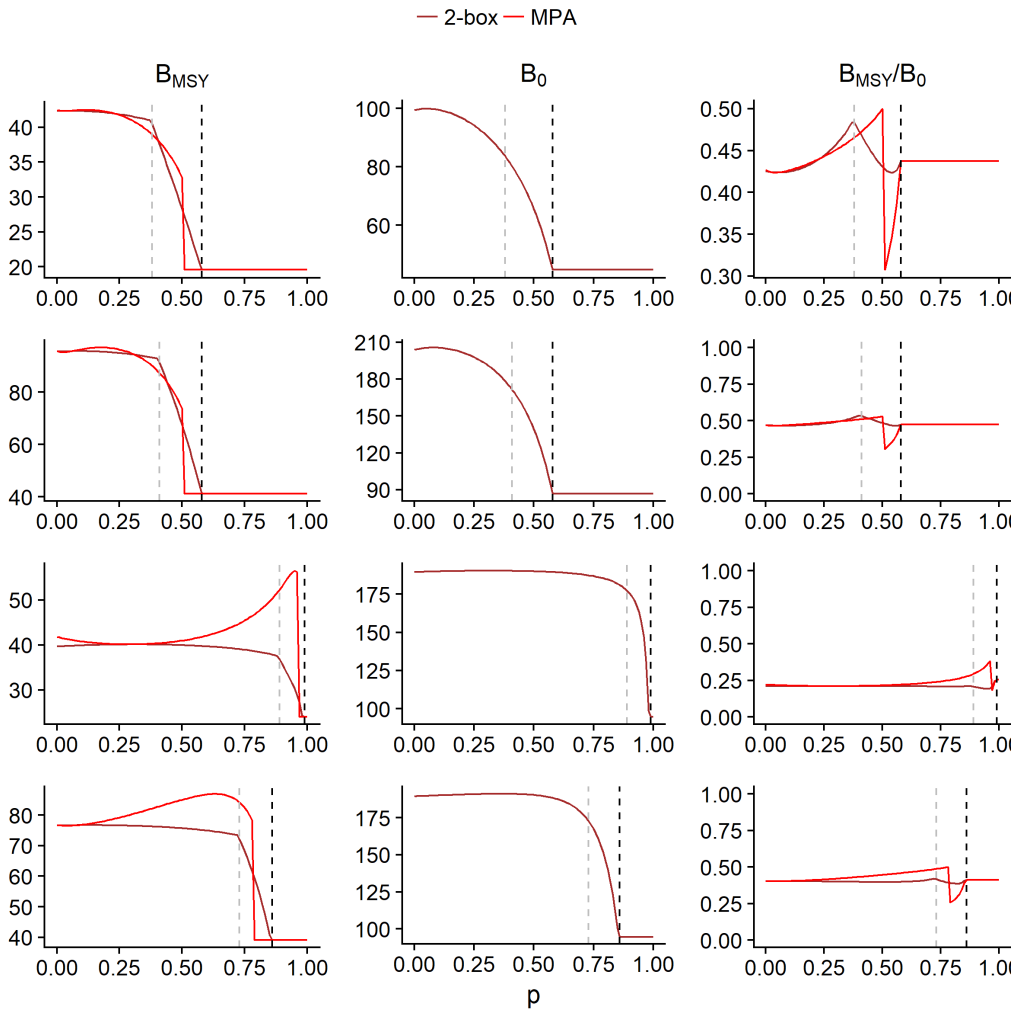

Figure 3.18: Total B_{MSY}, B_0, and biomass depletion at different ps, for a HL system using the BH_{50} (row 1), RK_{50} (row 2), BH_h (row 3), and RK_h (row 4) SR models. The vertical lines indicate p_{f0} (grey) and p_{ex} (black).

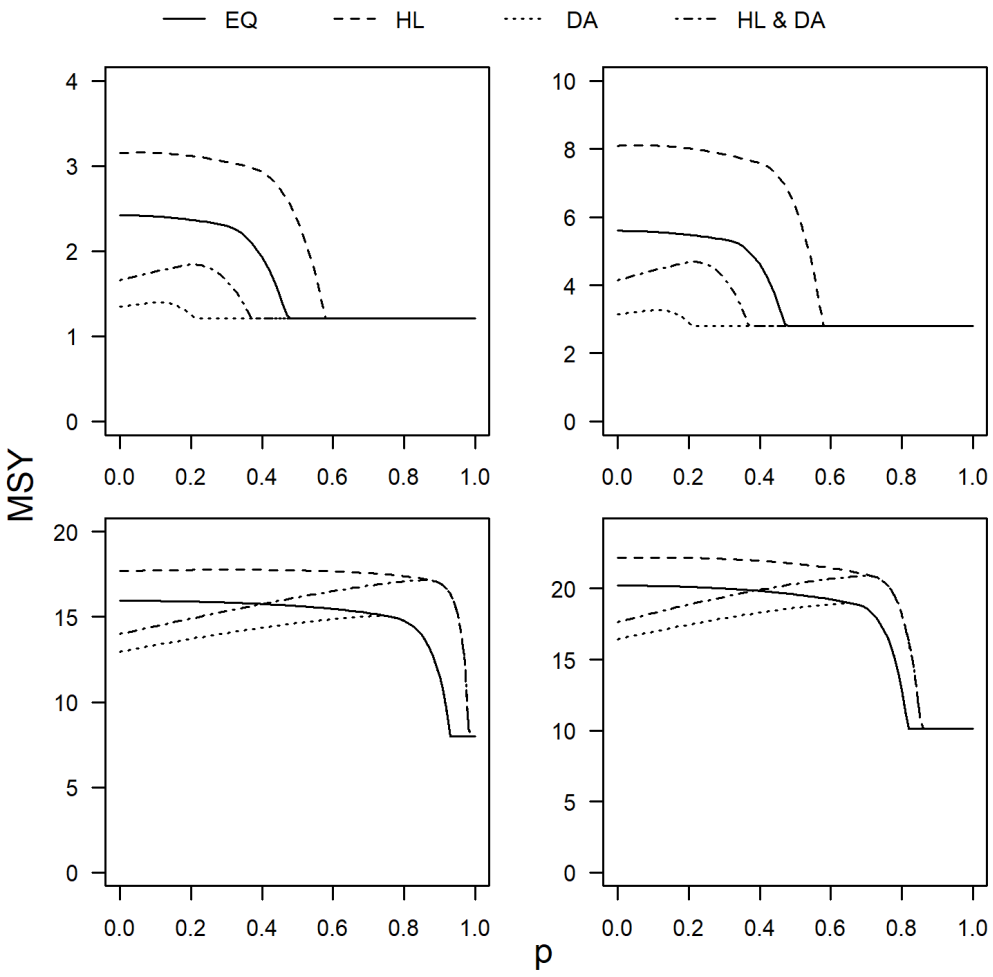

Figure 3.19: Total MSY from the optimal harvest strategy (i.e. $f_1 = f_{MSY,1}$ and $f_2 = f_{MSY,2}$) using the BH_{50} (top-left), RK_{50} (top-right), BH_h (bottom-left), and RK_h (bottom-right) SR models.

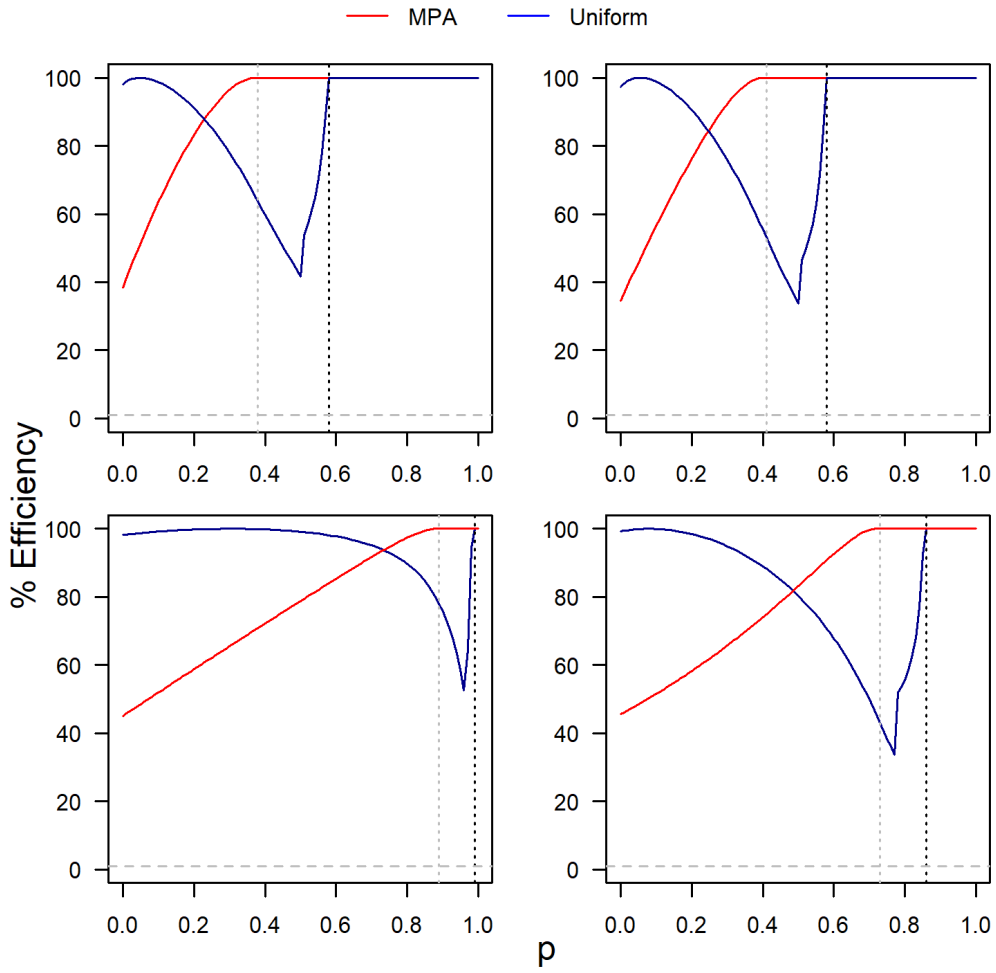

Figure 3.20: Efficiency of sub-optimal harvest strategies at different ps for a HL system, using the BH_{50} (top-left), RK_{50} (top-right), BH_h (bottom-left), and RK_h (bottom-right) SR models. The vertical lines indicate p_{f0} (grey) and p_{ex} (black).

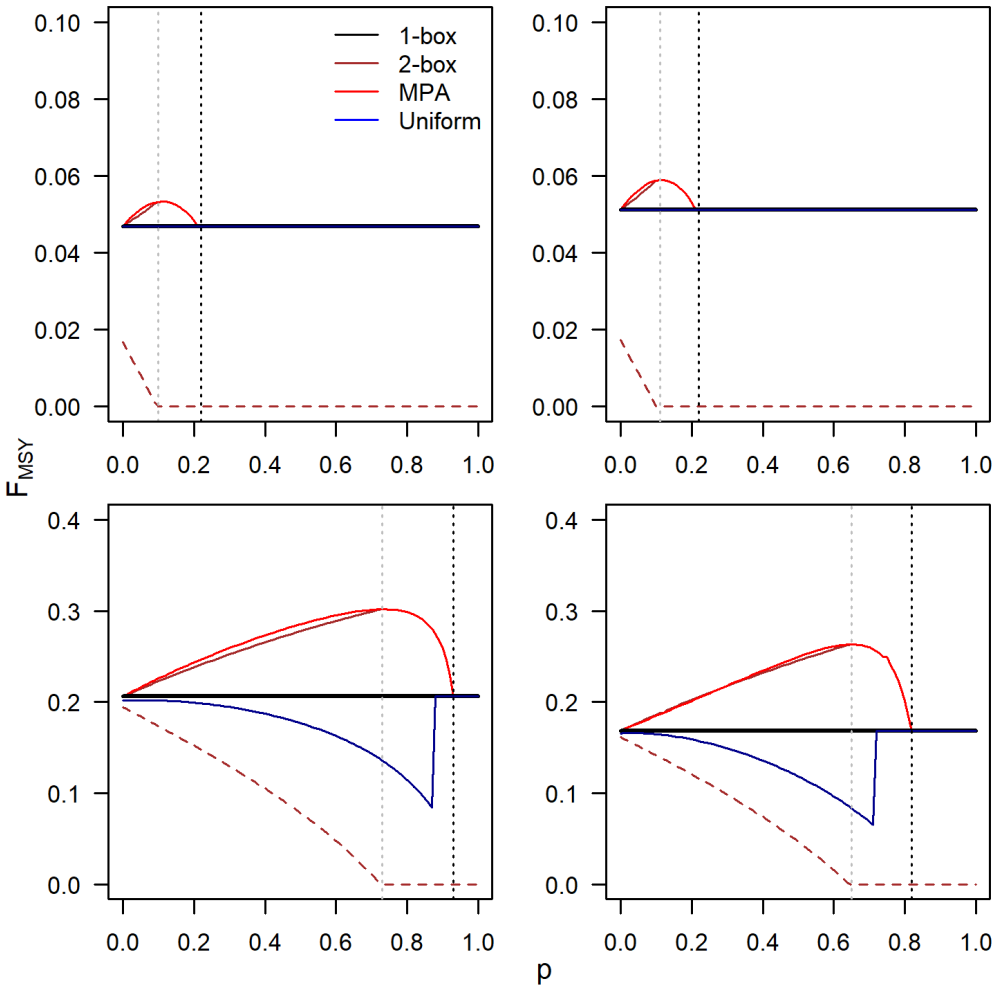

Figure 3.21: f_{MSY} at different p's, for a DA system using the BH_{50} (top-left), RK_{50} (top-right), BH_h (bottom-left), and RK_h (bottom-right) SR models. The vertical lines indicate p_{f0} (grey) and p_{ex} (black).

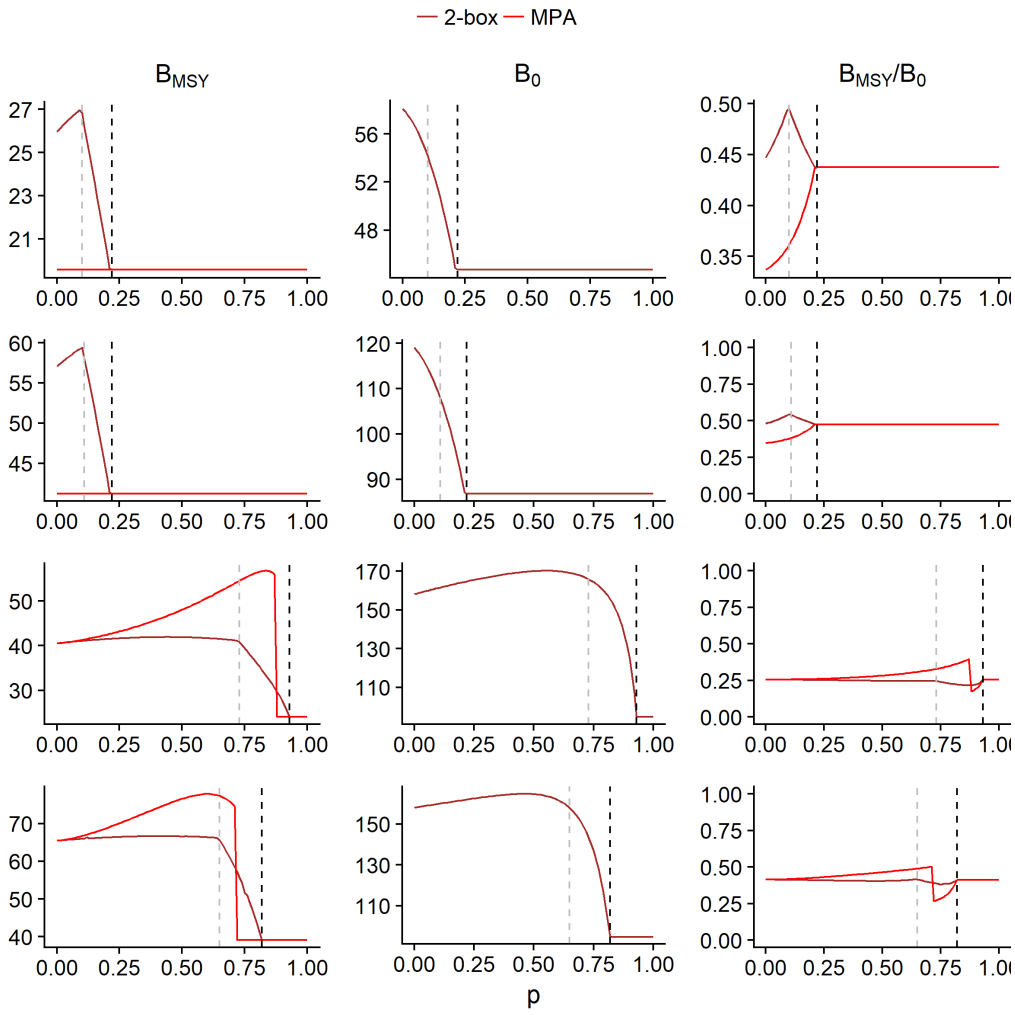

Figure 3.22: Total B_{MSY}, B_0, and biomass depletion at different p's, for a DA system using the BH_{50} (row 1), RK_{50} (row 2), BH_h (row 3), and RK_h (row 4) SR models. The vertical lines indicate p_{f0} (grey) and p_{ex} (black).

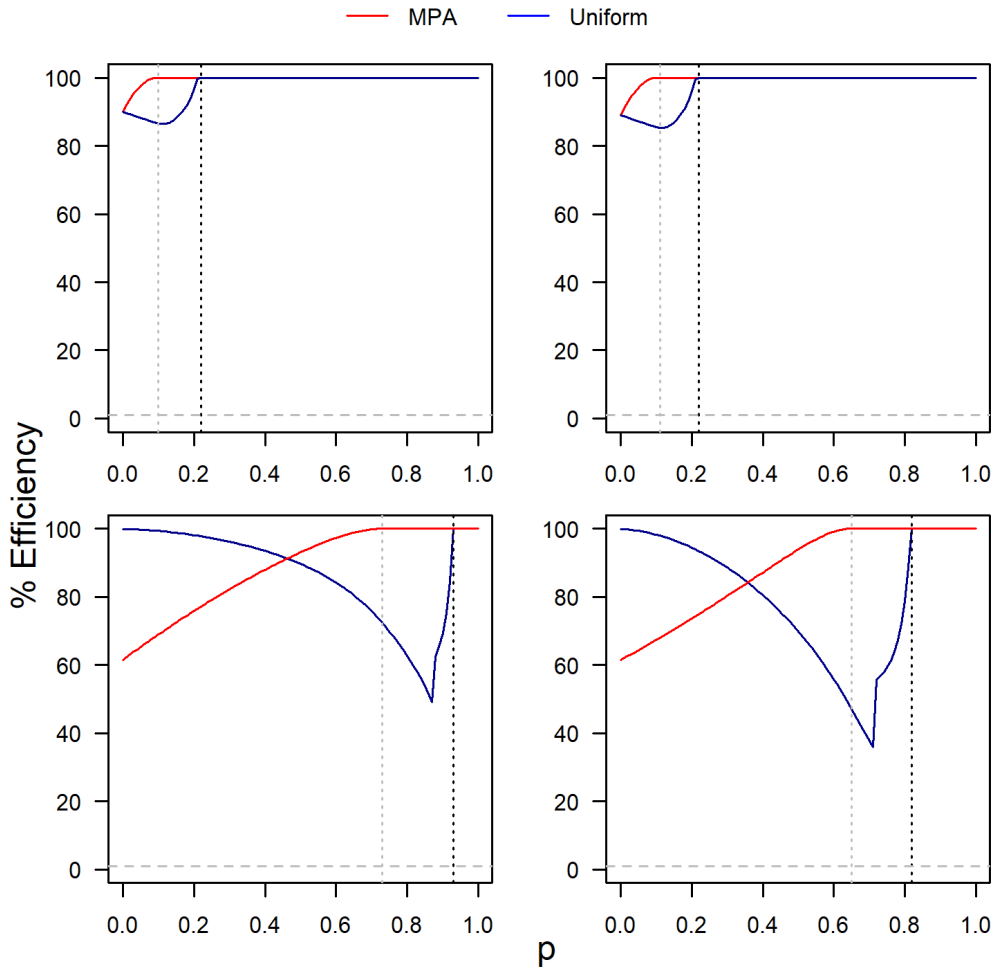

Figure 3.23: Efficiency of sub-optimal harvest strategies at different ps for a DA system, using the BH_{50} (top-left), RK_{50} (top-right), BH_h (bottom-left), and RK_h (bottom-right) SR models. The vertical lines indicate p_{f0} (grey) and p_{ex} (black).

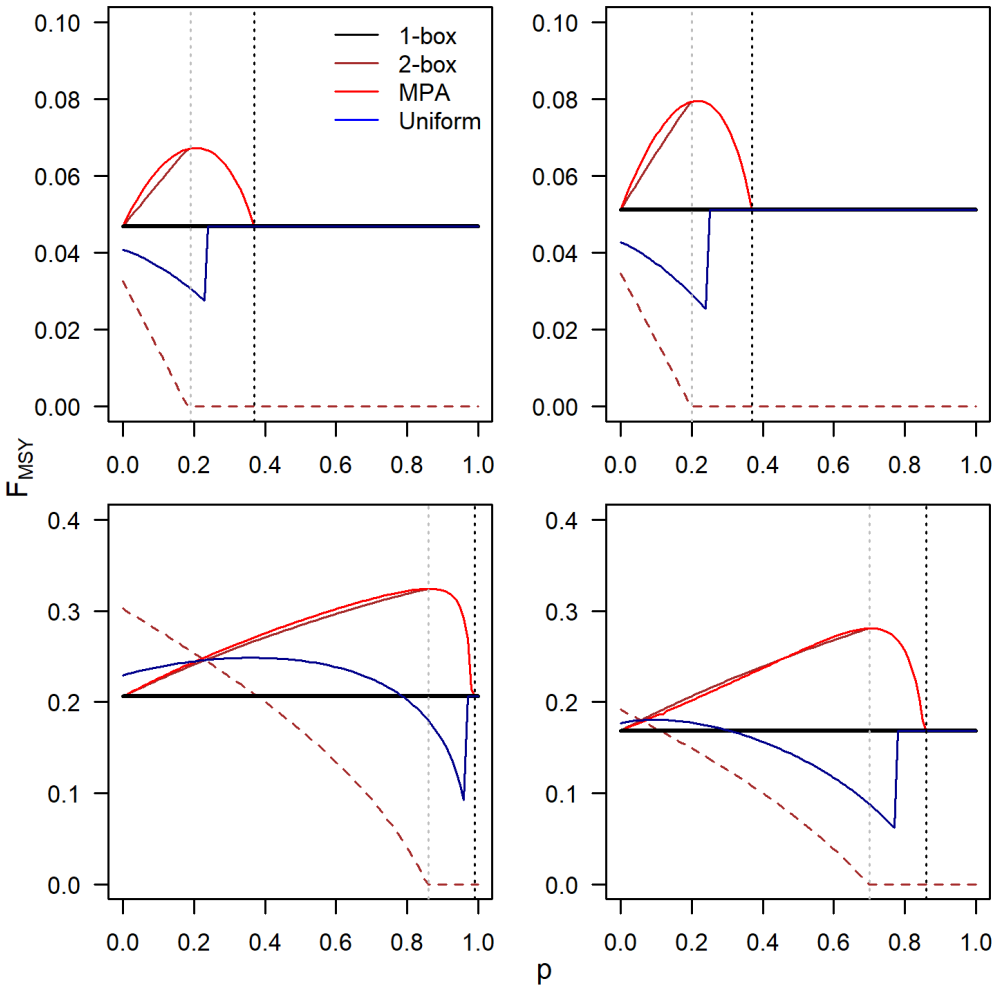

Figure 3.24: f_{MSY} at different p's, for a HL & DA system using the BH_{50} (top-left), RK_{50} (top-right), BH_h (bottom-left), and RK_h (bottom-right) SR models. The vertical lines indicate p_{f0} (grey) and p_{ex} (black).

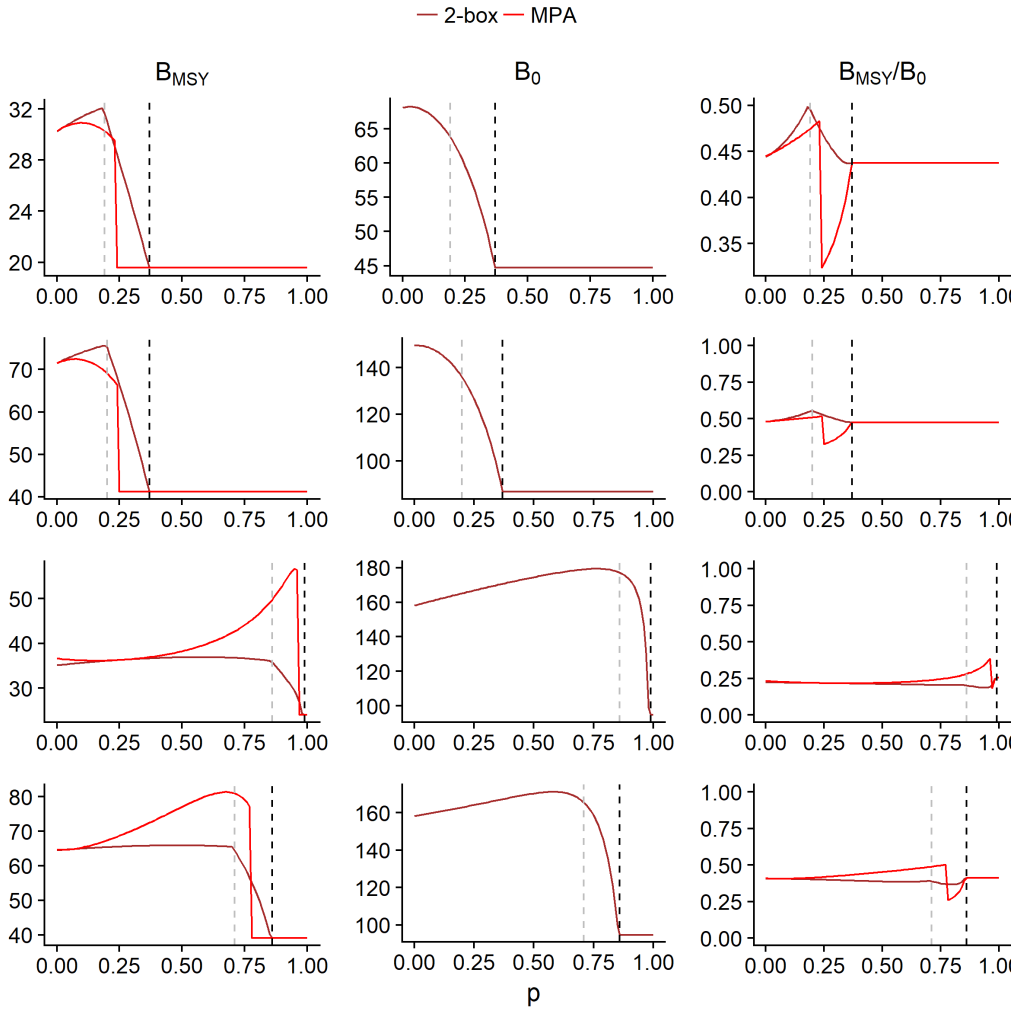

Figure 3.25: Total B_{MSY}, B_0, and biomass depletion at different ps, for a HL & NS system using the BH_{50} (row 1), RK_{50} (row 2), BH_h (row 3), and RK_h (row 4) SR models. The vertical lines indicate p_{f0} (grey) and p_{ex} (black).

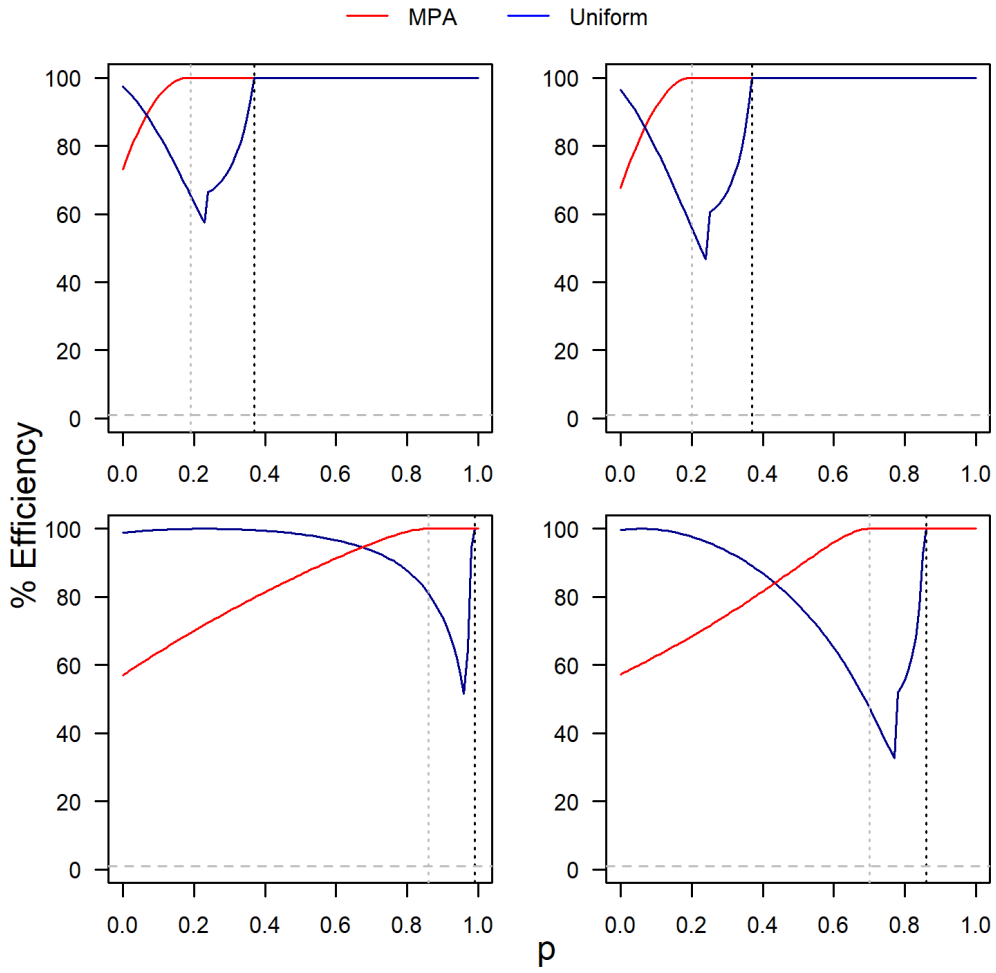

Figure 3.26: Efficiency of sub-optimal harvest strategies at different p's for a HL and DA system, using the BH_{50} (top-left), RK_{50} (top-right), BH_h (bottom-left), and RK_h (bottom-right) SR models. The vertical lines indicate p_{f0} (grey) and p_{ex} (black).

Chapter 4

The Three-Box Model

4.1 Methods

A model was developed in Chapter 3 to calculate spatially-explicit MSY RPs for a two-box, source-sink system. This framework can be expanded to model higher-dimension larval-advection dynamics. The two-box model involved a unidirectional advection pathway, where recruits transferred from source to sink. This resulted in a significant increase in complexity from the one-box model through the addition of the transfer proportion, spatially-segregated f's, and SR parameters and life history characteristics for each box. As the number of spatial dimensions increase, fish stocks may exhibit more complex connectivity patterns and variability between sub-populations. In this chapter, a three-box model will be developed to derive MSY RPs. However, model parameters must be heavily constrained to adequately present the dynamics of the metapopulation.

First, we define the SR relationships of each box to be proportional to

the area occupied by the sub-population, similar to the two-box model. We assume all sub-populations have the same areas, where $A_1 = A_2 = A_3$, and the density of SSB, ρ_S, and α and β are equal for all boxes, so all boxes have equal stock-recruitment relationships. Although this assumption isn't realistic, it provides a reasonable constraint and reduces complexity, and results that follow from the model will be optimistic by assuming recruitment is spatially invariant. Future research could expand on this to analyse the effect spatially-varying recruitment may have on RP estimates for each sub-population.

We only consider the BH SR model, since the effect of different SR models generally affects the scale of RPs, as demonstrated in Chapter 3. It can be shown that, for the BH model, α and β will be one third that for the one-box model. We assume $\alpha = \beta = 33$ (i.e. BH_{33}) and the total reproduction of all three boxes is equivalent to a one-box BH_{100} scenario.

For the three-box model, we simply assume all life history characteristics and SPR functions (and YPR functions) are equal for all boxes, where $SPR_1 = SPR_2 = SPR_3 = SPR$. We do this for two reasons: 1) we investigated spatially varying life history characteristics sufficiently in Chapter 3 and proceed by focusing primarily on the effects of population connectivity and overall stock persistence and harvest, and 2) a three-box model has far more degrees of freedom than the two-box model, and considering all possible assumptions and dynamics of three distinct sub-populations is too ambitious and beyond the scope of this thesis. Future studies may investigate spatially varying stock parametrizations and their impact on interconnectivity and management procedures, but we will focus mainly on developing and testing

the model for deriving such values.

There are five unique metapopulation advection patterns that can exist for a three-box larval advection model, assuming advection is unidirectional. These patterns are illustrated in Figure 4.1. The simplest one is a *Chain Advection* pattern (Figure 4.1a), where the SSB_{eq} depends on the R_{eq} of the sub-population before it in the chain. Let the transfer proportion from area i to j be denoted $p_{i\to j}$. Equilibrium SSB is defined as

$$SSB_{eq,1}(f_1) = (1 - p_{1\to 3})R_{eq,1}(f_1)SPR(f_1), \tag{4.1}$$

for sub-population P_1,

$$SSB_{eq,2}(f_1, f_2) = (1 - p_{2\to 3})R_{eq,2}(f_1, f_2)SPR(f_2) + p_{1\to 2}R_{eq,1}(f_1)SPR(f_2), \tag{4.2}$$

for P_2, and

$$SSB_{eq,3}(f_1, f_2, f_3) = R_{eq,3}(f_1, f_2, f_3)SPR(f_3) + p_{2\to 3}R_{eq,2}(f_1, f_2)SPR(f_3), \tag{4.3}$$

for P_3. This model is an extension of the source-sink model described in Chapter 3, where P_1 is a source, P_3 is a sink, and P_2 behaves as a sink for P_1 and a source for P_3.

Next is the *Converging Advection* pattern (Figure 4.1b). For this pattern, sub-populations P_1 and P_2 are reproductively isolated (i.e. sources), and recruits transfer from both sub-populations to P_3 (i.e. the sink). Therefore, the equilibrium recruitment for sub-populations P_1 and P_2 are independent

of all other sub-populations, but P_3 is dependent on the other two other sub-populations. Equilibrium SSB is defined as

$$SSB_{eq,1}(f_1) = (1 - p_{1\to3})R_{eq,1}(f_1)SPR(f_1), \tag{4.4}$$

for P_1,

$$SSB_{eq,2}(f_2) = (1 - p_{2\to3})R_{eq,2}(f_2)SPR(f_2), \tag{4.5}$$

for P_2, and

$$SSB_{eq,3}(f_1, f_2, f_3) = R_{eq,3}(f_1, f_2, f_3)SPR(f_3) + p_{1\to3}R_{eq,1}(f_1)SPR(f_3) \tag{4.6}$$

$$+p_{2\to3}R_{eq,2}(f_2)SPR(f_3), \tag{4.7}$$

for P_3.

In a *Branching Advection* pattern (Figure 4.1c), recruits from one sub-population, P_1, transfer to more than one other sub-population, in this case both P_2 and P_3. That is, sub-populations P_2 and P_3 are sinks to a single source sub-population, P_1. Equilibrium SSB is defined as

$$SSB_{eq,1}(f_1) = (1 - p_{1\to2} - p_{1\to3})R_{eq,1}(f_1)SPR(f_1), \tag{4.8}$$

for P_1,

$$SSB_{eq,2}(f_1, f_2) = R_{eq,2}(f_1, f_2)SPR(f_2) + p_{1\to2}R_{eq,1}(f_1)SPR(f_2), \tag{4.9}$$

for P_2, and

$$SSB_{eq,3}(f_1, f_3) = R_{eq,3}(f_1, f_3)SPR(f_3) + p_{1\to3}R_{eq,1}(f_1)SPR(f_3), \quad (4.10)$$

for P_3.

A *Detouring Advection* pattern (Figure 4.1d) models advection of recruits one sub-population, P_1, to more than one other sub-population, P_2 and P_3, but recruits from P_1 also transfer to P_2. Equilibrium SSB is defined as

$$SSB_{eq,1}(f_1) = (1 - p_{1\to2} - p_{1\to3})R_{eq,1}(f_1)SPR(f_1), \quad (4.11)$$

for P_1,

$$SSB_{eq,2}(f_1, f_2) = (1 - p_{2\to3})R_{eq,2}(f_1, f_2)SPR(f_2) + p_{1\to2}R_{eq,1}(f_1)SPR(f_2), \quad (4.12)$$

for P_2, and

$$SSB_{eq,3}(f_1, f_2, f_3) = R_{eq,3}(f_1, f_2, f_3)SPR(f_3) + \quad (4.13)$$

$$p_{1\to3}R_{eq,1}(f_1)SPR(f_3) + p_{2\to3}R_{eq,2}(f_1, f_2)SPR(f_3), \quad (4.14)$$

for P_3.

The last unique three-box connectivity pattern is the *Cyclical Advection* pattern (Figure 4.1e). This pattern is different from the previous patterns because equilibrium SSB and recruitment for any sub-population depends on itself, i.e. $S_1 = f(S_1) = (f \circ h \circ g \circ f)(S_1) = f(h(g(f(S_1))))$. To elaborate, for all other advection patterns, we assumed at least one sub-population was a

source, and SSB_{eq} of this source was independent of the SSB_{eq} for all other sub-populations. For the cyclical pattern, however, this independence does not exist, and all sub-populations act as either a source or sink to the other connected sub-populations. The equilibrium SSB for sub-population P_1 is defined as

$$SSB_{eq,1} = (1 - p_{1\to2})R_{eq,1}(f_1, f_2, f_3)SPR(f_1) + p_{3\to1}R_{eq,3}(f_1, f_2, f_3)SPR(f_1), \tag{4.15}$$

where $SSB_{eq,1}$ depends on $SSB_{eq,3}$, $SSB_{eq,3}$ depends on $SSB_{eq,2}$, $SSB_{eq,2}$ depends on $SSB_{eq,1}$, and so on. The Equilibrium SSB for the other sub-populations are defined as

$$SSB_{eq,2} = (1 - p_{2\to3})R_{eq,2}(f_1, f_2, f_3)SPR(f_2) + p_{1\to2}R_{eq,1}(f_1, f_2, f_3)SPR(f_2), \tag{4.16}$$

for P_2, and

$$SSB_{eq,3} = (1 - p_{3\to1})R_{eq,3}(f_1, f_2, f_3)SPR(f_3) + p_{2\to3}R_{eq,2}(f_1, f_2, f_3)SPR(f_3), \tag{4.17}$$

for P_3.

Equilibrium SSB values can be calculated from the above definitions for each pattern. Analytic equations can be derived for the BH SR model, but the RK must be numerically derived. In general, if the SSB_{eq} of the sub-population is independent of all other sub-populations and no recruits advect *into* the area, SSB_{eq} will be similar to Equation 3.1 (i.e. a source). However, for a three-box model, the amount of advecting recruits, p, will instead be

the sum of all transfer proportions of advecting recruits (e.g. $p = p_{1\to2} + p_{1\to3}$). If the SSB_{eq} of the sub-population depends on at least one other sub-population, SSB_{eq} will be similar to Equation 3.3 (i.e. a sink). In this case, the recruits transferring in will be the sum of all recruits transferring in. To be succinct, we calculated values for SSB_{eq} numerically rather than deriving explicit equations.

Total equilibrium yield can be calculated as

$$Y_{eq,tot}(f_1, f_2, f_3) = \sum_{i}^{3} \frac{YPR(f_i)}{SPR(f_i)} SSB_{eq,i}, \tag{4.18}$$

where $SSB_{eq,i}$ will depend on the connectivity pattern for the population and may depend on f_1, f_2, and f_3. Values for f_{MSY} for each area can be derived by optimizing the total equilibrium yield with respect to all f's, simultaneously. The optimal results will depend on the connectivity pattern and transfer proportions between each sub-population. Again, optimization is done using the *nlminb* function in **R**.

For each of the three-box model connectivity patterns, MSY RPs (e.g. f_{MSY}, B_{MSY} and biomass depletion) and MSY were calculated for each sub-population for varying transfer proportions. Values for total B_{MSY}, biomass depletion, and MSY were also calculated. RPs were derived using the BH_{33} SR model. The metapopulation for each pattern was modelled based on Figure 4.1.

4.2 Results

MSY RPs were derived for the five unique patterns for a three-box model. RPs were calculated for a range of $p_{1\to2}$, $p_{1\to3}$, and $p_{2\to3}$ for each pattern. Transfer proportions changes were mutually exclusive, where only one transfer proportion was allowed to vary at a time. The transfer proportions that did not change were fixed at a constant $p = 0.1$. The transfer proportions were changed one at a time to highlight the effect each proportion has on RP results.

The optimal f's for each sub-population were derived by optimizing the total equilibrium yield. B_{MSY} for each sub-population was calculated as the SSB_{eq} from the optimal f's. For example, $SSB_{eq,2}$ for the chain advection pattern depends on f_1 and f_2, so $B_{MSY,2}$ is calculated using $f_{MSY,1}$ and $f_{MSY,2}$. The total B_{MSY} is the sum of B_{MSY} for all sub-populations. Biomass depletion is calculated as the ratio of B_{MSY} to the unfished biomass for the sub-population, for example biomass depletion for P_2 for the chain advection pattern is $SSB_{eq,2}(f_1 = f_{MSY,1}, f_2 = f_{MSY,2})/SSB_{eq,2}(f_1 = 0, f_2 = 0)$. The total biomass depletion is the ratio of total B_{MSY} to the sum of unfished biomasses for each sub-population. The MSY for each sub-population is the equilibrium yield from the optimal f's, for example $MSY_2 = Y_{eq,2}(f_1 = f_{MSY,1}, f_2 = f_{MSY,2})$ for the chain advection pattern. Total MSY is the optimized total yield and also the sum of the MSYs for all sub-populations.

Like the two-box model, the three-box model has values of p for which f_{MSY} is zero (i.e. p_{f0}) and $SSB_{eq}(f = 0) = 0$ (i.e. p_{ex}). However, these values only exist for exclusive source sub-populations, since any amount of

immigrating recruits will make extirpation impossible, or populations that act as both a ource and sink if its respective source is depleted. These p values depend on the connectivity pattern, as well as the life history characteristics and SR relationships for each sub-population.

For several connectivity patterns, RP results exhibited trends similar to that of the two-box model RPs. For example, f_{MSY} for the two-box model (see Figure 3.12) strictly decreased in the source and increased in the sink as p increased, until $p = p_{f0}$ and $f_{MSY,1} = 0$. Once the source was unfished, $f_{MSY,2}$ decreased until $p = p_{ex}$, and $f_{MSY,2}$ remained constant for all further increases in p. For some connectivity patterns, f_{MSY} results for the three-box model followed a similar trend. We refer to this reoccurring trend in results as a "source-sink trend".

4.2.1 Chain Pattern

MSY RPs were derived for a chain advection pattern, where sub-populations are connected in a sequential order (see Figure 4.1a). Values for $f_{MSY,1}$, $f_{MSY,2}$ and $f_{MSY,3}$ were derived by optimizing the total equilibrium yield (Figure 4.2). Values for $f_{MSY,1}$ and $f_{MSY,2}$ exhibited a source-sink trend with respect to $p_{1\to2}$, where sub-population P_1 was the source and P_2 was the sink. Values for $f_{MSY,2}$ and $f_{MSY,3}$ had a similar trend with respect to $p_{2\to3}$, but the scales were larger and $f_{MSY,3}$ remained high when $p_{2\to3}$ was high. Also, $p_{1\to2}$ had slight effects on $f_{MSY,3}$ and $p_{2\to3}$ had slight effects on $f_{MSY,1}$.

Unsurprisingly, $p_{1\to3}$ had no effect on f_{MSY} values since sub-populations

P_1 and P_3 were not directly connected, and all MSY RPs are unaffected by changes in $p_{1\to3}$. Populations P_1 and P_2 are not connected and, although we include a $p_{1\to3}$ panel to facilitate comparisons with other figures below, this parameter has no effect on f_{MSY} for the chain advection pattern.

For the chain advection pattern, B_{MSY} for any sub-population was only significantly affected by recruits advecting out (Figure 4.3). For example, changing $p_{1\to2}$ reduced $B_{MSY,1}$ until $B_{MSY,1} = 0$, but $B_{MSY,2}$ and $B_{MSY,3}$ hardly changed. Also, $B_{MSY,2}$ decreased as $p_{2\to3}$ increased, but $B_{MSY,2} > 0$ even when $p_{2\to3} = 1$.

Biomass only became completely depleted for sub-population P_1 (Figure 4.4). Biomass depletion in sub-population P_2 decreased as $p_{2\to3}$ increased and increased as $p_{1\to2}$ increased, until sub-population P_1 was completely depleted. Biomass depletion in sub-population P_3 and the total biomass depletion were hardly affected by any transfer proportion.

Optimized yields followed similar trends to f_{MSY} for each sub-population (Figure 4.5). MSY_1 decreased and MSY_2 increased as $p_{1\to2}$ increased, until the $f_{MSY,1} = 0$, while MSY_2 decreased and MSY_3 increased as $p_{2\to3}$ increased, until the $f_{MSY,2} = 0$. The net change in total yields were always negative. The total MSY always decreased as any transfer proportion increased, and MSY was greatest when no recruits advected.

4.2.2 Converging Pattern

Sub-populations P_1 and P_2 behaved as sources for a single sink, P_3. MSY RPs showed a source-sink trend (see Figure 4.1b), where P_2 was the source

with respect to $p_{2\to3}$ and P_1 was the source with respect to $p_{1\to3}$. All MSY RPs were independent of $p_{1\to2}$ because sub-populations P_1 and P_2 were unconnected.

Values for $f_{MSY,1}$ were independent of changes in $p_{2\to3}$ and values for $f_{MSY,2}$ were independent of $p_{1\to3}$ (Figure 4.6). Values for $f_{MSY,2}$ with respect to changes in $p_{2\to3}$ were identical to values for $f_{MSY,1}$ with respect to changes in $p_{1\to3}$, and $f_{MSY,3}$ responded equally from changes in $p_{1\to3}$ and $p_{2\to_3}$. Values for $f_{MSY,3}$ were always higher than $f_{MSY,1}$ or $f_{MSY,2}$. This is because sub-population P_3 was supplied with recruits from two independent sources, and could allow more fishing than either sources. Similar to the chain advection connectivity pattern, $p_{1\to2}$ had no affect because sub-populations P_1 and P_2 were not connected in the converging advection connectivity pattern.

$B_{MSY,1}$ strictly decreased as $p_{1\to3}$ increased and $B_{MSY,2}$ decreased as $p_{2\to3}$ increased. $B_{MSY,1}$ and $B_{MSY,2}$ decreased more than $B_{MSY,3}$ increased from increasing transfer proportions, and $B_{MSY,3}$ changed very slightly from increases in either $p_{1\to3}$ or $p_{2\to3}$. Therefore, the total B_{MSY} strictly decreased with transfer proportions, and any amount of advecting recruits resulted in reduced total B_{MSY}.

Biomass became less depleted in the sources (i.e. P_1 and P_2) as the transfer proportions increased (Figure 4.8) until the source were extirpated. Biomass depletion for P_3, and total biomass depletion hardly changed for any changes in transfer proportions.

MSY for all sub-populations followed similar trends as f_{MSY} (Figure 4.9). Yields decreased in the sources (i.e. P_1 and P_2) as their respective transfer proportions increased, and yields in the sink (i.e. P_3) were increased as

long either source persisted to supply recruits. However, any amount of transferring recruits between sub-populations reduced the total MSY.

4.2.3 Branching Pattern

The branching advection pattern (Figure 4.1c) behaved as a source-sink systems with two sinks (P_2 and P_3) and once source (P_1). Of course, MSY RPs were independent of $p_{2\to3}$ because sub-populations P_2 and P_3 were unconnected.

Values for $f_{MSY,1}$ strictly decreased with $p_{1\to2}$ and $p_{1\to3}$, and $f_{MSY,2}$ and $f_{MSY,3}$ increased as $p_{1\to2}$ and $p_{1\to3}$ increased, respectively (Figure 4.10). Sub-population P_1 provide both other sub-populations with recruits, and if $p_{1\to2}$ increased, for example, $f_{MSY,3}$ would decrease because less recruits were available to advect from P_1 to P_3. The optimization of f's for both sink sub-populations depended on both sub-populations even though P_2 did not directly depend on $p_{1\to3}$ and P_3 did not directly depend on $p_{1\to2}$. Both sinks relied on the same source, and recruits advecting into one sink had indirect effects on the other.

Only $B_{MSY,1}$ was significantly affected by increases in any transfer proportions. $B_{MSY,2}$ and $B_{MSY,3}$ remained relatively constant, and the total B_{MSY} strictly decreased with any transfer proportion due to the decrease in $B_{MSY,1}$ (Figure 4.11).

Biomass depletion changed significantly with $p_{1\to2}$ and $p_{1\to3}$ for P_1, while biomass depletion for P_2 and P_3, as well as the total biomass depletion, changed very little for any transfer proportion (Figure 4.12).

Yields, similar to the optimal f's, followed the source-sink trend (Figure 4.13). Most MSYs decreased as any transfer proportion increased, the exceptions being MSY_2 for $p_{1\to2}$ when $p_{1\to2}$ was low and MSY_3 for $p_{1\to3}$ when $p_{1\to3}$ was low. The total MSY always decreased as transfer proportions increased.

4.2.4 Detouring Pattern

The detouring advection pattern (Figure 4.1d) is one of two fully interconnected connectivity patterns, where all sub-populations are directly connected, and all transfer proportions affected MSY RPs. In this case, sub-population P_1 is a source to sub-populations P_2 and P_3, while P_2 is also a source to P_3.

Sub-population P_3 could allow higher f's than P_2, and P_2 could allow higher f's than P_1 (Figure 4.14). Both sink sub-populations allowed higher f's because they both had an influx of recruits from P_1. Values for $f_{MSY,1}$ (source) and $f_{MSY,2}$ (sink) followed the source-sink trend with respect to $p_{1\to2}$, and $f_{MSY,3}$ decreased with $p_{1\to2}$. Also, $f_{MSY,1}$ (source) and $f_{MSY,3}$ (sink) followed a source-sink trend with respect $p_{1\to3}$, and $f_{MSY,2}$ decreased with $p_{1\to3}$. The transfer proportion $p_{2\to3}$ hardly affected $f_{MSY,1}$ because $p_{2\to3}$ did not directly affect sub-population P_1. Values for $f_{MSY,2}$ and $f_{MSY,3}$ followed a somewhat source-sink trend, but with higher sustainable f's, and $f_{MSY,3}$ was higher when $p_{2\to3} = 1$ than when $p_{2\to3} = 0$.

$B_{MSY,1}$ decreased as $p_{1\to2}$ and $p_{1\to3}$ increased, and $B_{MSY,2}$ decreased as $p_{2\to3}$ increased (Figure 4.15). Otherwise, B_{MSY} values changed minimally with transfer proportions. The total B_{MSY} strictly decreased with an increase

in any transfer proportion.

Sub-population P_1 became depleted if $p_{1\to2}$ or $p_{1\to3}$ was high enough, and P_2 became less depleted as $p_{2\to3}$ increased and P_1 persisted (Figure 4.16). However, in most cases, sub-population biomass depletion and total biomass depletion changed minimally with any transfer proportions.

Yields for each sub-population followed the same trends as f_{MSY} (Figure 4.17), and total MSY strictly decreased with an increase in any transfer proportion.

4.2.5 Cyclical Pattern

For a cyclical advection pattern (Figure 4.1e), all sub-populations are connected similar to the detouring pattern. However, all sub-populations behave as either a source or sink to the other sub-populations, and no sub-population is reproductively independent. Note, recruits transfer from P_3 to P_1 and not from P_1 to P_3, and so $p_{1\to3}$ instead denotes the transfer proportion of recruits from P_3 to P_1.

MSY RPs for each sub-population followed the same trends between changing transfer proportions because all sub-population were essentially identical. To elaborate, $f_{MSY,1}$ with respect to $p_{1\to2}$ had the same values as $f_{MSY,2}$ with respect to $p_{2\to3}$ and $f_{MSY,3}$ with respect to $p_{1\to3}$ (Figure 4.18). The same is true for all f_{MSY} values, B_{MSY} values (Figure 4.19), biomass depletion (Figure 4.20), and yields (Figure 4.21). No one population is distinct, and all sub-populations are identical in how they respond to the emigrating proportions (e.g. $p_{1\to2}$ for P_1) assuming reproduction rates and life history

characteristics are the same.

Furthermore, no sub-population became depleted even when transfer proportions were $p = 1$. A cyclical connectivity pattern would create a hyperstable stock, where sub-populations could only be depleted if all sub-populations were depleted, which could only occur from overfishing in all areas since there is no p that would result in population extirpation.

4.3 Discussion

Augmenting a two-box spatial equilibrium yield model to feature three dimensions increases the precision and complexity of the dynamics, and preforming an overall analysis of these dynamics and the effects population connectivity have on MSY RPs is difficult. Therefore, the investigation of three-box model RPs requires constraints to glean practical information.

MSY RP results depended heavily on the connectivity pattern of the metapopulation, and RPs for each sub-population responded differently to each transfer proportion. Some RPs behaved similarly to the two-box source-sink model, while many RPs for the three-box model were unresponsive to transfer proportions.

In general, RPs are typically unaffected by transfer proportions that do not exist within their respective connectivity patterns, for example $p_{2\to3}$ did not affect $f_{MSY,1}$ for a branching pattern (see Figure 4.10). In several cases, however, transfer proportions (and therefore MSY RPs) had indirect effects on populations not directly linked to their particular sub-population configuration. For example, increasing $p_{1\to3}$ in a Branching pattern decreased

$f_{MSY,2}$ (Figure 4.10). Indeed, when assessing fish stocks, the metapopulation must be considered as a whole rather than a composition of its constituents to account for these indirect effects of interconnectivity.

Similar to the two-box model, the total B_{MSY} and MSY strictly decreased with the increases of any transfer proportion, for any connectivity pattern, and the total biomass depletion remained about constant with the increase of any transfer proportion. That is, for both the two- and three-box model, total RP values (and MSY) had similar trends with respect to the amount of transferring recruits.

Although values for MSY RPs were dependent on the transfer proportions, results were constrained by forcing transfer proportions to be $p = 0.1$. Exact RP results may be situational to these constraints, and the general trends in RPs may not be consistent, for example, if sub-populations become extirpated. When deriving MSY RPs for a three-box model, results will depend heavily on the assumptions made about the connectivity of the sub-populations.

RP values change based on the connectivity pattern of the sub-populations and depend on the transfer proportion between sub-populations. Overall, total yield relies on the f's of each sub-population (3) and the transfer proportion between each sub-population (3), and MSY has 6 degrees of freedom. When deriving MSY RPs, constraints must be placed on these variables to visualize how they change in response to one another. It is also difficult to clearly visualize how equilibrium values (e.g. Y_{eq} and SSB_{eq}) respond to f_1, f_2, f_3, $p_{1\to2}$, $p_{2\to3}$, and $p_{1\to3}$ simultaneously.

Although RP results may be analysed based on SSB_{eq} and Y_{eq} equations,

deriving these functions for each sub-population with specific connectivity patterns can be tedious, and is only possible for the BH SR model. Deriving equilibrium solutions and MSY RPs numerically is quicker and does not require explicit equations, which can be overwhelming to derive, especially when more than two sub-populations are present. In the next chapter, we develop a matrix model to numerically derive MSY RPs for n boxes, for any connectivity pattern, and for any SR model.

4.4 Figures

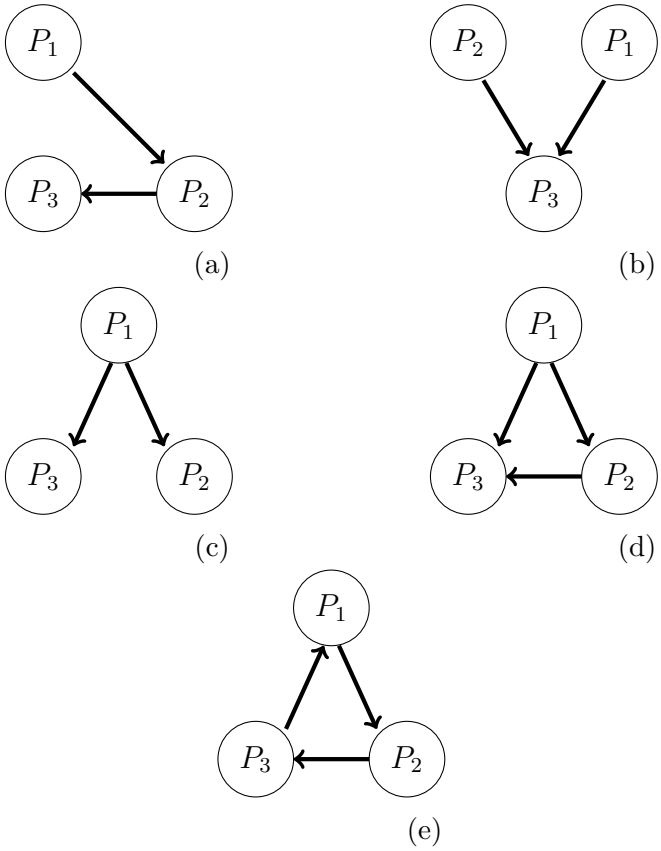

Figure 4.1: Three-box metapopulation structures with unidirectional transfer, where sub-populations P_1, P_2, and P_3 are connected through a (a) chain, (b) converging, (c) branching, (d) detouring, and (e) cyclical advection pattern.

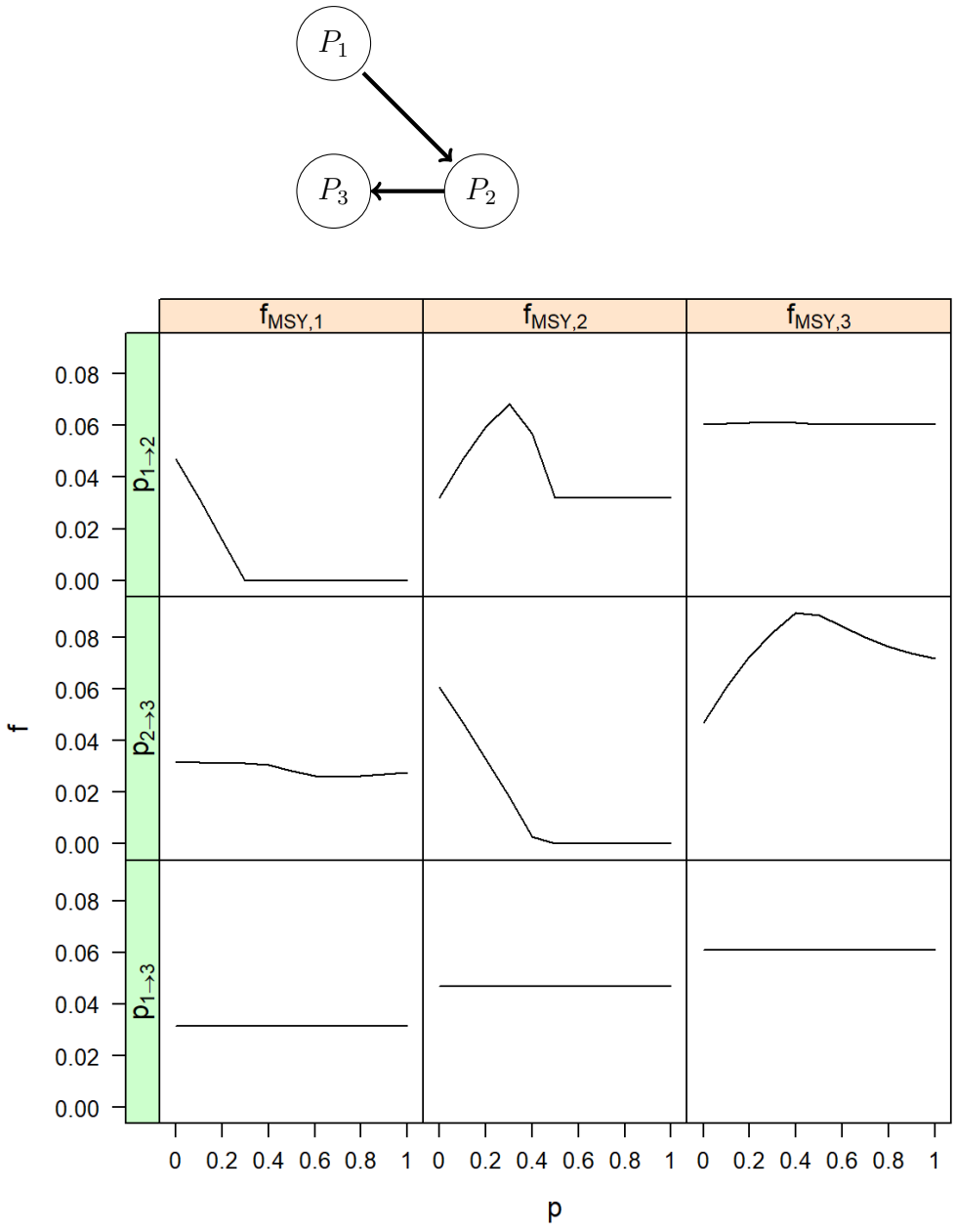

Figure 4.2: Values for f_{MSY} for a three-box model with a chain advection connectivity pattern. Values are calculated for each sub-population according to Figure 4.1a. Changes in transfer proportions are mutually exclusive, where only one transfer proportion changes at a time (indicated by row). All non-changing transfer proportions a fixed at a constant $p = 0.1$.

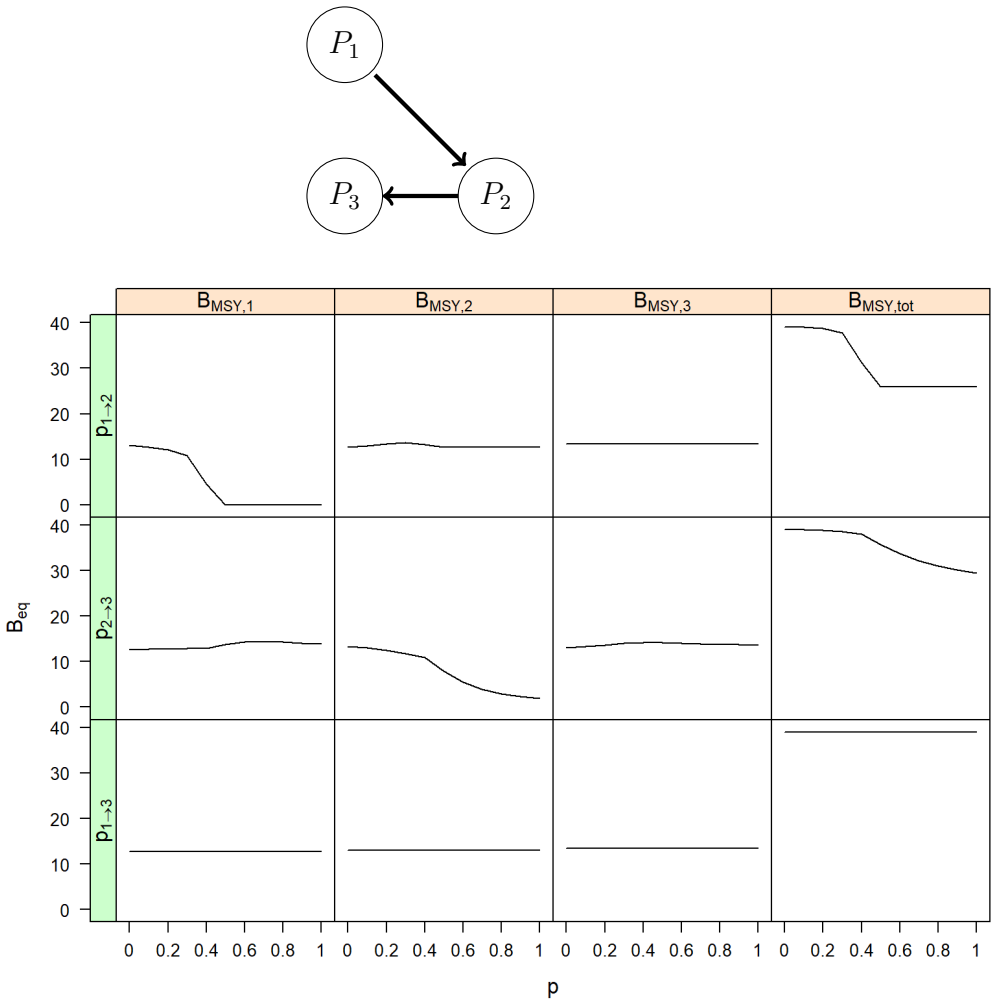

Figure 4.3: Values for B_{MSY} for a three-box model with a chain advection connectivity pattern. Values are calculated for each sub-population according to Figure 4.1a. Total B_{MSY} is the sum of all B_{MSY} values for each sub-population. Changes in transfer proportions are mutually exclusive, where only one transfer proportion changes at a time (indicated by row). All non-changing transfer proportions a fixed at a constant $p = 0.1$.

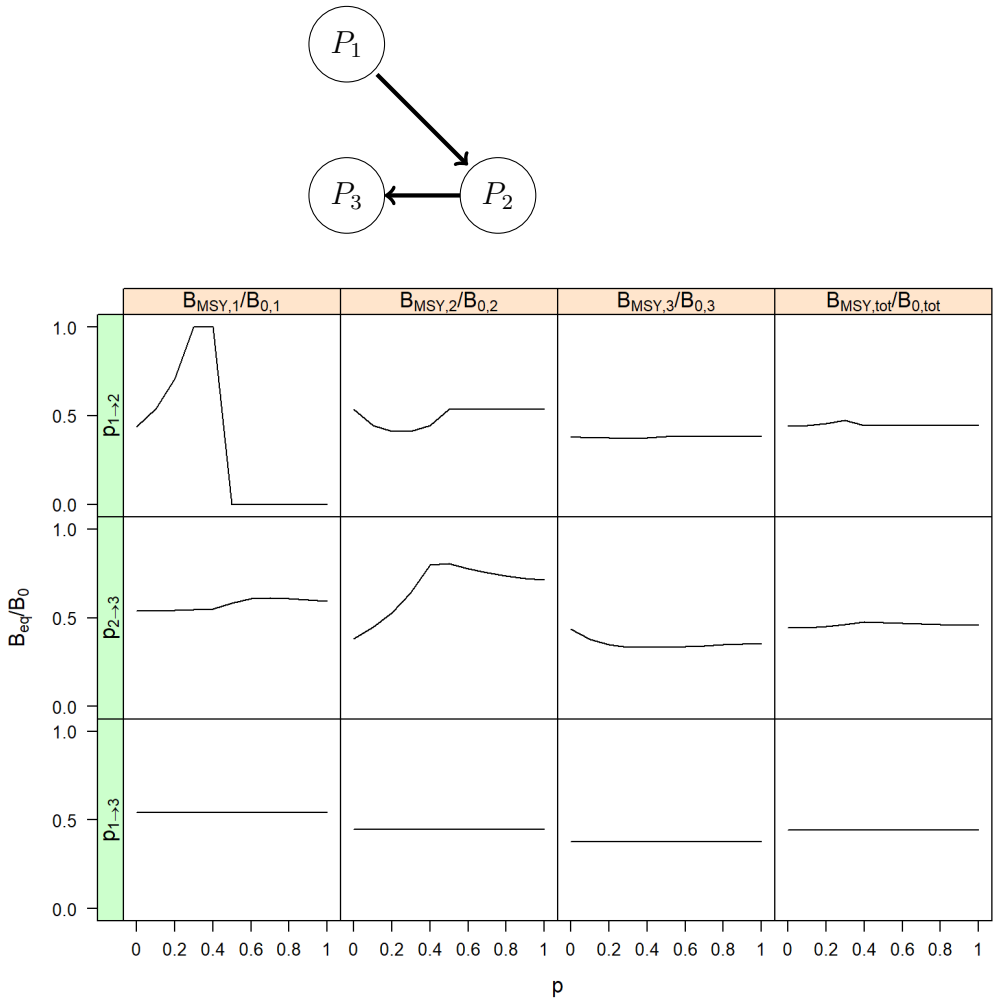

Figure 4.4: Biomass depletion for a three-box model with a chain advection connectivity pattern. Values are calculated for each sub-population according to Figure 4.1a. Biomass depletion is the ratio of B_{MSY} to unfished biomass for each sub-population, and total biomass depletion is the ratio of the sum of all B_{MSY} values to the sum of all unfished biomasses. Changes in transfer proportions are mutually exclusive, where only one transfer proportion changes at a time (indicated by row). All non-changing transfer proportions a fixed at a constant $p = 0.1$.

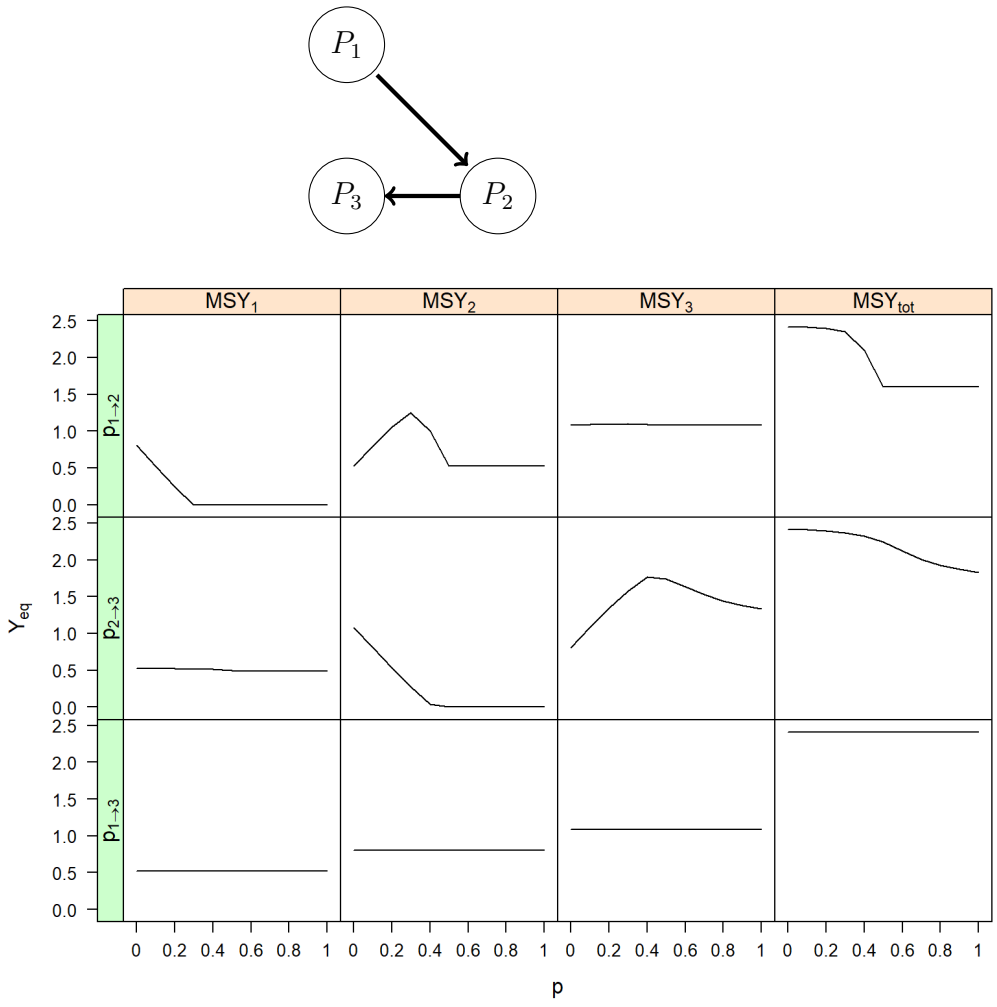

Figure 4.5: MSY for a three-box model with a chain advection connectivity pattern. Values for MSY are calculated for each sub-population according to Figure 4.1a. Total MSY is the sum of optimized yields for all sub-populations. Changes in transfer proportions are mutually exclusive, where only one transfer proportion changes at a time (indicated by row). All non-changing transfer proportions a fixed at a constant $p = 0.1$.

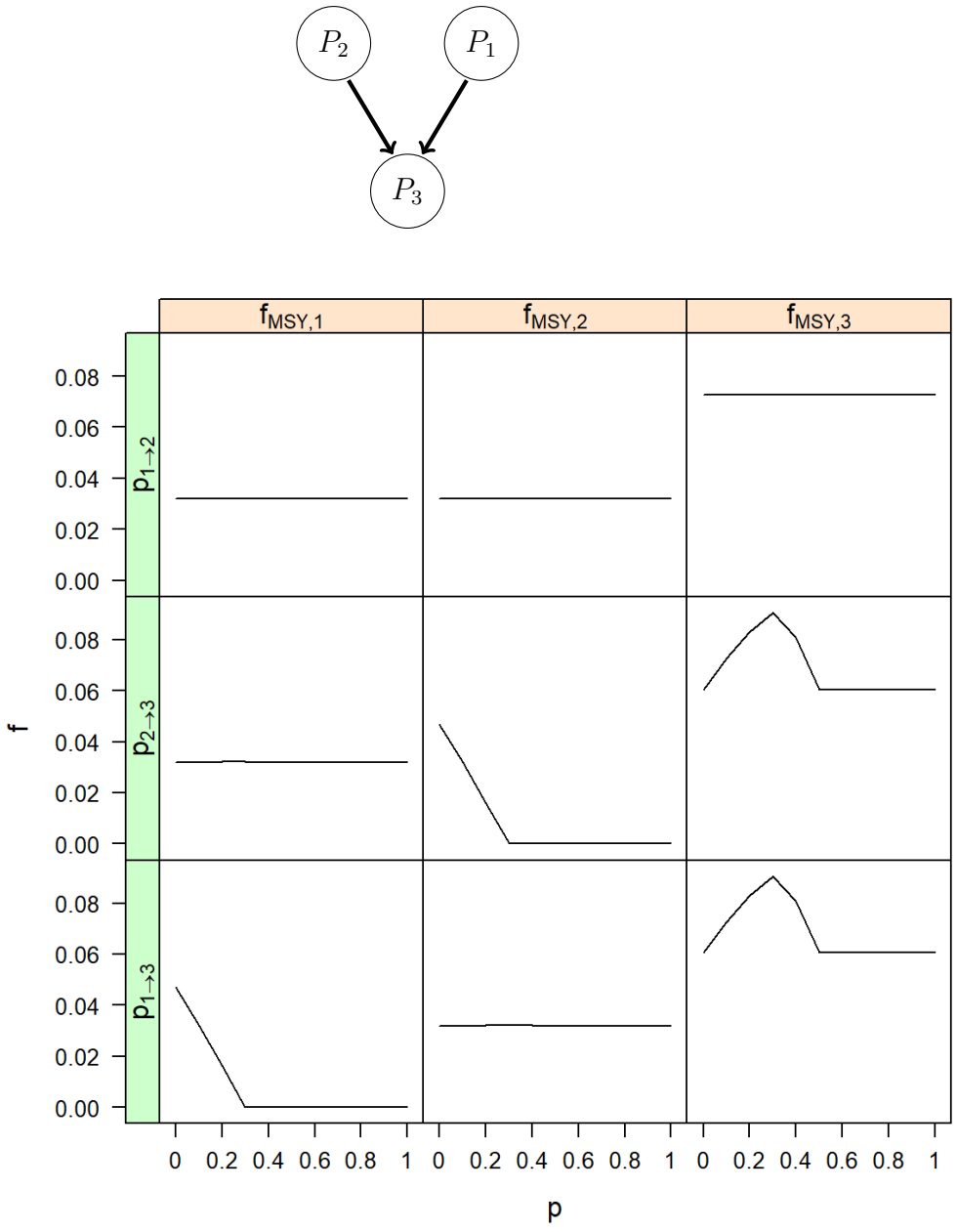

Figure 4.6: Values for f_{MSY} for three-box model with a converging advection connectivity pattern. Values are calculated for each sub-population according to Figure 4.1b. Changes in transfer proportions are mutually exclusive, where only one transfer proportion changes at a time (indicated by row). All non-changing transfer proportions a fixed at a constant $p = 0.1$.

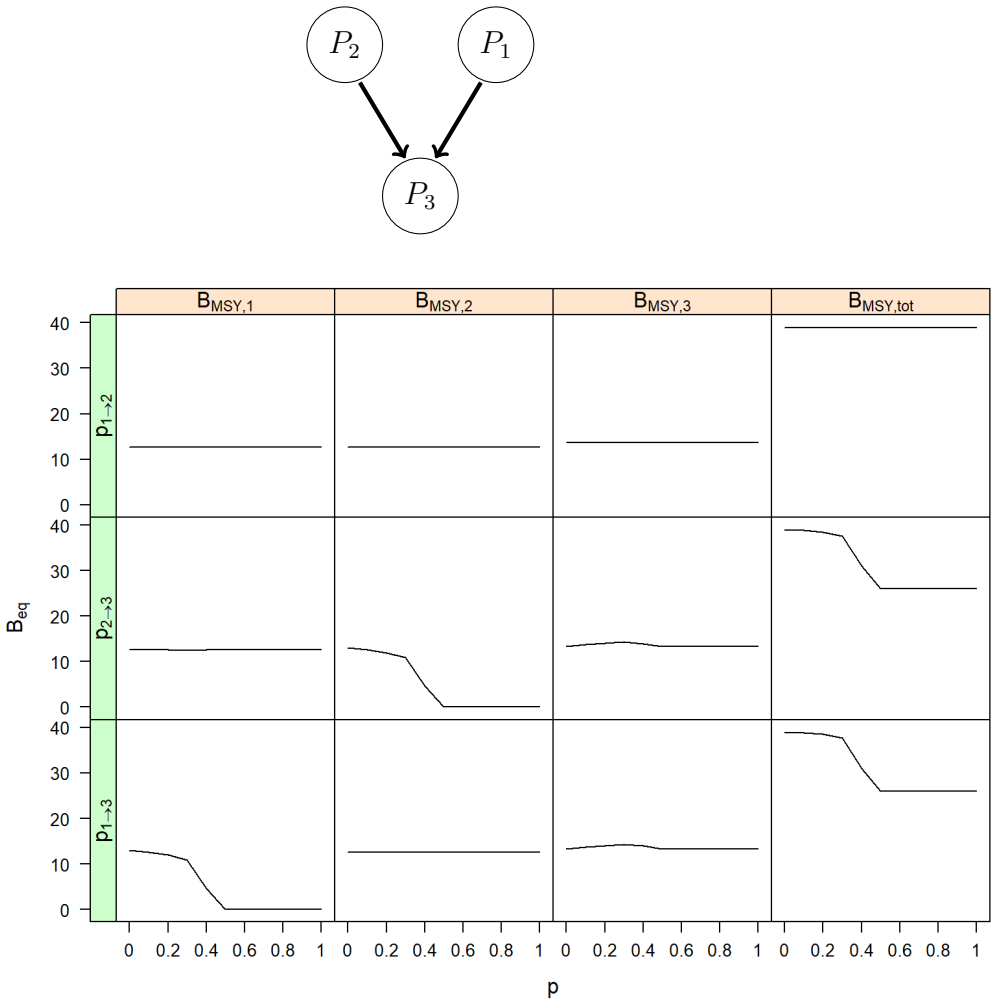

Figure 4.7: Values for B_{MSY} for three-box model with a converging advection connectivity pattern. Values are calculated for each sub-population according to Figure 4.1b. Total B_{MSY} is the sum of all B_{MSY} values for each sub-population. Changes in transfer proportions are mutually exclusive, where only one transfer proportion changes at a time (indicated by row). All non-changing transfer proportions a fixed at a constant $p = 0.1$.

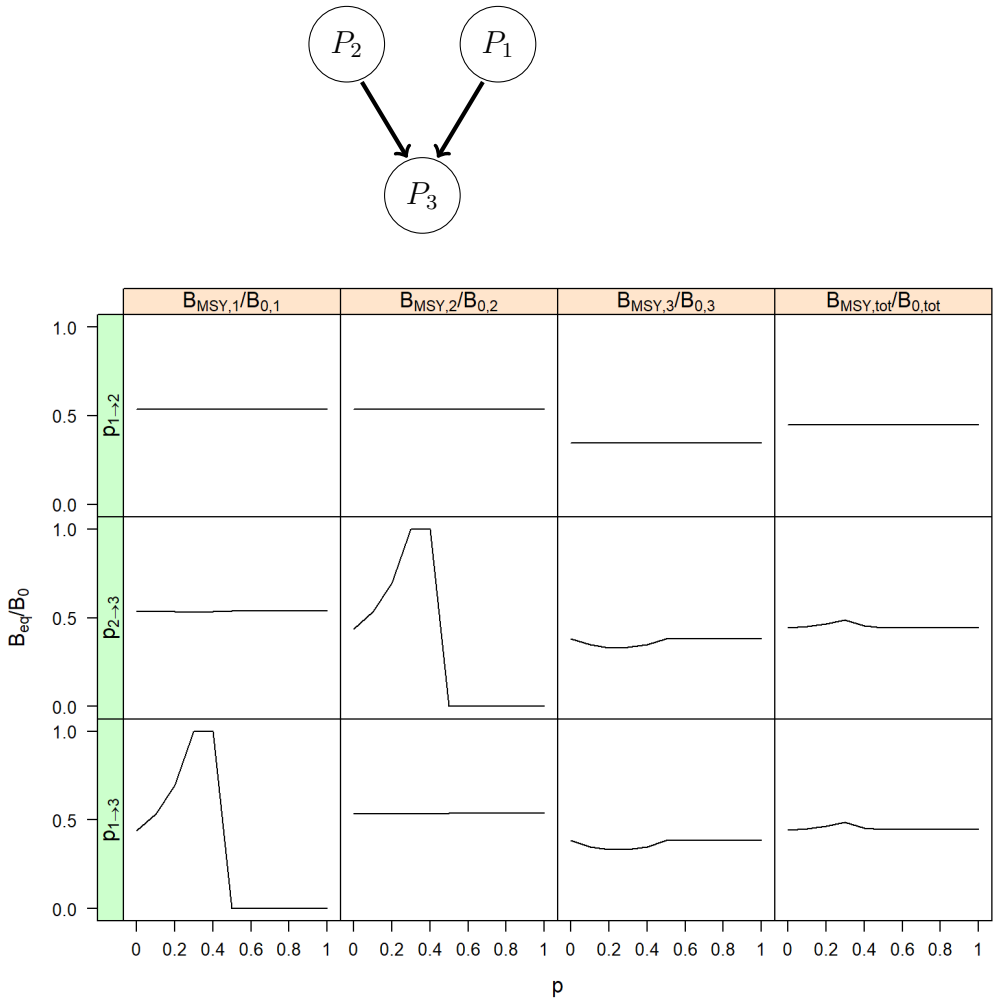

Figure 4.8: Biomass depletion for a three-box model with a converging advection connectivity pattern. Values are calculated for each sub-population according to Figure 4.1b. Biomass depletion is the ratio of B_{MSY} to unfished biomass for each sub-population, and total biomass depletion is the ratio of the sum of all B_{MSY} values to the sum of all unfished biomasses. Changes in transfer proportions are mutually exclusive, where only one transfer proportion changes at a time (indicated by row). All non-changing transfer proportions a fixed at a constant $p = 0.1$.

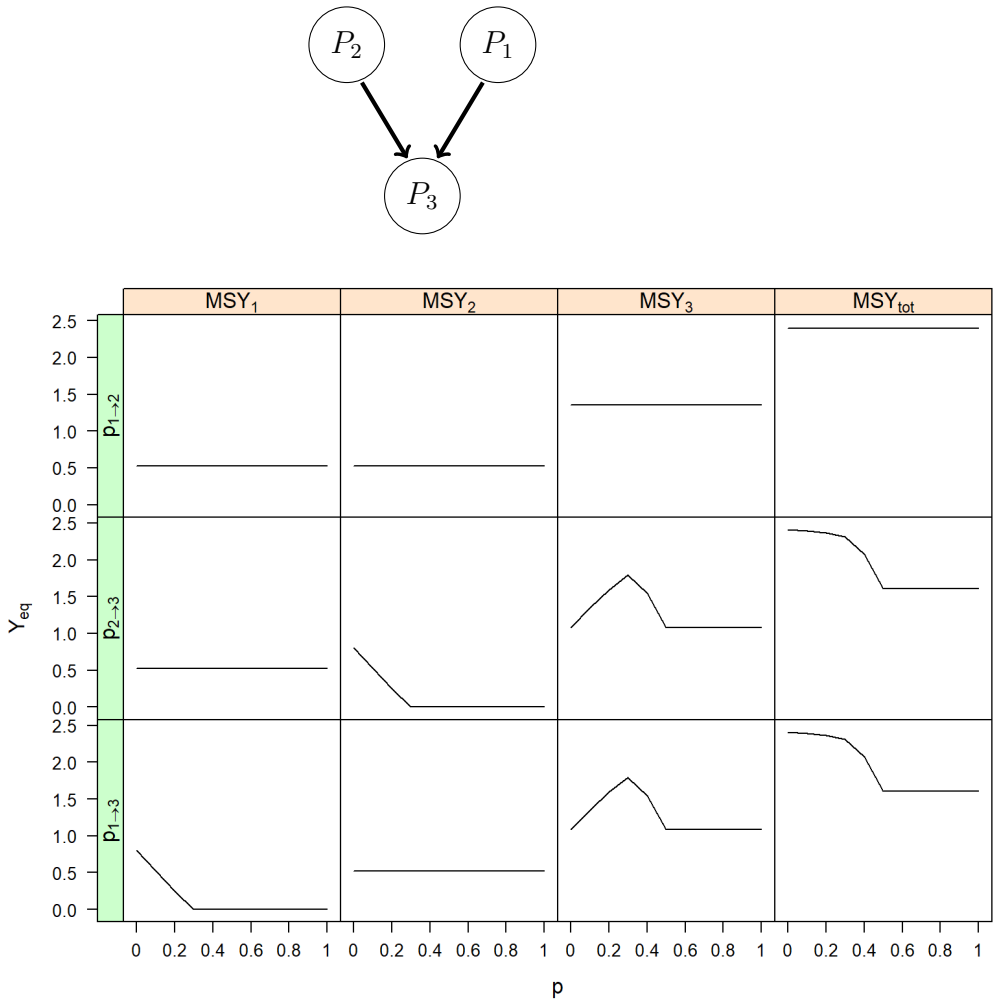

Figure 4.9: MSY for a three-box model with a converging advection connectivity pattern. Values for MSY are calculated for each sub-population according to Figure 4.1b. Total MSY is the sum of optimized yields for all sub-populations. Changes in transfer proportions are mutually exclusive, where only one transfer proportion changes at a time (indicated by row). All non-changing transfer proportions a fixed at a constant $p = 0.1$.

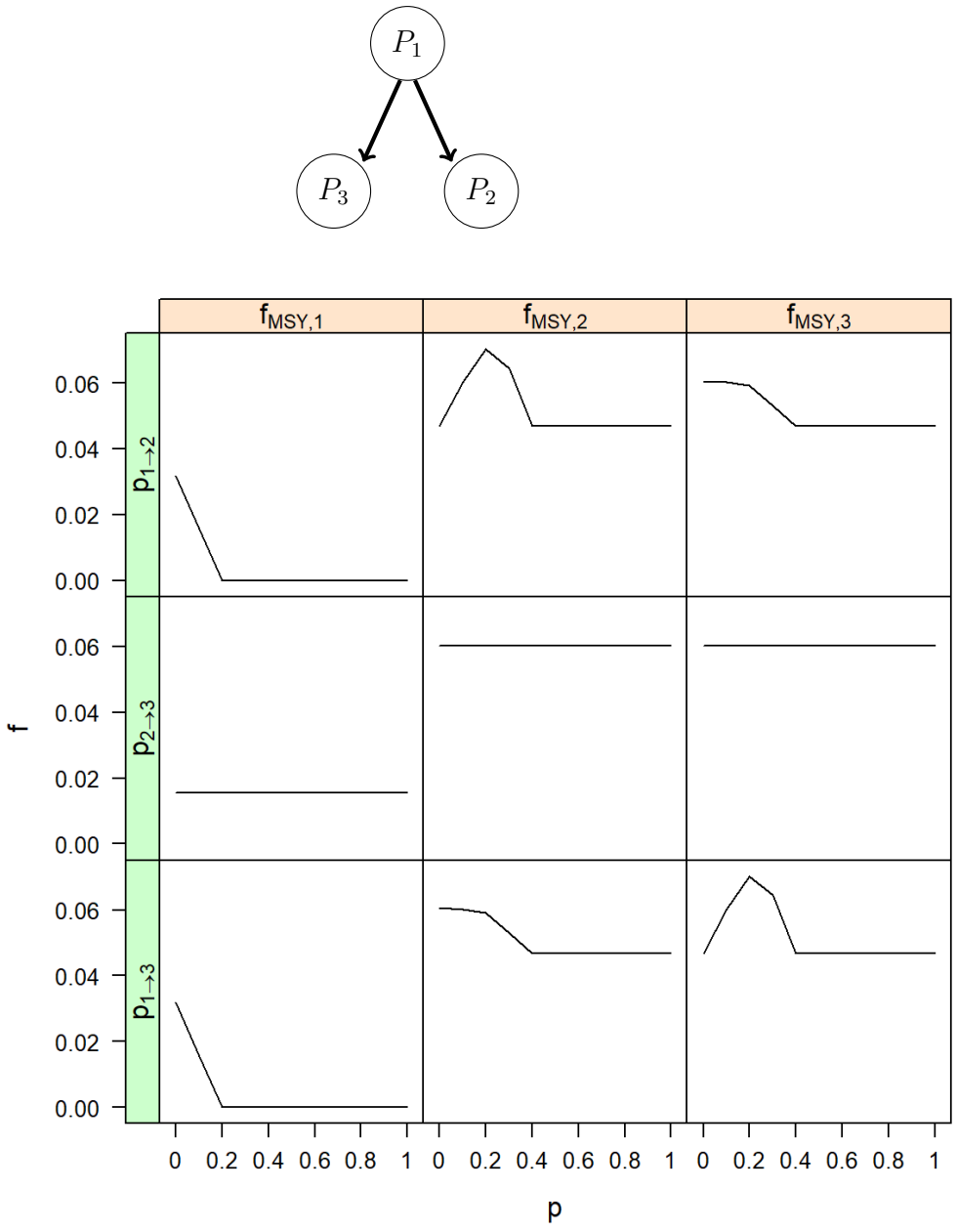

Figure 4.10: Values for f_{MSY} for three-box model with a branching advection connectivity pattern. Values are calculated for each sub-population according to Figure 4.1c. Changes in transfer proportions are mutually exclusive, where only one transfer proportion changes at a time (indicated by row). All non-changing transfer proportions a fixed at a constant $p = 0.1$.

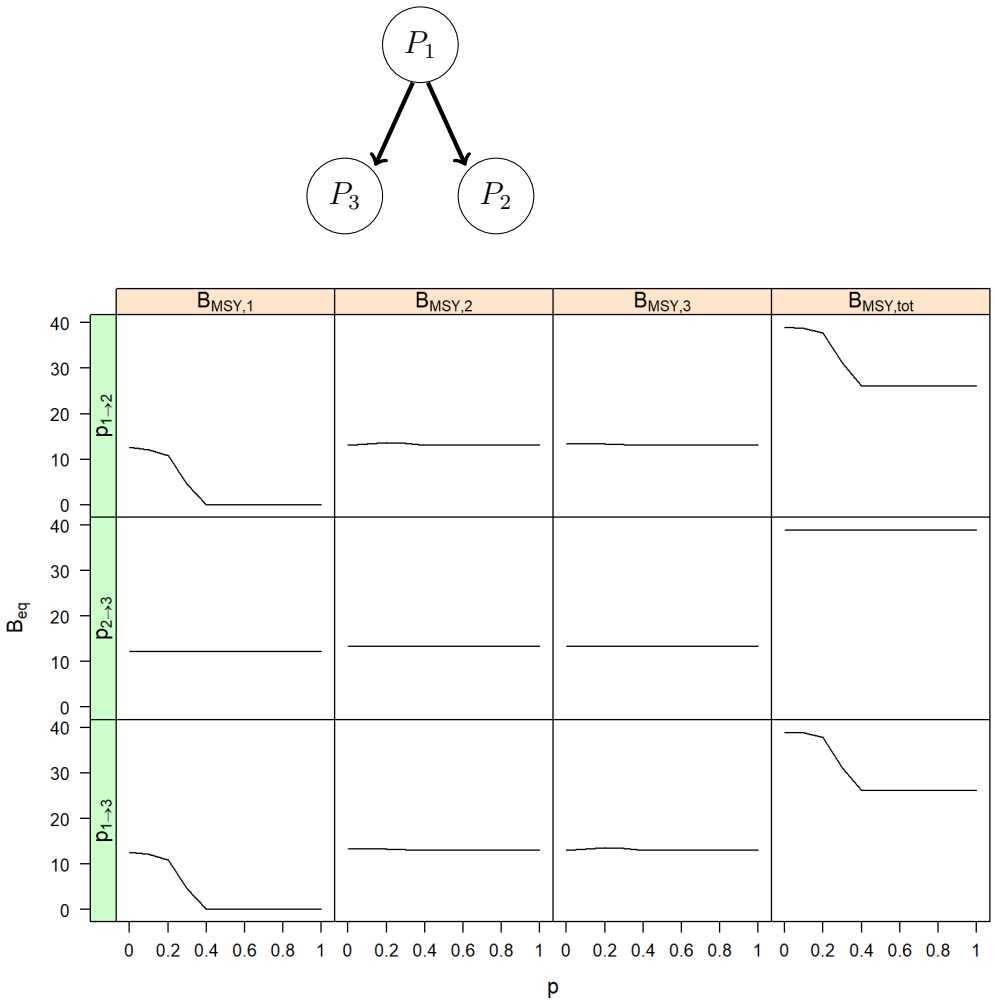

Figure 4.11: Values for B_{MSY} for three-box model with a branching advection connectivity pattern. Values are calculated for each sub-population according to Figure 4.1c. Total B_{MSY} is the sum of all B_{MSY} values for each sub-population. Changes in transfer proportions are mutually exclusive, where only one transfer proportion changes at a time (indicated by row). All non-changing transfer proportions a fixed at a constant $p = 0.1$.

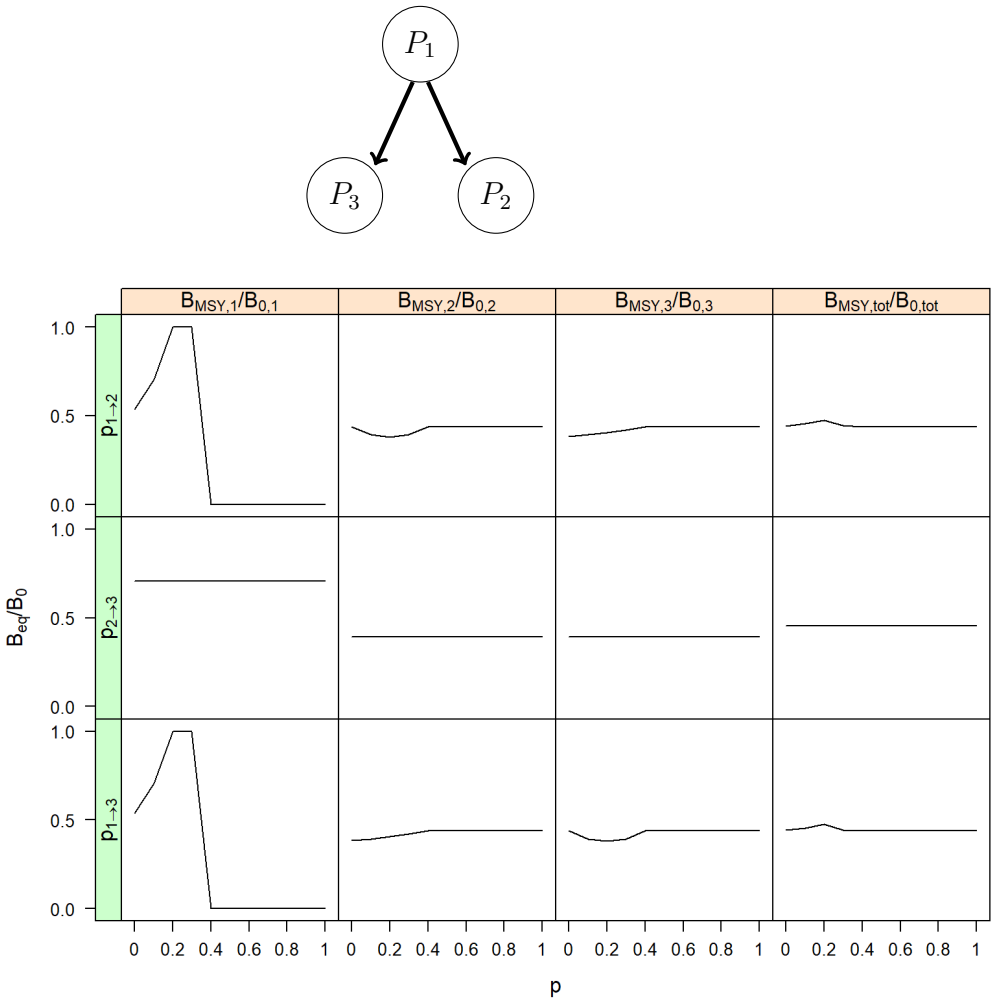

Figure 4.12: Biomass depletion for a three-box model with a branching advection connectivity pattern. Values are calculated for each sub-population according to Figure 4.1c. Biomass depletion is the ratio of B_{MSY} to unfished biomass for each sub-population, and total biomass depletion is the ratio of the sum of all B_{MSY} values to the sum of all unfished biomasses. Changes in transfer proportions are mutually exclusive, where only one transfer proportion changes at a time (indicated by row). All non-changing transfer proportions a fixed at a constant $p = 0.1$.

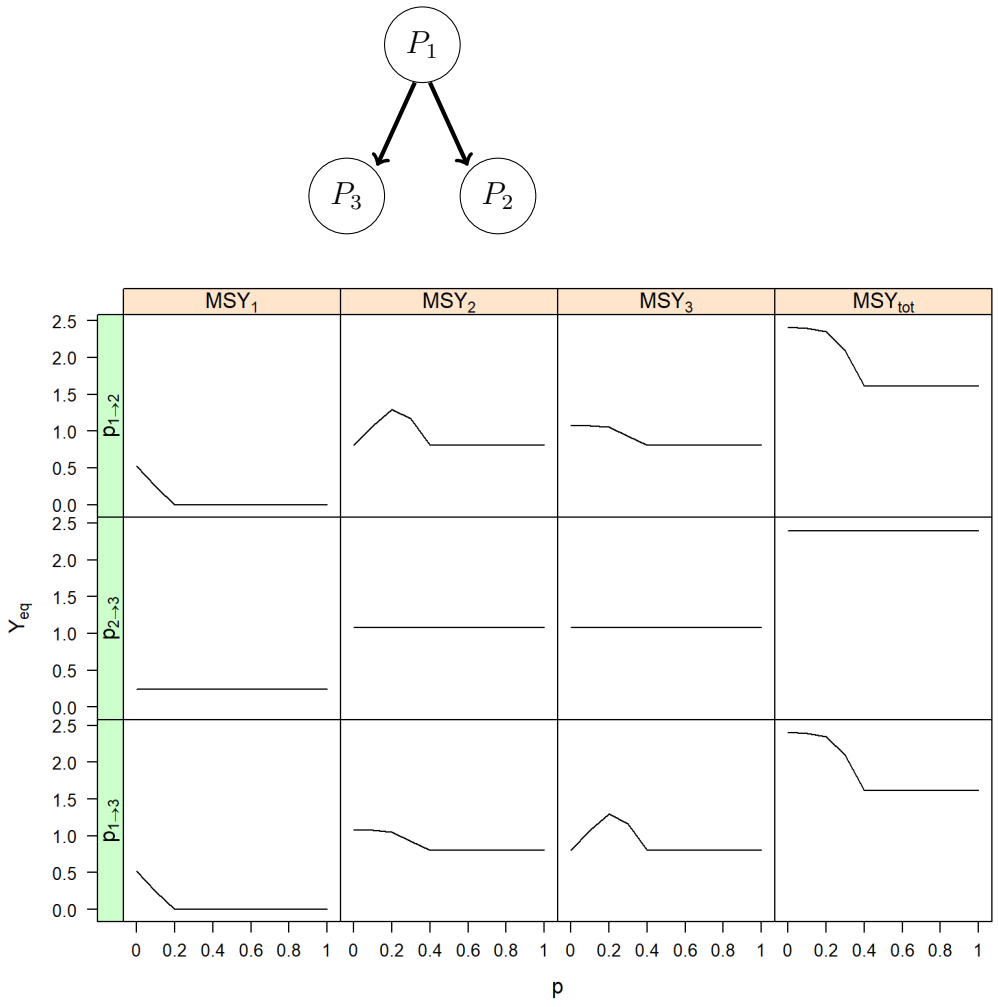

Figure 4.13: MSY for a three-box model with a branching advection connectivity pattern. Values for MSY are calculated for each sub-population according to Figure 4.1c. Total MSY is the sum of optimized yields for all sub-populations. Changes in transfer proportions are mutually exclusive, where only one transfer proportion changes at a time (indicated by row). All non-changing transfer proportions a fixed at a constant $p = 0.1$.

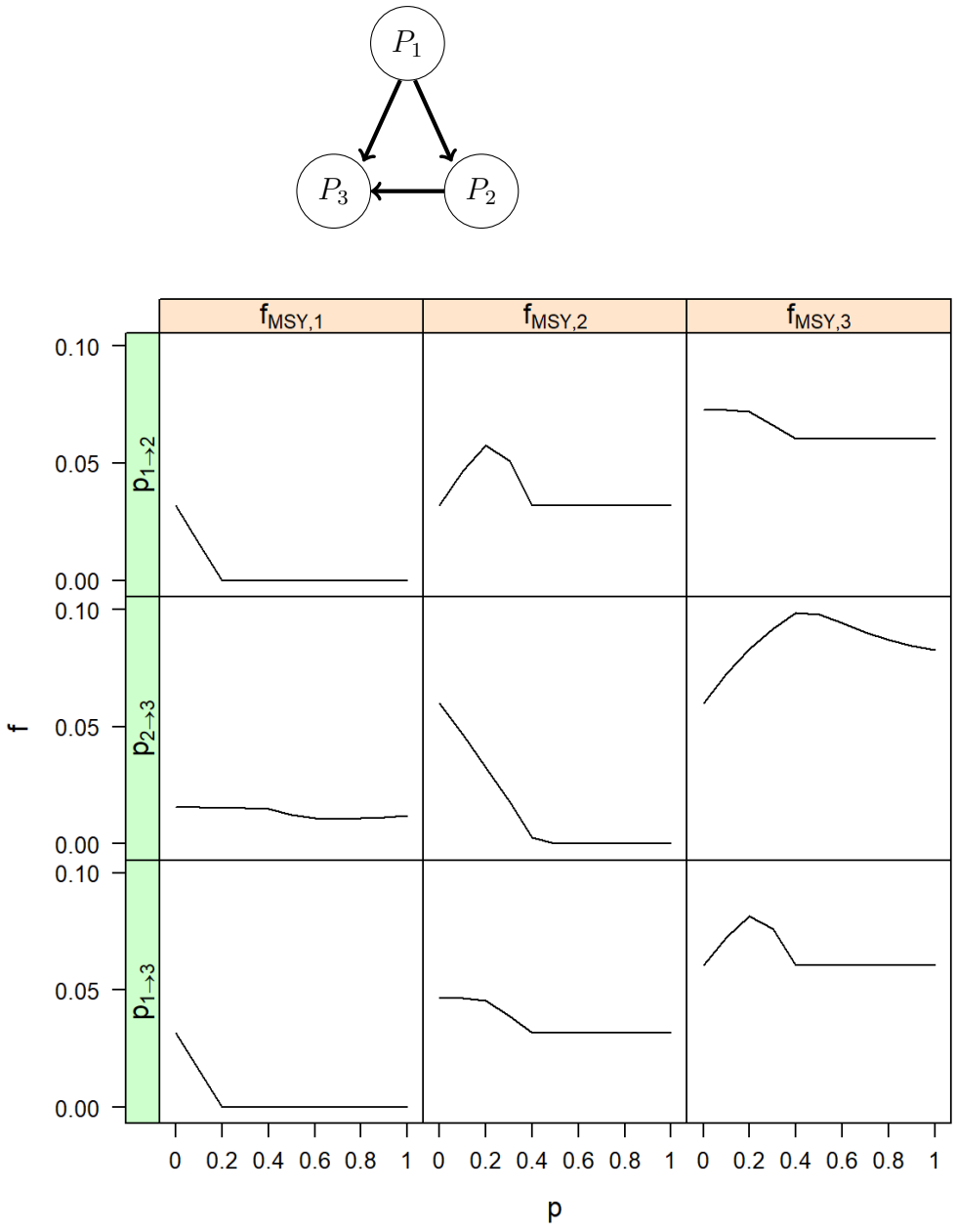

Figure 4.14: Values for f_{MSY} for a three-box model with a detouring advection connectivity pattern. Values are calculated for each sub-population according to Figure 4.1d. Changes in transfer proportions are mutually exclusive, where only one transfer proportion changes at a time (indicated by row). All non-changing transfer proportions a fixed at a constant $p = 0.1$.

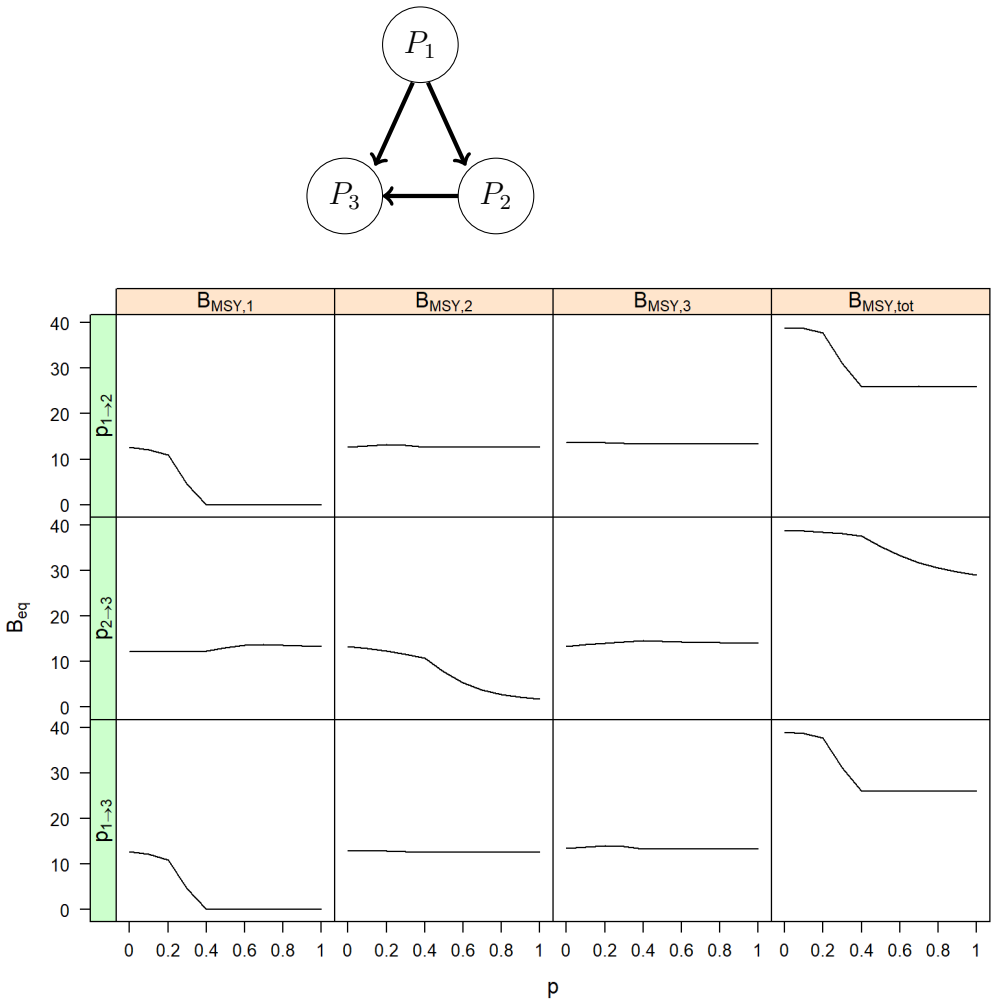

Figure 4.15: Values for B_{MSY} for a three-box model with a detouring advection connectivity pattern. Values are calculated for each sub-population according to Figure 4.1d. Total B_{MSY} is the sum of all B_{MSY} values for each sub-population. Changes in transfer proportions are mutually exclusive, where only one transfer proportion changes at a time (indicated by row). All non-changing transfer proportions a fixed at a constant $p = 0.1$.

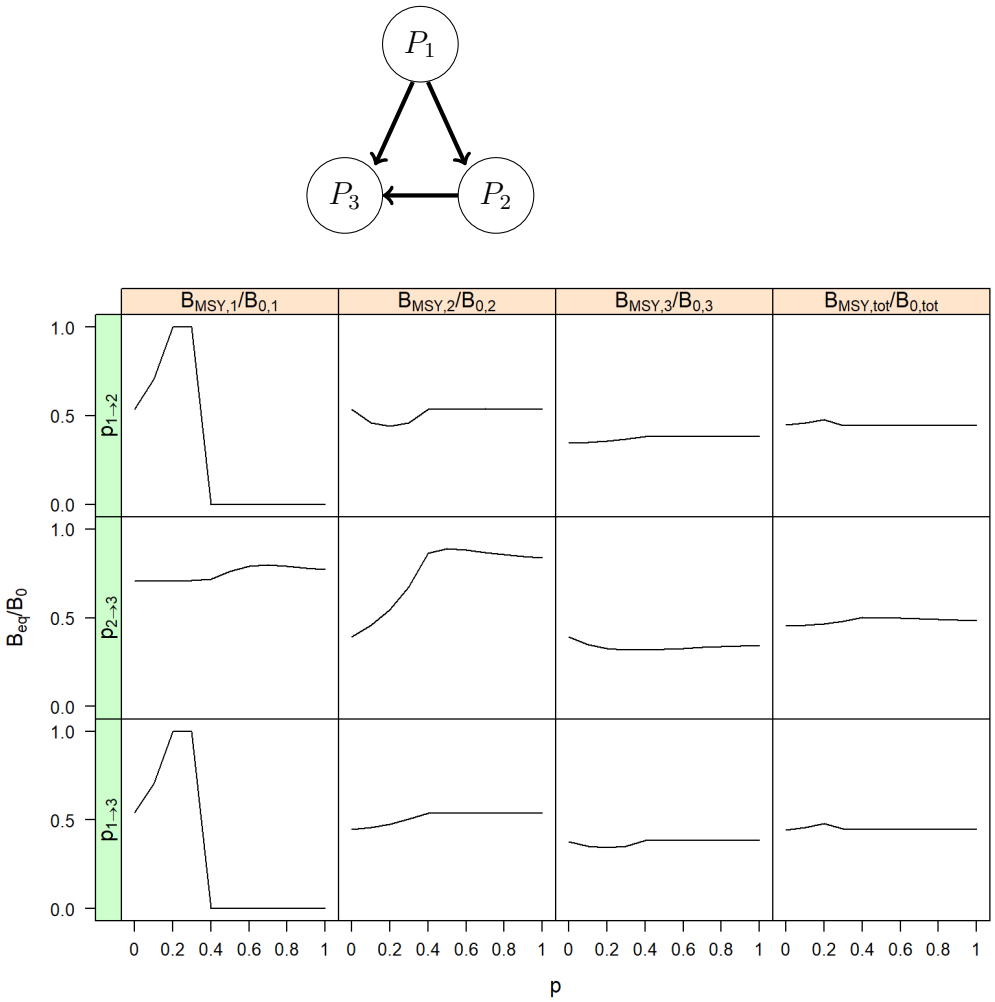

Figure 4.16: Biomass depletion for a three-box model with a detouring advection connectivity pattern. Values are calculated for each sub-population according to Figure 4.1d. Biomass depletion is the ratio of B_{MSY} to unfished biomass for each sub-population, and total biomass depletion is the ratio of the sum of all B_{MSY} values to the sum of all unfished biomasses. Changes in transfer proportions are mutually exclusive, where only one transfer proportion changes at a time (indicated by row). All non-changing transfer proportions a fixed at a constant $p = 0.1$.

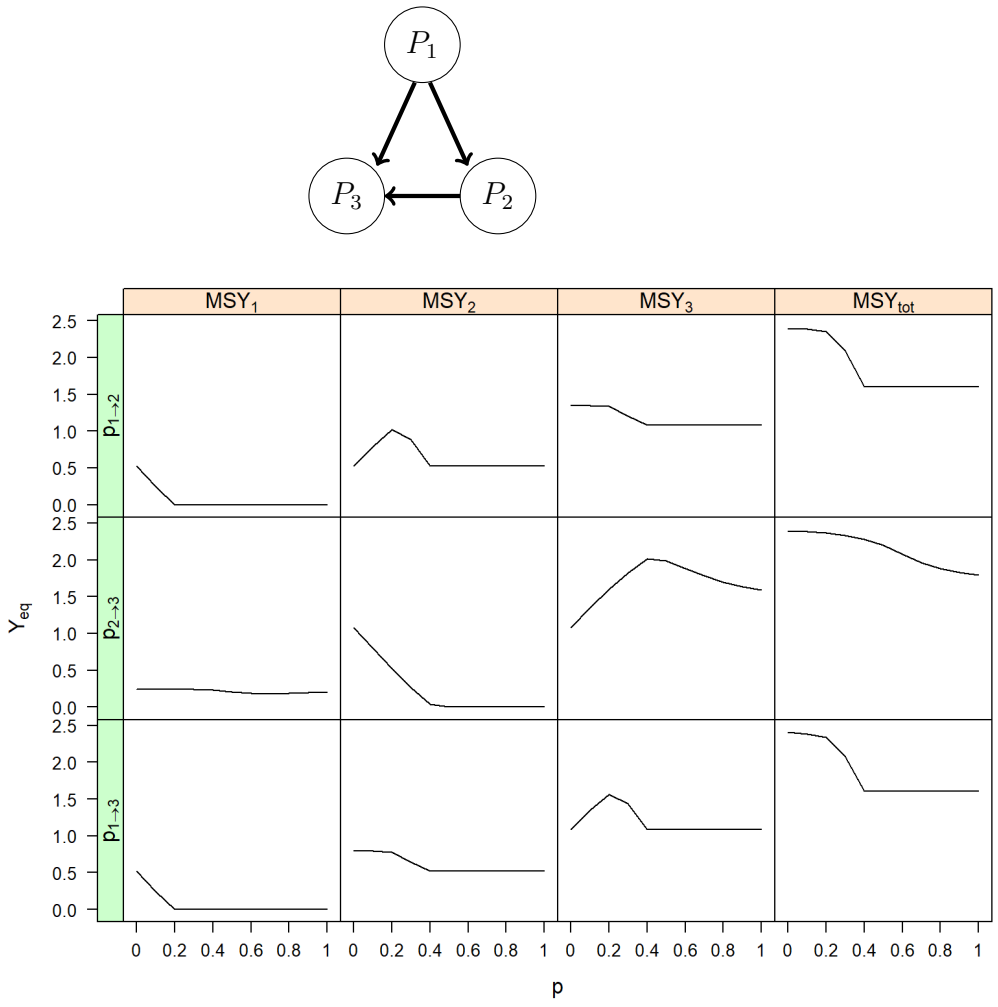

Figure 4.17: MSY for a three-box model with a detouring advection connectivity pattern. Values for MSY are calculated for each sub-population according to Figure 4.1d. Total MSY is the sum of optimized yields for all sub-populations. Changes in transfer proportions are mutually exclusive, where only one transfer proportion changes at a time (indicated by row). All non-changing transfer proportions a fixed at a constant $p = 0.1$.

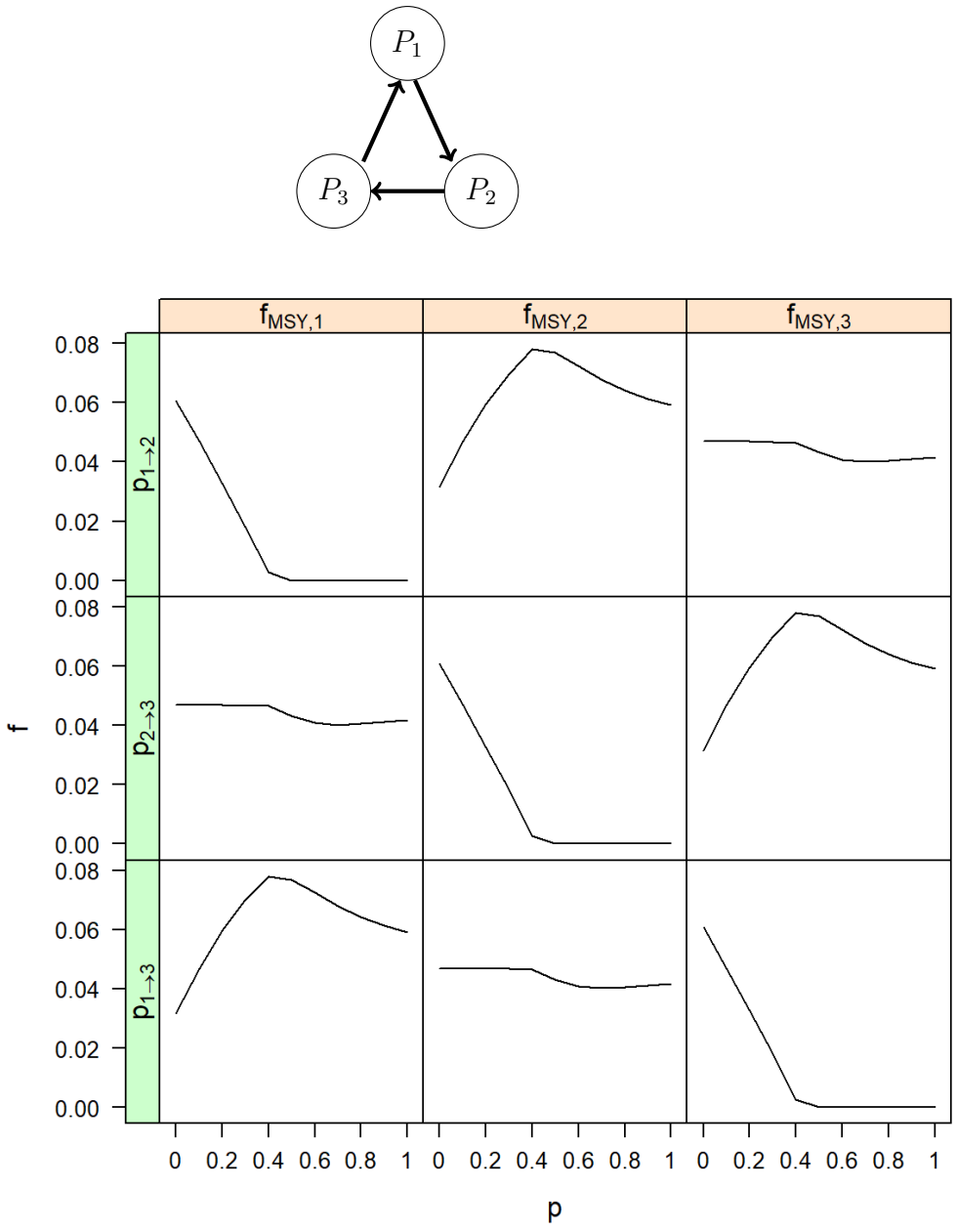

Figure 4.18: Values for f_{MSY} for a three-box model with a cyclical advection connectivity pattern. Values are calculated for each sub-population according to Figure 4.1e. Changes in transfer proportions are mutually exclusive, where only one transfer proportion changes at a time (indicated by row). All non-changing transfer proportions a fixed at a constant $p = 0.1$.

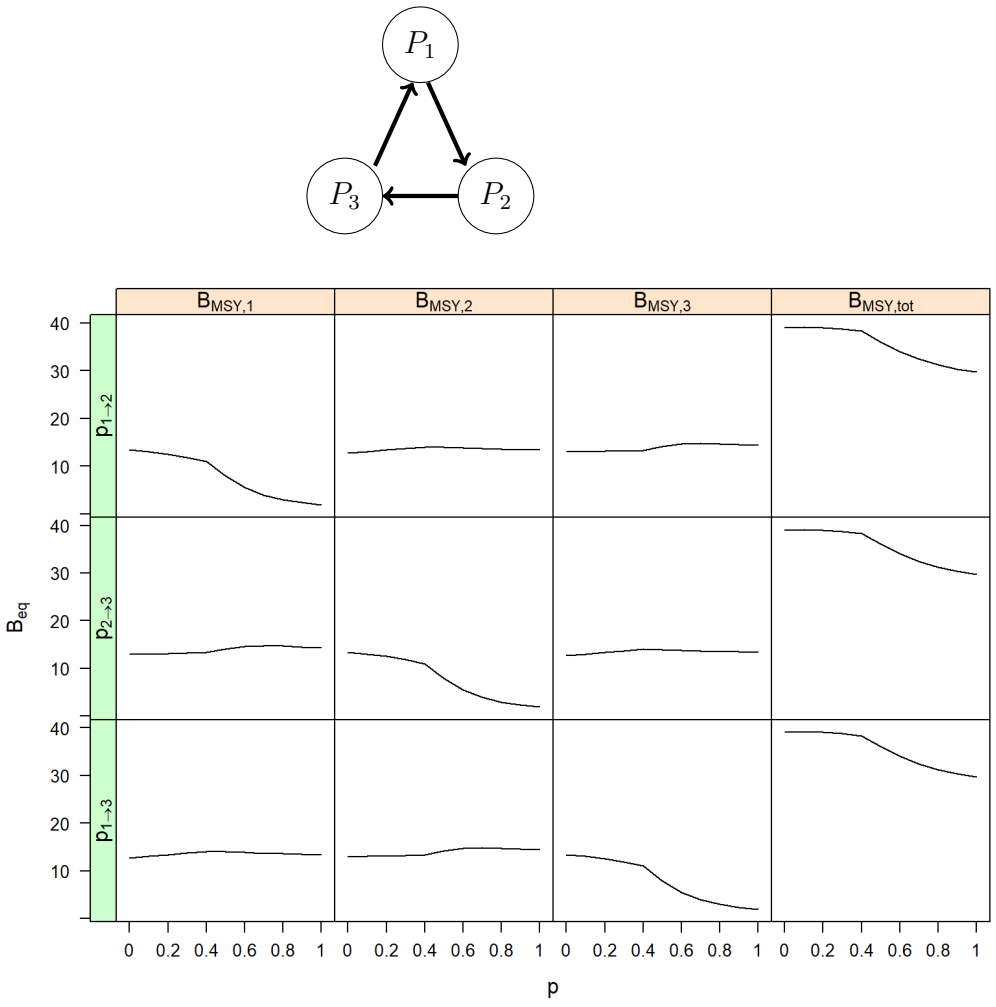

Figure 4.19: Values for B_{MSY} for a three-box model with a cyclical advection connectivity pattern. Values are calculated for each sub-population according to Figure 4.1e. Total B_{MSY} is the sum of all B_{MSY} values for each sub-population. Changes in transfer proportions are mutually exclusive, where only one transfer proportion changes at a time (indicated by row). All non-changing transfer proportions a fixed at a constant $p = 0.1$.

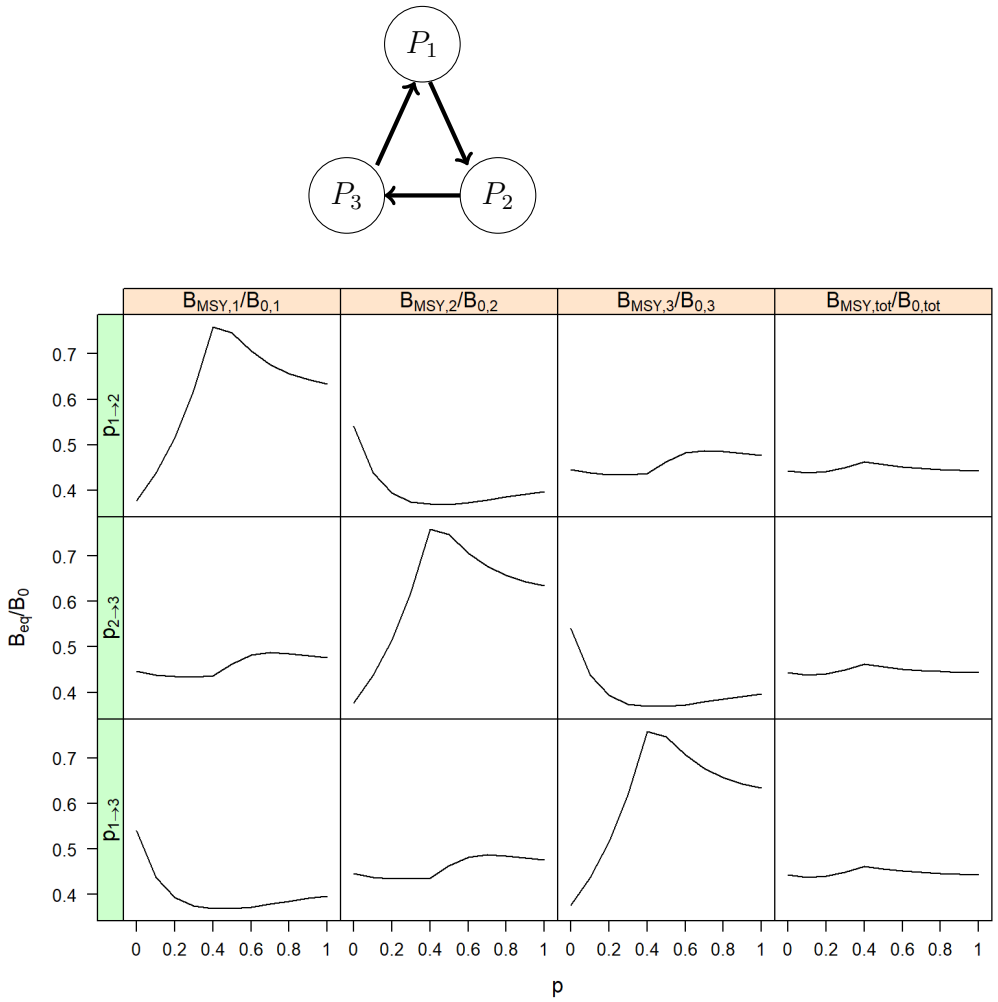

Figure 4.20: Biomass depletion for a three-box model with a cyclical advection connectivity pattern. Values are calculated for each sub-population according to Figure 4.1e. Biomass depletion is the ratio of B_{MSY} to unfished biomass for each sub-population, and total biomass depletion is the ratio of the sum of all B_{MSY} values to the sum of all unfished biomasses. Changes in transfer proportions are mutually exclusive, where only one transfer proportion changes at a time (indicated by row). All non-changing transfer proportions a fixed at a constant $p = 0.1$.

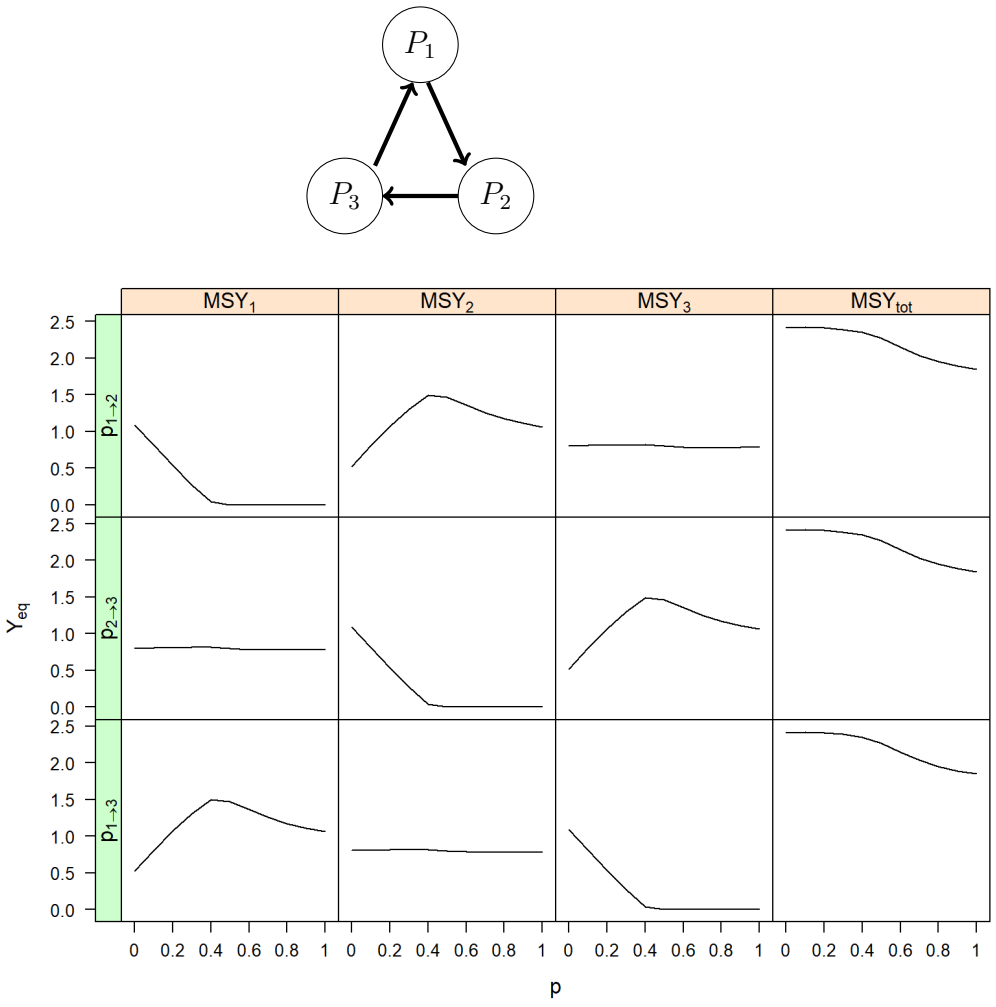

Figure 4.21: MSY for a three-box model with a cyclical advection connectivity pattern. Values for MSY are calculated for each sub-population according to Figure 4.1e. Total MSY is the sum of optimized yields for all sub-populations. Changes in transfer proportions are mutually exclusive, where only one transfer proportion was change at a time (indicated by row). All non-changing transfer proportions a fixed at a constant $p = 0.1$.

Chapter 5

Multiple dimensions and the n-Box Model

5.1 Theory

Explicit spatial models which include two or three separate populations can be complex and inefficient when used to derive MSY RPs, as demonstrated in Chapters 3 and 4, which may deter their implementation. Therefore, in this chapter we present a concise, numerical method to derive MSY RPs for spatial models of any dimension via the per-recruit method. Matrix representations of key values, which can be far more effective for analysing overall stock dynamics, are formulated and illustrated using a mock metapopulation.

Multi-dimensional larval advection models have various potential population dynamic structures, and some of the general patterns are outlined in Figure 4.1. An n-box model can be a combination of several of these population dynamics patterns, and the number of possible patterns depends on

n. However, among these connectivity patterns, population connectivity can be described using two general components: an emigration component and an immigration component.

- **Emigration:** Assume P_1 is connected to m other sub-populations, denoted $P_2, P_3, ...P_m$, with transfer proportions $p_{1\to2}, p_{1\to3}, ...p_{1\to m}$, and assume recruits from P_1 advect into all other sub-populations. The equilibrium SSB for P_1 is defined as

$$SSB_{eq,1} = (1 - \sum_{i=2}^{m} p_{1\to i}) R_{eq,1} SPR_1(f_1), \tag{5.1}$$

  where $\sum_{i=2}^{m} p_{1\to i} \leq 1$ and $p_{1\to i} \in [0, 1]$.

- **Immigration:** Assume P_1 is the sink for sub-populations $P_2, P_3, ...P_m$, where the transfer proportions are $p_{2\to1}, p_{3\to1}, ...p_{m\to1}$. The equilibrium SSB for P_1 is then defined as

$$SSB_{eq,1} = R_{eq,1} SPR_1(f_1) + \sum_{i=2}^{m} (p_{i\to1} \cdot R_{eq,i} SPR_1(f_1)), \tag{5.2}$$

  where $p_{i\to1} \in [0, 1]$.

Closed-form solutions for equilibrium SSB may be derived from Equations 5.1 and 5.2 using the BH SR model. However, numerical solutions are necessary for the RK SR model, and are preferred for higher-dimension models. Also, to maintain generality, we assume the SPR and YPR functions are defined as SPR_i and YPR_i for some sub-population P_i.

To elaborate, assume we have a metapopulation of $n = 6$ sub-populations that has the population structure illustrated in Figure 5.1. The equilibrium

SSB equations for each sub-population are defined as:

$$SSB_{eq,1} = (1 - p_{1\to3})R_{eq,1}SPR_1(f_1), \tag{5.3}$$

$$SSB_{eq,2} = (1 - p_{2\to3})R_{eq,2}SPR_2(f_2), \tag{5.4}$$

$$\begin{aligned} SSB_{eq,3} = (1 - p_{3\to4} - p_{3\to5})R_{eq,3}SPR_3(f_3) \\ + p_{1\to3} \cdot R_{eq,1}SPR_3(f_3) \\ + p_{2\to3} \cdot R_{eq,2}SPR_3(f_3), \end{aligned} \tag{5.5}$$

$$SSB_{eq,4} = (1 - p_{4\to6})R_{eq,4}SPR_4(f_4) + p_{3\to4} \cdot R_{eq,3}SPR_4(f_4), \tag{5.6}$$

$$SSB_{eq,5} = R_{eq,5}SPR_5(f_5) + p_{3\to5} \cdot R_{eq,3}SPR_5(f_5), \tag{5.7}$$

and

$$SSB_{eq,6} = R_{eq,6}SPR_6(f_6) + p_{5\to6} \cdot R_{eq,5}SPR_6(f_6). \tag{5.8}$$

For any n-box model, equilibrium SSB for each sub-population can instead be expressed as a matrix equation. That is,

$$\boldsymbol{A}\vec{R} = \vec{S}, \tag{5.9}$$

where $\mathbf{A}$ is an nxn matrix, and $\vec{R}$ and $\vec{S}$ are vectors of length n for the recruitment, $R(S)$, and SSB, S, for each sub-population, expressed as

$$\vec{R} = \begin{bmatrix} R_1(S_1) \\ R_2(S_2) \\ \vdots \\ R_n(S_n) \end{bmatrix}, \qquad \vec{S} = \begin{bmatrix} S_1 \\ S_2 \\ \vdots \\ S_n \end{bmatrix}. \tag{5.10}$$

Matrix **A** is a matrix representation of the transferring spawning potential of each sub-population, and is defined as

$$\boldsymbol{A} = \begin{bmatrix} (1-\sum_{j,j\neq 1} p_{1\to j})SPR_1(f_1) & p_{2\to 1}SPR_1(f_1) & \dots & p_{n\to 1}SPR_1(f_1) \\ p_{1\to 2}SPR_2(f_2) & (1-\sum_{j,j\neq 2} p_{2\to j})SPR_2(f_2) & & \vdots \\ \vdots & & \ddots & \\ p_{1\to n}SPR_n(f_n) & \dots & & (1-\sum_{j,j\neq n} p_{n\to j})SPR_n(f_n) \end{bmatrix}, \tag{5.11}$$

where j is the sub-population into which recruits are advecting.

In matrix **A**, the diagonal terms represent the emigration component of equilibrium SSB (or residual recruits) for each sub-population, while all remaining terms are the immigration components of equilibrium SSB for the sub-populations. For example, the diagonal term in row five, $\boldsymbol{A}_{5,5}$, represents spawning potential of recruits remaining in (i.e. not advecting from) sub-population P_5, while the remaining terms in row five represent the immigration of spawning potential into sub-population P_5. Naturally, if there is no connection between any two sub-populations P_i and P_j $(i \neq j)$, then $\boldsymbol{A}_{i,j} = 0$ since $p_{i\to j} = p_{j\to i} = 0$. Matrix diagonal terms are only zero if the net emigration $\sum_{j,j\neq i} p_{i\to j} = 1$ for sub-population P_i. Moreover, if net emigration $\sum_{j,j\neq i} p_{i\to j} = 0$, the matrix diagonal term for sub-population P_i is $SPR_i(f_i)$. If we assume unidirectionality for transferring recruits, **A** could be expressed as a lower or upper triangular matrix, where transfer proportions $p \in [-1, 1]$, and the sign of the transfer proportion indicates the advection direction (e.g. $p_{1\to 2} = -p_{2\to 1}$).

The steady-state matrix, **A**, can be expressed as product of a transfer

matrix, $\boldsymbol{P}$, and a SPR diagonal matrix, $\boldsymbol{S_n}$,

$$\boldsymbol{A} = \boldsymbol{S_n P}. \tag{5.12}$$

The transfer matrix is a matrix representation of the transfer proportions between each region,

$$\boldsymbol{P} = \begin{bmatrix} p_{1\to1} & p_{2\to1} & \dots & p_{n\to1} \\ p_{1\to2} & p_{2\to2} & \dots & p_{2\to2} \\ \vdots & \vdots & \ddots & \vdots \\ p_{1\to n} & p_{2\to n} & \dots & p_{n\to n} \end{bmatrix}, \tag{5.13}$$

where any transfer proportion $p_{i\to i} = (1 - \sum_{j,j\neq i} p_{i\to j})$. This connectivity matrix may be represented by a stochastic matrix describing the probabilistic exchange of recruits between regions, where $p_{i\to j}$ is the probability of recruits advecting from region i to j. Further, this may be described as a left stochastic matrix, where the terms of each column sum to 1, i.e. $\sum_j p_{i\to j} = 1$.

The SPR matrix is the diagonal matrix

$$\boldsymbol{S}_n = \begin{bmatrix} SPR_1(f_1) & 0 & \dots & 0 \\ 0 & SPR_2(f_2) & \dots & 0 \\ \vdots & \vdots & \ddots & \vdots \\ 0 & 0 & \dots & SPR_n(f_n) \end{bmatrix}, \tag{5.14}$$

where n defines the dimensions of the SPR matrix (i.e. nxn). Equilibrium SSB for each area can be derived numerically (or analytically for the BH SR model) from Equation 5.9 for some set of f's.

To demonstrate this matrix format, the transfer matrix for the metapopulation illustrated in Figure 5.1 is

$$\boldsymbol{P} = \begin{bmatrix} (1-p_{1\to3}) & 0 & 0 & 0 & 0 & 0 \\ 0 & (1-p_{2\to3}) & 0 & 0 & 0 & 0 \\ p_{1\to3} & p_{2\to3} & (1-p_{3\to4}-p_{3\to5}) & 0 & 0 & 0 \\ 0 & 0 & p_{3\to4} & (1-p_{4\to6}) & 0 & 0 \\ 0 & 0 & p_{3\to5} & 0 & 1 & 0 \\ 0 & 0 & 0 & 0 & p_{5\to6} & 1 \end{bmatrix}, \tag{5.15}$$

and $\boldsymbol{A} = \boldsymbol{S}_6\boldsymbol{P}$. Note, the immigration transfer proportions in the matrix $\boldsymbol{P}$, denoted $p_{i\to j}$, are always placed in column i and row j. Expressing definitions for SSB_{eq} in this matrix form is much easier to write and visualize compared to closed-form equations typically used (e.g. Equations 5.3 to 5.8).

The equilibrium yield for a sub-population would be

$$Y_{eq,i}(\vec{f}_i) = \frac{YPR_i(f_i)}{SPR_i(f_i)} S_i \tag{5.16}$$

where S_i is the equilibrium SSB for sub-population P_i. The total equilibrium yield for a metapopulation of n sub-populations is the sum of equilibrium yields of each sub-population,

$$Y_{eq,tot}(\vec{f}) = \sum_i Y_{eq,i}(\vec{f}_i), \tag{5.17}$$

where $\vec{f}$ is the vector of f's for all sub-populations in the metapopulation, and $\vec{f}_i$ is the vector of f's upon which equilibrium yield for some sub-population,

P_i, depends. For example, if a metapopulation is comprised of four sub-populations,

$$\vec{f} = \begin{bmatrix} f_1 \\ f_2 \\ f_3 \\ f_4 \end{bmatrix}, \tag{5.18}$$

and if sub-population P_1 has recruits immigrating in from sub-populations P_3 and P_4,

$$\vec{f_1} = \begin{bmatrix} f_1 \\ f_3 \\ f_4 \end{bmatrix}, \tag{5.19}$$

because sub-population P_1 depends on fishing in sub-populations P_3 and P_4. Values for f_{MSY} can be derived by optimizing the sum of equilibrium yields with respect to all f's, simultaneously.

This framework allows quick numerical calculations of MSY RPs for any n-box model ($n \geq 1$) for any SR model. It is recommended that this framework be used to derive spatial MSY RPs for any system that explicitly models larval advection between sub-populations.

5.2 Figures

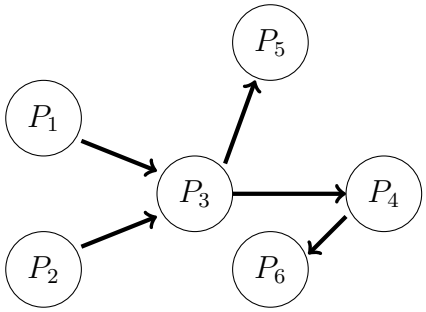

Figure 5.1: A six-box metapopulation model with several advection connectivity patterns between sub-populations.

Chapter 6

Conclusion

6.1 Future Research

In this thesis, we assume that recruits move between areas through a unidirectional larval advection process. Future studies could extend on this to allow movement of more age-classes and bidirectional movement of fish between sub-populations. Goethel and Berger (2017) used simulations to study the effects of misdiagnosing spatial complexity and connectivity dynamics of populations in source-sink systems. They noted that the movement of adults was a more important factor on B_{MSY} results than just larval movements, yet when movement was bidirectional, B_{MSY} results were nearly identical to results from a unidirectional model when productivity was different between populations. Nevertheless, bidirectional larval advection and the advection of older age classes may have significant effects on f_{MSY} and other RPs, as well. Including these alternative assumptions into the deterministic, metapopulation model detailed in this thesis may provide more insight on these effects.

Implementing such changes in to the proposed model would be minimalistic using the matrix model structure by adjusting $\mathbf{P}$ appropriately.

Our model also assumes that the annual transfer of recruits (i.e. p) is consistent over time. The proportion of transferring recruits may not only change between year, but also vary inter-annually (see Rice et al., 1999). Future research could analyse MSY RPs and the robustness of these results when p varies in time. Additionally, our model could be modified to allow stochastic variation in the transfer proportion p, as well as in the parameters for SR relationships and life history characteristics. Doing so may also provide insight into the robustness of spatially-explicit RPs

6.2 Final Remarks

Spatially-explicit MSY RPs depend on the movement of fish, the life history characteristics and SPR and YPR functions of each population, and their SR relationships. The amount of transferring pre-recruits directly affects the sustainability of populations, and allowing life history characteristics and SR relationships to vary by area can substantially affect RP results.

Incorporating unidirectional pre-recruit movement into population dynamics models results in a lower MSY and B_{MSY} compared to when pre-recruits are stationary because the survival of fish in early-life stages are assumed to be density-dependent. Any amount of advecting pre-recruits reduces overall stock-recruitment, and as a result lowers the total sustainable spawning biomass and yield. Additionally, implementing an MPA-like or uniform harvest strategy always provides sub-optimal yields compared to

the optimal f_{MSY}'s, but can potentially increase B_{MSY} when only a small proportion of pre-recruits transfer between populations. Nonetheless, RPs like f_{MSY} must be properly spatially allocated for yields to be optimized.

It is clear that spatially-explicit RPs are important for sustainable fisheries management. Not only is it important to account for the spatial distributions and movements of fish, but neglecting fish movements can be detrimental to a stock's status. In particular, larval advection processes can have significant impacts on MSY RPs, and RP derivations that do not account for these movements may result in overfishing.

When deriving spatially-explicit MSY RPs, it is important to consider sub-population interconnectivity. In the future, fisheries managers and scientists alike should be mindful of potential metapopulation structures of stocks, especially when deriving MSY RPs for management purposes, and should develop an appropriate stock-specific spatial model to do so.

Bibliography

Baranov, F. I. (1918). *On the question of the biological basis of fisheries.*

Berkes, F., Hughes, T. P., Steneck, R. S., Wilson, J. A., Bellwood, D. R., Crona, B., Folke, C., Gunderson, L., Leslie, H., Norberg, J., et al. (2006). Globalization, roving bandits, and marine resources. *Science*, 311(5767):1557–1558.

Beverton, R. J. and Holt, S. J. (1957). *On the dynamics of exploited fish populations*, volume 11. Springer Science & Business Media.

Bosley, K. M., Goethel, D. R., Berger, A. M., Deroba, J. J., Fenske, K. H., Hanselman, D. H., Langseth, B. J., and Schueller, A. M. (2019). Overcoming challenges of harvest quota allocation in spatially structured populations. *Fisheries Research*, 220:105344.

Botsford, L. W., Brumbaugh, D. R., Grimes, C., Kellner, J. B., Largier, J., O'Farrell, M. R., Ralston, S., Soulanille, E., and Wespestad, V. (2009). Connectivity, sustainability, and yield: bridging the gap between conventional fisheries management and marine protected areas. *Reviews in Fish Biology and Fisheries*, 19(1):69–95.

Botsford, L. W., Castilla, J. C., and Peterson, C. H. (1997). The management of fisheries and marine ecosystems. *Science*, 277(5325):509–515.

Branch, T. A., Hilborn, R., Haynie, A. C., Fay, G., Flynn, L., Griffiths, J., Marshall, K. N., Randall, J. K., Scheuerell, J. M., Ward, E. J., et al. (2006). Fleet dynamics and fishermen behavior: lessons for fisheries managers. *Canadian Journal of Fisheries and Aquatic Sciences*, 63(7):1647–1668.

Cadigan, N. G. (2013). Fitting a non-parametric stock–recruitment model in r that is useful for deriving msy reference points and accounting for model uncertainty. *ICES Journal of Marine Science*, 70(1):56–67.

Cadrin, S. X. and Secor, D. H. (2009). Accounting for spatial population structure in stock assessment: past, present, and future. In *The future of fisheries science in North America*, pages 405–426. Springer.

Carruthers, T. R., McAllister, M. K., and Taylor, N. G. (2011). Spatial surplus production modeling of atlantic tunas and billfish. *Ecological applications*, 21(7):2734–2755.

Cook, R. (1998). A sustainability criterion for the exploitation of north sea cod. *ICES Journal of Marine Science*, 55(6):1061–1070.

Cowen, R. K., Paris, C. B., and Srinivasan, A. (2006). Scaling of connectivity in marine populations. *Science*, 311(5760):522–527.

Cowen, R. K. and Sponaugle, S. (2009). Larval dispersal and marine population connectivity. *Annual review of marine science*, 1:443–466.

Crowder, L. B., Lyman, S., Figueira, W., and Priddy, J. (2000). Source-sink population dynamics and the problem of siting marine reserves. *Bulletin of Marine Science*, 66(3):799–820.

DFO (2014). Stock assessment of nafo subdivision 3ps cod.

DFO, A. (2006). A harvest strategy compliant with the precautionary approach. *DFO Can. Sci. Advis. Sec. Sci. Advis. Rep*, 23:2006.

EC (2010). Facts and figures on the common fisheries policy-basic statistical data.

FAO (2018). The state of the world fisheries and aquaculture 2018 - meeting the sustainable development goals.

Fogarty, M. J. and Botsford, L. W. (2007). Population connectivity and spatial management of marine fisheries. *Oceanography*, 20(3):112–123.

Francis, R. I. C. (1992). Use of risk analysis to assess fishery management strategies: a case study using orange roughy (hoplostethus atlanticus) on the chatham rise, new zealand. *Canadian Journal of Fisheries and Aquatic Sciences*, 49(5):922–930.

Gaines, S. D. and Lafferty, K. D. (1995). Modeling the dynamics of marine species the: The importance of incorporating larval dispersal. In McEdward, L., editor, *Eology of Marine Invertabrate Larvae*, chapter 12, pages 389–412. CRC Press, Florida.

Gawarkiewicz, G., Monismith, S., and Largier, J. (2007). Observing larval

transport processes affecting population connectivity: progress and challenges. *Oceanography*, 20(3):40–53.

Geromont, H., De Oliveira, J., Johnston, S., and Cunningham, C. (1999). Development and application of management procedures for fisheries in southern africa. *ICES Journal of Marine Science*, 56(6):952–966.

Goethel, D. R. and Berger, A. M. (2017). Accounting for spatial complexities in the calculation of biological reference points: effects of misdiagnosing population structure for stock status indicators. *Canadian Journal of Fisheries and Aquatic Sciences*, 74(11):1878–1894.

Goethel, D. R., Legault, C. M., and Cadrin, S. X. (2014). Testing the performance of a spatially explicit tag-integrated stock assessment model of yellowtail flounder (limanda ferruginea) through simulation analysis. *Canadian journal of fisheries and aquatic sciences*, 72(4):582–601.

Goethel, D. R., Quinn, T. J., and Cadrin, S. X. (2011). Incorporating spatial structure in stock assessment: movement modeling in marine fish population dynamics. *Reviews in Fisheries Science*, 19(2):119–136.

Haddon, M. (2010). *Modelling and quantitative methods in fisheries*. CRC press.

Haltuch, M. A., Punt, A. E., and Dorn, M. W. (2008). Evaluating alternative estimators of fishery management reference points. *Fisheries Research*, 94(3):290–303.

Hart, D. R. (2003). Yield- and biomass-per-recruit analysis for rotational

fisheries, with an application to the atlantic sea scallop (placopecten magellanicus). *Fishery Bulletin*, 101(1):44–57.

Hilborn, R. (2010). Pretty good yield and exploited fishes. *Marine Policy*, 34(1):193–196.

Hilborn, R. and Ovando, D. (2014). Reflections on the success of traditional fisheries management. *ICES Journal of Marine Science*, 71(5):1040–1046.

Hilborn, R. and Stokes, K. (2010). Defining overfished stocks: have we lost the plot? *Fisheries*, 35(3):113–120.

Hilborn, R. and Walters, C. J. (2013). *Quantitative fisheries stock assessment: choice, dynamics and uncertainty*. Springer Science & Business Media.

Hintzen, N. T., Roel, B., Benden, D., Clarke, M., Egan, A., Nash, R. D. M., Rohlf, N., and Hatfield, E. M. C. (2015). Managing a complex population structure: exploring the importance of information from fisheries-independent sources. *ICES Journal of Marine Science*, 72(2):528–542.

Horbowy, J. and Luzeńczyk, A. (2012). The estimation and robustness of f msy and alternative fishing mortality reference points associated with high long-term yield. *Canadian journal of fisheries and aquatic sciences*, 69(9):1468–1480.

Hutchings, J. A. and Rangeley, R. W. (2011). Correlates of recovery for canadian atlantic cod (gadus morhua). *Canadian Journal of Zoology*, 89(5):386–400.

ICES, C. (2016). Report of the meeting between ices and recipients of ices advice. *ICES CM*.

ICES, C. (2018). Ices advice bssis. *ICES CM*.

Jonzén, N., Lundberg, P., and Gårdmark, A. (2001). Harvesting spatially distributed populations. *Wildlife Biology*, 7(3):197–203.

Kanik, Z., Kucuksenel, S., et al. (2015). Implementation of the maximum sustainable yield under an age-structured model. *Department of Economics, METU Working Papers*.

Kritzer, J. P. and Sale, P. F. (2010). *Marine metapopulations*. Elsevier.

Larkin, P. (1977). An epithaph for the concept of maximum sustainable yield. *Transactions of the American Fisheries Society*, 106(1).

Lindegren, M., Andersen, K. H., Casini, M., and Neuenfeldt, S. (2014). A metacommunity perspective on source–sink dynamics and management: the baltic sea as a case study. *Ecological applications*, 24(7):1820–1832.

Lipcius, R. N., Eggleston, D. B., Schreiber, S. J., Seitz, R. D., Shen, J., Sisson, M., Stockhausen, W. T., and Wang, H. V. (2008). Importance of metapopulation connectivity to restocking and restoration of marine species. *Reviews in Fisheries Science*, 16(1-3):101–110.

Lundberg, P. and Jonzén, N. (1999). Optimal population harvesting in a source–sink environment. *Evolutionary Ecology Research*, 1(6):719–729.

Luzeńczyk, A. (2017). Change in biological reference points under different biological, fishery, and environmental factors. *Acta Ichthyologica et Piscatoria*, 47(1).

MacCall, A. D. (1990). *Dynamic geography of marine fish populations*. Washington Sea Grant Program Seattle, WA.

Munroe, D. M., Klinck, J. M., Hofmann, E. E., and Powell, E. N. (2012). The role of larval dispersal in metapopulation gene flow: local population dynamics matter. *Journal of Marine Research*, 70(2-3):441–467.

Murawski, S. A. (2010). Rebuilding depleted fish stocks: the good, the bad, and, mostly, the ugly. *ICES Journal of Marine Science*, 67(9):1830–1840.

Myers, R., Rosenberg, A., Mace, P., Barrowman, N., and Restrepo, V. (1994). In search of thresholds for recruitment overfishing. *ICES Journal of Marine Science*, 51(2):191–205.

Myers, R. A., Bowen, K. G., and Barrowman, N. J. (1999). Maximum reproductive rate of fish at low population sizes. *Canadian Journal of Fisheries and Aquatic Sciences*, 56(12):2404–2419.

NAFO (18 September 2004). Nafo precautionary approach framework. *NAFO/FC Doc*, (No. 04/18).

Needle, C. L. (2001). Recruitment models: diagnosis and prognosis. *Reviews in Fish Biology and Fisheries*, 11(2):95–111.

Neubert, M. G. (2003). Marine reserves and optimal harvesting. *Ecology Letters*, 6(9):843–849.

Nowlis, J. S. and Bollermann, B. (2002). Methods for increasing the likelihood of restoring and maintaining productive fisheries. *Bulletin of Marine Science*, 70(2):715–731.

Oceana (2018). Fishery audit 2018.

Okamura, H., McAllister, M. K., Ichinokawa, M., Yamanaka, L., and Holt, K. (2014). Evaluation of the sensitivity of biological reference points to the spatio-temporal distribution of fishing effort when seasonal migrations are sex-specific. *Fisheries research*, 158:116–123.

Parma, A. M. (2002). In search of robust harvest rules for pacific halibut in the face of uncertain assessments and decadal changes in productivity. *Bulletin of Marine Science*, 70(2):423–453.

Pineda, J., Hare, J. A., and Sponaugle, S. (2007). Larval transport and dispersal in the coastal ocean and consequences for population connectivity. *Oceanography*, 20(3):22–39.

Powers, J. E. (2014). Age-specific natural mortality rates in stock assessments: size-based vs. density-dependent. *ICES Journal of Marine Science*, 71(7):1629–1637.

Punt, A. E. and Cope, J. M. (2017). Extending integrated stock assessment models to use non-depensatory three-parameter stock-recruitment relationships. *Fisheries Research*.

Punt, A. E., Haddon, M., and Tuck, G. N. (2015). Which assessment configurations perform best in the face of spatial heterogeneity in fishing mortal-

ity, growth and recruitment? a case study based on pink ling in australia. *Fisheries research*, 168:85–99.

Quinn, T. J. and Deriso, R. B. (1999). *Quantitative fish dynamics*. Oxford University Press.

Ralston, S. and O'Farrell, M. R. (2008). Spatial variation in fishing intensity and its effect on yield. *Canadian Journal of Fisheries and Aquatic Sciences*, 65(4):588–599.

Rice, J. A., Quinlan, J. A., Nixon, S. W., Hettler Jr, W. F., Warlen, S., and Stegmann, P. M. (1999). Spawning and transport dynamics of atlantic menhaden: inferences from characteristics of immigrating larvae and predictions of a hydrodynamic model. *Fisheries Oceanography*, 8(Suppl. 2):93–110.

Ricker, W. (1958). Maximum sustained yields from fluctuating environments and mixed stocks. *Journal of the Fisheries Board of Canada*, 15(5):991–1006.

Scott, R. D. and Sampson, D. B. (2011). The sensitivity of long-term yield targets to changes in fishery age-selectivity. *Marine Policy*, 35(1):79–84.

Sethi, S. A. (2010). Risk management for fisheries. *Fish and Fisheries*, 11(4):341–365.

Shelton, P. A. and Morgan, M. J. (2014). Impact of maximum sustainable yield-based fisheries management frameworks on rebuilding north atlantic cod stocks. *Journal of Northwest Atlantic Fishery Science*, 46.

Shertzer, K. W. and Conn, P. B. (2012). Spawner-recruit relationships of demersal marine fishes: prior distribution of steepness. *Bulletin of Marine Science*, 88(1):39–50.

Smedbol, R. K. and Wroblewski, J. (2002). Metapopulation theory and northern cod population structure: interdependency of subpopulations in recovery of a groundfish population. *Fisheries Research*, 55(1-3):161–174.

Takashina, N. and Mougi, A. (2014). Effects of marine protected areas on overfished fishing stocks with multiple stable states. *Journal of theoretical biology*, 341:64–70.

Takashina, N. and Mougi, A. (2015). Maximum sustainable yields from a spatially-explicit harvest model. *Journal of theoretical biology*, 383:87–92.

Thorson, J. T., Ianelli, J. N., Munch, S. B., Ono, K., and Spencer, P. D. (2015). Spatial delay-difference models for estimating spatiotemporal variation in juvenile production and population abundance. *Canadian journal of fisheries and aquatic sciences*, 72(12):1897–1915.

Tyler, J. A. and Rose, K. A. (1994). Individual variability and spatial heterogeneity in fish population models. *Reviews in Fish Biology and Fisheries*, 4(1):91–123.

Walsh, S. J., Simpson, M., and Morgan, M. J. (2004). Continental shelf nurseries and recruitment variability in american plaice and yellowtail flounder on the grand bank: insights into stock resiliency. *Journal of Sea Research*, 51(3-4):271–286.

Werner, F. E., Cowen, R. K., and Paris, C. B. (2007). Coupled biological and physical models: present capabilities and necessary developments for future studies of population connectivity. *Oceanography*, 20(3):54–69.

White, J. W. (2010). Adapting the steepness parameter from stock–recruit curves for use in spatially explicit models. *Fisheries Research*, 102(3):330–334.

Wilberg, M. J., Irwin, B. J., Jones, M. L., and Bence, J. R. (2008). Effects of source–sink dynamics on harvest policy performance for yellow perch in southern lake michigan. *Fisheries Research*, 94(3):282–289.

Worm, B., Hilborn, R., Baum, J. K., Branch, T. A., Collie, J. S., Costello, C., Fogarty, M. J., Fulton, E. A., Hutchings, J. A., Jennings, S., et al. (2009). Rebuilding global fisheries. *science*, 325(5940):578–585.

Ying, Y., Chen, Y., Lin, L., and Gao, T. (2011). Risks of ignoring fish population spatial structure in fisheries management. *Canadian Journal of Fisheries and Aquatic Sciences*, 68(12):2101–2120.

Zhang, Z. (2013). Evaluation of logistic surplus production model through simulations. *Fisheries research*, 140:36–45.

Zheng, N., Wang, S., and Cadigan, N. (2019). Sensitivity of maximum sustainable yield reference points.

Appendices

Appendix A

Equilibrium SSB for the sink using the BH model is

$$S_2 = \frac{\alpha_2 S_2}{\beta_2 + S_2} SPR_2(f_2) + p\frac{\alpha_1 S_1}{\beta_1 + S_1} SPR_1(f_2),$$

where $S_2 \equiv SSB_{eq,2}(f_1, f_2)$ and $S_1 \equiv SSB_{eq,1}(f_1)$. The equilibrium SSB from the source is constant in terms of f_2, so we can rewrite it as

$$S_2 = \frac{\alpha_2 S_2}{\beta_2 + S_2} SPR_2(f_2) + cSPR_1(f_2),$$

where $c = pR(SSB_{eq,1}(f_1))$.This can be expanded and rearranged as

$$S_2(\beta_2 + S_2) = \alpha_2 S_2 SPR_2(f_2) + cSPR_1(f_2)(\beta_2 + S_2),$$

$$S_2^2 + \beta_2 S_2 - SPR_2(f_2)\alpha_2 S_2 - cSPR_1(f_2)S_2 - cSPR_1(f_2)\beta_2 = 0,$$

$$S_2^2 + [\beta_1 - SPR_2(f_2)\alpha_2 - cSPR_1(f_2)]S_2 - cSPR_1(f_2)\beta_2 = 0.$$

We can solve for S_2 by using the quadratic formula, where $A = 1$, $C = cSPR_2(f_2)\beta_2$, and B is

$$B(f_1, f_2) = \beta_2 - SPR_2(f_2)\alpha_2 + p \cdot R(SSB_{eq,1}(f_1))SPR_1(f_2).$$

The solution to the quadratic formula is provided by Equation 3.3.

The quadratic formula provides two roots (i.e. two solutions) for $SSB_{eq,2}$. One solution derives from the positive-root and the other from the negative-root. The solution, however, must be greater than zero, since $SSB_{eq} < 0$ is not possible. If we use the negative-root, then the solution is

$$\frac{-B(f_1, f_2) - \sqrt{B(f_1, f_2)^2 + 4\beta_2 \cdot p \cdot R(SSB_{eq,1}(f_1))SPR(f_2)}}{2} > 0.$$

Removing the denominator and rearranging, we get

$$-B(f_1, f_2) > -\sqrt{B(f_1, f_2)^2 + 4\beta_2 \cdot p \cdot R(SSB_{eq,1}(f_1))SPR_1(f_2)}.$$

Since we know the magnitude of the root is always greater than or equal to $B(f_1, f_2)$, that is,

$$B(f_1, f_2)^2 + 4\beta \cdot p \cdot R(SSB_{eq,1}(f_1))SPR(f_2) \geq B(f_1, f_2)^2,$$

because

$$4\beta \cdot p \cdot R(SSB_{eq,1}(f_1))SPR_1(f_2) \geq 0,$$

the negative-root solution for $SSB_{eq,2} \leq 0$ for any $p \geq 0$, and the positive-root solution for $SSB_{eq,2} \geq 0$ for any $p \geq 0$. Therefore, the positive-root is

the only plausible solution.

Appendix B

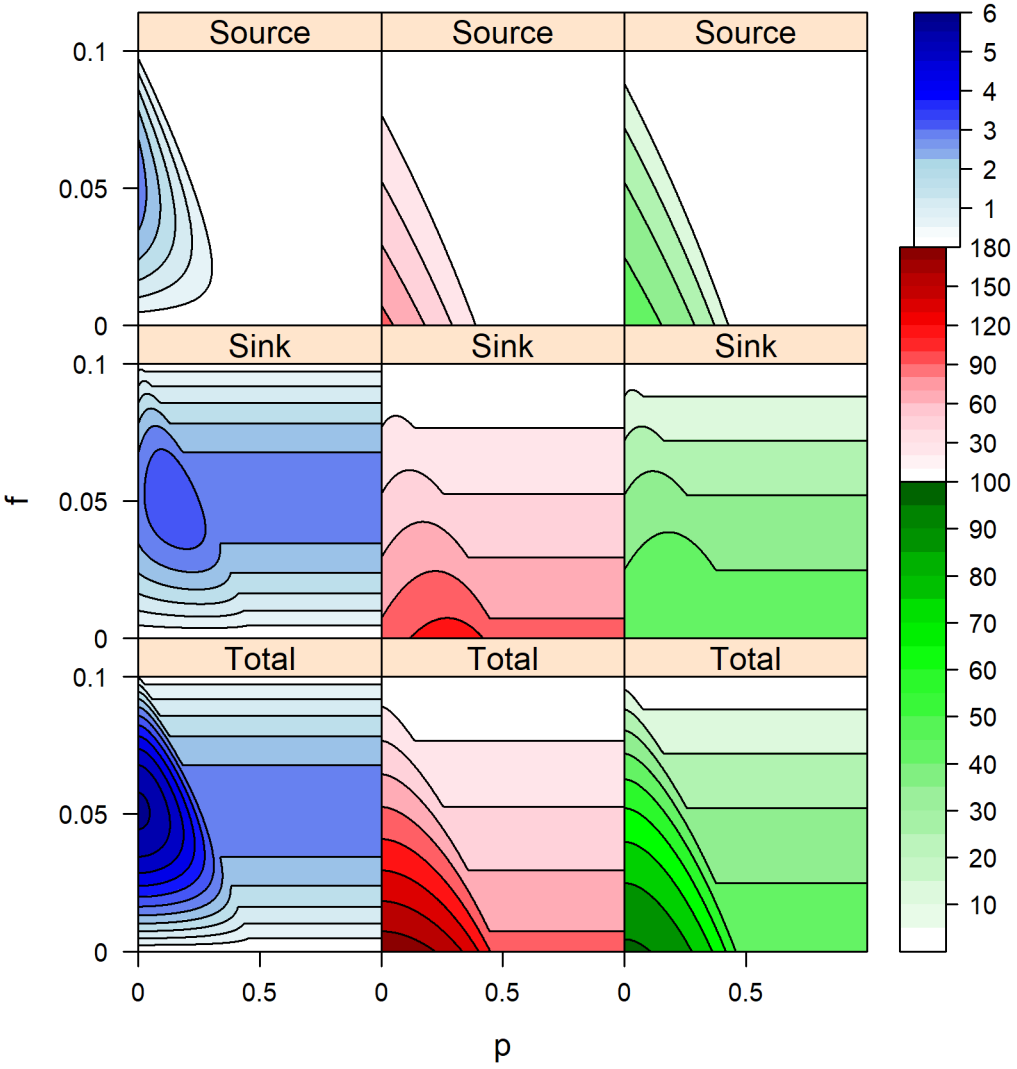

Figure B.1: Contour plots of the source, sink, and total equilibrium yield (blue), SSB (red), and local recruitment (green) for $f = f_1 = f_2$. Yields were calculated using the RK_{50} under an EQ system.

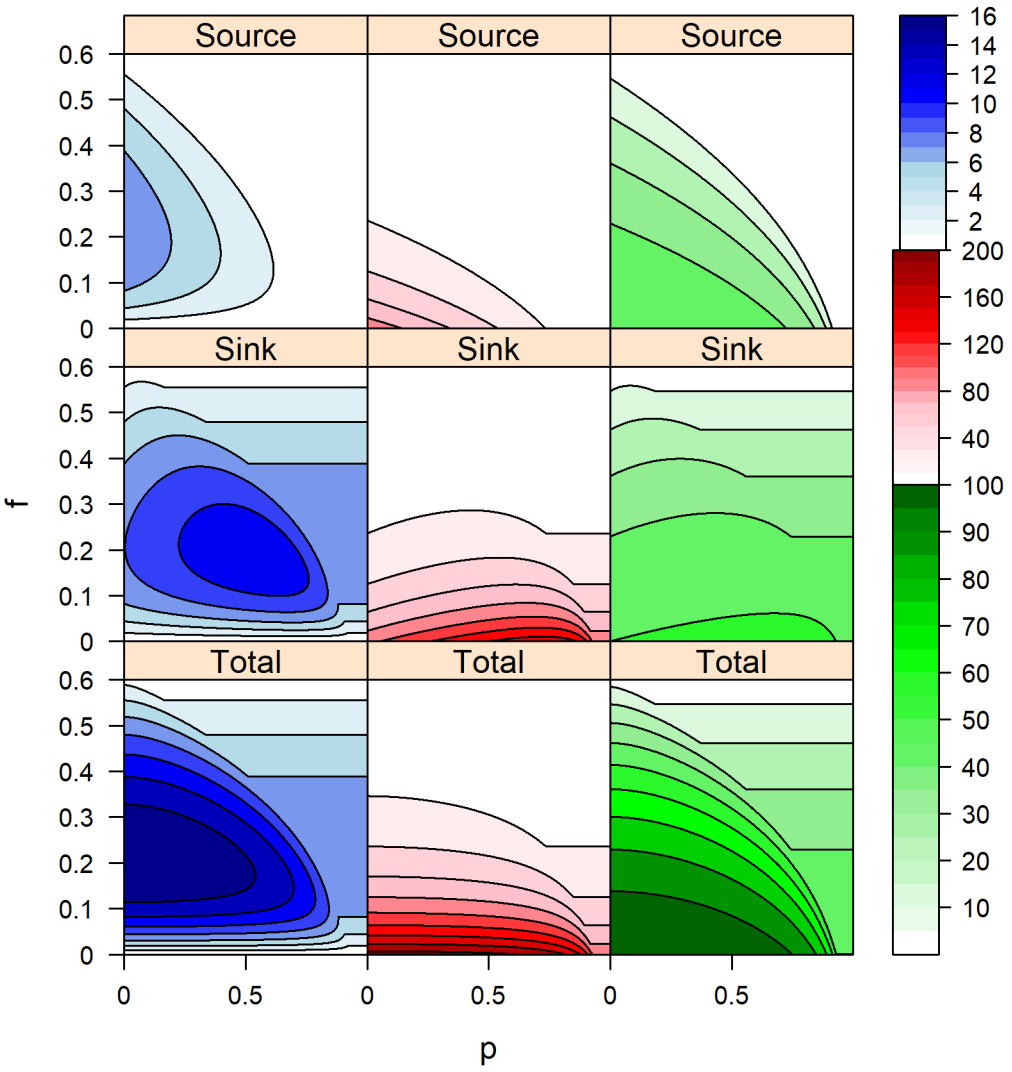

Figure B.2: Contour plots of the source, sink, and total equilibrium yield (blue), SSB (red), and local recruitment (green) for $f = f_1 = f_2$. Yields were calculated using the BH_h under an EQ system.

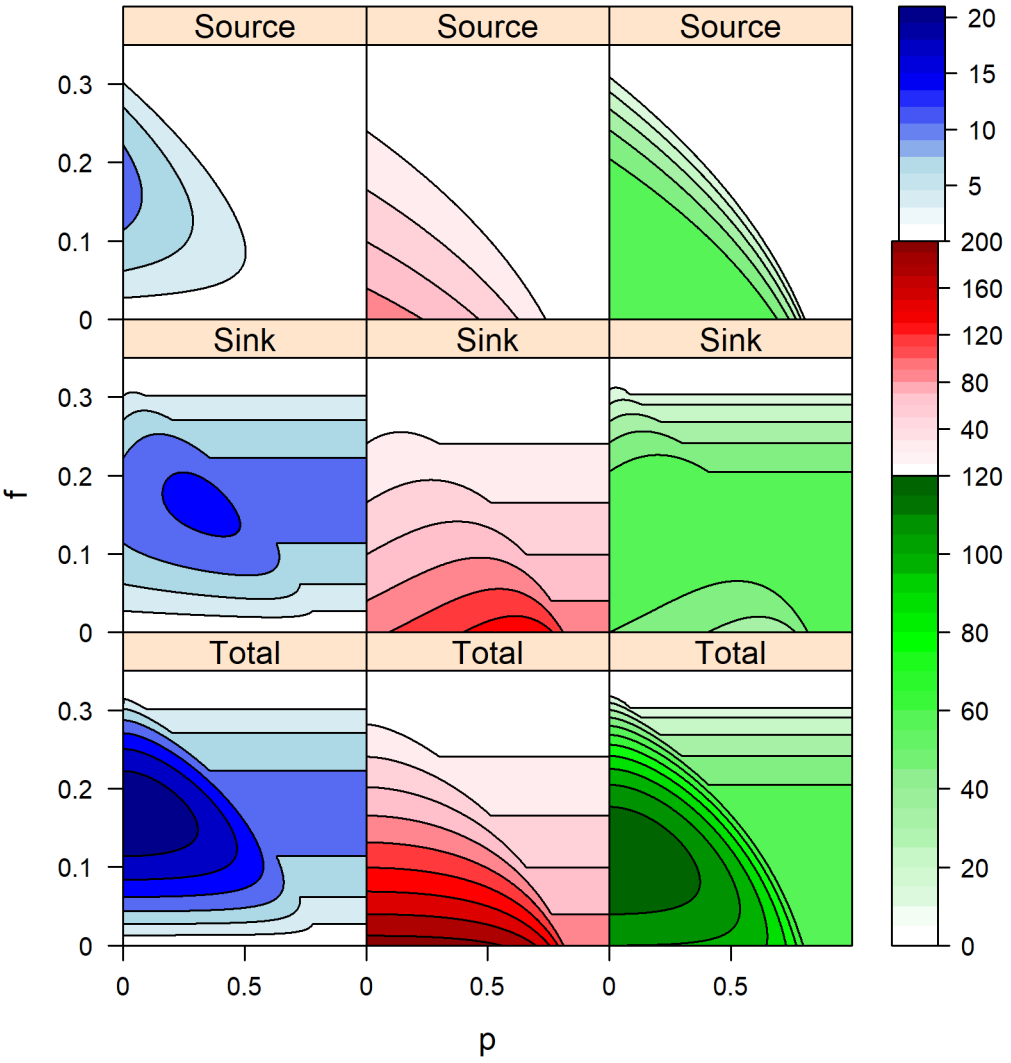

Figure B.3: Contour plots of the source, sink, and total equilibrium yield (blue), SSB (red), and local recruitment (green) for $f = f_1 = f_2$. Yields were calculated using the RK_h under an EQ system.

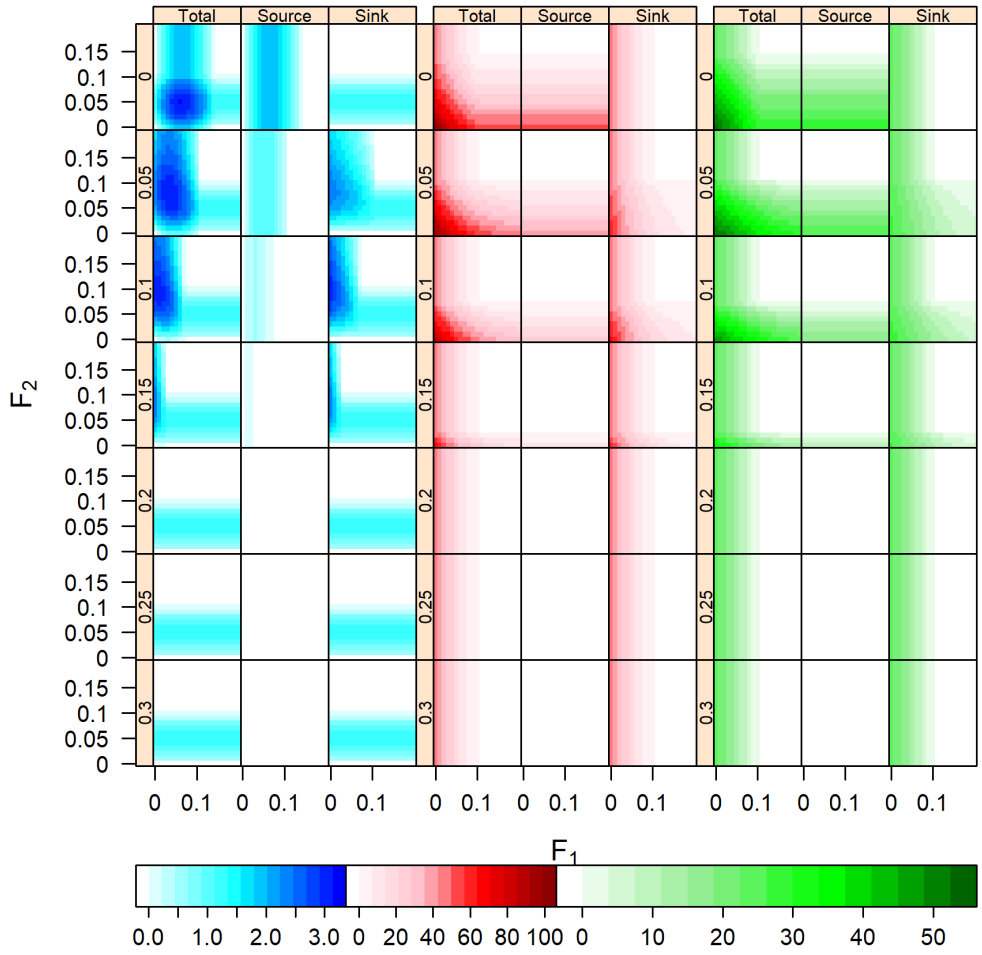

Figure B.4: Equilibrium values for a HL system using the BH_{50} SR model. Shown are the equilibrium yield (blue), SSB (red), and recruitment (green) for the source and sink, and the total of both. The value of p varies by row.

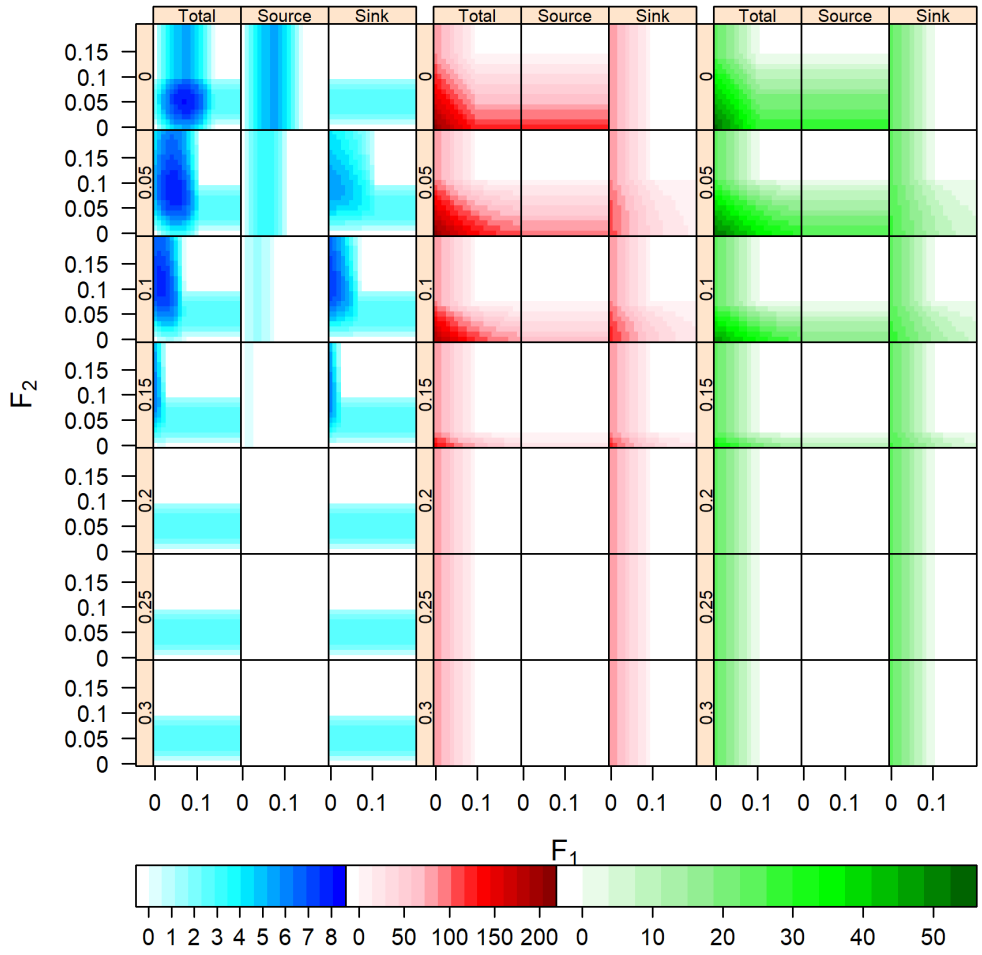

Figure B.5: Equilibrium values for a HL system using the RK_{50} SR model. Shown are the equilibrium yield (blue), SSB (red), and recruitment (green) for the source and sink, and the total of both. The value of p varies by row.

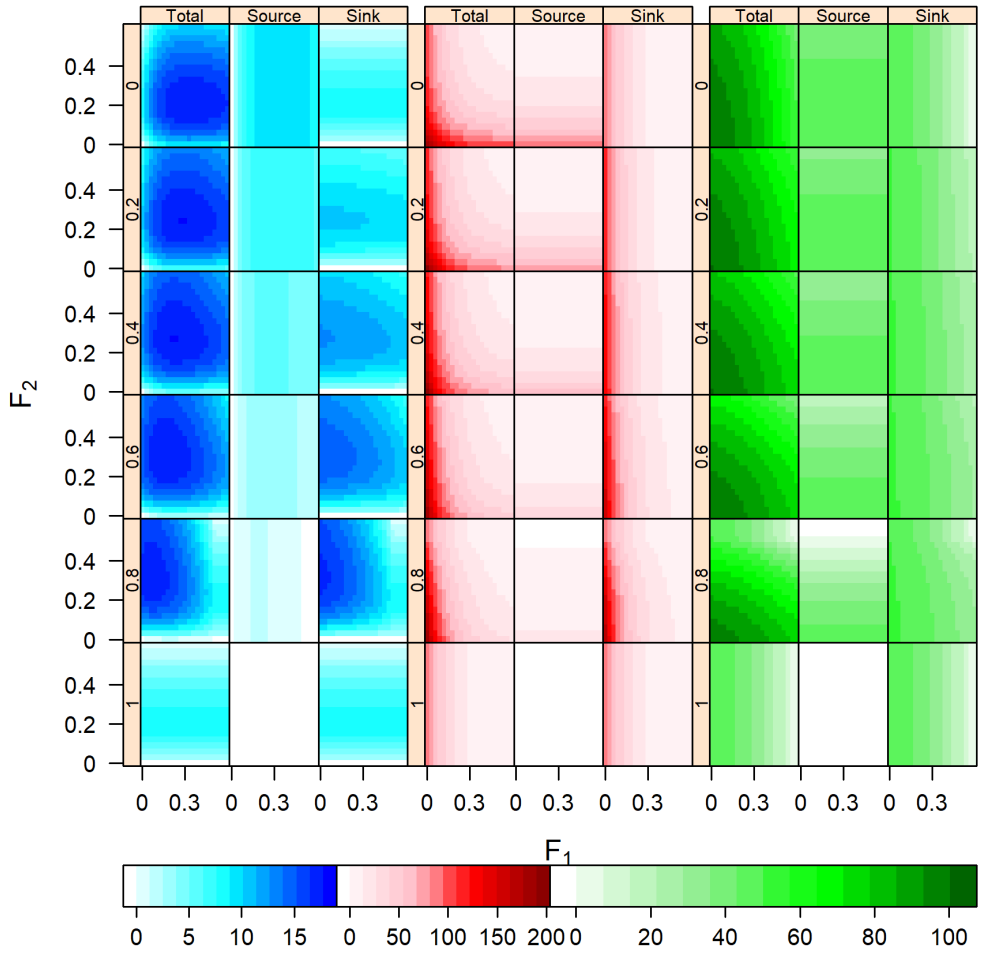

Figure B.6: Equilibrium values for a HL system using the BH_h SR model. Shown are the equilibrium yield (blue), SSB (red), and recruitment (green) for the source and sink, and the total of both. The value of p varies by row.

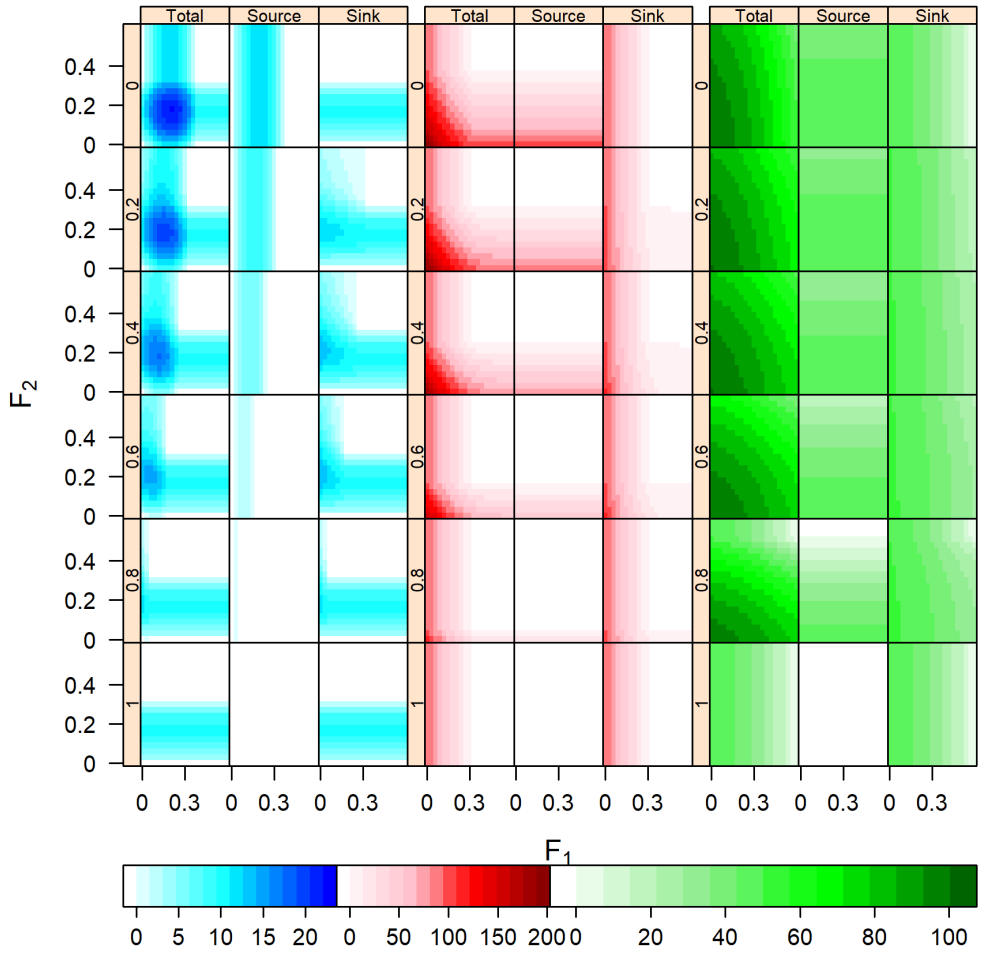

Figure B.7: Equilibrium values for a HL system using the RK_h SR model. Shown are the equilibrium yield (blue), SSB (red), and recruitment (green) for the source and sink, and the total of both. The value of p varies by row.

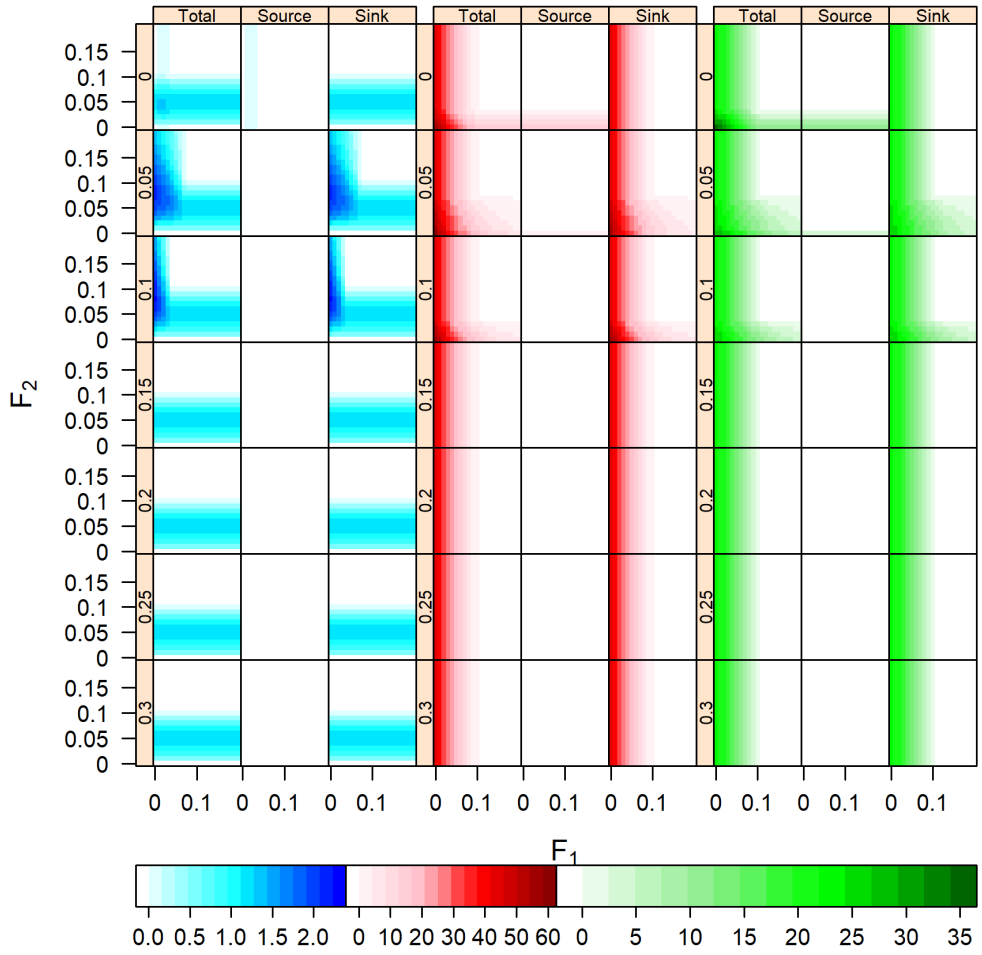

Figure B.8: Equilibrium values for a DA system using the BH_{50} SR model. Shown are the equilibrium yield (blue), SSB (red), and recruitment (green) for the source and sink, and the total of both. The value of p varies by row.

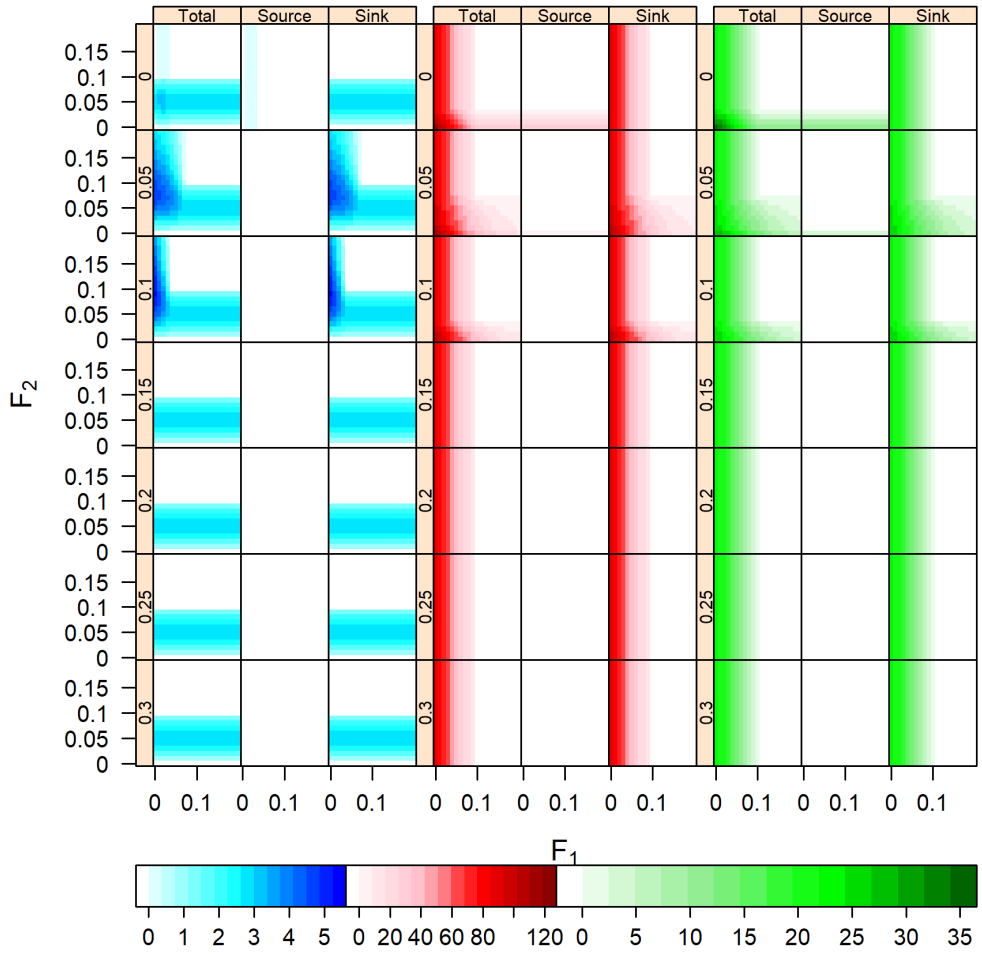

Figure B.9: Equilibrium values for a DA system using the RK_{50} SR model. Shown are the equilibrium yield (blue), SSB (red), and recruitment (green) for the source and sink, and the total of both. The value of p varies by row.

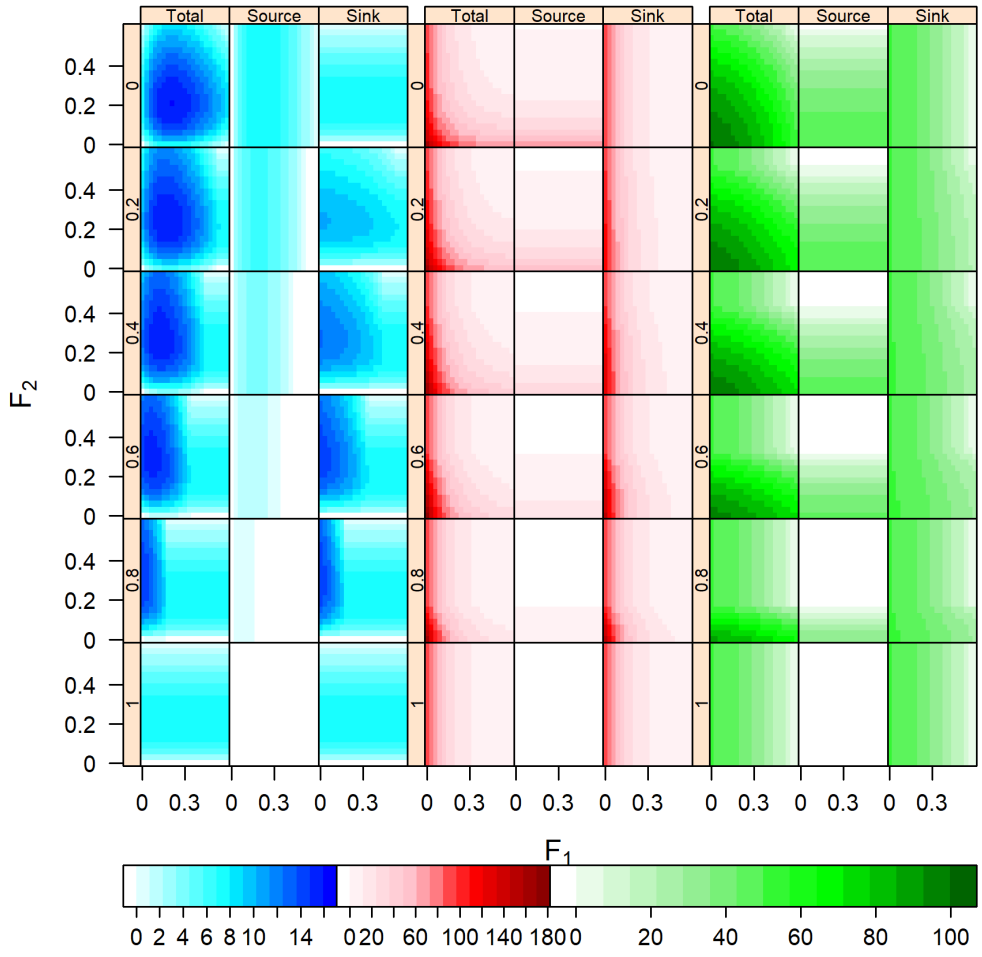

Figure B.10: Equilibrium values for a DA system using the BH_h SR model. Shown are the equilibrium yield (blue), SSB (red), and recruitment (green) for the source and sink, and the total of both. The value of p varies by row.

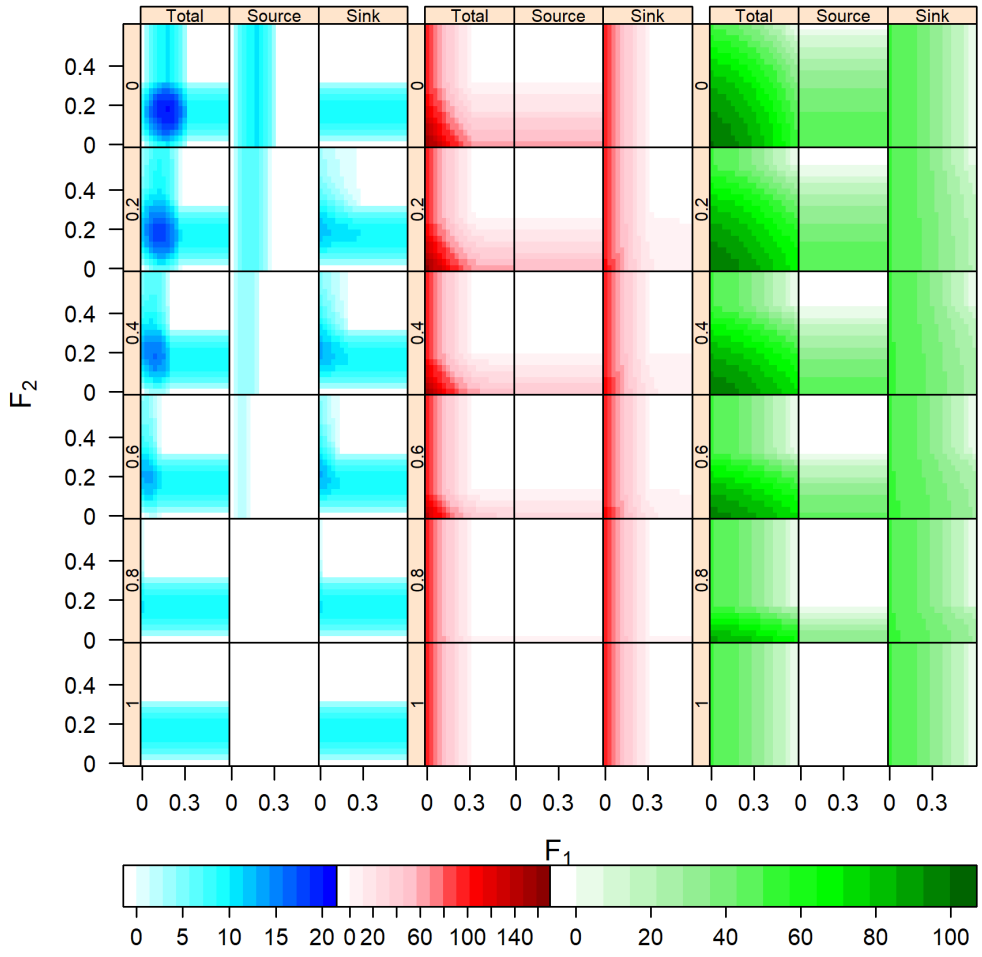

Figure B.11: Equilibrium values for a DA system using the RK_h SR model. Shown are the equilibrium yield (blue), SSB (red), and recruitment (green) for the source and sink, and the total of both. The value of p varies by row.

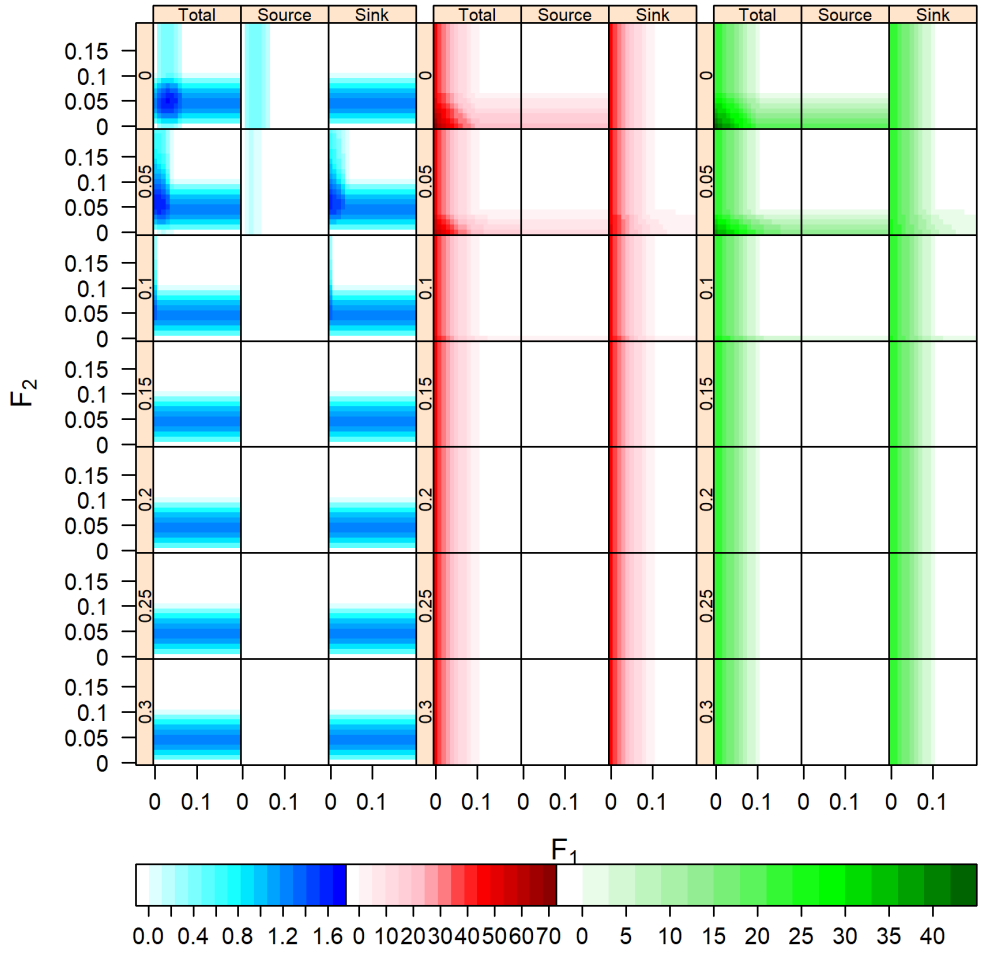

Figure B.12: Equilibrium values for a HL & DA system using the BH_{50} SR model. Shown are the equilibrium yield (blue), SSB (red), and recruitment (green) for the source and sink, and the total of both. The value of p varies by row.

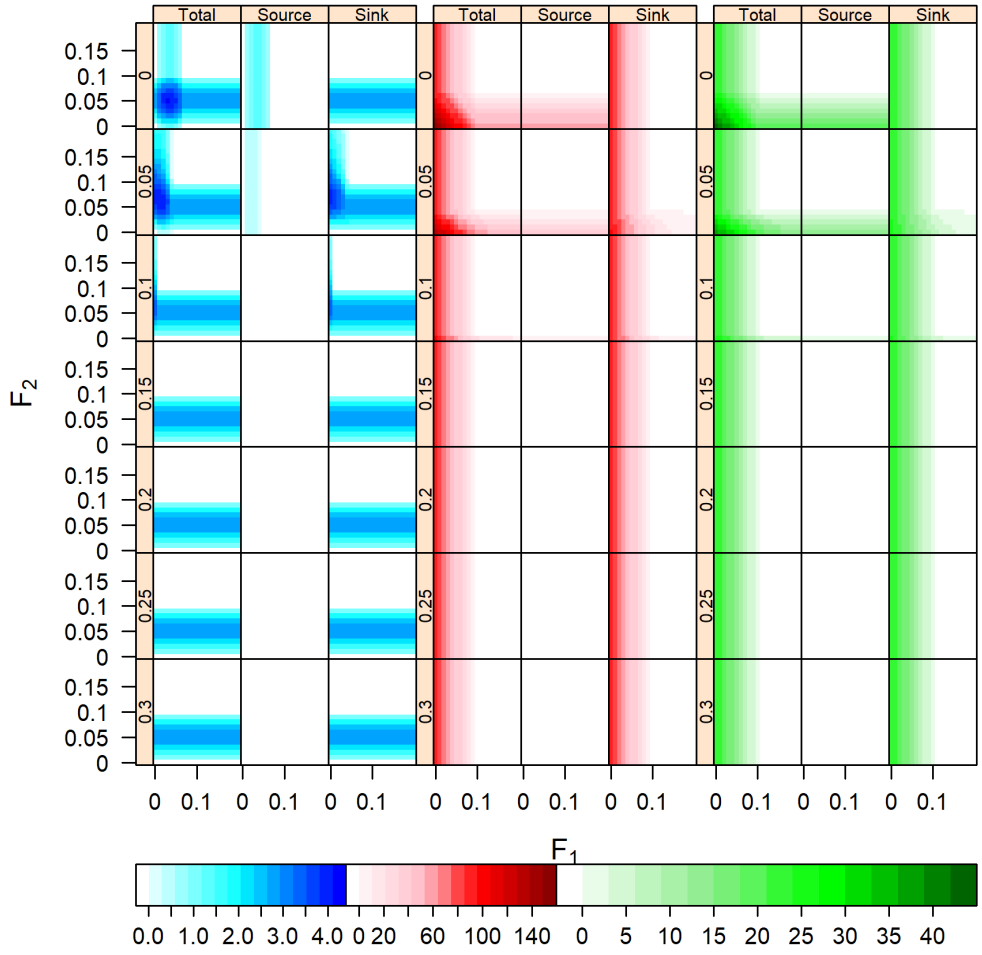

Figure B.13: Equilibrium values for a HL & DA system using the RK_{50} SR model. Shown are the equilibrium yield (blue), SSB (red), and recruitment (green) for the source and sink, and the total of both. The value of p varies by row.

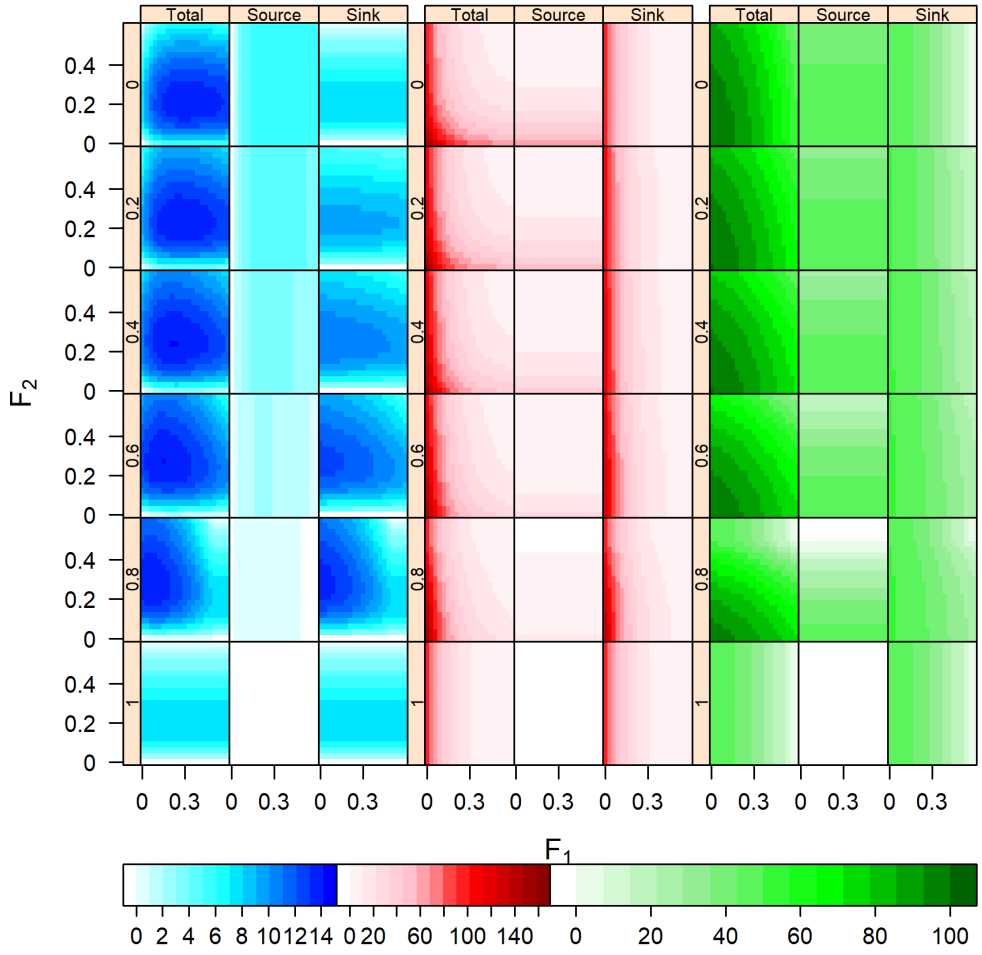

Figure B.14: Equilibrium values for a HL & DA system using the BH_h SR model. Shown are the equilibrium yield (blue), SSB (red), and recruitment (green) for the source and sink, and the total of both. The value of p varies by row.

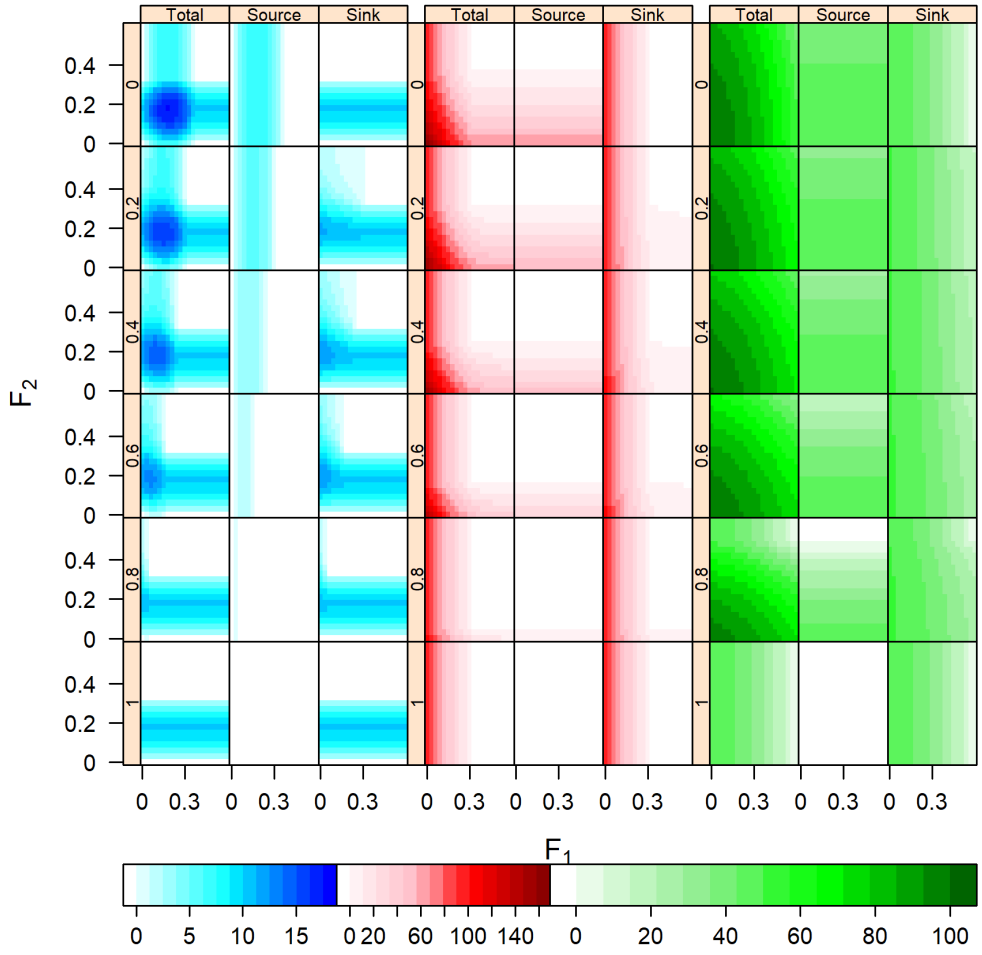

Figure B.15: Equilibrium values for a HL & DA system using the RK_h SR model. Shown are the equilibrium yield (blue), SSB (red), and recruitment (green) for the source and sink, and the total of both. The value of p varies by row.